Understanding HS6ST1 and heparan sulfate 6-O-sulfation in cartilage

Oliver McClurg

Doctor of Philosophy (PhD)

University of East Anglia

Norwich Medical School

April 2024

Abstract

Osteoarthritis (OA) is a common, degenerative musculoskeletal disease for which treatment options are lacking due to limited understanding of the molecular pathogenesis of joint degradation and repair. OA is characterised by loss of aggrecan and type II collagen from the joint, partly due to dysregulated growth factor signalling. Heparan sulfate (HS) proteoglycans in the pericellular matrix surrounding chondrocytes regulates growth factor signalling through their negatively-charged sulfate groups. HS 6-O-sulfation regulates the signalling of many growth factors and is therefore tightly regulated, being the only sulfate group that is modified during and after biosynthesis. In OA, HS 6-O-sulfation is increased due to increased expression of the 6-O-sulfotransferase, *HS6ST1*. Therefore, it has been hypothesised that increased 6-O-sulfation, driven by *HS6ST1,* contributes to OA progression.

In this thesis, I set out to investigate the effect of *HS6ST1* on the C28/I2 chondrocyte-like cell line. *HS6ST1* overexpression reduced sulfated glycosaminoglycan (sGAG) content *in vitro*, which could be reversed by addition of exogenous ligands (TGF-β1, BMP4). This suggests that 6-O-sulfated HS sequesters an endogenous anabolic ligand, which can be competed off by exogenous HS ligands. Label-free quantitative mass spectrometry of healthy and OA human cartilage identified proteins with high affinity for 6-O-sulfated HS, but candidates chosen for further study (endostatin, SERPINF1) could not account for the reduced sGAG. RNASeq functional enrichment analyses suggest that *HS6ST1*-overexpresison reduced cell-ECM interactions, driven by reduced integrin expression. This was accompanied by reduced phosphorylation of several signalling pathways, including SRC kinases and BMP4-induced SMAD1/5/8 phosphorylation.

Therefore, I propose that increased HS 6-O-sulfation is deleterious for cartilage as it inhibits growth factor signalling, and so downregulates expression of integrins, reducing mechano-responses of chondrocytes and impairing their attachment to the matrix and sGAG accumulation. Targeting HS 6-O-sulfation may therefore be of therapeutic benefit in OA.

Table of contents

List of figures

List of tables

Acknowledgements

My DPhil has been a challenging and enjoyable 4 years. Since 2019 life has been tumultuous, yet a steady and enduring aspect has been the strong supervision by Dr Linda Troeberg. I would like to thank her for her patience, wit, and scientific knowledge. I could not have asked for a better supervisor, as few would have managed to keep my interest high during periods of scientific lulls. I sincerely hope we maintain a good relationship as we both move forward in our careers. To all the past and present members of the Troeberg lab, thank you for your advice and questions. Secondly, I'd like to thank my secondary supervisor, Dr Ian Clark, for prompt help and his wisdom over the past 4 years.

Scientific advancement is impossible without collaboration, and I'd like to thank Dr Matteo Calligaris and Dr Simone Scilabra (and many others at RiMED) not only for their LfQ MS analysis of cartilage extracts, but for memories shared over a glass of wine in Palermo. I'd like to thank Professor Jeremy Turnbull and Dr Ed Yates for their synthesis of custom heparin-Sepharose resins, without which my project would have been seriously delayed. Finally, Dr Romain Vives, from the University of Grenoble, who so generously offered recombinant SULF2 as thunder clapped overhead whilst we were at the Gordon Proteoglycan conference together.

I'd like to thank Versus Arthritis for their scholarship, this work would not have been possible without their funding, and I will sincerely miss the Fellows days. To

the Oxford OA Pathogenesis Centre, in particular Dr Angus Wann, I'd like to thank you for your invite to the weekly meetings and conferences.

To my friends, there is not enough space to adequately express my thanks for your support. To Dr Benjamin Johnson, thank you for our scientific and non-scientific discussions in the kitchen of our flat, to Scott Johnson thank you for extending my horizons and encouraging me to take more risks, and to Svenja, I will always treasure the memories of suffering through writing together, being dragged on early morning cycles and constantly being humbled about not truly working at the JIC, despite my insistence at working in the library. To my other friends, Aaron, Angel, Ben, Dan, Franziska, John, Magdalena, Oliver F, Pediro, Sarah, Tom B and Tom F, thank you for being there to cry over a beer, to climb a wall, to swim in the mornings, or to cycle a mad distance.

Finally, to my parents, Andrew and Heather McClurg, I'd like to thank you for supporting me through my scientific adventure and through life. I am where I am today because of your support.

Chapter 1. Introduction

1.1 Osteoarthritis and cartilage

1.1.1 An old disease that needs new therapies

Musculoskeletal (MSK) conditions cover a wide range of disorders affecting bones, joints, muscles, and connective tissues. One of the most prevalent MSK diseases is osteoarthritis (OA). OA patients suffer from pain, stiffness, and reduced quality of life. Latest estimates[1] calculate ten million people in the UK suffer from OA, with the majority (>5 million) suffering from OA of the knee, however hip and/or hand OA is also common[2] . By 2030, working days lost due to OA are expected to cost the UK economy over £3 billion a year[1].

The primary risk factor for symptomatic OA is age. Of those diagnosed, only 1% are below the age of 40, whilst over 50% of people diagnosed with OA are aged 80 or over. Older age is associated with increased frailty and reduced physical activity, both of which contribute to symptomatic OA[3,4]. The second largest risk factor is biological sex as women are 1.5x more likely to develop OA than men[5].

Despite the prevalence of OA, there are no effective disease-modifying OA drugs that improve a patient's quality of life[6]. Current treatments for OA focus on improving pain and joint function, and therefore comprise mainly analgesics, such as paracetamol, nonsteroidal anti-inflammatory drugs, and opioids. The only effective treatment for late-stage OA is joint replacement surgery. A major reason for the lack of effective drugs is due to the poor understanding of the molecular mechanisms underpinning OA progression, cartilage loss and joint pain.

Healthy joints have a smooth layer of tough but compressible cartilage covering the surface of opposing bones. This layer of cartilage enables smooth articulation

of the opposing bones within the joint. OA cartilage exhibits surface fibrillation that contributes to the loss of smooth articulation of opposing bones. However, other symptoms observed include osteophyte formation[7], synovitis[8], and angiogenesis of the synovium, osteocytes, and deep layers of cartilage[9]. Structurally, cartilage has a superficial zone at the joint interface, a middle zone and a deep zone that connects with the surface of the bones within the joint. Macroscopically, the structure of cartilage is remarkably simple.

1.1.2 OA disease pathology and biochemical aetiology

There are three major components of articular cartilage. Type II collagen and aggrecan make up the ~90-95% of the dry weight of cartilage, and chondrocytes compose the final 5%. Type II collagen forms a super-helical structure that consists of three identical α1(II) chains. Initially synthesised as procollagen, modifications occur that are crucial for stabilization of the triple helix. Procollagen processing occurs by procollagen C-proteinases and members of the ADAMTS protease family. The removal of propeptides results in decreased procollagen solubility, thereby promoting organisation of the triple helical structure into a higher order organisation[10–12]. Whilst the orientation and arrangement of collagen fibrils was initially thought to be random, it is now known that collagen fibrils arrange perpendicular to the joint surface in the deep zone, and parallel to the surface in the superficial zone (**Figure 1.1**). Mutations of type II collagen are known to result in several types of chondrodysplasias, and lead to premature osteoarthritis development in both adults[13] and children[14]. The stability and strength of type II collagen contributes to cartilage integrity and resilience to stress.

Aggrecan is a proteoglycan that is found homogenously through healthy cartilage. It consists of core globular regions (G1, 2, 3) interspersed with interglobular regions that are substituted with chondroitin sulfate glycosaminoglycan (GAG) chains. These globular regions are important for aggrecan function and synthesis, as heat shock protein 25 guides aggrecan synthesis in the ER through interactions with its G3 domain[15]. Aggrecan molecules aggregate together along large filaments of the non-sulfated GAG hyaluronan (HA). As many as 50 aggrecan molecules can be linked to a single HA chain, which is retained in cartilage through binding to a chondrocyte HA cell surface receptor, CD44[16]. The importance of CD44 to cartilage integrity has been shown using anti-CD44 antibodies. Cleavage of the HA polysaccharide with hyaluronidase caused loss of the gel-like structure that can be observed surrounding chondrocytes. Addition of exogenous HA:aggrecan aggregates re-established the gel-like structure but was inhibited in the presence of anti-CD44 antibodies[17]. Therefore, integration of HA:aggrecan into cartilage is significantly dependent upon CD44. The GAG chains located between G2 and G3 act to draw water into the joint and contribute to the mechanoproperties of cartilage. They do this through osmotic imbalance, as the negatively charged sulfate groups on the CS GAG chains are counter-charged by Na^+ ions. This difference in ionic charge draws water into cartilage, causing the tissue to expand and promotes its function. Loss of aggrecan is therefore a critical step in OA pathogenesis as this osmotic potential is lost.

Finally, chondrocytes are the only cells found within articular cartilage and are responsible for synthesizing the cartilaginous matrix. They form linear clusters in the deep zone, but closer to the superficial zone of cartilage they are generally

found as single cells (**Figure 1.1**)

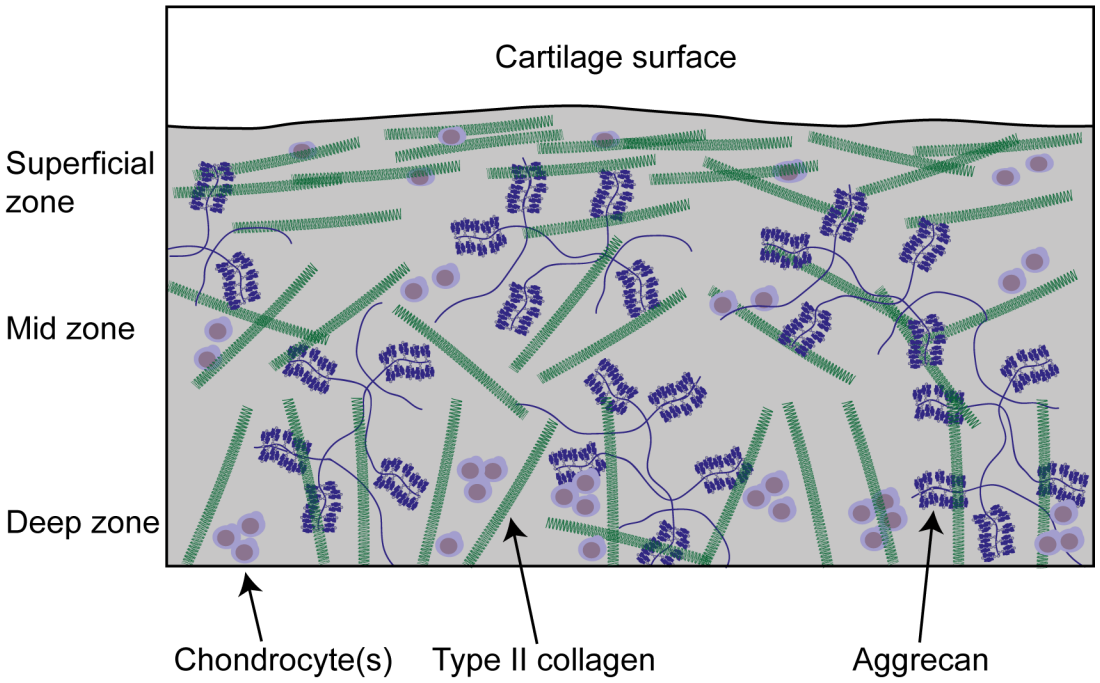

Figure 1.1 Schematic representation of cartilage composition.

Schematic representation showing the deep, mid- and superficial zones of cartilage. Type II collagen (green) radiate up to the superficial zone from the deep zone, organising into bundles parallel to the surface of cartilage. Aggrecan (blue) proteoglycans lay interspersed throughout cartilage. Chondrocytes are sparsely found in the superficial zone, and group together in the deeper areas of cartilage.

Cartilage formation begins prenatally when mesenchymal cells condense and differentiate into two different cell lineages: chondrocytes and perichondral cells. Commitment of mesenchymal cells into the chondrocyte lineage is induced by paracrine factors secreted from neighbouring mesodermal cells. These committed cells condense into nodules and differentiate into chondrocytes that begin to proliferate and start forming the model for bone. Expression of the transcription factor *SOX9* is induced in this phase, therefore making it a master transcriptional regulator for chondrocytes. Expression of SOX9 marks the transition towards the proliferation phase. During this phase, chondrocytes secrete the cartilage-specific extracellular matrix described above, with the

expression of type II collagen, aggrecan, fibroblast growth factor receptor 3 (*FGFR3*) and parathyroid hormone-related hormone (*Pthlh*) increasing, the latter promoting chondrocyte proliferation. Chondrocytes subsequently become prehypertrophic, expressing parathyroid hormone-related peptide receptor and Indian hedgehog (Ihh). Ihh promotes Pthlh expression thereby promoting chondrocyte proliferation[18]. Proper control of Ihh signalling is crucial for bone development, as shown by reduced long bone development in Ihh null mice[19], and control of this process is discussed further in **1.3.1**. The secreted matrix is then modified as chondrocytes stop proliferating, become hypertrophic and begin to secrete type X collagen and increase their secretion of fibronectin. Following this, this cartilage-bone model is invaded by cells that establish the primary centre of ossification thus promoting mineralization of the cartilage. Interestingly, expression of both type X collagen and fibronectin alongside chondrocyte hypertrophy are notably increased in OA, possibly indicating a move towards an endochondral-ossification phenotype in OA chondrocytes.

In the final phase of bone growth, secondary ossification centres form and hypertrophic chondrocytes undergo apoptosis, and perichondral cells, now differentiated into osteoblasts, form bone on the neo-cartilage. The primary and secondary ossification centres are separated by the growth plate, a region of both hypertrophic and proliferating chondrocytes. Expansion of this zone through Pthlh and Ihh signalling and subsequent mineralization, is responsible for bone growth. This process is termed endochondral ossification. At birth, the secondary ossification centre is capped by embryonic articular cartilage, which will form the articular-epiphyseal cartilage complex[20]. The immature articular-epiphyseal cartilage complex has 5 zones, the zone of articular cartilage is at the surface of

what will become the joint and has the characteristic features of mature cartilage. The remaining zones are typical of cartilage that will become bone, namely having proliferating chondrocytes, mature enlarged chondrocytes, hypertrophic chondrocytes and finally a zone of apoptotic chondrocytes with an ECM undergoing vascular invasion. Therefore, the articular-epiphyseal cartilage complex is crucial for demarcating where bone ends, and articular cartilage begins. A brief overview of some signalling pathways and their roles in cartilage and bone development is shown in **Figure 1.2**.

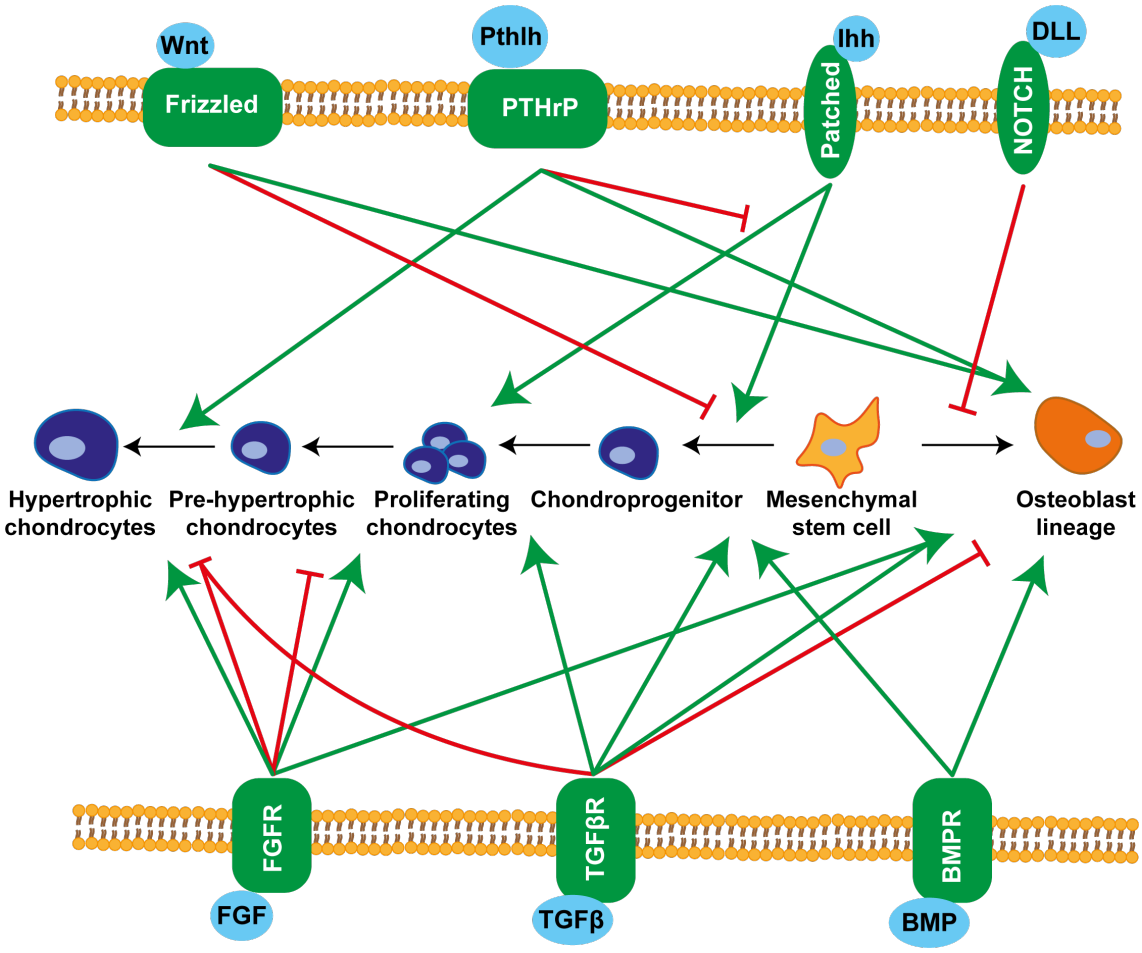

Figure 1.2 Schematic of important signalling events in endochondral ossification.

Schematic showing signalling events that either promote (green arrows) or inhibit (red arrows) progression down either the chondrocyte lineage or osteoblast lineage.

Given the importance of type II collagen and aggrecan, the productive capacity of chondrocytes would be expected to be consumed almost entirely by their production of type II collagen and aggrecan, but the half-lives of these molecules has proven to be exceptionally long. Type II collagen was measured to have a half-life of over 100 years[21], whereas aggrecan turnover is estimated to be between 3-25 years, depending on the aggrecan fraction investigated. Therefore, chondrocytes productive capacity must be predominantly occupied by the production of other matrix components. Given this, the finely tuned regulation of these components must play a critical role in regulating cartilage homeostasis. In conjunction with the increased protease activity observed in OA, dysregulated synthesis of matrix components results in loss of aggrecan and cartilage from the joint. In fact, OA chondrocytes have dysregulated expression of a wide variety of genes. A characteristic hallmark of an OA chondrocyte is expression of hypertrophic markers and matrix calcification genes.

1.1.3 Proteolytic activity increases in OA cartilage.

The irreversible loss of type II collagen in OA is preceded by the loss of aggrecan[22]. The loss of these macromolecules is mediated predominantly through the action of two families of proteases. The major aggrecanases in cartilage are a disintegrin and metalloproteinase with thrombospondin motif (ADAMTS) 4 and 5. Evidence suggests that ADAMTS-5 is primarily responsible for aggrecan loss *in vivo*, as cartilage loss is reduced in ADAMTS-5 deficient mice but not in ADAMTS-4 deficient mice[23–25]. Aggrecan turnover is a normal aspect of cartilage homeostasis, and it is thought that dysregulation of this process is the

driver of aggrecan loss in OA. MMP activity has been linked to homeostatic turnover of aggrecan, whereas the increased activity of ADAMTS in OA partially explains the increased turnover[26,27]. A summary of the major ADAMTS and MMPs cleavage sites of aggrecan by ADAMTS and MMPs is shown in **Figure 1.3**.

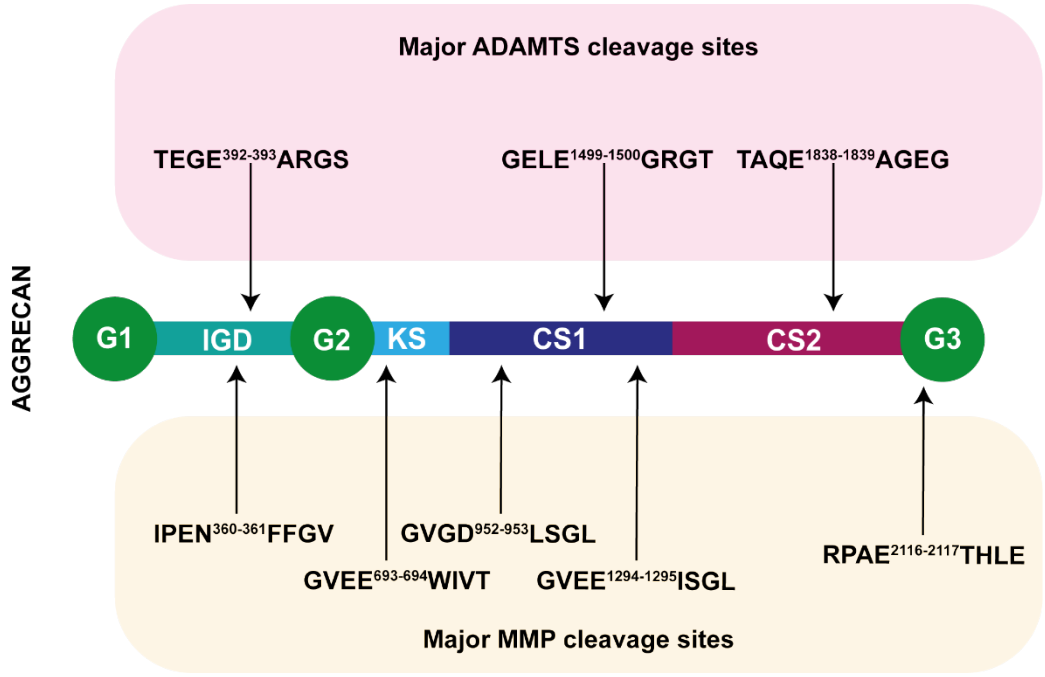

Figure 1.3 ADAMTS activity is linked to pathogenic aggrecan turnover

Schematic of aggrecan cleavage sites by ADAMTS (top) and MMP (bottom) proteases. MMP cleavage of aggrecan has been linked to normal turnover of aggrecan within cartilage, whereas ADAMTS proteolysis of aggrecan is increased in disease.

Following initial loss of aggrecan from cartilage, collagen is then also broken down. Type II collagen is primarily broken down by MMP-13 in articular cartilage. Expression of MMP-13 is elevated in OA and in rodent OA models[28], conditional MMP-13 expression in murine cartilage induced spontaneous cartilage degradation[29] whilst *Mmp13*$^{-/-}$ mice had reduced cartilage loss following surgically-induced OA[30]. The role of other MMPs is less clear. For example, *MMP3* is strongly expressed in OA cartilage, however expression reduces in later

stages of disease[31]. Conflicting evidence exists on the role for MMP-3 in the joint as, despite it having roles in MMP-13 activation, *Mmp3*$^{-/-}$ mice show both reduced and increased collagen and aggrecan loss[32,33].

1.1.4 The pericellular matrix is rich in structural and signalling proteins.

Surrounding the chondrocyte is the pericellular matrix (PCM). Together, the chondrocyte and PCM have historically been termed the 'chondron'. Compared to the interterritorial matrix, which is composed mainly of aggrecan and type II collagen, the PCM is rich and diverse in proteins. It not only transduces signals (biochemical and biomechanical) to the chondrocyte[34–36], but is also responsible for proper processing of procollagen to mature collagen[37]. Type VI collagen, a major component of the PCM, aggregates alongside biglycan, decorin and βig-h3[38] to promote formation of a collagen fibril network. Type VI collagen is composed of three distinct α-chains that form triple helices, with non-helical globular-appearing domains. The triple helical region contains 11 RGD repeats, which enable anchoring of chondrocytes to the PCM through binding to cell surface integrins[39] and to the chondroitin sulfate proteoglycan NG2. NG2 promotes chondrocyte adhesion to integrins through type VI collagen, and this is lost in OA[40], potentially contributing to disease progression. Interestingly, type VI collagen appears to have location-dependent effects, as *Col6a1*$^{-/-}$ mice had reduced Young's modulus of the PCM from hip chondrocytes[41], but no effect was observed in the PCM of knee chondrocytes[42].

Integrins are heterodimeric transmembrane proteins that consist of α and β subunits. Their extracellular regions cooperate with matrix components, and their

short cytoplasmic domains both interact with kinase-mediated intracellular signalling pathways and bind and organise cytoskeletal structures. There are 24 different heterodimers, consisting of α and β subunits. Chondrocytes have previously been observed to predominantly express α1, 2, 3, 5 and β1 and 3 subunits[43].

Integrins signal into and out of cells. It is thought that integrin activation is one aspect of a cell's response to an altered environment. Integrins are normally present in an inactive conformation, where they are unable to bind ECM components. Integrin-independent signalling initiates signalling cascades that lead to integrin activation, through recruitment of talin and kindlin to the cytoplasmic tails of β integrins. Activation increases the affinity of integrins for ECM proteins by clustering integrins into focal adhesions, and further into streak-like fibrillar adhesions. This is part of the 'inside-out' signalling mechanism. Once integrins are activated, they bind ECM molecules and activate numerous tyrosine and serine kinases alongside their respective adaptor proteins. This is termed 'outside-in'. A schematic of this is shown in **Figure 1.4.**

.

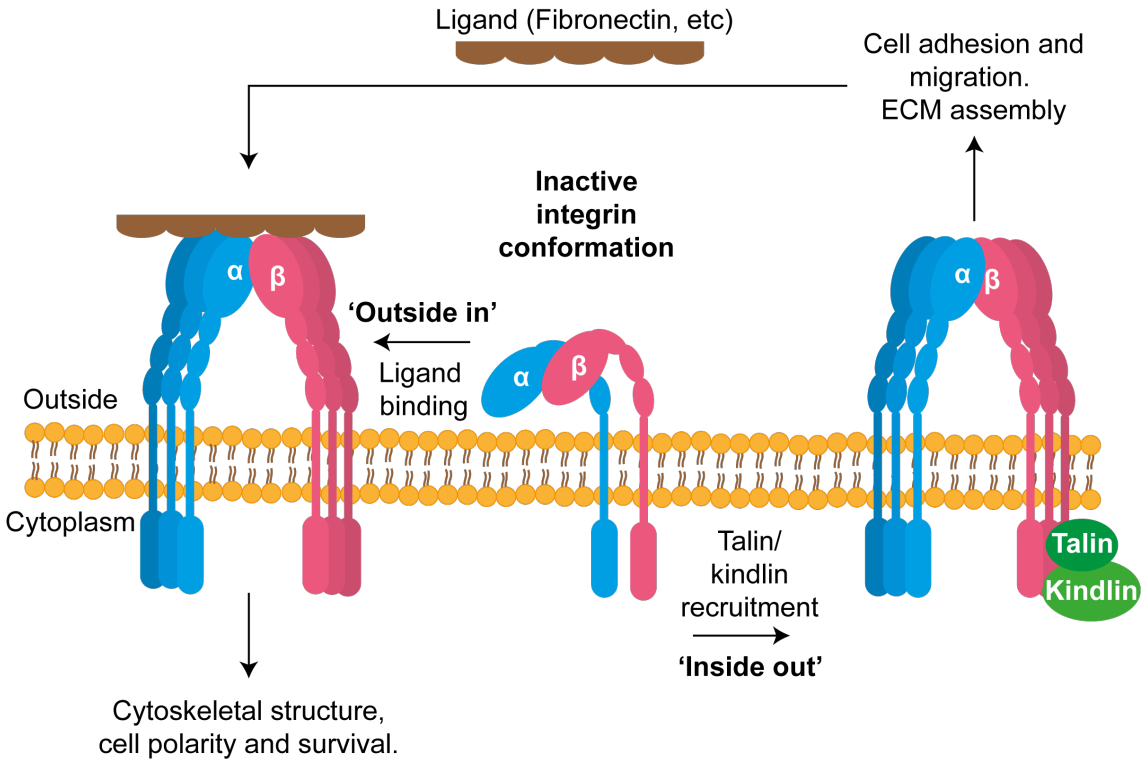

Figure 1.4 Integrins signal through both 'inside-out' and 'outside-in' mechanisms.

Inactive integrins form α and β heterodimers. Through binding of multi-valent intracellular ligands (such as talin and kindlin) to the cytoplasmic tails of β integrins, heterodimers become heterooligomers. Alongside other membrane components, these hetero-oligomers become focal adhesions, which interact with the ECM. This is termed 'inside-out' signalling. Binding of ECM molecules to focal adhesions, or integrins, can activate intracellular signalling, termed 'outside-in' signalling.

In this manner, integrins control how cells both respond to and change their environment. In healthy articular cartilage, chondrocytes express proteins that bind to a number of integrins, e.g., COLII and COLVI (which bind promiscuously to α1β1, α2β1 and α10β1, helping to control PCM organisation[44]) laminin (α6β1), osteopontin (αVβ3) and fibronectin (α3,4,5β1). Changes to integrin expression have been linked to OA progression. Both β3 and α5 deficient mice had reduced OA progression in response to surgically-induced OA[45] whilst α5β1 induced ACAN expression following cyclic compression of chondrocytes was abrogated

with anti-α5 antibodies[46]. There is partial evidence that loss of integrin function may play a role in OA pathophysiology, as, unlike normal chondrocytes, OA chondrocytes did not respond to cyclic compression in an α5β1-dependent manner[46], and activation of α5β1 upregulated inflammatory markers (NO, PGE2) in OA chondrocytes[47].

Heparan sulfate proteoglycan 2 (HSPG2, otherwise known as perlecan) is a second major constituent of the PCM that colocalises with type VI collagen and is thought to be the most abundant heparan sulfate proteoglycan in cartilage. *Hspg2*$^{-/-}$ mice die shortly after birth, displaying severe skeletal dysplasia[48,49]. Endochondral ossification was severely defective in *Hspg2*-deficient mice, and cartilage displayed disorganized collagen fibril organisation and glycosaminoglycan synthesis. The phenotype of these mice closely resembles that of mice with activating mutations of *Fgfr3*, indicating that dysregulated signalling prevented proper development. Much like aggrecan, HSPG2 consists of a core protein with GAG chains covalently attached. Unlike aggrecan, which functions to draw water into the joint, it is believed that the GAG side chains of HSPG2 binds growth factors, chemokines and/or matrikines, and thus may offer a repository of proteins that can be released in response to loading or damage[34,50–53].

The PCM therefore serves as a reservoir of proteins that can activate both anabolic and catabolic activities within a chondrocyte. As discussed, a number of these proteins bind to the GAG side chains of HSPG2. For example, FGF2 colocalised with HSPG2 in cartilage explants and was displaced following mechanical loading, thus inducing a signalling response[34]. Debate around FGF2

signalling in cartilage rages[54], as it can both promote cartilage repair [52,55] and cartilage catabolism[56,57]. It is likely that this is controlled through receptor expression, as FGF2 can signal through both FGFR1 and FGFR3 with signalling inducing catabolic or anabolic responses respectively, and the balance of FGFR1 and FGFR3 is dysregulated in OA.

Connective tissue growth factor, CTGF, which binds to latent TGF-β[51] and controls signalling through binding to TGF-βR3 (otherwise known as betaglycan), also colocalises with HSPG2 and Type VI collagen. Loss of CTGF is known to protect the joint from surgically-induced OA[51]. Binding of FGF18, a well-known anabolic growth factor in cartilage, to domain III of HSPG2 inhibits its mitogenic activity[58], perhaps by sequestering it from its receptor. TIMP-3, an endogenous inhibitor of cartilage-relevant proteases, such as MMP-13 and ADAMTS-5, co-localised with HSPG2 in cartilage cryosections[53]. Many of these proteins may not exclusively interact with HSPG2. For example, ADAMTS-5 is known to also bind the HS side chains of SDC4[59]. Furthermore, unlike syndecan and glypicans (see **1.2.5**) HSPG2 is not localised to the cell surface, so displacement of growth factors from HSPG2 may allow binding to cell surface HSPGs and thereby promote signalling.

Finally, another important protein found on the chondrocyte surface is LRP1. LRP1 is a scavenger receptor that mediates the endocytosis of a large number (>40) of proteins, and the activity of LRP1 is crucial for chondrocyte health, as LRP1 inhibition induces chondrocyte death[60]. Many proteins that bind to LRP1 are also known HS-binding proteins[60,61], raising the question of whether the 'ligandome' of HS and LRP1 are shared, and whether changes to HS structure

may alter LRP1 activity in chondrocytes. A comprehensive analysis of this question is required. A cartoon of some of the components discussed is shown in **Figure 1.5**.

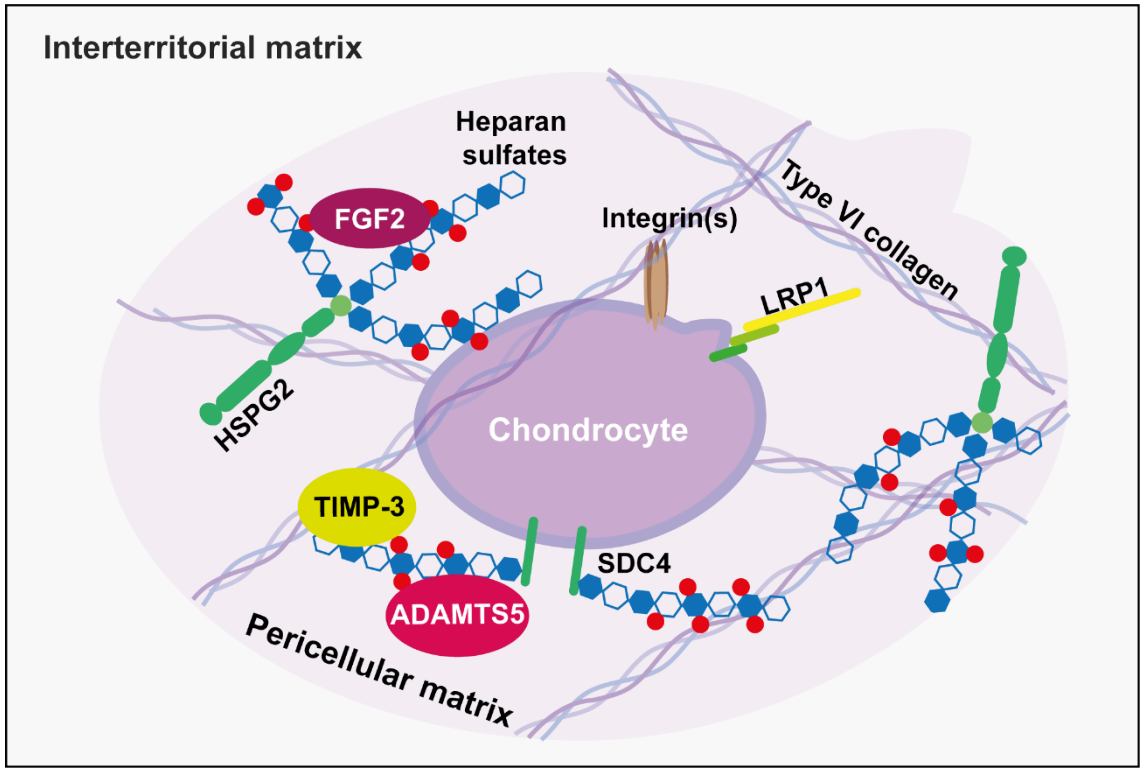

Figure 1.5 The pericellular matrix of chondrocytes is rich in growth factors, proteases, and structural proteins.

Immediately surrounded a chondrocyte is the pericellular matrix (PCM) which is rich in HSPGs and proteins that connect chondrocytes to the ECM. Type VI collagen is a major PCM component that binds to both integrins on the cell surface and the HS side chains of HSPG2. HSPG2 is one of the major HSPGs of the PCM and is believed to be a reservoir for growth factors, morphogens and cytokines. SDC4, another HSPG, is known to bind ADAMTS5, a major protease within cartilage, and binding of ADAMTS-5 to SDC4-HS side chains may present it to its endogenous inhibitor TIMP-3, another HS binding protein. Finally, LRP1, a scavenger receptor, is responsible for the endocytosis and turnover of a number of PCM components, including TIMP-3 and ADAMTS-5.

A common property that many proteins found within the PCM share, including all those discussed here, is affinity for the heparan/chondroitin sulfate side chains of proteoglycans[62–64].

1.2 Proteoglycans are core components of cartilage.

1.2.1 Chondroitin- and heparan sulfate proteoglycans are abundant in the joint.

Proteoglycans are core proteins with glycosaminoglycan chains covalently bound to serine residues on the protein backbone. Proteoglycans exist predominantly in two forms, chondroitin sulfate proteoglycans (CSPGs) and heparan sulfate proteoglycans (HSPGs). The major CSPG in cartilage, as discussed, is aggrecan. Two other CSPGs, CSPG4 and biglycan are both located on chondrocyte cell membranes and have functions in cartilage[65,66]. HSPGs also vary in localisation, some are present on the cell membrane such as syndecan 1-4 (SDC1-4) (also a CSPG), and glypican 1-6 (GPC1-6), others localise to secretory vesicles (serglycin) and finally some, such as HSPG2, agrin and COLXVIII, are exported to the extracellular matrix[67]. In cartilage, these exported HSPGs are almost exclusively observed in the pericellular matrix. Alongside loss of the CSPG aggrecan, dysregulation of HSPG core protein expression has been observed in OA[68,69]. Proteins can bind to the HS side chains of HSPGs, driven predominantly by ionic interactions between positively charged amino acids on the protein surface and negatively charged groups on HS. HS can bind a huge number of biomolecules (>600)[70], and regulate their biological activity, localisation and half-life. As such, control of HS biosynthesis must be tightly regulated.

1.2.2 Heparan sulfate structure and biosynthesis is complex

Heparan sulfates glycosaminoglycans are linear polysaccharides, containing a characteristic repeating disaccharide. HS biosynthesis consists of initial synthesis of a Ser-Xyl-Gal-Gal linker, following which chain elongation occurs as D-glucuronic acids (GlcA) and N-acetylglucosamines (GlcNAc) are sequentially added by *EXT1* and *EXT2* enzymes, connected by β(1-4) glycosidic linkages, to give the characteristic [-GlcA-GlcNAc-] disaccharide. During chain elongation, the HS chain is extensively modified by a series of modification enzymes.

The first modification step involves removal of the acetyl group from GlcNAc and addition of a sulfate group by GlcNAc N-deacetylase/N-sulfotransferases (NDST1-4). GlcA can then undergo epimerisation by GlcA C5 epimerase (GLCE) to form L-iduronic acid (IdoA). Following this, sulfate groups can be added to the second carbon of the uronic acid (GlcA or IdoA) (2-O-sulfate) by heparan sulfate 2-O-sulfotransferases (HS2ST), to the sixth carbon of the glucosamine (6-O-sulfate) by HS6ST1-3 and finally to the third carbon of the glucosamine (3-O-sulfate) by HS3ST1-5. An example schematic of sequential HS biosynthesis and domain architecture is shown in Error! Reference source not found..

The structure of HS is not dissimilar to that of chondroitin sulfate, whose polysaccharide backbone consists of N-acetylated galactosamine residues compared to the N-acetylated glucosamines of HS, to give a general repeat structure of [-GlcA-GalNAc-]. Much like HS, the glucuronic acid residue of CS can be epimerised to give a polysaccharide termed dermatan sulfate (DS) with a general repeat structure of [-IdoA-GalNAc-]. Both CS and DS can then be sulfated

on either their fourth or sixth carbon of the galactose, or the second carbon of the uronic acid. Unlike HS, CS/DS cannot have its N-acetyl group sulfated. Finally, hyaluronic acid (or hyaluronan, HA) has the same general repeat structure as HS, however HA is non-sulfated. As discussed, its main role in cartilage is to link molecules of aggrecan together and integrate these into the matrix, whilst also providing lubrication for the joint (alongside lubricin).

Importantly, none of these modification steps go to completion and many subsequent modifications require preceding modifications. For example, the epimerisation activity of GLCE (GlcA -> IdoA) is almost entirely dependent on an adjacent glucosamine being N-sulfated[71], and the activity of HS2ST has a strong preference for IdoA over GlcA[72]. Indeed, HS2ST has previously been observed to co-purify with GLCE, helping to explain the HS2ST substrate specificity[73]. The processive steps of modification result in a HS chain that has extended areas of non-modification (NA domains [-GlcA-GlcNAc-]), regions of alternating N-sulfated/N-acetylated glucosamines that can also contain 3-O and 6-O sulfate groups (NA/NS domains [-GlcA-GlcNAc-GlcA-GlcNS(6S)-]) and finally regions of N-sulfated glucosamines (NS domains [-IdoA2S-GlcNS(6S)-]). NS domains are generally believed to be highly sulfated, containing extensive IdoA, 2-O-, 6-O- and 3-O-sulfate modifications. An example schematic of sequential HS biosynthesis, and domain architecture is shown in **Figure 1.6**.

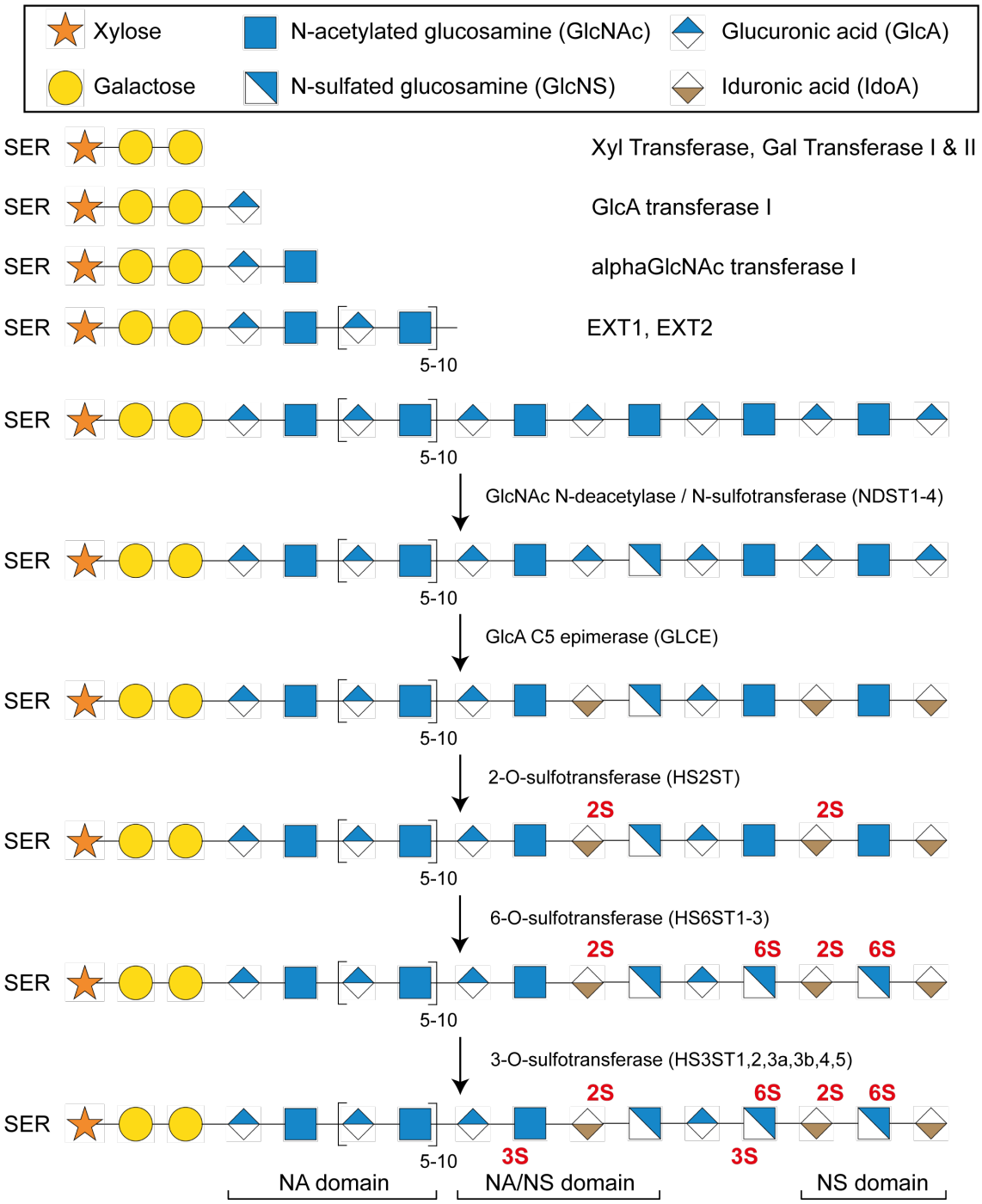

Figure 1.6 HS biosynthesis generates an information-rich polysaccharide.

HS chains are synthesised by *EXT1* and *EXT2*. N-acetyl groups are then sulfated, following by epimerisation and subsequent 2-O-, 6-O- and 3-O- sulfation by the *NDST, GLCE, HS2ST, HS6ST* and *HS3ST* enzymes respectively. None of these modifications go to completion, and therefore generate an information-rich polysaccharide. The length of the HS chains is not biologically representative. Monosaccharides are presented according to SNFG guidelines[74].

HS structure can then be 'fine-tuned' by the sulfatases 1 and 2 (SULF1 and SULF2). The SULFs are unique amongst HS modifying enzymes, as they are

secreted and modify both existing and nascent HS chains. First identified in quails[75], they are now known to exist in mice, rats, zebrafish and humans[76] and are likely to exist in all other multicellular organisms, given the presence of HS in these organisms. SULFs selectively remove 6-O-sulfate groups from HS chains, therefore making 6-O-sulfation of HS unique in that it is the only modification that can be altered at both the synthesis and post-synthesis level. Remarkably, SULF2, but not SULF1, was identified to be a CSPG[77]. The presence of a CS chain on SULF2 was found to modulate its endosulfatase activity, likely by electrostatic interference with target HS chains. Depolymerisation of the CS chain by hyaluronidase was observed, which may be a regulatory mechanism to modulate SULF2 activity. The mechanisms that regulate CS chain attachment to SULF2, but not SULF1, are currently unknown as the glycosylated residue in SULF2 is conserved in SULF1.

The final mammalian HS modifying enzymes is heparanase (not to be confused with heparitinase, HS-degrading enzymes secreted by bacteria). Heparanase is the only known endoglycosidase that is capable of HS cleavage. It specifically targets HS in regions of low sulfation, releasing polysaccharide fragments of sufficient size to still interact with ligands[78]. Heparanase has a close homolog, heparanase-2 which displays no enzymatic activity but competitively inhibits heparanase action through binding to HS-chains[79,80]. In healthy tissues, heparanase expression is low and is tightly controlled through methylation of its promoter region[81]. In freshly purified OA chondrocytes, heparanase is expressed at both the RNA and protein level, where its activity was shown to induce mRNA expression of proteases *MMP13* and *ADAMTS4* and -*5*[82].

Finally, an often-overlooked aspect of HS variation is its stereochemical conformation. IdoA (and to a minor extent GlcA) residues switch between two conformers. Often called chair and skew boat conformers, $^{1}C_{4}$ and $^{2}S_{0}$ respectively, the switch between these two conformers depends on the sulfation of IdoA and adjacent residues. Non-sulfated IdoA residues adjacent to GlcN are more likely to form $^{1}C_{4}$ conformers, due to a stabilizing hydrogen bond. IdoA2S adjacent to GlcN(6S) residues are more likely to form $^{2}S_{0}$ IdoA conformers, again due to a stabilizing hydrogen bond[83,84]. This means that NA/NS domains (which contain fewer 2-O-sulfated IdoA and 6-O-sulfated GlcN residues) are more likely to have a higher proportion of $^{1}C_{4}$ IdoA, whereas NS domains contain more $^{2}S_{0}$ IdoA conformers. Rather than being a quirk of chemistry, these conformers can drastically alter the conformation of an HS chain, and therefore bioavailability of its negatively charged groups and its biological role[85].

Due to the extensive variation in its modifications, HS is information-rich. Much like DNA, which encodes chemical information through its negatively charged bases, HS encodes information through its negatively charged groups (hydroxyl, carbonyl, ring oxygens and sulfates) through which it binds proteins. The main contributors to the 'information' encoded by HS are 1) its sulfate groups 2) carboxyl and carbonyl oxygens and 3) the conformation of the polysaccharide, given the electrostatic repulsion between its negatively charged groups and the conformation of the uronic acid residues. It is the combination of these factors that promotes HS binding to positively charged lysine and arginine residues on a protein surface. Due to the similarity in structure of CS/DS with HS, some HS-binding proteins (HSBPs) also bind CS with appreciable affinity (e.g. FGF7 and

10)[86] although many HSBPs show high selectivity for HS over CS/DS, such as antithrombin III-HS[87].

1.2.3 Heparan sulfate can promote protein-receptor interactions

As discussed, glycosaminoglycans bind proteins through their negatively charged groups. HS can control the diffusion[88], localisation[89], presentation and the degradation of proteins[90]. Protein binding to HS has been extensively studied, with numerous crystal structures of protein-HS and protein-HS-receptor complexes being solved (such as FGF2 and follistatin)[91,92]. However, even in the most well-studied systems debate endures about the exact effect HS has on its ligands. For example, with FGF2, crystal structures show heparan sulfate is involved in binding directly to FGF2 and to FGFR1c, making it a critical component of ternary receptor complex formation[92], however other evidence suggests the critical function of HS is to stabilise FGF2 against denaturation (or proteolysis)[93]. Furthermore, even the precise stoichiometry of HS within the receptor complex is debated, as crystal structures showing a 2:2:2 stoichiometry of FGF2:HS:FGFR1 (symmetric) and 2:1:2 (asymmetric) stoichiometry have been resolved by the same research group[92,94]. In the symmetric model, 1:1:1 stoichiometric complexes are formed that dimerize to form an active signalling complex, and in the asymmetric model 1:1 FGF:FGFR complexes form that further associate through interaction with HS. The two models diverge drastically in their view of the role of HS: in the symmetric model the sugar is only one of the components enabling dimerization as dimerization can still occur without HS due to the extensive protein interfaces formed, whereas in the asymmetric model

formation of the signalling complex requires HS as there are few protein:protein interactions between the respective 1:1 complexes.

Whilst both complexes have been identified in mass spectromic preparations[95] the asymmetric model is inconsistent with available biochemical data. For example, sulfated glycosaminoglycan-deficient fibroblasts do have FGF2-stimulated receptor activation (albiet transient)[96], which suggests signalling can occur without HS and so supports the symmetric model. Furthermore, cell proliferation was stimulated by addition of a heparin tetrasaccharide[93] that is too short to bridge the two 1:1 FGF:FGFR complexes, also supporting the symmetric model. Site-directed mutagenesis of the FGF2 secondary receptor binding site attenuated signalling due to reduced dimerization[97], and thermally stabilised mutants of FGF2 promoted increased ERK phosphorylation compared to wild-type FGF2[93]. This indicates that HS does serve role in thermal stabilization of FGF2 and does not support the role for HS binding to preformed 1:1 FGF:FGFR complexes[93], thus, again favouring the symmetrical model. This highlights the complexity of researching heparan sulfate, and why extensive structural biology and biochemical studies are required to properly elucidate mechanisms behind the signalling of even a single protein when HS is involved.

1.2.4 FGFs and signalling in cartilage

As discussed, HS has a critical role in regulating FGF signalling, including within the joint. Phylogenetic analysis of FGFs divides FGF1 - 23 into 7 families: the FGF1, FGF4, FGF7, FGF8, FGF9, FGF11 and FGF18 subfamilies. Most FGFs (3-8, 10, 17-19, 21 and 23) possess N-terminal signal peptides and are thus

secreted, however FGF9, 16, and 20 are secreted despite lacking a signal peptide, and FGF1 and -2 also lack signal peptides but are nevertheless observed in the extracellular space. FGF22 remains attached to the cell surface, and FGF11-14 remain intracellular and function in a receptor-independent manner. Intriguingly, FGF2 has both high- (24, 23 and 22 kDa) and low-molecular weight forms (18 kDa) that have been observed to localise predominantly to either the nucleus or cytoplasmic/membrane-associated regions respectively. It is interesting to note that functionally both the low- and high-molecular weight forms can exert similar effects. That is, low-molecular weight FGF2 can signal in the nucleus similar to high-molecular weight FGF2, and high-molecular weight FGF2 can signal through FGFRs with HS as a cofactor similar to low-molecular weight FGF2[98,99]. Therefore, the functional differences between the two are determined by their targeting to different cellular compartments (either the nucleus or the extracellular space) and not by intrinsic differences in their binding specificities.

Differential expression of these FGFs is involved in bone formation, as high-molecular weight *FGF2* is expressed by proliferating chondrocytes of epiphyseal growth plate cartilage, whereas low-molecular weight *FGF2* is expressed throughout the growth plate by resting, proliferating and hypertrophic chondrocytes[100]. In the developing skeleton, FGF9 and 18 are predominantly involved in bone growth. Whereas mice lacking *Fgf2* have decreased bone mass but have phenotypically and functionally normal growth plates, *Fgf9* null mice exhibit a shortened appendicular skeleton, and *Fgf18*-null mice have decreased chondrocyte proliferation[101–103].

FGFs signal almost exclusively through FGF receptors, which are receptor tyrosine kinases that contain an FGF- and HS-binding domain, a transmembrane region and two intracellular tyrosine kinase domains. Binding of FGFs to FGFRs induces receptor dimerization and autophosphorylation of the tyrosine kinase domains, activating a cytoplasmic signalling cascade. Four functional FGFR genes have been identified (*FGFR1-4)* with each having preferential affinity for a particular FGF ligand. FGFR isoforms contribute to specificity within a signalling system, and contribute to development of tissues from endothelial and mesenchymal lineages. FGFRb splice variants are mainly observed in endothelial tissues but bind to FGFs from mesenchymal lineage tissues, whereas FGFRc variants are observed in mesenchymal tissues and bind to FGFs from both endothelial and mesenchymal tissues. FGFRc isoforms are the predominant variants observed in cartilage, specifically FGFR1 and FGFR3c[104,105], which is expected given the mesenchymal origin of the tissue.

In the developing skeleton, there is a level of redundancy in expression of FGFRs. *Fgfr1* and *Fgfr2* are co-expressed in the developing distal limb bud of mice, and inactivation of either results in a milder skeletal phenotype[106] than inactivation of both[107]. FGFR1/2-induced ERK signalling negatively regulates Wnt-induced methylation of the *Sox9* promoter, thereby promoting Sox9 expression, which thus induces FGFR3 expression. As *Fgfr3* expression increases *Fgfr2* expression decreases during differentiation, resulting in a stable ratio of *Fgfr1* and *Fgfr3* expression. This ratio is preserved through bone growth and cartilage development and can be subsequently observed in articular cartilage of adults. Activation of FGFR1/2 is therefore crucial for beginning the pathways of endochondral ossification described above. As chondrocytes hypertrophy during

endochondral ossification, *Fgfr1* expression increases and *Fgfr3* expression decreases, promoting mineralization. In this manner the temporal and spatial regulation of FGFR1/3 expression during chondrocyte differentiation controls endochondral bone growth and therefore cartilage formation. The homeostatic ratio of these receptors is also dysregulated in osteoarthritic cartilage, further highlighting the importance of a delicate balance in FGFR activation in cartilage[105,108].

Finally, as discussed above (**1.2.3**) HS is involved in regulating the affinity of some FGFs for FGFRs. HS is involved in the recruitment of most FGFs to their respective FGFR, although the extent and manner in which it is involved is still debated. However, some FGFs have little to no affinity for HS and instead are recruited to FGFRs with a cofactor. These are known as hormonal FGFs and very little is known about their role in cartilage.

FGF23, derived from bone, forms a trimeric signalling complex with α-klotho and FGFRs, independent of HS, to mediate its physiological functions. Recently, increased cartilage matrix stiffness was linked to a reduction in expression of α-klotho[109], highlighting the neglected importance of non-FGF2 and FGF18 FGFs in regulating cartilage homeostasis. Independent of α-klotho, FGF23 can drive *MMP13* expression[110], suggesting that reductions in α-klotho expression in aged cartilage may promote a catabolic environment by promoting an α-klotho-independent FGF23 signalling mode. Indeed, FGF23 has been shown to drive chondrocyte hypertrophy by upregulation of *RUNX2* expression[111]. Further work is required to understand the extent to which FGF23 activity is controlled by klotho in cartilage, or what role it may play in maintaining homeostasis of adult joints.

Other hormonal FGFs, such as FGF19 and 21 have also been detected in the joint, however research around the role of these proteins in cartilage is severely lacking.

As with the hormonal FGFs, intracellular FGFs belonging to the FGF11 subfamily (FGF11-14) are also remarkably understudied in chondrocytes. FGF12 and -14 are known to bind to voltage-gated sodium channels, e.g. FGF12 binds $Na_V1.5$, however the role of FGF12 in chondrocyte biology is unknown. Research suggests a potential involvement of these FGFs in OA pathogenesis, as the expression of sodium channels on the surface of chondrocytes is increased in OA, and deletion of $Na_V1.7$, which interacts with FGF13 to promote heat nocioception[112], protects mice from surgically-induced OA[113].

1.2.5 HS binding can control protein diffusion.

Besides promoting receptor-complex formation, HS has also been implicated in the control of diffusion gradients. HS has been shown to modulate protein diffusion using FGF2 conjugated to a gold nanoparticle, with FGF2 observed 'hopping' between high affinity to high affinity binding sites[114], and using Halo-tagging of FGF1,2 and 6 (each with different affinity for HS) were observed diffusing into photobleached HS-rich extracellular matrix at different rates[115]. HS-controlled diffusion of Indian hedgehog (Ihh) during endochondral ossification was also elegantly shown using *Ext1*$^{Gt/Gt}$ mice, which have reduced HS levels compared to control littermates. E15.5 *Ext1*$^{Gt/Gt}$ mice showed reduced bone growth and increased Ihh domain expression. Binding of Ihh to HS was therefore

proposed to inhibit its diffusion, negatively regulating its activity, and thus inhibiting bone growth[89].

1.2.6 Heparan sulfate binding can control presentation to proteases or receptors

The ability of HS to prevent proteolysis of bound ligands is well-studied for chemokines, where proteolysis of even a single amino acid can alter their function. For example, stromal cell-derived factor-1 (SDF-1) binds to HS and is protected from proteolysis by CD26/dipeptidyl peptidase IV[116]. Alternatively, HS can prevent proteolysis by promoting oligomerisation, as is observed with CXCL12[117].

HS can also block endocytosis of its ligands and increase their interactions with other HS ligands. For example, ADAMTS-5 is a known HS-binding protein, and exogenous heparin inhibits its LRP-1-mediated endocytosis[118], as it also does for TIMP-3, an endogenous inhibitor of ADAMTS-5[53]. Confoundingly however, binding of TIMP-3 to HS increased TIMP-3 affinity for ADAMTS-5 by 1000-fold[53]. Binding of ADAMTS-5 to HS therefore acts both to promote accumulation of extracellular ADAMTS-5 and to promote association with its endogenous inhibitor. Further work must be done to understand the role of endogenous HS in regulating ADAMTS-5 activity and in ADAMTS-5-TIMP-3 interactions.

Finally, HS can prevent protein-receptor interactions. Wnt8 binds strongly to heparan sulfate in a 6-O-sulfate-dependent manner, and modulation of which can

prevent protein-receptor interactions, as shown in by increased Wnt activity in Frizzled-3-expressing wild-type compared to HS-deficient CHO cells[75].

A summary of HS effects on its ligands is shown in **Figure 1.7.**

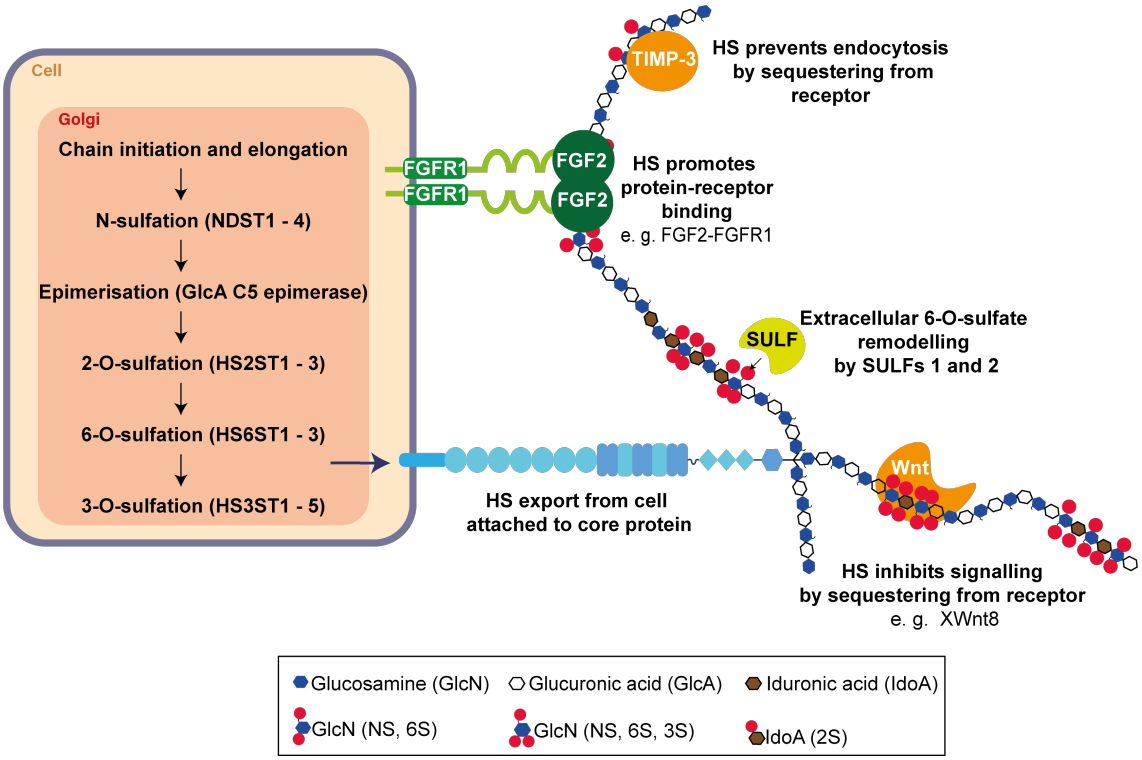

Figure 1.7 Heparan sulfate binds proteins and controls their activity.

Heparan sulfate is synthesised in the Golgi apparatus, attached to core proteins, and exported out of the cell. Outside the cell, HS 6-O-sulfate groups can be removed by the endosulfatases SULF1 and SULF2. HS can influence the activity of its protein ligands by sequestering them from endocytic receptors, promoting protein-receptor interactions, or inhibiting signalling by sequestering from receptors.

1.2.7 Cells shed HSPGs to control activity.

The activity of syndecans and glypicans, which are transmembrane HSPGs, can be controlled by shedding of their ectodomains from the cell surface.

Glypicans are retained on the cell surface by a GPI-anchor. GPI-anchored proteins can be shed by proteolysis of the core protein or by cleavage of the GPI-anchor by GPIases[119]. Whilst expressed at the RNA level, glypicans are not thought to be major HSPGs in chondrocytes[120], however expression of glypican-1 is increased in OA[68,121,122]

Each of the four syndecans can be rapidly shed by proteolytic cleavage of the core protein. SDC shedding can be activated by phorbol-12-myristate-13-acetate activation of protein kinase C, thrombin and epidermal growth factor receptors, and inhibited by TIMP-3, but not TIMP-1 or -2 nor inhibitors of serine or cysteine proteases[123]. This suggests shedding is mediated by either an ADAM or ADAMTS family protease or metalloprotease, as these are selectively sensitive to TIMP-3 inhibition. The shedding of syndecans is likely to be disease-relevant in cartilage, as loss of SDC4 is protective against surgically-induced OA[59] and correlates with disease severity[124]. *Sdc4*$^{-/-}$ mice had reduced Mankin scores following surgically induced OA and reduced aggrecanase activity[59]. ADAMTS-5 was shown to bind the HS chains of SDC4, therefore shedding of SDC4 ectodomains may promote ADAMTS-5 diffusion into the interterritorial matrix. Increased shedding of SDC4 is observed as OA progresses, with SDC4 concentrations increased in the synovial fluid of patient samples with Kellgran-Lawrence (KL) scores 3 and 4 compared to KL1-2[124].

Finally, GAG-protein binding is regulated in an unusual way in cartilage. As discussed in **1.1.2**, cartilage has high osmotic charge due to the highly-negatively charged GAG chains of aggrecan. In an elegant study, Keppie *et al.*[50] showed that compression of cartilage released sodium, most likely from aggrecan GAG

chains. Intriguingly, this sodium release was higher in the superficial zone of cartilage compared to the deeper zones, and the authors concluded this was due to decreased stiffness in the superficial compared to the deep zone. It was proposed that compression of cartilage and subsequent sodium release competes off HS-bound proteins and so promotes their signalling. As aggrecan is degraded in OA, this mechanism is lost and released of matrix-bound growth factors is reduced. Interestingly, there was more release of HS-bound growth factors in early OA samples than in healthy tissue, suggesting this mechanism may support cartilage repair in early OA by favouring release of pro-anabolic growth factors.

1.2.8 HS research faces many technical challenges

Due to their high structural heterogeneity, there are numerous technical challenges in studying HS and glycosaminoglycans. Firstly, the purification of HS from tissues is a distinctly non-trivial matter, highlighted by the pharmaceutical heparin contamination crisis[125]. This is largely due to the high structural heterogeneity of HS and glycosaminoglycans. Glycans encode exponentially more information than the genome or the proteome. For example, for an octosaccharide (dp 4) there are theoretically 4096 possible structures, although the actual number is likely to be significantly lower due to structural constraints. As the length of HS chains generally vary between 50-200 disaccharides (dp 50 – 200), there is a large 3-dimensional conformational space that can be occupied by HS. As conformation of HS is critically linked to its activity, prioritisation of methods that can measure HS confirmation in tissues would be hugely informative for research. Purification of HS from tissues is difficult due to its

negative charge, and purification procedures must be undertaken with care as other negatively charged macromolecules, such as DNA/RNA can be co-purified. Purification by size is also complicated by the heterogeneity of HS lengths.

Structural analysis of HS sulfation offers information as to how HS biosynthesis changes with age or in disease, but the hydrophilic nature of HS along with their lack of an effective endogenous chromophore, means that direct analysis of HS is difficult. This can be partially overcome by conjugating the reducing-end with a radio- or hydrophilic tag to aid detection. Alternatively, enzymatic degradation utilising heparitinases cleaves HS molecules between the C4 and C5 carbon of uronic acids introducing an unsaturated double bond that can be detected at a UV wavelength of 232 nm. The cleavage by heparitinases further simplifies detection by producing disaccharides, drastically reducing the number of species that are detected. Detection of HS using UV is complicated as contaminating CS/DS structures will also be detected in samples. This can be resolved by the introduction of a fluorescent tag, such as BODIPY FL hydrazide[126], which both improves sensitivity (to femtomolar ranges) and is beneficial as it has a fluorescence emission wavelength close to that of commercially available fluorescence detectors. Alternatively, mass spectrometry can be used for structural characterization. The negative charge of HS makes ionization more complex. This can be overcome with the use of a positively charged peptide that binds to HS, thus 'neutralizing' the negative charge and promoting ionization. This technique was used to identify the heparin decasaccharide that binds to antithrombin III[127]. ESI-MS has advantages over MALDI-TOF for structural analysis, as it enables direct mass calculation of HS fragments, with improved peak retention time and shape[128]. Highlighted by Puvirajesinghe and Turnbull[129],

these structural analytical techniques have technical limitations that make comparative analysis difficult: 1) It is difficult to quantify the abundance of disaccharides for which standards are unavailable (e.g. 3-O-sulfated HS disaccharides), 2) The high dimensionality (such as sulfate loss, disaccharide retention, signal intensity) of the data results in noisy spectra that must be processed potentially inducing data loss and 3) Simultaneous and routine analysis of multiple samples provides vast quantities of data which must be processed. Together, this makes for a time-consuming process that is not widely commercially available.

Functional analyses of HS are thus undertaken in a systematic manner. Ablation of HS using enzymes (e.g. heparanases/heparitinases), inhibiting HS synthesis by addition of sodium chlorate[130] to cell cultures, or inhibiting HS binding to ligands using the small molecule surfen[131] , can reveal insights into HS control of protein activity (such as signalling) with appropriate downstream assays. Exogenous heparins can be utilised to further study the role of endogenous HS through their addition to cell cultures. For example, addition of heparin to HS-deficient CHO cells restored fibronectin fibril formation to the level seen in wild-type CHO cells[132]. Alternatively binding of proteins to HS can be measured using techniques such as surface plasma resonance (SPR)[133], differential scanning fluorimetry (DSF)[133] or heparin affinity chromatography[134]. The density of GAG chains in these analyses is unlikely to replicate the biological density of GAG chains, and this must be taken into account when drawing conclusions from the data, but these approaches have significant advantages as GAG concentrations, chain length and chain sulfation can be strictly controlled. The use of heparin affinity chromatography allows tissue-scale purification of HS-binding proteins.

This has been used to identify novel HS-binding proteins that selectively bind particular sulfate groups using chromatography resins derivatized with chemically-modified heparin oligosaccharides followed by quantitative mass spectrometry[135]. A final approach for investigating HS is use of murine (or cell line) knockout models. A non-exhaustive list of the phenotypes exhibited by HS-mutant mice is shown in **Table 1.1**. Several different methods to target HS biosynthesis in mice are required, due to the frequency of embryonically lethal phenotypes, such as those seen in *Ext* knockout lines. Therefore, tissue-specific or inducible knockout strategies are commonly employed, such as the Cre-lox method, which enables tissue-specific investigation of HS functions.

Table 1.1 HS mutant mice show genetic and experimentally dependent phenotypes

Gene knockout	Phenotype	Murine death	Reference
Ext1$^{-/-}$	Embryonic lethal	E6.25	[136]
Col2-Cre;Ext1$^{(f/f)}$	Reduced bone growth and chondrocyte hypertrophy	N/A	[137]
Ext1$^{gt/gt}$	Embryonic lethal	E6.25	[89]
Ndst1$^{-/-}$	Embryonic lethal, chondrogenic defects and neural or immunological defects	E14.5-E16.5	[138–140]
Glce$^{-/-}$	Chondrogenic and immunological defects	N/A	[141,142]
Hs2st$^{gt/gt}$ *or* $^{-/-}$	Neonatal lethal, or neurological defects	Neonatal	[143,144]
Hs6st$^{-/-}$	Embryonic lethal, or severe neurological defects	E16.5 - Perinatal	[145]
Hs3st1$^{-/-}$	Genetic background lethality, reduced coagulation, increased inflammation	Genetic background lethality	[146,147]
Sulf1 & 2$^{-/-}$	Embryonic lethality, skeletal defects, neurological defects	E15-5 – birth, post-natal	[148–151]

1.3 Heparan sulfate in development and disease

1.3.1 Heparan sulfate is crucial for proper development.

The importance of specific HS sulfation motifs in development has been highlighted across several tissues and developmental processes. The importance of HS, as discussed, lays in its ability to control growth factor signalling of bound ligands. In the lung, for example, HS controls the activity of several growth factors and morphogens during development. Heparinase III treatment of lung explants reduced branching morphogenesis which could be overcome by addition of exogenous FGF10, but not when lung explants were pre-treated with sodium chlorate[152]. Given the specificity of heparinase III, this indicates that FGF10 binds to HS with lower affinity for 6-O-sulfate groups than 3-O-, 2-O-, or N-sulfated HS. *Ndst1*$^{-/-}$ mice display defective differentiation of lung cells and have increased cell proliferation compared to their wild-type littermates. This was concluded to be due to increased BMP signalling, as Noggin (a BMP antagonist) rescued the phenotype[153]. Finally, mice deficient in heparin-binding isoforms of VEGF (VEGF$^{164/188}$) exhibited impaired peripheral lung vascular development, with a reduced number of air-blood barriers and delayed airspace formation[154].

In cardiac development, loss of function of B3GAT3, one of the enzymes involved in the initial synthesis of the GAG tetrasaccharide linker, resulted in bicuspid aortic valve and aortic root dilation[155]. *Ndst1*$^{-/-}$ mice displayed increased ventricular and arterial developmental defects caused by reduced FGF8 signalling[156]. Finally, Gpc3 loss of function mutations in mice (representative of Simpson-Golabi-Behmel syndrome) caused high incidences of congenital

cardiac malformations, such as ventricular septal defects and coronary artery fistulas[157].

Bone and cartilage development is also highly dependent upon HS-orchestrated signalling. As reviewed by Jochmann *et al.*[158] mesenchymal cells form condensates whereby these cells become chondrocytes. Chondrocytes secrete cartilage components and, eventually, stop proliferating, becoming hypertrophic and secreting type X collagen. These hypertrophic chondrocytes direct mineralization of the surrounding matrix, attract blood vessels through VEGF secretion, and attract chondroclasts. Hypertrophic chondrocytes direct adjacent perichondral cells to become osteoblasts which form a collar of bone around the cartilage. After hypertrophic chondrocyte cell death, osteoblasts migrate into the cartilage matrix and form bone. Many of the growth factors identified to be important for growth plate function are known HS-binding proteins. For example, Ihh, expressed by prehypertrophic chondrocytes, travels past a zone of proliferating chondrocytes to activate expression of parathyroid related hormone (Pthlh)[159]. PthIh is a positive regulator of bone growth as it prevents chondrocyte hypertrophy. The importance of HS for bone and cartilage development was clearly demonstrated by Koziel *et al.*[89] who showed that *Ext1* deficient mice were both small in stature and displayed joint fusion with delayed (albeit variable) hypertrophic differentiation that was linked to defective HS-control of Ihh signalling. Further work by Dierker *et al.*[142] found that *Glce*$^{-/-}$ deficient mice also had increased Ihh signalling, characterised by increased proliferating chondrocytes and a delay in hypertrophic chondrocyte differentiation. Therefore, control of Ihh diffusion is likely dependent upon IdoA residues and 2-O-sulfation of these residues.

Prx1-Cre;Ext1$^{fl/fl}$ mice have conditional ablation of *Ext1* expression in their limb bud mesenchyme starting at E9.5. By E16.5 they displayed smaller fore- and hind limbs, joint fusion, and defects in digit patterning[160]. This was accompanied by abnormal chondrocyte condensation and accelerated ossification due to increased BMP-induced-Smad1/5/8 phosphorylation. This may be due to differential regulation of BMP signalling, such as receptor binding and sequestration of BMP proteins, as these results agree with results from a Gdf5-Cre;*Ext1* knockout mouse model, which also had increased BMP signalling and ectopic cartilage formation, alongside joint fusions and abnormal digit development[161,162]. In agreement with this overall data on the importance of EXT1 for bone formation, post-natal *Ext1* deficient mice had reduced body length, disorganised growth plate architecture, increased chondrocyte hypertrophy, exostosis-like outgrowths and increased HSPG2 staining in chondrocytes close to the growth plate reserve zone[137]. Loss of HS biosynthesis is therefore highly detrimental to endochondral ossification.

1.3.2 Heparan sulfate has a complex role in orchestrating the cancerous phenotype.

Given the importance of HS in development, it is unsurprising that HS is dysregulated in a wide variety of diseases. Dysregulation of nearly every HS biosynthesis gene has been observed across cancer types as mutations of HS biosynthesis genes can be either protective or pathogenic. For example, *NDST*, *GLCE* and *HS3ST2* have been shown to have tumour suppressive functions. 54% of colorectal carcinomas had significantly reduced expression of *NDST4*

compared with matched, normal, mucosae[163], indicating a tumour suppressive role for NDST4. In contrast, mice with endothelial deletion of NDST1 (TekCre^{+};Ndst1$^{fl/fl}$) had reduced tumour growth compared to (Tek-Cre^{-};Ndst1$^{fl/fl}$) controls, indicating a tumour promoting effect for endothelial NDST1. This correlated with reduced response to FGF2 and VEGF164[164]. Expression of C5-epimerase, *GLCE*, was reduced in breast cancer MCF7 cells compared to healthy human breast tissue and re-expression of *GLCE* inhibited MCF7 proliferation due to increased expression of the tumour suppressor genes p53 and BRCA1[165]. *HS3ST2* promoter methylation was found to be increased in six lung cancer cell lines and induction of *HS3ST2* expression inhibited cell migration, invasion, and proliferation in H460 and H23 cells. Thus, lung cancer patients with hypermethylation of *HS3ST2* had poorer prognosis than patients without [166]. Meanwhile, 2-O- and 6-O-sulfation have also been implicated in cancer pathogenesis. HS6ST2 expression was increased in colorectal cancer tissues[167] and positively correlated with proliferation and invasion of prostate cancer cells whilst siRNA knockdown of *HS2ST* significantly reduced invasion in *in vitro* assays [168]. Given the examples above, it is clear that it is difficult to predict how a mutation in HS biosynthesis genes will impact cancer progression, as activating and silencing mutations can both improve or worsen cancer prognoses. It most likely depends on the tissue-specific pattern of growth factor expression and how these proteins interact with the mutant HS-structures.

1.3.3 Heparan sulfate is protective for pancreatic β-cell survival and diabetic phenotype.

Current research indicates that HS plays a protective role in the pathogenesis of both type 1 diabetes and type 2 diabetes mellitus. In mice, HS is highly expressed by pancreatic islet β-cells. Heparitinase-induced loss of HS reduced glucose-induced insulin secretion and expression of genes involved in insulin secretion. β-cell-specific deletion of *Extl3* resulted in abnormal islet morphology and glucose intolerance as well as β-cell death[169]. *In vivo* autoimmune destruction of islets in type 1 diabetic-susceptible mice was associated with secretion of heparanse by infiltrated mononuclear cells. Subsequent development of type 1 diabetes could be inhibited by treatment with a chemical inhibitor of heparanase, PI-88[170].

In type 2 diabetes mellitus, ER-stress of both young and aged diabetic (db/db) and insulin-deficient mice preceded loss of HSPG and HS. *In vitro* replacement of HS with exogenous heparin significantly increased survival of wild type and db/db mice β-cells[171]. In accordance with these murine studies, three SNPs in the EXT2 gene have been identified as risk-loci for human type 2 diabetes mellitus[172], and there is increased heparanase protein in the plasma and urine of type 2 diabetes mellitus patients compared to healthy controls[172]. Therefore, loss of HS on the surface of β-cells promotes diabetes pathogenesis.

1.3.4 Heparan sulfate sulfation increases in idiopathic pulmonary fibrosis.

Fibrosis is characterized by accumulation of extracellular matrix components, usually caused by aberrant responses to injury. Idiopathic pulmonary fibrosis (IPF) is thought to be caused by recurrent epithelial cell injury that leads to aberrant repair processes that leads to a loss of dysregulate myofibroblasts.

Altered expression of both HSPG core proteins and HS biosynthesis proteins are implicated in fibrotic progression.

Amongst core proteins, much research has focused in SDC4, which was found to protect against fibrosis in mice, as *Sdc4*$^{-/-}$ mice have increased fibrotic injury compared with *Sdc4*$^{+/+}$ mice. CXCL10, an HS-binding IFN-γ inducible protein, was found to bind directly to syndecan-4 and inhibit fibrotic progression. This inhibitory activity was lost in *Sdc4*$^{-/-}$ mice[173]. Furthermore, oxidative injury of lung tissue induced syndecan-1 shedding, which in turn recruited neutrophils and increased reactive oxygen species expression and TGF-β1 release from fibroblasts, promoting further fibrosis[174].

There was increased deposition of GAGs in IPF tissues, including increased sulfation of CS/DS and HS. In particular, N- and 6-O-sulfation of HS was dramatically increased, and the highly sulfated forms of HS localised to fibrotic border regions, potentially implicating this highly sulfated form of HS in disease progression[175]. The elevated 6-O-sulfation of HS was accompanied by increased expression of both the HS 6-O-sulfotransferases[176] and 6-O-endosulfatases[177] in IPF. Functionally, the increased HS 6-O-sulfation was found to positively regulate TGF-β1 signalling which in turn induced SULF2 expression. This negative feedback mechanism may reflect a response by diseased tissue to return to a homeostatic HS structure.

1.3.5 Heparan sulfate in bone and cartilage disorders

One of the most well-known HS-dependent bone disorders involves loss of heterozygosity mutations in the *EXT1* gene in growth plate chondrocytes causing multiple hereditary exosotoses. There is some debate as to the extent of *EXT2* involvement, however most studies identify *EXT1* mutations as the primary risk factor[178]. This was further confirmed with the development of *Ext1*$^{+/-}$ and *Ext2*$^{+/-}$ mice, as *Ext2*$^{+/-}$ mice did not develop exostoses, whereas *Ext1*$^{+/-}$ mice did[179,180]. In human disease, these loss of heterozygosity mutations, followed by somatic second-hit mutations, cause cells to cease synthesis of functional HS. The loss of HS synthesis causes abnormal signalling, perhaps primarily by Ihh, in the chondrocytes of the external columns of the proliferative chondrocyte region of long bones. This causes the cells to lose polarity and so change the direction in which they proliferate, generating bony exostoses.

In mice, mutations of core protein genes and HS modification genes are all implicated in bone and cartilage disorders. *Ndst1*$^{-/-}$ mutant mice show impaired skull development alongside delayed mineralization of both vertebrae and long bones which was linked to reduced N-sulfation inhibiting FGF2 and sonic hedgehog signalling *in vitro* [181]. Likewise, Grobe *et al*.[182] concluded that impaired Shh and FGF signalling in *Ndst1*$^{-/-}$ mice caused forebrain and forebrain-derived structural defects[183]. However, some *Ndst1*$^{-/-}$ null mice display a mild phenotype of dysfunctional condylar growth plates and thicker superficial and polymorphic cell zones, due to an increased zone of Ihh activity[184]. It may be, given the mild phenotype, that there is compensatory activity of the other NDST isoforms in this strain, or that Hh signalling is regulated by HS in a tissue-dependent manner depending perhaps on domain, inhibitor, and activator expressions.

Alongside being required for proper bone formation heparan sulfate modulates cartilage homeostasis. Mice lacking *Hspg2* or *Sdc4* showed reduced OA development following surgically-induced OA[59,185] indicating a pro-catabolic role for these core proteins in cartilage. Furthermore, *Hspg2* expression was required for osteophyte formation in a surgical OA model, as it increased cell proliferation of osteophyte forming chondrocytes[186]. Studies on *Ext1* knockout mice have generated conflicting data on cartilage, with both unaltered[160] and increased[187] SMAD1/5/8 phosphorylation reported, with the latter leading to increased chondrocyte hypertrophy compared to control littermates. Gerstner *et al.*[188] showed increased GAG synthesis by chondrocytes in *Ext1*-deficient mice that was linked to increased BMP4/6-induced SMAD1/5/8 phosphorylation, agreeing with a role for HS in inhibiting BMP activity within the joint. Ultimately, the role of *Ext1* in cartilage is not wholly clear, and differences in experimental outcomes may be down to differences in the genetic backgrounds of murine models or experimental set ups.

Ndst1$^{+/-}$ mice show increased cartilage thickness compared to *Ndst1*$^{+/+}$ mice up to 18 months of age, which was accompanied by reduced progression of surgically-induced OA[189]. As N-sulfation is a prerequisite for subsequent modifications (see **1.2.2**), this raised the question whether the observed phenotype was specifically due to changes in N-sulfation. *Hs2st1*$^{-/-}$ mice showed reduced HS sulfation at embryonic day 15.5 show, driven primarily by reductions in 2-O- and 6-O-sulfation, and increased CS synthesis[190] .

A series of studies have shown that SULFs are protective in cartilage. First, *Sulf* expression was found to be upregulated in human OA cartilage and increased as

mice aged[191]. Subsequent studies in *Sulf1*$^{-/-}$ and *Sulf2*$^{-/-}$ mice showed greater degeneration of articular cartilage at 6 months of age and following surgically-induced OA. This was accompanied by reduced mRNA expression of *Col2a1* and *Acan (aggrecan),* and increased *Adamts5* expression[151]. The protective role of SULFs in cartilage was supported by a subsequent study investigating intervertebral disk cartilage, which identified increased expression of both SULF-1 and -2 in degenerated human intervertebral disks, with *Sulf1*$^{-/-}$ mice showing more severe IVD pathology than wild-type mice[150].

In a comprehensive analysis of HS biosynthesis enzymes, *Chanalaris et al.*[68] identified 15 HS biosynthesis enzymes that were significantly dysregulated in cartilage from age- and sex-matched healthy and OA cartilage samples. Of the 3 HS modifications (N-, 2-O-, and 6-O- sulfation) investigated, only 6-O-sulfation was significantly increased in OA samples. This was driven by increased expression of *HS6ST1,* as there was no significant change in expression of either *HS6ST2* or *-3.* Furthermore, in chondrosarcomas, malignant cartilage-forming tumours, there is increased expression of the *HS6ST* enzymes, alongside increased 6-O-sulfation of HS, that correlated with disease severity[192]. Taken together, these studies indicate that 6-O-sulfation is likely to be deleterious for cartilage homeostasis.

1.4 Heparan sulfate 6-O-sulfation is critical for development and disease.

One of the ways in which cells control growth factor signalling is through balancing HS 6-O-sulfation by expression of both *HS6ST1-3* and *SULF1/2,* with

6-O-sulfation being the only HS modification that is altered in the extracellular environment after HS synthesis. By controlling 6-O-sulfation, tissues can carefully orchestrate signalling cascades that direct tissues down correct developmental lineages, so it is unsurprising that 6-O-sulfation is regulated in development and dysregulated in many diseases. Here, I will briefly go over how 6-O-sulfation regulates developmental processes, and how changes in this structural motif can promote or inhibit disease progression.

1.4.1 HS 6-O-sulfation in development

As described **1.3**, the control of growth factor signalling by heparan sulfate is crucial for development of several organs. This is highlighted by the reduced viability of *Hs6st1*$^{-/-}$ mice which show high pre- and postnatal mortality[145]. This is likely explained by an inability to orchestrate signalling cascades required for proper development. For example, HS purified from murine neuroepithelia showed a shift to more highly 2-O- and 6-O-sulfated HS from days E10 to E12. This increased HS affinity for FGF1, whilst reducing the affinity for FGF2[193], likely representing the temporal demands for growth factor signalling in embryonic brain development. SULF deficiency resulted in neurite outgrowth defects [194] and a reduction in cerebellar cell survival *in vitro*[195], whilst *Sulf1/2* double knockout mice had glomerular abnormalities linked to changes in VEGF, PDGF-B and TGF-β signalling[196]. In the heart, *Sulf1* knockdown resulted in severe vascular patterning and maturation defects such as arterial dysmorphogenesis, leading to distal aortal occlusion, linked to a reduction in VEGFA signalling[197]. Finally, BMP4-induced SULF1 expression reduced FGF10 signalling in human urogenital tissue, therefore helping to direct prostate development[198]. Control of 6-O-

sulfation through the expression of *HS6ST* and *SULF* enzymes is thus one of the multiple layers of regulation that controls developmental processes.

Accordingly, 6-O-sulfation has been reported to change with age, with an age-dependent increase in 6-O-sulfation reported in murine muscle[199] and human aorta[200] and an age-dependent decrease in murine brains[201]. Mechanisms regulating these changes are unknown, but these observations raise the question of whether these are age-dependent changes that make tissues more susceptible to disease or are a disease-dependent response to conditions that present as tissues age.

In developing bones, there is a shift in expression from *Sulf2 to Sulf1* in developing mouse joints as cells transition from proliferating to hypertrophic chondrocytes[202]. *Sulf1*$^{-/-}$ and *Sulf2*$^{-/-}$ mice have different HS structures across a range of tissues[203–205] indicating different substrate specificity, which is supported by the sequence divergence of their substrate recognition domain, the C-terminal highly basic domain[206]. This difference in substrate recognition likely helps direct growth factor signalling at specific time points in development, by switching on and switching off signalling through expression of either *Sulf1* or *Sulf2.*

1.4.2 Dysregulation of 6-O-sulfation promotes neurological degeneration.

Ageing is highly correlated with neurological disease[207]. Tau aggregation is a common theme in numerous neurodegenerative diseases, from Parkinson's to Huntington's, and HS promotes both the aggregation of partially folded proteins into amyloid plaques, and the internalization of tau aggregates, a critical step for

fibril propagation[208]. Internalization can be blocked by knockdown of *EXT1* or following heparanase treatment[209]. Further work by Zhao *et al.*[210] identified 6-O-sulfate groups as potential mediators of HS-Tau interactions. This was further shown *in* and *ex vivo* by Rauch *et al.*[211] who observed that exogenous differentially sulfated heparins prevented Tau internalisation in a 6-O-sulfate dependent manner, and knockdown of *HS6ST1 (*or *EXT2)* inhibited Tau internalisation by up to 50%. In a comprehensive analyses of HS biosynthetic gene expression in the brain, *HS6ST1* expression was found to be increased in patients with severe Alzheimer's disease, whilst *SULF2* expression was decreased, indicating increased 6-O-sulfation[212]. *In vivo* this was shown using Alzheimer's disease mice, which showed increased abundance of tri-sulfated HS compared to control mice[213]. HS is therefore an important factor in the pathogenesis of tau aggregate-mediated neurological disease, and that this is promoted by HS 6-O-sulfation.

1.4.3 HS 6-O-sulfation increases in lung and renal fibrosis.

In IPF tissue HS 6-O-sulfation was increased, with specific increases in the quantity of UA-GlcNS(6S) and UA2S-GlcNS(6S) disaccharides which correlated with significantly increased expression of both *HS6ST1* and *HS6ST2. HS6ST1* knockdown reduced TGF-β1-induced SMAD2 phosphorylation and TGF-β1-induced α-smooth muscle actin expression[176]. This suggests that increased 6-O-sulfation may support a pathogenic feedback cycle, where increased TGF-β1 signalling increased fibrosis.

A similar mechanism may operate in renal fibrosis, which is characterised by connective tissue deposition on the kidney parenchyma, leading to deterioration of kidney function. Epithelial to Mesenchymal Transition is a core aspect of renal fibrosis and is mediated through TGF-β1 signalling[214]. In late-stage renal disease, kidney transplant is a potential therapeutic option, but runs the risk of allograft rejection. Work by Alhasan *et al*.[215] showed increased binding of antibodies (HS3A8, HS4C2 and RB4EA12) directed against tri-sulfated HS domains in chronic graft rejection samples and in mice models of progressive renal fibrosis, indicative of increased 6-O-sulfated domains. This was confirmed by overexpression of *HS6ST1* in renal epithelial cells, which also exhibited increased binding of HS3A8, HS4C2 and RB4EA12 antibodies. Thus, increased 6-O-sulfation has been observed as a hallmark of fibrosis in two independent tissues, and due to its potentiation of TGF-β1 signalling likely promotes disease progression.

1.4.4 HS 6-O-sulfation modulates activity of bioactive proteins in cartilage.

Given the effects of increased 6-O-sulfation described above, it is possible that increased 6-O-sulfation of HS observed in OA cartilage plays a role in osteoarthritis progression[68].

Numerous proteins with important roles in cartilage biology bind to and are likely to be regulated by 6-O-sulfated HS. ADAMTS-5 and MMP-13 degrade aggrecan and type II collagen, respectively, and are thought to be the main enzymes responsible for loss of cartilage from the joint in OA. LRP1-mediated endocytic clearance of ADAMTS-5 and MMP-13 was blocked by heparin[118,216], and binding

of immobilised heparin to FLAG-tagged ADAMTS-5 or FLAG-tagged TIMP-3 (an endogenous inhibitor of both ADAMTS-5 and MMP-13) was shown to be N- and 6-O-sulfate-dependent[53]. Increased 6-O-sulfation of HS may help prevent the endocytosis of these proteases, thus increasing their concentration in the pericellular matrix from where they may subsequently diffuse into the interterritorial matrix and cleave aggrecan and type II collagen. Binding to heparin increased the affinity of TIMP-3 for ADAMTS-5 1000-fold. It is unclear whether 6-O-sulfation may similarly regulate MMP-13 and TIMP-3 affinity.

Cartilage can regenerate following injury, but this process is reduced in OA. The observed increase in 6-O-sulfation in OA may impair repair, as signalling of several growth factors is known to be modulated by 6-O-sulfation. For example, SULF1 activity promotes WNT3a signalling[217]. WNT signalling is carefully balanced in cartilage, with canonical WNT ligands, such as WNT3a having catabolic effects[218] and non-canonical WNT ligands, such as WNT16, being anti-catabolic[219]. Expression of WNT3a is increased in rat OA models[220], and catabolic signalling of these elevated levels of Wnt3a may be promoted by the increased 6-O-sulfation in OA cartilage.

TGF-β1 has long been associated with OA risk, as a dominant-negative form of the TGF-β receptor II accelerates OA *in vivo*[221]. TGF-β1 preferentially binds to N- and 6-O-sulfate groups of HS[222], however the role of 6-O-sulfation in endogenous signalling is unclear as both *Sulf1*$^{-/-}$ mice[196] and lung fibroblasts treated with siRNA against *HS6ST1*[176] showed reduced SMAD2/3 phosphorylation. BMPs are also known to be important for chondrogenic health. BMP signalling is potentiated by HS[223], as loss of heparan sulfate antagonised BMP-induced p38

phosphorylation[223]. Signalling was not however completely ablated in these experiments, suggesting that whilst HS potentiates BMP signalling, it is not an absolute requirement. Binding of a BMP6 peptide to heparin was reduced by de-6-O-sulfation[224], but the sulfation motifs preferentially bound by most BMPs is currently unknown and the role of 6-O-sulfation in BMP signalling is also currently unclear.

As described in section **1.2.3** signalling of FGF2 (which can be both pro-catabolic and anabolic) is dependent upon the 6-O-sulfate group of HS to form the FGF2:HS:Receptor ternary complex, due to extensive interactions between the 6-O-sulfate group of HS and FGFR1c[92]. Unlike FGF1, which interacts directly with the 6-O-sulfate group, FGF2 does not. FGF18, another important anabolic protein in cartilage, is known to bind to both the 2-O and 6-O-sulfate groups of HS[225] and signalling can be induced with chondrocyte-derived perlecan, providing HS chains are intact[226]. Therefore, increased 6-O-sulfated HS may promote both FGF2 and FGF18 signalling in OA cartilage.

Given its effects on both anabolic (FGF18, FGF2, TIMP-3, BMP) and catabolic proteins (ADAMTS-5, WNT3a) in cartilage, it is unclear what the effect of increased 6-O-sulfation is on cartilage homeostasis. It is also likely to alter the bioactivity of a number of proteins of relevance in cartilage biology that are currently unknown or understudied. Therefore, given that 6-O-sulfation of HS is increased in OA cartilage[68], and the activity of SULFs has been shown to be protective[151], it is important to investigate whether this change in 6-O-sulfation plays a role in disease progression (as it does in other diseases) or is a by-product of an altered joint environment. To do this, I aimed to investigate how *HS6ST1*

expression regulated sGAG content of a chondrocyte cell line, and to identify cartilage proteins with high affinity for 6-O-sulfated. Finally, I planned to investigate how *HS6ST1* overexpression altered the transcriptome of the cell and how this changed the response of a chondrocyte cell line to stimulus.

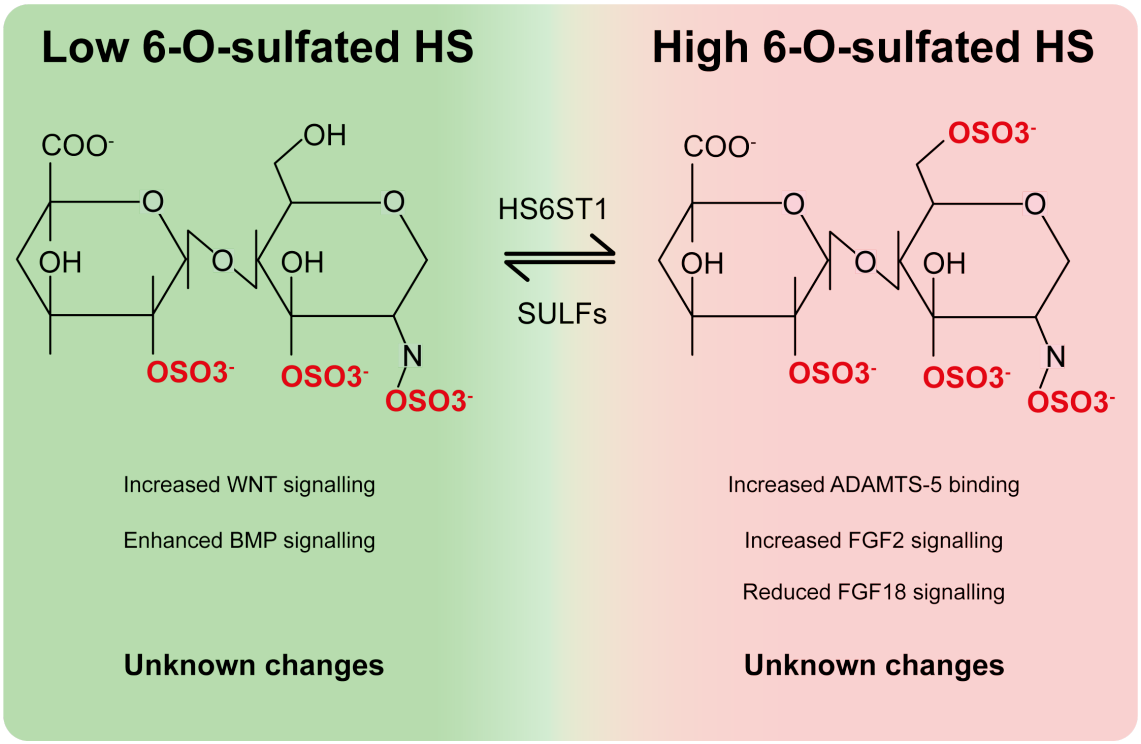

Figure 1.8 Heparan 6-O-sulfation binds known and unknown proteins in cartilage.

Low 6-O-sulfation of HS in healthy cartilage is regulated by the activity of SULFs and low expression of *HS6ST1*. In OA, due to increased *HS6ST1,* HS is more highly 6-O-sulfated. The change in sulfation may alter the binding of a large number of biomolecules, some known such as WNT, BMP, FGFs and proteases, and many more that are currently unknown, as no comprehensive analysis of the 6-O-sulfatome has been performed in cartilage.

1.5 Hypothesis and aims

I hypothesis that HS6ST1 inhibits anabolic growth factor activity in cartilage.

This hypothesis was tested with the following specific aims:

1. To investigate the effect of HS6ST1 overexpression on the phenotype of C28/I2 chondrocyte cell line (Chapter 3 and 4).
2. To identify human cartilage proteins with high affinity for 6-O-sulfated heparin (Chapter 5)
3. To investigate the effect of HS6ST1 overexpression on the transcriptome of the C28/I2 cell line (Chapter 6).

Chapter 2. Materials and methods

2.1 Reagents

2.1.1 Cell lines and cell culture reagents

HTB94 (SW1353) cells were obtained from laboratory stocks, originally purchased from American Type Culture Collection. C28/I2 cells were a kind gift from Professor Ian Clarks laboratory. **Table 2.1** summarises cell culture reagents used. All cells were cultured in growth medium, defined as Dulbecco's Modified Eagle medium (DMEM) supplemented with 10% foetal bovine serum (FBS) with 1% penicillin/streptomycin (P/S) and 1% sodium pyruvate. All proteins, otherwise specified, were purchased from Peprotech.

Table 2.1 Tissue culture reagents used for culturing C28/I2 cells and porcine chondrocytes

Reagent	Manufacturer
DMEM	Gibco
Non-heat inactivated FBS	First Link (UK)
Heat-inactivated FBS	Sigma
P/S	Lonza
Sodium pyruvate	Gibco
Opti-Mem	Gibco
4-(2-hydroxyethyl)-1-piperazineethanesulfonic acid (HEPES)	Gibco
Amphotericin B	Sigma
Trypsin-ethylenediaminetetraacetic acid (0.25%) (Trypsin-EDTA)	Gibco
Collagenase II	Gibco
Pronase E	Sigma
Sodium perchlorate	Fisher Scientific
Heparin	Sigma
Phosphate buffered saline (PBS)	In-house
Vrirkon RELY-ON	LANXESS

2.1.2 Human cartilage

Human cartilage samples were obtained from Articular Engineering from post-mortem donors with osteoarthritis or no diagnosed or macroscopically-evident arthritis. Human samples were obtained in full compliance with institutional, national and international ethical requirements (Faculty of Medicine and Health Sciences Research Ethics Committee, the UK Human Tissue Act and the Declaration of Helsinki).

2.2 Cell Culture and transfection optimisation

2.2.1 Cell line culture

HTB94 cells were cultured in DMEM supplemented with 10% heat-inactivated FBS, 1% P/S and 1% sodium pyruvate. C28/I2 cells were cultured in DMEM supplemented with 10% non-heat inactivated FBS, 1% P/S and 1% sodium pyruvate. Both cell lines were grown at 37 °C at 5% CO_2. Cells were passaged with trypsin-EDTA twice a week.

2.2.2 Porcine chondrocyte isolation and culture

Pig feet were collected fresh from HG Blake abattoir and sterilised for 30 minin Virkon (1 tablet / L). Cartilage explants were dissected from the metacarpophalangeal joints under sterile conditions washed in sterile PBS and incubated for 2 h with Pronase E (3.3 U/mL) (MedChemExpress) in serum-free

DMEM. Cells were washed in sterile PBS and left to digest overnight in collagenase II (185 U/mL) (Gibco) in growth medium, supplemented with 1% HEPES and 1% amphotericin B, at 37 °C at 5% CO_2. Following digestion, cells were strained through a 70 μm cell strainer and pelleted at 2500 revolutions per minute (RPM) for 10 min. Cells were resuspended in growth medium and pelleted a further two times. Cells were then plated out in growth medium at a density of one joint per 10 cm^3 plate.

2.2.3 Interleukin-1β response

The response of C28/I2 cells to IL-1β was investigated as shown in **Figure 2.1.** $1x10^5$ cells were seeded into a 12 well plate and cultured in growth medium for 48 h. Cells were serum starved for 24 h and stimulated with 5 ng/mL IL-1β for 6 h before being lysed for RNA and gene expression analyses as described in **2.3.1** and **2.3.2**. The response of HS6ST1-transfected cells was also investigated as described above.

The response to IL-1β in conditions of HS depletion or anatagonism was also investigated. Cells were cultured in the presence of sodium chlorate (30 mM), or surfen (20 μM). Chlorate is a competitive inhibitor of 3'-phosphoadenosine 5'-phosphosulfate thus preventing HS chain sulfation and enabling investigation of the effects of non-sulfated HS is on the cellular response to stimulus. Surfen is an HS antagonist that prevents protein-HS binding. A schematic of these timelines is shown in **Figure 2.1.**

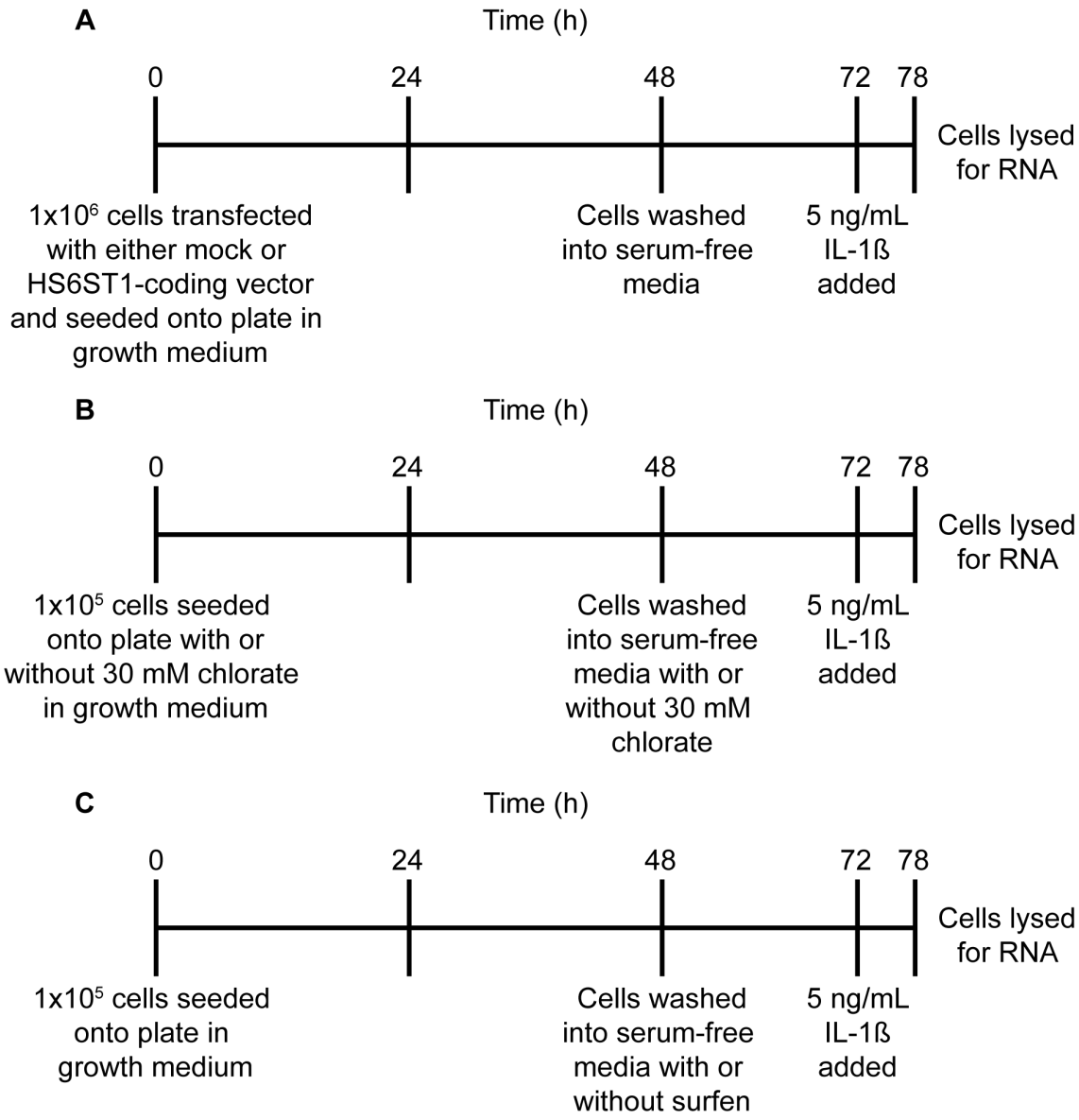

Figure 2.1 Transfected or treated cells were stimulated with IL-1ß for 6 h.

(A) C28/I2 cells ($1x10^6$) were transfected with either mock or HS6ST1-coding plasmids (2 μg) and grown for 48 h in growth medium. Cells were washed with PBS and cultured in serum-free medium for 24 h. Cells were treated with IL-1β (5 ng/mL) for 6 h before lysis for RNA isolation and cDNA synthesis. The effect of IL-1β on gene expression was measured using RT-qPCR. (B) C28/I2 cells ($1x10^5$) cells were treated with 30 mM sodium-chlorate for 48 h in growth medium. Cells were washed with PBS and cultured in serum-free medium with 30 mM sodium chlorate a further 24 h to silence signalling. Cells were then treated with IL-1β (5 ng/mL) for 6 h before lysis for RNA isolation and cDNA synthesis. The effect of chlorate treatment on IL-1β-induced gene expression was measured using RT-qPCR. (C) C28/I2 cells ($1x10^5$) were grown for 48 h in growth medium. Cells were washed with PBS and cultured in serum-free medium for 24 h. Cells were treated with IL-1β (5 ng/mL) for 6 h before lysis for RNA isolation and cDNA synthesis. The effect of surfen on IL-1β-induced gene expression was measured using RT-qPCR.

2.2.3 Bacterial transformation and plasmid purification

One Shot TOP10 chemically competent *E. coli* (Thermo Fisher) were transformed with a pcDNA3.1 *HS6ST1-FLAG*-coding plasmid custom-synthesised by GenScript. *E. coli* were transformed using the heat-shock method[227] as described by the manufacturer.

Transformed bacteria were plated out onto agar containing 50 μg/mL ampicillin and cultured overnight at 37 °C. Single colonies were picked and cultured sequentially in 5 mL LB-Broth and then 100 mL LB-Broth. Cells were pelleted by centrifugation at 4000 RPM for 15 min. Plasmid was isolated using QIAGEN Maxi kit according to manufacturer's instructions.

To generate a non-coding vector, the plasmid was digested in Xba1 restriction enzyme for 1 h at 37 °C. Digested plasmid was electrophoresed on a 0.5% agarose gel and imaged under UV. The plasmid was cut out of the gel and digested with NT1 reagent (Machery-Nagel) at 50 °C. The plasmid was cleaned using NucleoSpin Gel and PCR Clean-Up Columns (Machery-Nagel), religated using T4 DNA Ligase (37 °C, 16 h) and transformed into *E.coli* as described above.

2.2.3 Transfection of C28/I2 cells with *HS6ST1* plasmid

C28/I2 cells were transfected with an empty vector plasmid or an *HS6ST1*-encoding plasmid using the Lonza chondrocyte nucleofector protocol. Briefly, 2 μg plasmid was added to 100 μL primary P3 cell transfection buffer (Lonza).

Confluent cells were incubated with trypsin-EDTA to generate single cell suspensions. One million cells were resuspended in the plasmid-P3 buffer mix and electroporated using the 4D-Nucleofector apparatus. Following electroporation, cells were recovered for 5 min at 37 °C. Next, 500 μL of pre-warmed growth medium was gently added, before cells were seeded at a density of 1 million cells per 9.6 cm^2 . Medium was changed 24 h post-transfection.

Alternatively, cells were transfected using Lipofectamine 3000 (Invitrogen) according to manufacturer's instructions. Briefly, cells were seeded at a density of 300 000 per 9.6 cm^2 and grown overnight. 7.5 μL Lipofectamine 3000 reagent was diluted in 125 uL Opti-MEM. 2 μg plasmid and 4 μL P3000 reagent were mixed in 125 μL Opti-MEM. Diluted DNA and Lipofectamine 3000 were mixed 1:1 and incubated 10 min at room temperature (RT). DNA-reagent complex was added dropwise to cells in Opti-MEM. Cells were cultured for 24 h after which the medium was changed.

2.2.4 Measuring transfection efficiency with GFP

Transfection efficiency was evaluated by transfecting C28/I2 cells with a GFP-encoding plasmid as described in **2.2.3.** Transfected cells were grown for 48 or 72 h, and green fluorescence was quantified using ImageJ or flow cytometry.

For ImageJ quantification, green fluorescence was observed in the green channel of an EVOS M5000 (Invitrogen). Three wells were seeded per condition and three images were taken per well. Images were converted to greyscale in ImageJ

(v1.53a), and non-fluorescent sections of the image were thresholded out. Pixel intensity was quantified and used as a procy measured of transfection efficiency.

Fluorescence was also measured using flow cytometry on a CyFlow Cube 6 (SYSMEX). Briefly, transfected cells were dissociated using a cell dissociation buffer (Gibco), pelleted at 1500 RPM for 5 min and resuspended in PBS, supplemented with 1 mM EDTA to prevent cell aggregation by chelation of divalent cations. Green fluorescence was measured, and data were analysed with FlowJo (v10.7)

2.2.5 Cell viability assay

Cell viability was measured using the CellTiter 96 Aq_{ueous} One Solution Cell Proliferation Assay (Promega) following the manufacturer's instructions. This assay utilises a tetrazolium compound, [3-(4,5-dimethylthiazol-2-yl)-5-(3-carboxymethoxyphenyl)- 2-(4-sulfophenyl)-2H-tetrazolium, inner salt; (MTS), that couples with phenazine methosulfate, to produce formazan. This coupling reaction is directly proportional to the number of living cells in culture, and therefore the amount of formazan, measured at 490 nm absorbance, can be used to measure cell viability. Briefly, $1x10^4$ cells were grown in a 96-well tissue culture plate. Cells were washed into 80 μL growth medium with 20 μL MTS reagent and incubated for 1 h at 37 °C. Cells were shaken briefly before having absorbance measured at 490 nm was measured.

2.3 Phenotypic characterisation of C28/I2 cells

2.3.1 RNA isolation and reverse transcription-PCR

Cells were washed twice with PBS before RNA was extracted with the RNEasy kit (QIAGEN) according to the manufacturer's protocol. 100 – 500 ng of RNA was reverse transcribed to cDNA using the High-capacity cDNA reverse transcription kit (Applied Biosystems) according to manufacturer's instructions. RT-PCR was performed in a T100 Thermal Cycler (BioRad). PCR products were diluted 1 in 4 with RNAse-free water (Invitrogen).

2.3.2 Quantitative real time PCR

qPCRs were performed in 384-well plates (Armadillo, ThermoFisher Scientific), in a Quantstudio 7 Flex system (Applied Biosystems) using SYBR Green master mix (Applied Biosystems), with a total reaction volume of 5 μL including 1 μL of diluted cDNA. Data were analysed using the -ΔΔCT method, using *GAPDH* as a housekeeper gene. Primers sequences used are shown in Table 2.2. All primers were purchased as KiCqStart primers from Sigma. Melt curves were analysed for each primer pair after initial solubilisation and every 6 months to ensure generation of a single PCR product.

Table 2.2 SYBR-Green RT-qPCR primer sequences

Gene	Forward (5'-3')	Reverse (5'-3')
HS6ST1	5'-AGGAAGTTCTACTACATCACC	5'-CCCATCACACATATGCAAC
HS6ST2	5'-GACAGTCCATAAACTCTTTGAG	5'-AGAACTTCCACTACATCACC
HS6ST3	5'-CCACACCAGGAATTTCTATTAC	5'-GAAGAGAGGTTTTCCAAGTG
HS2ST	5'-ACTTTAGATGAGGAAGAGGAC	5'-CCTGATCTTGCAATGACATC
GLCE	5'-AGGTATGGTCTGAATATGCG	5'-GTACTGTGACCAAAGTGAAG
SULF1	5'-AGACCTAAGAATCTTGATGTTGGAA	5'-CCATCCCATAACTGTCCTCTG
SULF2	5'-GACCCCTACCAGCTGATGAA	5'-GCTTGTAACCCTTGCAGCTC
XYLT1	5'-TCAGGATGGCTACTTTTCTC	5'-TGTTGTCGACATTCTCAAG
CHPF2	5'-TACAAGAAGGTGCTAGG	5'-TGAAGTAGAGTAACCGAGG
ACAN	5'-CACCCCATGCAATTTGAG	5'-AGATCATCACCACACAGTC
SOX9	5'-CTCTGGAGACTTCTGAACG	5'-AGATGTGCGTCTGCTC
COL2A1	5'-GAAGAGTGGAGACTACTGG	5'-CAGATGTGTTTCTTCTCCTT
LRP1	5'-ACATATAGCCTCCATCCTAATC	5'-GCTTATACCAGAATACCACTC
CAPN	5'-CAAGATCAACGGATGCTATG	5'-GATGATCTTGAACAGGTTGG
ADAMTS4	5'-AGAAGAAGTTTGACAAGTGC	5'-CACATTGTTGTATCCGTACC
ADAMTS5	5'-CCCACCCAATGGTAAATC	5'-GACTCCTTTTGCATCAGAC
IL1B	5'-GCCTCAAGGAAAAGAATCTG	5'-GGATCTACACTCTCCAGC
B3GALT6	5'-AACTGGGTAACTTATTGGG	5'-TTCCAGGTTGAGATTCTTTATTC
MMP3	5'-GCAGTTAGAGAACATGGAG	5'-ACGAGAAATAAATTGGTCCC
MMP8	5'-AAGTTGATGCAGTTTTCCAG	5'-CTAACTTCCCTTCAACATTC5
MMP9	5'-AAGGATGGGAAGTACTGG	5'-GCCCAGAGAAGAAGAAAAG
MMP13	5'-AGGCTACAACTTGTTTCTTG	5'-AGGTGTAGATAGGAAACATCAG
HYAL1	5'-CAGATCTTCTATGACACGAC	5'-CTGACATGATTCCTTGGTTC
HYAL2	5'-GGACCTCATCTCTACCATTG	5'-AGGTAACTTTGAGGTACTGG
GAPDH	5'-ACAGTTGCCATGTAGACC	5'-TTGAGCAGCAGGGTACTTTA
CHPF	5'-GAGATCCAGGAGTTACAGTG	5'-CTGCTCCGTGAAGTAGTC
CSGALNACT1	5'-CTGGTCATAAAGAAGGAAACTG	5'-CCACCTATATTGATGAAGTC
CHST3	5'-AAGATGAGAAGCAAATACGC	5'-TGTCTGAGACCCTTGATATG
CHST11	5'-TATTTCCAAATCATGCGGAG	5'-ATTGGGTTGTAGAGTTCCTG
CHST15	5'-TGGGATAATAATGCCTGGAC	5'-TAGTCTGAGTACAACCTCTC

2.3.3 Immunoblotting

Cell lysates were collected using reducing sodium dodecyl sulfate–polyacrylamide gel electrophoresis (SDS-PAGE) sample buffer supplemented with protease inhibitor cocktail (Sigma) and denatured by heating at 100 °C for 5 min. Conditioned medium were collected, and proteins precipitated by addition of 6.1 N trichloroacetic acid (to 5% v/v) (MPbio). Following precipitation, proteins were pelleted at 15000 RPM for 15 min, before being resuspended in SDS-PAGE

sample buffer. Protein samples were separated by molecular weight on SDS polyacrylamide gels (**Table 2.3**) at 180 V for up to 70 min. Proteins were transferred to low fluorescence polyvinylidene difluoride (Invitrogen) membranes using Trans-Blot Turbo apparatus (BioRad). Prior to blocking, total protein was quantified using Revert Total Protein Stain (LiCOR) following the manufacturer's instructions. Non-specific binding was blocked using Tris-buffered saline-based Intercept blocking buffer (LiCOR) for 1 h at RT. Membranes were incubated with primary antibodies in primary antibody solution (**Table 2.3**) for 1 h at RT. Membranes were washed with TBS-Tween20 (0.1% v/v) for 4x5 min, before being incubated with secondary antibodies in secondary antibody solution (**Table 2.3**) for 1 h at RT. Membranes were washed for 4x5 min before imaging on a LiCOR Odyssey (LiCOR) at 700 and 800 nm. Bands of interest were normalised against total protein, or a housekeeper protein using ImageStudioLite (LiCOR v5.2.5). Antibodies used and dilutions are shown in **Table 2.4**.

Table 2.3 Immunoblotting lysis and buffer recipes

Buffer	Recipe
SDS-PAGE running buffer	100 mM Tris-HCl, pH 6.8, 2% SDS, 5% β-mercaptoethanol, 15% glycerol, 0.01% Bromophenol blue
12% polyacrylamide lower gel	(3.3 mL) Milli-Q H_2O, (4.0 mL) 30% acrylamide, (3.8 mL) 1.5 M Tris-HCl pH 8.8, (0.1 mL) 10% (w/v) SDS, (0.1 mL) 10% (w/v) ammonium persulfate, (4.0 μL) Tetramethylethylenediamine
Polyacrylamide upper gel	(4.1 mL) Milli-Q H_2O, (1.0 mL) 30% acrylamide, (0.75 mL) 1 M Tris-HCl pH 6.8, (60 μL) 10% (w/v) SDS, (60 μL) 10% (w/v) APS, (6 μL) Tetramethylethylenediamine
Primary antibody solution	Primary antibody, (2.5 mL) Tris-buffered saline-based Intercept blocking buffer, (2.5 mL) Tris-buffered saline, (20 μL) Tween-20
Secondary antibody solution	Secondary antibodies, (2.5 mL) Tris-buffered saline-based Intercept blocking buffer, (2.5 mL) Tris-buffered saline, (20 μL) Tween-20, (20 μL) 10% (m/v) SDS

Table 2.4 Antibodies used for immunoblotting

Antibody targets	Dilution	Host species	Manufacturer	Detected by
ANTI-FLAG M2	1/1000	Mouse	Sigma	HRP-conjugated anti-mouse
P44/42 MAPK (ERK1/2)	1/1000	Mouse	Cell Signalling Technologies	IRDye 800 CW anti-mouse IgG (H + L)
Phospho-p44/42 MAPK (ERK1/2) (Thr202/Tyr204)	1/1000	Rabbit	Cell Signalling Technologies	IRDye 680RD anti-rabbit IgG (H + L)
TIMP-3 (clone AB6000)	1/1000	Rabbit	Sigma	HRP-conjugated IgG anti-rabbit
Phospho-SMAD1/5 (S463/465)	1/2000	Rabbit	Cell Signalling Technologies	IRDye 680RD anti-rabbit IgG (H + L)
Phospho-SMAD2/3 (S465/467)	1/1000	Rabbit	Cell Signalling Technologies	IRDye 680RD anti-rabbit IgG (H + L)
Human Endostatin	1/500	Goat	R&D Biosystems	HRP-conjugated IgG anti-goat
IRDye 800 CW anti-mouse IgG (H + L)	1/2500	Goat	LiCOR	N/a
IRDye 680RD anti-rabbit IgG (H + L)	1/2500	Goat	LiCOR	N/a
HRP-conjugated IgG anti-mouse	1/2500	Rabbit	Fisher	N/a
HRP-conjugated IgG anti-rabbit	1/2500	Goat	Abcam	N/a
HRP-conjugated IgG anti-goat	1/2500	Rabbit	Agilent Dako	N/a

2.3.4 Human phosphokinase antibody arrays

Phosphorylation of proteins in response to *HS6ST1* transfection was investigated using the Human Phospho-Kinase Antibody Array (R&D Biosystems) according to the manufacturer's instructions. A brief schematic of the experimental plan can be seen in **Figure 2.2.**

Briefly, 1x10^6 *HS6ST1*-transfected cells were seeded onto a 6-well plate and cultured in growth medium for 48 h. Signalling was silenced by 24 h of serum starvation, then cells were treated with serum-containing growth medium for 30 min before being lysed using Lysis Buffer 6. Protein concentrations were quantified using the Bradford assay according to the manufacturer's instructions and 400 μg of protein was loaded onto a set of membranes.

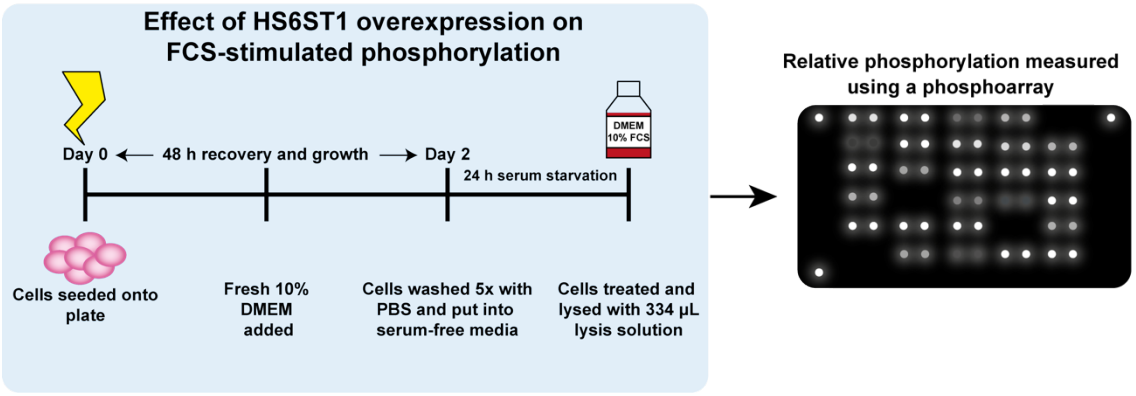

Figure 2.2 Schematic of phosphorylation array method for *HS6ST1* overexpressing cells.

C28/I2 cells (1x10^6) were transfected with 2 µg of mock or HS6ST1-encoding plasmid and cultured for 48 h. Cells were serum starved for 24 h and stimulated with growth medium for 30 min (37 ºC, 5% CO_2). Cells were washed twice in ice-cold PBS and cell lysates were collected in SDS sample buffer supplemented with protease and phosphatase inhibitors. Cell lysates (400 µg) were incubated with membranes as per the manufacturer's instructions to quantify phosphorylation of proteins. Reference spots on each membrane were used to control for signal between membranes. Data were analysed using ImageJ (v1.53a).

2.3.4 Alcian blue staining

Sulfated glycosaminoglycan content of cultured cells was quantified using the dye Alcian blue, as described previously[228]. Briefly, cells were washed twice with PBS, then fixed for 30 min with ice-cold methanol at -20 °C. Cells were washed twice with water, then stained at 4 °C overnight with Alcian blue stain [0.5% Alcian

blue 8GX (Sigma) in 0.1 N HCl]. Cells were washed to remove unbound dye, and destained at 4 °C overnight with 6 M Guanidine-HCl. 1 volume of 6 M Guandine-HCl was added in the morning, and samples were left to complete de-stain at RT for a further 3.5 h. Absorbance at 630 nm was then quantified in duplicate on a SPECTROstar Omega plate reader (BMG).

2.3.5 Protease activity assays

Protease activity in a sample can be measured using Förster resonance energy transfer-quenched fluorogenic substrates which exhibit increased fluorescence upon cleavage. One of the first substrates to measure MMP activity was Mca-PLGL-Dpa-AR-NH_2 developed by Knight *et al.*[229]. This was used to measure protease activity in the conditioned medium of transfected cells. 50 µL of conditioned medium from transfected cells was incubated in Eppendorf tubes with 100 µL of Tris/sodium/calcium assay buffer (TNC, 50 mM Tris.HCl, pH 7.5, 150 mM NaCl, 10 mM $CaCl_2$, 0.05% v/v Brij35) and 50 µL Knight substrate (Bachem, 6 µM, giving a final concentration of 1.5 µM) for 16 h, at 37 ºC. Endpoint fluorescence was measured in an opaque walled, clear bottomed 96-well plate using a SPECTRAmax GEMINI XPS fluorometric plate reader (Molecular Devices) (excitation 325 nm, emission 393 nm). Purified MMP-13 (Bio-techne) was used as a positive control at a final concentration of 3 µM.

ADAMTS-5 activity was measured using the fluorogenic peptide Abz-TESE~SRGAIY-Dpa-KK (5 mM) at a final concentration of 20 µM per well[230]. 90 µL of conditioned medium from transfected cells was incubated with 90 µL TNC and 20 µL of a 200 µM working solution of ADAMTS-5 substrate (24 h, 37 ºC).

Endpoint fluorescence was measured in an opaque walled clear bottomed 96-well plate using a SPECTRAmax GEMINI XPS fluorometric plate reader (Molecular Devices) (excitation 300 nm, emission 430 nm). ADAMTS-5 purified by Dr Linda Troeberg (UEA) was used as a positive control, at a final concentration of 10 nM.

2.3.6 mRNA sequencing

C28/I2 cells transfected with mock- or HS6ST1-encoding plasmids (n=5) were cultured for 48 h in growth medium. Cells were washed twice with PBS, and RNA was isolated. 280/260 and 230/260 nm absorbance values were assessed using a Nanodrop 3000. Per treatment group, 4 samples with highest RNA quality (lowest 280/260 and 230/260) were sent to Novogene for mRNA sequencing and quantification.

Briefly, samples underwent poly-A tail enrichment, fragmentation, and cDNA synthesis. Sample quality was assessed using Qubit and RT-PCR for quantification and using bioanalyzer for analysis of size distribution. Samples were sequenced on an Illumina platform using paired end reading at a depth of 6 Gb.

Raw data were processed using fastp to remove reads containing adapter or poly-N and low-quality reads. Reads were aligned to the *Homo sapiens* reference genome using Hisat2 (v2.0.5). Gene expression was quantified using featureCounts (v1.5.0-p3). Differential gene expression was calculated with DESeq2 (v1.20.0).

Differentially expressed genes underwent functional enrichment analysis using the online webserver gProfiler[231] .

2.4 Affinity chromatography isolation of heparin-binding proteins and mass spectrometric characterization.

2.4.1 Protein extraction from cartilage

Efficiency of protein extraction from porcine cartilage was tested with a range of buffers (**Table 2.5**). Porcine extracts (120 mg) (**2.2.2**) were incubated in the buffers (3 mL) shown in **Table 2.5** on a roller at 4 °C overnight. RIPA, SDS and Gdn-HCl extracts were dialysed against 50 mM Tris-HCl, pH 7.4, 150 mM NaCl. Briefly, samples were added to 3.5k MWCO Slide-A-Lyzer dialysis cassettes (ThermoFisher Scientific) and dialysed against 266 volumes of 50 mM Tris-HCl pH 7.4 for 24 h at 4 °C . Samples were dialysed for an initial 8 h, followed by replacement of the 50 mM Tris-HCl pH7.4 buffer and dialysis for a further 16 h overnight. Efficiency of protein extraction was then evaluated by immunoblotting for the heparin-binding protein TIMP-3.

Table 2.5 Extraction buffers used to extract proteins from cartilage explants.

Buffer	Recipe
RIPA	50 mM Tris-HCl pH 7.4, 150 mM NaCl, 1 mM EDTA, 1% (v/v) NP-40, 0.25% (w/v) Na-deoxycholate
Tris-HCl	500 mM Tris-HCl pH 7.0, 100 mM NaCl, 0.5% (v/v) NP-40
SDS buffer	100 mM Tris-HCl, pH 6.8, 2% SDS, , 15% glycerol, 0.01% bromophenol blue
Guanidine-HCl	4 M guanidine HCl, 50 mM L-arginine

2.4.2 Heparin affinity chromatography

Heparin affinity chromatography was performed on commercial heparin-Sepharose (Cytavia) as well as custom-synthesised heparin- and 6-O-desulfated heparin-Sepharose (IntelliHep). Heparin-Sepharose resins were prepared in Poly-Prep chromatography column reservoirs (Bio-Rad). Resins were washed with 10x column volumes of water to remove the ethanol-containing storage solution and then sequentially washed with 10x column volumes of equilibration solution, 5x volumes of elution solution 2, and 20x column volumes of equilibration buffer. Columns were stored in equilibration buffer supplemented with 0.05% sodium azide to prevent bacterial growth.

Prepared heparin-Sepharose resins (1 mL column resin final volume) were added to dialysed cartilage extracts in a 15 mL Falcon tube, and left on a roller at 4 °C overnight. Resins were transferred to reservoirs and the unbound fraction was

collected. Resins were washed with 50 column volumes of equilibration buffer and heparin-binding proteins were then eluted using 6 column volumes of 50mM Tris-HCl, pH 7.4, 1 M NaCl in 1.5 mL fractions. Resins were then eluted with 6x column volumes of 50 mM Tris-HCl, pH 7.4, 2 M NaCl this was collected in 1.5 mL fractions. Resins were then washed with a further 10 column volumes of 50 mM Tris-HCl 2 M NaCl pH 7.4, before being equilibrated with 20 column volumes of equilibration buffer.

Samples were stored at -80 °C prior to preparation for mass spectrometry.

2.4.3 Mass Spectrometry (MS)

1 M NaCl elutions from heparin and 6-O-desulfated heparin-Sepharose resins eluates were analysed by Dr Matteo Calligaris and Dr Simone Dario Scilabra (RiMED, Sicily).

To eliminate issues with sample degradation, samples were freeze-dried prior to shipping. Samples were reconstituted in UB buffer (**Table 2.6**) and concentrated on a 10 kDa Vivacon column. Samples were reduced in UA buffer with 50 mM DTT, and then alkylated with 50 mM iodoacetamide in UA buffer. Samples were washed with UB buffer and digested with LysC and trypsin. Samples were collected in NaCl (0.5 M) and peptides acidified with formic acid (8%). Resulting peptides were desalted by Stop-and-Go Extraction (STAGE)[232]. Mass spectrometry was then performed as previously described[233]

Table 2.6 Buffers used in MS sample preparation

Buffer	Recipe
UB Buffer	8 M Urea, 100 mM Tris-HCl pH 8.0
UA Buffer	8 M Urea, 100 mM Tris-HCl, pH 7.5
UC buffer	2 M Urea, 25 mM Tris-HCl, pH 8.0

2.4.4 Analysis of MS data

Raw data were analysed using MaxQuant, v. 2.0.1.0 (Max-Planck Institute). MS data were searched against a reviewed canonical database of *Homo sapiens* downloaded from UniProt on November 5th 2020. Trypsin/P was the defined protease, with up to two missed cleavages allowed for the database search. “First search” was used to recalibrate the peptide masses within a window of 20 ppm. The main peptide search and peptide fragment mass tolerances were set to 4.5 and 20 ppm respectively. Carbamidomethylation of cysteine was defined as a static modification. Acetylation of protein N-termini as well as methionine oxidation were chosen as variable modifications. The False Discovery Rate (FDR) for both proteins and peptides were adjusted to less than 1%. The “match between runs” option was enabled with a match time window of 1.5 min. Label-free quantification (LfQ) of proteins required at least on ratio count of unique peptides. Protein LfQ reports of MaxQuant were processed in Perseus. Protein LfQ intensities were Log2 transformed and filtered for LfQ intensities detected in at least three biological replicates per group to be quantified. Statistical significance was considered at $p < 0.05$.

2.5 Statistical analysis

Data were analysed using Prism 9.0.0. Data were assessed for normality using Shapiro-Wilks test. Normally-distributed data involving multiple samples in a single group were analysed using One-way ANOVA, normally distributed data involving multiple samples with multiple groups were analysed using 2-way ANOVA. Sample to sample comparisons were analysed using a paired t-test.

Chapter 3. Optimisation of *HS6ST1* overexpression in the chondrocyte cell line C28/I2.

3.1 Introduction

Due to the lack of readily available primary human chondrocytes, I investigated whether chondrocyte-like cell lines were appropriate for investigating the role of *HS6ST1* in cartilage. I investigated two different cell lines, HTB94, an osteosarcoma cell line, and the immortalised chondrocyte cell line C28/I2. Due to differences in gene expression profiles, certain cells lines have been used for studying different aspects of cartilage biology. For example, HTB94 cells can be used for studying catabolic responses to inflammatory stimuli[234] , whereas C28/I2 cells have previously been used for research into cartilage anabolism[228,235]. As the main aim of my project was to investigate the role of heparan sulfate in cartilage, I was interested whether these cell lines expressed relevant heparan sulfate biosynthesis and modifying enzymes. I also measured the expression of three anabolic genes characteristic of cartilage repair in primary chondrocytes: *ACAN, SOX9* and *COL2A1*. The profile of expression of these genes helped me to determine which cell line was suitable for investigating HS in a cartilage cell culture model.

Different culture conditions can change the gene expression in chondrocyte cell lines, as well as their extracellular matrix composition and response to stimuli. For example, culturing of C-20/A4 cells, an immortalised juvenile costal chondrocyte cell line, in alginate upregulated expression of several genes involved in pericellular matrix formation, such as fibronectin, biglycan and decorin[236]. No such change was observed when C28/I2 cells were cultured in alginate[237], but increased anabolic activity was observed when C28/I2 cells were cultured in micromass, with increased expression of *ACAN*, *SOX9* and *COL2A1*

mRNA, and elevated synthesis of sulfated glycosaminoglycans compared with monolayer cultures[228]. Therefore, I investigated how culturing C28/I2 cells in micromass effected their mRNA expression of GAG- and cartilage-related genes (using RT-qPCR) and their matrix deposition (by Alcian blue staining). Finally, I optimised transfection of the selected cell line with an HS6ST1-coding plasmid and confirmed overexpression using qPCR and western blotting.

3.2 C28/I2 cells express chondrocyte-related genes and synthesise sulfated glycosaminoglycans

HTB94 and C28/I2 cells were cultured for 2 days in growth media and had their gene expression of several HS biosynthesis and modifying genes and three prototypic cartilage genes was measured using RT-qPCR. The difference in mRNA expression of these genes in the two cell lines is shown in **Figure 3.1**. Neither cell line expressed appreciable levels of *HS6ST3* (Ct > 35), and there was no significant difference in expression of 7 of the other genes investigated. Expression of SULF1 was significantly reduced in C28/I2 cells compared to HTB94s (HTB94: Ct 7, C28/I2 Ct: 11.7). Importantly, HTB94 cells had no expression of *ACAN* (Ct > 35), whereas C28/I2 cells showed moderate expression compared to the housekeeper GAPDH. Due to the importance of aggrecan in cartilage[238], C28/I2 cells were thus selected for further study.

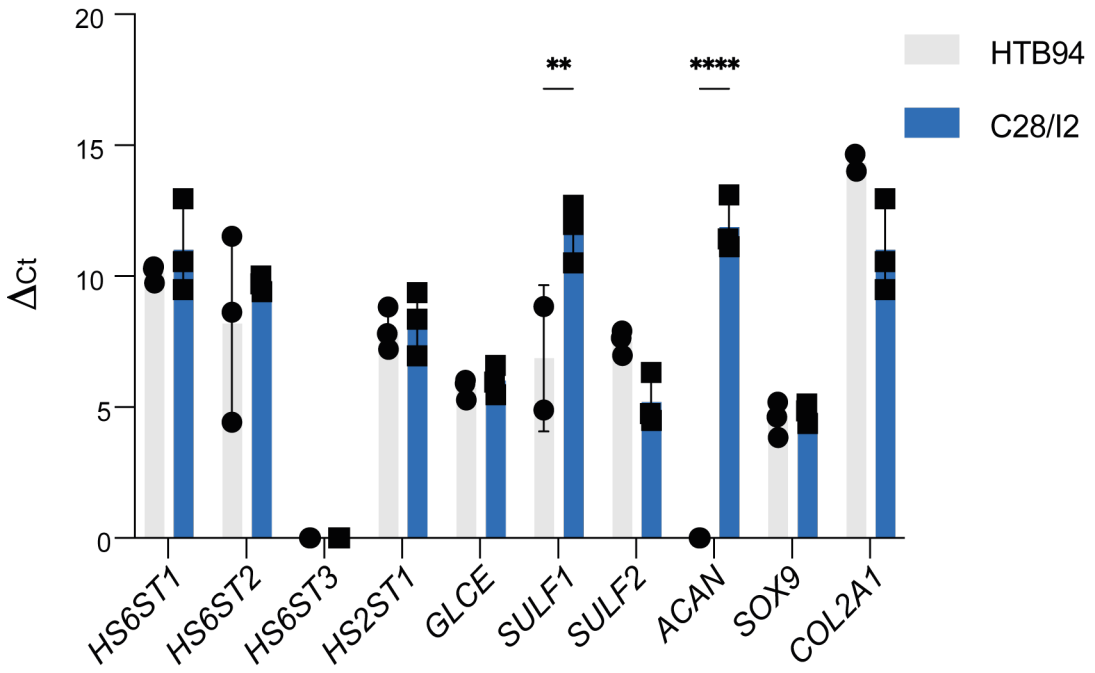

Figure 3.1 RT-qPCR analysis showed C28/I2 cells, but not HTB94 cells, expressed detectable levels of aggrecan mRNA.

HTB94 and C28/I2 cells ($3x10^5$) were cultured for 48 h before RNA was isolated and reverse transcribed into cDNA. Expression of selected HS biosynthesis and anabolic cartilage genes was measured by RT-qPCR using SybrGreen primers and ΔCt values normalised against GAPDH housekeeper. Data were assessed for normality with Shapiro-Wilks test. (n = 3, mean ± SD. Data analysed with 2-way ANOVA and corrected for multiple comparisons with Dunnett's multiple comparisons test. * $p \leq 0.05$, ** $p \geq 0.001$, *** $p \leq 0.001$).

The effect of culturing conditions on the phenotype of C28/I2 cells was then investigated. Continuous passage of chondrocytes in the presence of TGF-β1 has been shown to increase sGAG deposition and increase the expression of genes related to GAG synthesis[239,240]. Furthermore, work by Greco *et al.*[228] showed that culturing C28/I2 cells in micromass increased their expression of genes typically associated with anabolism, such as *ACAN* and *COL2A1*, and their sGAG content. Therefore, C28/I2 cells were cultured in monolayer or in micromass, and/or supplemented with TGF-β1, and the change in expression of the GAG biosynthesis and modifying genes and the prototypic cartilage genes

described earlier was examined by RT-qPCR, and accumulation of sGAG quantified using Alcian blue staining.

Culturing cells in micromass had no effect on the expression of genes associated with initial sulfation of the HS chain (e.g. *HS6ST1, HS6ST2* are shown in **Figure 3.2 A,B**, with similar data obtained for *HS2ST1* and *GLCE* not shown). Culturing cells in micromass also had no significant effect on the expression of either *SULF1* or *SULF2*. However, addition of TGF-β1 to both the monolayer and micromass cultures significantly increased *SULF2* expression, by 4- and 6-fold respectively (**Figure 3.2 C**), as has been observed previously by others in other cell types[241] .

As TGF-β1 treatment is predicted to increase the amount of sGAG content of the C28/I2 cells[228], the gene expression of two genes, *XYLT1* and *B3GALT6*, two genes involved in the initial biosynthesis of both HS and CS was examined. Culturing in micromass had no significant effect on the expression of *XYLT1*, but TGF-β1 treatment significantly increased expression in both monolayer and micromass, by 3.5- and 5.5-fold respectively (**Figure 3.2 B**). There was no significant effect on *B3GALT6* expression (**Figure 3.2 B**). *CSGALNACT1,* which adds N-acetylglucosamine residues to the core CS tetrasaccharide linker, and *CHPF,* which promotes CS chain elongation. *CSGALNACT1* expression was significantly reduced by TGF-β1 treatment in monolayer cultures, but not in micromass (**Figure 3.2 D**). *CHPF* expression was significantly reduced in micromass culture compared to monolayer, with this expression restored by addition of TGF-β1 (**Figure 3.2 D**).

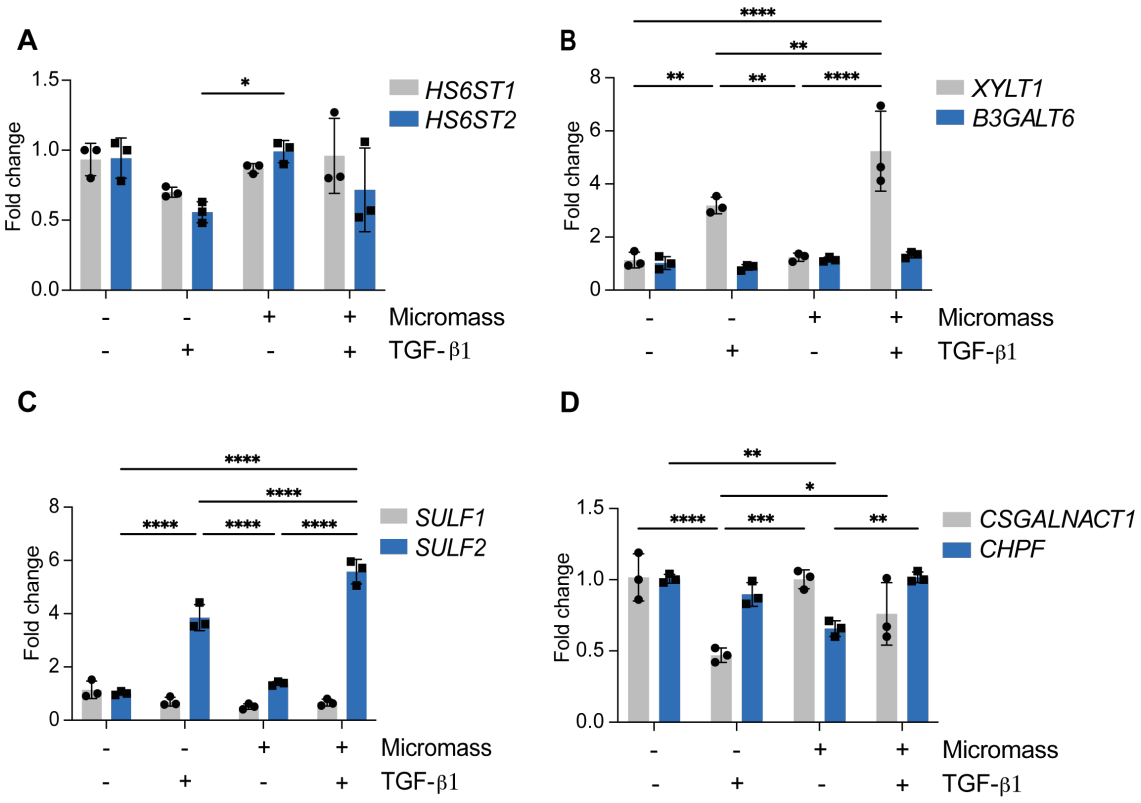

Figure 3.2 RT-qPCR showed that TGF-β1 treatment increased expression of *SULF2* and *XYLT1* in C28/I2 cells.

(A-D) C28/I2 ($5x10^5$) cells were grown in monolayer or micromass, in serum-free media supplemented with or without 5 ng/mL TGF-β1 for 4 days. RNA was extracted and reverse transcribed to cDNA. mRNA expression of selected GAG biosynthesis and modifying genes was analysed with RT-qPCR and normalised against the housekeeper GAPDH using the -ΔΔCt method and expressed relative to untreated cells grown in monolayer. Expression of *HS6ST1* and *HS6ST2* (A) *XYLT1* and *B3GALT* (B), *SULF1* and *SULF2* (C) and *CSGALNACT1* and *CHPF* (D) was quantified. Data were assessed for normality with Shapiro-Wilks test (n = 3, mean ± SD, analysed with 2-way ANOVA, and corrected for multiple comparisons with Tukey's multiple comparisons test * $p \leq 0.05$, ** $p \geq 0.001$, *** $p \leq 0.001$).

Contrary to the work by Greco *et al.*[228], I found that culturing C28/I2 cells in micromass or in the presence of TGF-β1 had no significant effect on *ACAN* expression (**Figure 3.3 A**). Addition of TGF-β1 to monolayer-cultured C28/I2 cells had no significant effect on *SOX9* expression, but micromass culture significantly increased *SOX9* expression compared to monolayer cells, and this was increased further by addition of TGF-β1 to the micromass cultures. This resulted

in 2.5-fold greater *SOX9* expression in TGF-β1-treated micromasses compared to monolayer cells (**Figure 3.3 A**). There was no significant change in *COL2A1* expression with TGF-β1 treatment or micromass culture (**Figure 3.3 A**).

Finally, as TGF-β1 treatment changed the expression of genes (*XYLT1, CHPF)* involved in GAG synthesis and sulfation, the effect of TGF-β1 on sGAG accumulation in monolayer and micromass cultures was investigated using Alcian blue staining. Cultures were grown for 5 days before being fixed and stained as described previously[228] and in **2.3.4.** Culturing in micromass had no significant effect on sGAG accumulation (**Figure 3.3 B**). TGF-β1 marginally increased sGAG synthesis in both monolayer and micromass cultures, however there was no significant difference in sGAG accumulation between TGF-β1 supplemented monolayer and micromass cultures (**Figure 3.3 B**) nor were there any obvious changes to culturing phenotype observed under a microscope between TGF-β1 treated micromass cultures **(Figure 3.3 C, D)**.

Whilst TGF-β1-induced changes in sGAG accumulation were marginal (**Figure 3.3 B**), and TGF-β1 increased *SULF2* expression (**Figure 3.2 C**), thereby potentially reducing levels of 6-O-sulfation, I decided that conditions increasing expression of this gene were inappropriate for investigating the role of increased 6-O-sulfation caused by HS6ST1. Therefore, cells were not cultured with TGF-β1 in future experiments. Furthermore, due to there being no significant improvements in sGAG accumulation in non-TGF-β1-treated micromass cultures (**Figure 3.3 B**), I decided to use monolayer cultures for optimising and investigating *HS6ST1* overexpression.

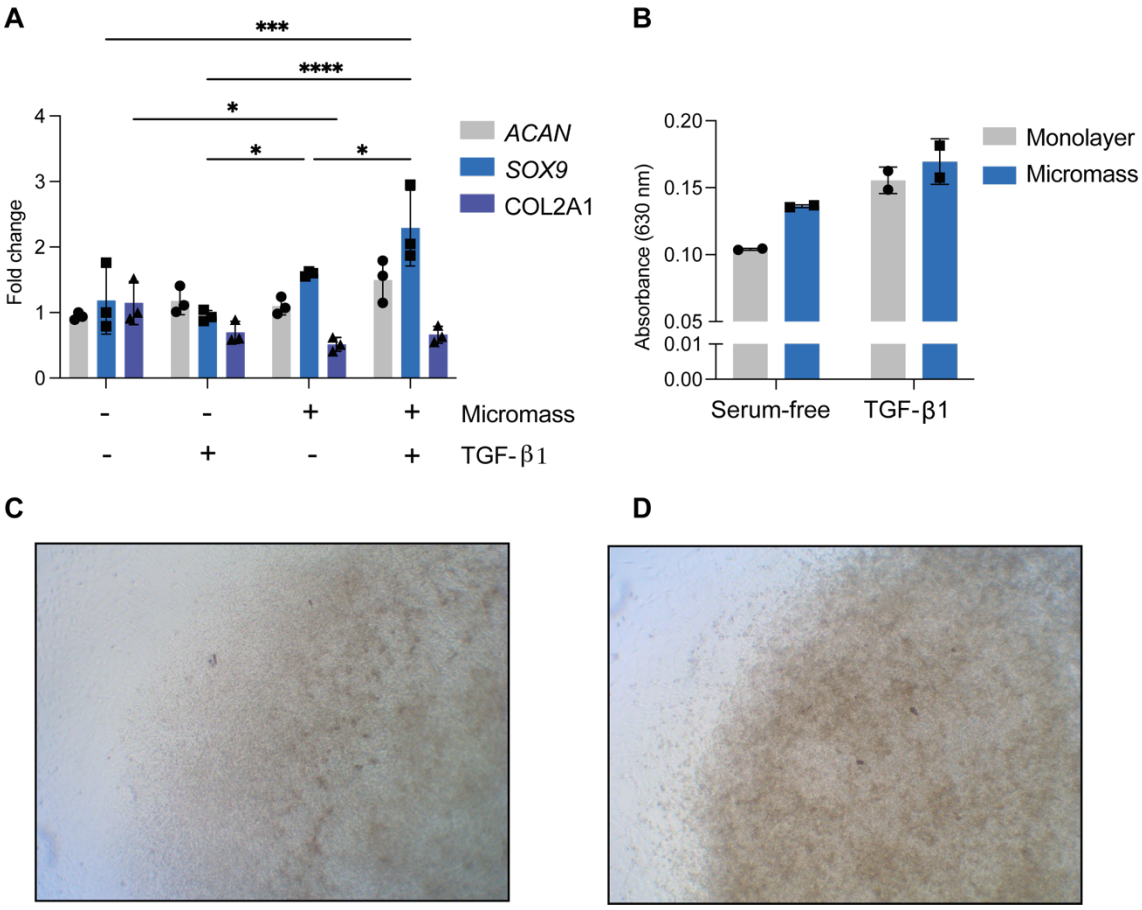

Figure 3.3 TGF-β1 has no significant effect on *ACAN* expression, but significantly increased sGAG content.

C28/I2 ($5x10^5$) cells were grown in monolayer or micromass, in serum-free media supplemented with or without 5 ng/mL TGF-β1 for 4 days. (A) RNA was extracted and reverse transcribed to cDNA. mRNA expression of *ACAN, SOX9* and *COL2A1* was analysed with RT-qPCR and normalised against the housekeeper *GAPDH* using the -ΔΔCt method and expressed relative to untreated cells grown in monolayer (B) Cells were stained for sGAG using Alcian blue and absorbance at 630 nm quantified. (C) Micromass photomicrograph after 5 days culture in serum-free medium. (D) Micromass photomicrograph after 5 days culture in serum-free medium supplemented with TGF-β1. Data were assessed for normality with Shapiro-Wilks test, ((A n = 3), (B n=2), mean ± SD, analysed with 2-way ANOVA, and corrected for multiple comparisons with Tukey's multiple comparisons test * $p \leq 0.05$, ** $p \geq 0.001$, *** $p \leq 0.001$).

3.3 Transfection with *HS6ST1*-encoding plasmid increased HS6ST1 expression for at least 96 hours.

To investigate the effect of *HS6ST1* in a cartilage cell culture model, transient transfection was utilised with an *HS6ST1*-encoding plasmid. The *HS6ST1*-encoding plasmid was commercially synthesised by GenScript based on a pcDNA3.1 (5.4 kb) backbone (**Figure 3.4 A**) and including the human *HS6ST1*-encoding sequence (1.8 kb) with a C-terminal FLAG-encoding sequence, giving a total plasmid size of 7.2 kb.

To properly discriminate effects driven by increased *HS6ST1* activity from those caused by the transfection method, the *HS6ST1*-encoding sequence was excised out using the restriction endonuclease XbaI. After incubation of the plasmid with XbaI, samples were run on a 0.5% agarose gel (**Figure 3.4 B**), and the plasmid backbone at the correct expected size (5.4 kb) was cut out of the gel, purified and religated using DNA Ligase IV. This non-*HS6ST1*-encoding plasmid, henceforth named ‘mock’, was used as a control for all future transfection experiments.

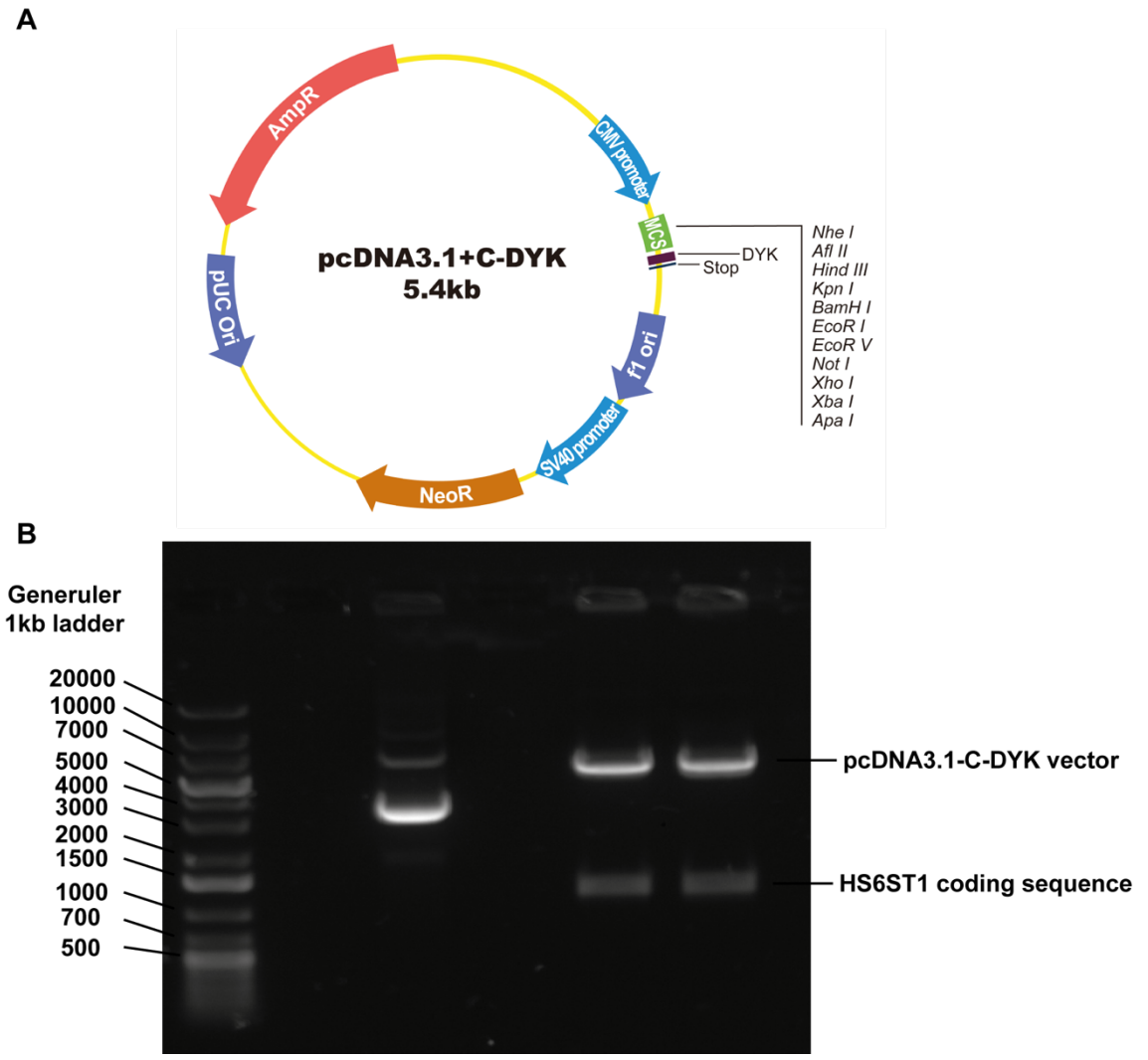

Figure 3.4 Generation of mock pcDNA3.1 vector from HS6ST1-FLAG-encoding pcDNA3.1 plasmid.

(A) Plasmid map, showing features of the pcDNA3.1 plasmid, coding for C-terminally FLAG-tagged HS6ST1 (custom synthesised by GenScript). (B) The HS6ST1 coding sequence (1.8 kb) was cut out from the plasmid using the restriction enzyme Xba I and the empty plasmid then religated using T4 DNA Ligase.

Next, the optimal amount of plasmid and method of transfection were investigated. Cells were transfected with 1 – 8 µg of plasmid (**Figure 3.5 A**) and viability was measured using MTS (**2.2.5**). Cells transfected with 2 µg of plasmid were found to have significantly increased viability 72 h post transfection while cells transfected with 8 µg of plasmid had a significant reduction in viability at this timepoint (**Figure 3.5 A**).

Next, two different transfection methods were investigated using a GFP-encoding plasmid. GFP fluorescence in transfected cells was first measured using ImageJ which allowed GFP fluorescence of the same well to be measured at both 48 h and 72 h. Using Lipofectamine 3000, maximal transfection efficiency of 20% at both 48 and 72 h was observed after transfection with 1 and 2 µg of plasmid, compared to 10 and 5% with fluorescence in cells transfected with 4 µg of plasmid at 48 and 72 h (**Figure 3.5 B**). This transfection efficiency using lipid-based reagents is comparable to that observed in other studies[228].

C28/I2 cells were transfected with a GFP-encoding plasmid using electroporation. GFP fluorescence at both 48 and 72 h was measured using ImageJ as described above, and a marked increase in fluorescence with each plasmid amount was observed (**Figure 3.5 D,E**). The percentage of cells positive for GFP fluorescence increased from 20% using Lipofectamine 3000 to 70% using electroporation (**Figure 3.5 B,D**).

Flow cytometry was then used to directly compare lipofection and electroporation. Cells were transfected with 2 µg of GFP-encoding plasmid using either Lipofectamine 3000 or electroporation, and their fluorescence measured. Compared to control, non-transfected, cells 31.8% of events measured in the Lipofectamine 3000-transfected cells were determined to fluoresce green, compared to 93.6% of events in the electroporated cells (**Figure 3.5 F**). Therefore, I determined that electroporation was the most efficient transfection method for C28/I2 cells.

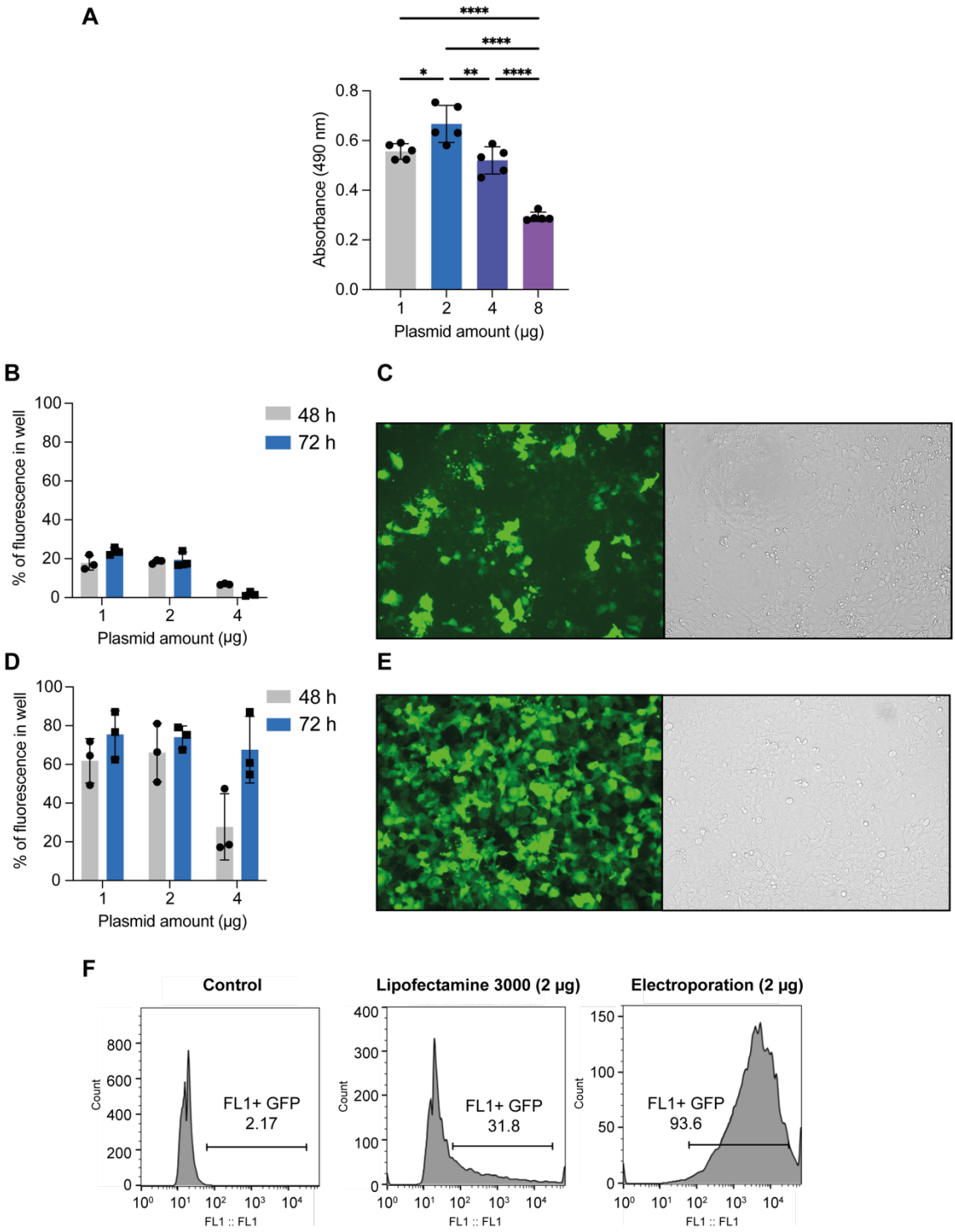

Figure 3.5 Comparison of transfection methods showed that electroporation was the most effective method for transfecting C28/I2 cells with a GFP-coding plasmid.

C28/I2 ($1x10^5$) cells were transfected with an *HS6ST1*-encoding pcDNA3.1 plasmid, cultured for 72 h, and cell viability assessed after 1 h incubation with MTs as described in **2.2.5**. (B) C28/I2 ($3x10^5$) cells were transfected with 1-4 µg of a pmaxGFP vector using Lipofectamine 3000, and GFP fluorescence as a percentage of pixel count was measured 48 and 72 h later as described in **2.2.4**. (C) Representative GFP and equivalent photomicrograph image of cells transfected with

2 µg of a GFP-encoding plasmid using lipofection. (D) C28/I2 ($1x10^6$) cells were transfected with 1-4 µg of a GFP-encoding plasmid by electroporation, and GFP fluorescence as a percentage of pixel count was measured 48 and 72 h later using ImageJ. (E) Representative GFP and equivalent photomicrograph image of cells transfected with 2 µg of a GFP-encoding plasmid using electroporation. (F) 72 h post transfection, cells were dissociated using cell dissociation solution and resuspended in PBS supplemented with 1 mM EDTA. Green fluorescence (excitation 482 nm, emission 524 nm) was measured by flow cytometry as described in **2.2.4**. Data were assessed for normality with Shapiro-Wilks test (n = 3, mean ± SD, analysed with 2-way ANOVA, and corrected for multiple comparisons with Tukey's multiple comparisons test * $p \leq 0.05$, ** $p \geq 0.001$, *** $p \leq 0.001$).

Finally, the effect of transfection on the mRNA and protein levels of *HS6ST1* was investigated using RT-qPCR and western blotting. Following transfection with 2 µg of plasmid, there was a significant increase (64-fold) in mRNA expression of *HS6ST1* at 24 h compared to mock transfected cells, Expression rapidly reduced to a non-significant 12-fold difference by 48 h (**Figure 3.6 A**).

Using an M2 anti-FLAG antibody, the levels of HS6ST1 in the conditioned medium of transfected cells was measured. A strong band was visible between 40 and 55 kDa in the *HS6ST1*-transfected samples, correlating with the predicted size of HS6ST1 of 48 kDa. This band was detectable for up to 96 h post-transfection and was not detected in mock-transfected samples (**Figure 3.6 B**). The reduction in *HS6ST1* mRNA thus did not correlate to a reduction in detectable FLAG-tagged HS6ST1 protein.

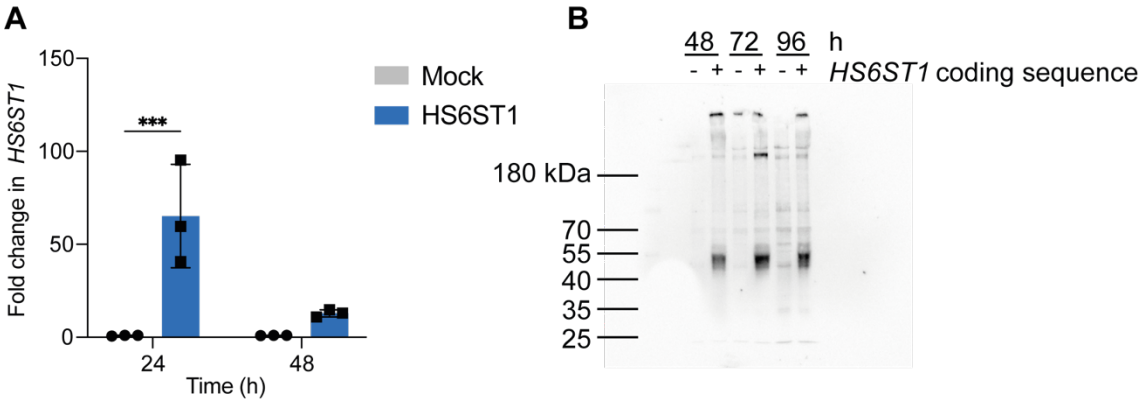

Figure 3.6 mRNA and protein expression of HS6ST1 was increased in HS6ST1-transfected cells compared to mock-transfected cells.

C28/I2 cells ($1x10^6$) were transfected with 2 μg of empty vector (mock) or HS6ST1-encoding plasmid by electroporation. After 24 or 48 h, RNA was extracted, and cDNA synthesised. The mRNA expression of *HS6ST1* was evaluated against the housekeeper *GAPDH* by RT-qPCR using the -ΔΔCt method. Expression of HS6ST1 was significantly increased in cells transfected with the HS6ST1-encoding plasmid compared to mock at 24 h, but not at 48 h. (B) Conditioned media were harvested from cells in (A), concentrated by TCA precipitation, and analysed by western blotting with an anti-FLAG M2 antibody to evaluate HS6ST1 protein expression. FLAG-tagged HS6ST1 was detected in conditioned media from HS6ST1-transfected cultures but not in mock transfected cultures at 48, 72, and 96 h post transfection. Data were assessed for normality with Shapiro-Wilks test (n = 3, mean ± SD analysed with 2-way ANOVA, and corrected for multiple comparisons with Sidak's multiple comparisons test * $p \leq 0.05$, ** $p \geq 0.001$, *** $p \leq 0.001$).

3.4 Discussion

In this Chapter, I set out to determine which cell line could be used to investigate the role of heparan sulfate in the regulation of cartilage homeostasis. I compared two different cell lines, HTB94 and C28/I2, and investigated their expression of 7 genes involved in the biosynthesis and modification of HS and 3 genes involved in cartilage anabolism. Whilst the cell lines had similar gene expression profiles overall, HTB94 cells did not express detectable levels of *ACAN* mRNA (**Figure 3.1**). In comparison, C28/I2 cells expressed detectable, albeit low, levels of *ACAN*.

Aggrecan makes up 45% of the dry weight of cartilage and is important for many of the mechanical properties of the joint[238]. The highly-negatively charged sulfate groups present on the CS chains of aggrecan draw water into the cartilage and thus allows smooth articulation of opposing bones in the joint. Loss of aggrecan is therefore a key event in the progression of OA[238]. Furthermore, as a CSPG, aggrecan likely contributes overwhelmingly to the signal observed when chondrocyte cell cultures are stained for sulfated GAG content[242] and understanding whether aggrecan is lost in response to stimuli is critical for understanding cartilage homeostasis. I thus decided that expression of aggrecan was a critical requirement for any cell line that was to be used for analysis of cartilage anabolism and therefore HTB94 cells were inappropriate for my research. C28/I2 cells were thus used for future experiments.

Articular chondrocytes rapidly lose their phenotype in monolayer culture[243–246], therefore methods to maintain their phenotype have been extensively studied. One such method involves growing articular chondrocytes or chondrocyte cell lines in micromass cultures[247,248]. Several studies have investigated using micromass culture to increase the chondrocytic phenotype of C28/I2 cells, or to investigate anabolic activity of proteins, such as agrin[249]. Therefore, I investigated whether C28/I2 cells could be made more chondrocytic by optimising culturing conditions.

Previous work by Greco *et al.* [228] showed that culturing C28/I2 cells in micromass, combined with TGF-β1 treatment increased the expression of core chondrocyte-related genes, including *ACAN*, *SOX9* and *COL2A1* and increased sulfated glycosaminoglycan accumulation. As expected, I saw increased *SOX9*

expression when C28/I2 cells were cultured in micromass, and this was further increased by TGF-β1 addition. As *SOX9* is a master regulator of chondrocyte phenotype[250] this was not unexpected and is in-line with the previously discussed work[228]. Unexpectedly, I saw no significant change in *ACAN* or *COL2A1* expression when C28/I2 cells were cultured in micromass compared to monolayer (**Figure 3.3 A**). Nor was there significant change in expression when these cells were cultured in micromass with TGF-β1. This may be partly explained by the difference in culture conditions used, as the Greco *et al.*[228] micromass cultures were supplemented with Insulin-Transferring-Selenium. Chuea *et al.*[251] showed that Insulin-Transferring-Selenium supplementation alone significantly increased *ACAN* and *COL2A1* expression in human nasal septum chondrocytes. Therefore, the lack of *ACAN* and *COL2A1* responsiveness I observed could, in part, be due to the lack of ITS supplementation.

TGF-β1 moderately increased sGAG synthesis, as indicated by increased staining with Alcian blue (**Figure 3.3 B**). This effect has been reported previously[252,253] and indicates that TGF-β1 improved the chondrocyte-like phenotype. TGF-β1 also induced expression of *XYLT1* in both monolayer and micromass cultures, as has been previously reported[254,255] . Since *XYLT1* is involved in the initial biosynthesis of both HS and CS, this could be one of the mechanisms by which TGF-β1 increased sGAG accumulation.

TGF-β1 also significantly increased expression of *SULF2* in both monolayer and micromass cultures. This is in agreement with previously published work, which showed that TGF-β1 increased *SULF1* expression[256]. Previous work on IPF lung

fibroblasts showed that knockdown of *HS6ST1* reduced TGF-β1-induced SMAD2 phosphorylation[176]. It is likely therefore that 6-O-sulfation acts as a regulator of TGF-β1 signalling, and the TGF-β1-induced expression of *SULF*, and therefore reduced 6-O-sulfation, acts to inhibit further TGF-β1 signalling. I observed that TGF-β1 induced expression of *SULF2* more than *SULF1*, which reflects the tissue-specific expression pattern of the sulfatases[205] with *SULF2* being the more highly expressed *SULF* in both C28/I2 cells (**Figure 3.1**) and chondrocytes isolated from articular cartilage[191].

So, while addition of TGF-β1 promoted slight increases in sGAG synthesis, it also markedly increased mRNA expression of *SULF2*. Increased *SULF2* expression would increase 6-O-endosulfatase activity and so lead to a reduction in heparan sulfate 6-O-sulfation. As the aim of my study was to investigate the role of increased 6-O-sulfation, adding a growth factor that induced expression of a 6-O-endosulfatase would therefore be counterproductive. Consequently, I decided against culturing in the presence of TGF-β1.

Next, transfection of *HS6ST1* was optimised. Two different transfection methods were tested, a cationic lipid-based method utilising Lipofectamine 3000, or nucleofection using a chondrocyte-specific protocol recommended by the manufacturer of the apparatus. Efficient transfection of chondrocytes has historically been poor, with transfection efficiencies ranging from single digit percentages to ~40% using lipid-based reagents[257,258]. Indeed, transfection efficiency of C28/I2 cells has only reached ~30% using lipid-based reagents[228]. Previous work on primary chondrocytes has shown that nucleofection can be significantly more efficient than lipid-based methods, with transfection efficiencies

reaching 80%[259,260]. Here, I optimised electroporation of a GFP-coding plasmid that achieved transfection efficiencies ~90%, measured using flow cytometry (Figure 3.5 **D**). This high level of transfection efficiency significantly increased mRNA expression of *HS6ST1* when cells were transfected with a FLAG-tagged *HS6ST1* coding vector. HS6ST1 was detected in the conditioned medium of transfected cells using an anti-FLAG antibody. The FLAG-tagged protein was detected in the conditioned medium of transfected cells for up to 96 h after transfection in comparison to mRNA expression where the overexpressed mRNA is undetectable after 48 h (**Figure 3.6**).

HS6ST1 is functionally active within the Golgi, where it is responsible for addition of 6-O-sulfate groups to nascent N-sulfated HS chains[261]. Here HS6ST1 could was detected in the conditioned medium of transfected cells, in agreement with previously published data by Habuchi *et al.*[262] who found that 6-O-sulfotransferase activity in HS6ST1-transfected CHO cells was detected in the conditioned medium. It is tempting to speculate that this indicates a regulatory mechanism, in which HS6ST1 is shed from the Golgi and secreted out of the cell to control the level of 6-O-sulfation on newly synthesised HS chains. This explanation is supported by a previous report, which showed 6-O-sulfation of HS was increased 2-fold when *HS6ST3* export out of the cell was inhibited by mutating its N-terminal hydrophobic domain, to prevent β-secretase activity[263]. Habuchi *et al.*[262] did not investigate whether β-secretase is also responsible for *HS6ST1* secretion out of the cells, however given the sequence similarities between the proteins (~50%), it is likely that the same mechanisms controlling *HS6ST3* secretion are also responsible for *HS6ST1* secretion[264].

In summary, I found that C28/I2 cells were a suitable cell line for investigating the role of HS6ST1 in cartilage, as they express HS- and cartilage-related genes, and I was able to reliably overexpress *HS6ST1* by electroporation. In **Chapter 4** I investigate how overexpression of HS6ST1 altered the expression of candidate genes expressed by C28/I2 cells, and what effects *HS6ST1* overexpression had on anabolic activity and responses to inflammatory stimuli.

Chapter 4. Characterisation of an *HS6ST1*-overexpression phenotype.

4.1 Introduction

Chondrocytes are surrounded by a pericellular matrix that is structurally and functionally distinct from the interterritorial matrix. The PCM serves to transduce both biochemical and biomechanical signals to the chondrocyte[34,50–52], and has been shown to be rich in HSPGs, in particular HSPG2, which colocalises with type VI collagen[35]. As discussed in **1.4.2** a number of studies have examined whether pericellular HS has protective or detrimental effect on cartilage phenotype. Loss of HS from HSPG2 following heparinase digestion significantly increased the elastic modulus of the pericellular matrix in cartilage sections[36], indicating HSPG2 may help maintain the mechanical properties of cartilage. However, most studies suggest that elevated levels of sulfated HSPGs are detrimental for cartilage. For example, loss of HSPG2 was chondroprotective in a mouse surgically-induced OA model[185], and *Ext1*-deficient mice had reduced OARSI scores at 18 months of age and following surgically-induced OA[189]. HS and HSPGs are proposed to increase protease activity in cartilage, with *Ndst1*$^{-/-}$ murine cartilage exhibiting reduced protease activity following retinoic acid treatment[265] and the HS side chains of SDC4 are thought to promote activation of a major aggrecanase, ADAMTS-5[59]. Studies on *Sulf* knockout mice suggest that reduced HS sulfation is protective, with *Sulf* knockout mice having greater cartilage loss following surgically-induced OA[151,191]. Finally, knee OA cartilage was found to have significantly increased 6-O-sulfation of HS compared to healthy cartilage, and this correlated with increased expression of *HS6ST1*[68]*.* Together, this research indicates that the pattern of sulfation on heparan sulfate is not only dysregulated in OA, and that this contributes to the loss of cartilage homeostasis in OA.

As shown in the previous chapter, transfection of C28/I2 cells with a plasmid encoding FLAG-tagged HS6ST1 resulted in detectable expression of HS6ST1 protein in the conditioned medium of transfected cells. I wanted to investigate how changes to the expression of HS6ST1 altered the phenotype of C28/I2 cells. To do this, I investigated how the sGAG content changed in response to changes in HS 6-O-sulfation, through both overexpression of *HS6ST1* and addition of recombinant SULF2. Secondly, as heparan sulfate-binding proteins have been shown to bind and are involved in regulating of the activity of a number of key proteases in cartilage (ADAMTS-5, MMP-13[53,64,230,266,267]), the activity of these proteases was investigated using both western blotting for aggrecan fragments and then fluorescence-based assays. Finally, how heparan sulfate synthesis and overexpression of HS6ST1 altered responses of C28/I2 cells to inflammatory stimuli was investigated. Several different cytokines (e.g. IL-1β [268], TNF[269], retinoic acid[270], or oncostatin M[270]) can be used to induce an OA phenotype *in vitro* - I chose to use IL-1β as it is a potent stimulus, and its mechanisms of action are well studied.

4.2 Results

4.2.1 Sulfated GAG synthesis is reduced following *HS6ST1* overexpression and is recovered by SULF2 activity.

Alcian blue staining of C28/I2 cells was optimised as a means of evaluating the effect of HS6ST1 on cartilage ECM synthesis. This dye is widely used by many research groups to measure sulfated glycosaminoglycan content of cartilaginous extracellular matrices *in vitro*[271] and *in vivo*[272]. Conversely, incorporation of sulfate groups into glycosaminoglycans (HS and CS) can be inhibited by addition of sodium chlorate[130]. Consequently, C28/I2 cells were grown in serum-free or growth medium with or without 30 mM sodium chlorate, stained for the sGAG content using Alcian blue, and staining quantified by measuring absorbance at 630 nm (**2.2.5**). As shown in **Figure 4.1**, Alcian blue staining for sGAG content significantly increased when cells were cultured in serum-containing growth media. In both serum-free and serum-containing cultures, addition of sodium chlorate significantly reduced Alcian blue staining, indicating that as expected the majority of the staining was due to the presence of CS and/or HS. The absorbance of sodium chlorate-treated serum-free cultures was still significantly higher than background binding to an empty well, indicating either that sodium chlorate only partially inhibited sGAG production, or that Alcian blue stained other highly negatively-charged structures within the ECM or cell.

The effect of *HS6ST1* overexpression on the sGAG content of C28/I2 cells was then investigated. Overexpression of *HS6ST1* significantly reduced sGAG content at both 48 and 72 h post-transfection compared to mock-transfected cells (**Figure 4.2 A**). SULF2 is able to remove the 6-O-sulfate group from heparan

sulfate[76] and should therefore counteract the effect of *HS6ST1* overexpression on sGAG production. Addition of recombinant SULF2 reversed the reduction of sGAG content in *HS6ST1*-transfected cells but had no significant effect on mock-transfected cultures (**Figure 4.2 B**).

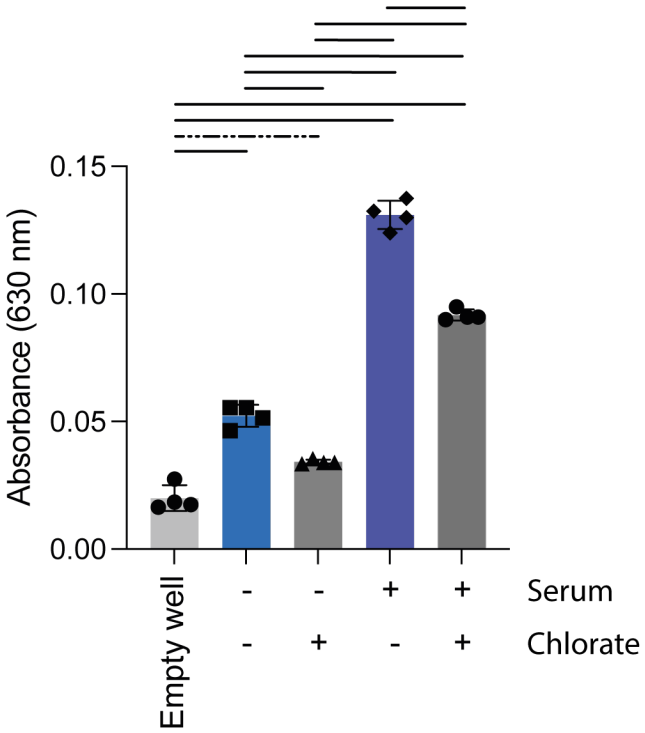

Figure 4.1 Alcian blue stained for sulfated GAGs and measured sodium chlorate inhibition of sGAG accumulation.

C28/I2 cells ($3x10^5$) were grown for 5 days in serum-free or serum-containing media with or without sodium chlorate (30 mM). Cells were fixed in methanol and stained for sGAGs with 0.5% Alcian blue. Alcian blue stain was extracted using 6 M Guanidine-HCl and absorbance at 630 nm measured on a plate reader. Data assessed for normality with Shapiro-Wilks test (n=4, mean ± SD, analysed with 2-way ANOVA, corrected for multiple comparisons with Šídák's multiple comparisons test) – – – $p < 0.05$ – – – – $p < 0.01$ —— $p < 0.001$

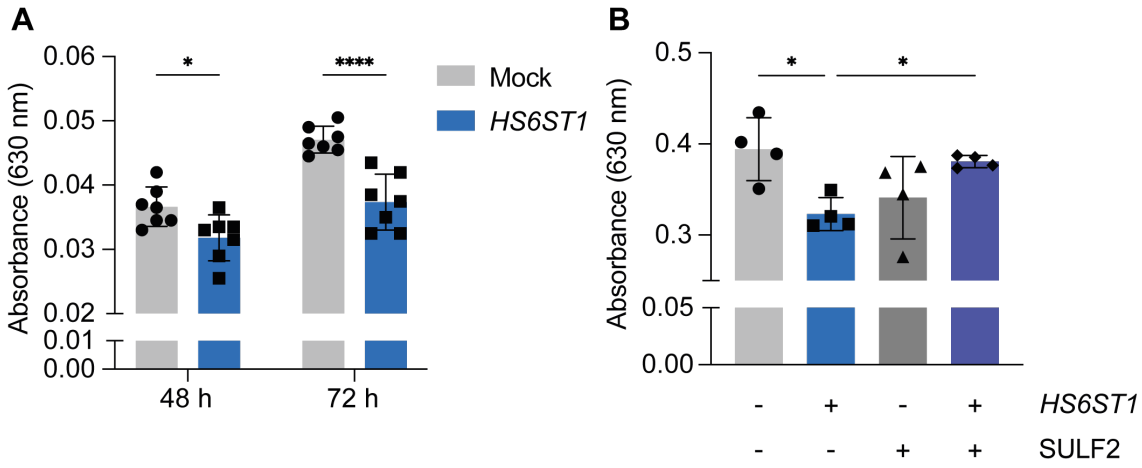

Figure 4.2 Alcian blue staining showed that *HS6ST1*-transfected cells accumulated less sulfated GAG, and this could be restored by adding recombinant SULF2.

C28/I2 cells were transfected with 2 µg of either mock or *HS6ST*-encoding plasmids and seeded at a density of $1x10^5$ / cm^2 (A) Cells were grown for 48 or 72 h and then stained for sGAG using Alcian blue (n = 7, mean ± SD analysed with 2-way ANOVA with Šídák's multiple comparisons test) or, (B) were incubated in the presence of recombinant SULF2 (3 µg/mL) for 5 days and stained for sGAG content using Alcian blue. Data assessed for normality with Shapiro-Wilks test ((A)n = 7 (B) n=4, mean ± SD, analysed with one-way ANOVA with Dunnett's multiple comparison test * $p \leq 0.05$, ** $p \geq 0.001$, *** $p \leq 0.001$).

As transfection and/or protein overexpression can be toxic to a cell, the effect of *HS6ST1* overexpression on cell growth was investigated. Overexpression of *HS6ST1* significantly increased cell growth compared to mock-transfected cells at both 48 h (**Figure 4.3 A**) and 72 h (**Figure 4.3 B**) when cells were cultured in growth medium.

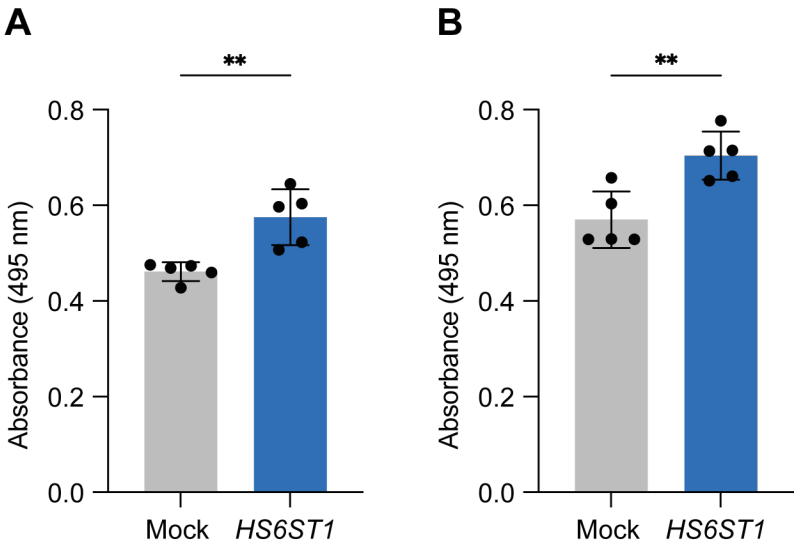

Figure 4.3 Cell viability was increased in *HS6ST1*-transfected cells.

C28/I2 ($1x10^6$) cells were transfected with 2 µg of either mock or *HS6ST1* coding plasmid and seeded ($3.1x10^5$ / cm^2) into a tissue culture plate. Cells were grown for 48 h (A) or 72 h (B) in growth medium. Media were changed to fresh growth medium supplemented with MTS reagent and incubated at 37 °C for 1 h before absorbance at 495 nm was measured. Data assessed for normality with Shapiro-Wilks test (n = 5, mean ± SD, analysed with unpaired two-tailed t-tests * $p \leq 0.05$, ** $p \geq 0.001$, *** $p \leq 0.001$)

To determine whether this effect on cell growth and sGAG accumulation was observed only when endogenous HS was altered, C28/I2 cells were treated with exogenous heparin or 6-O-desulfated heparin (100 µg/mL). Heparin- and 6-O-desulfated heparin had no significant effect on viability of C28/I2 cells (**Figure 4.4 A**). Unexpectedly, treatment with 6-O-desulfated heparin significantly reduced sGAG accumulation compared to untreated and heparin-treated cells (**Figure 4.4 B**).

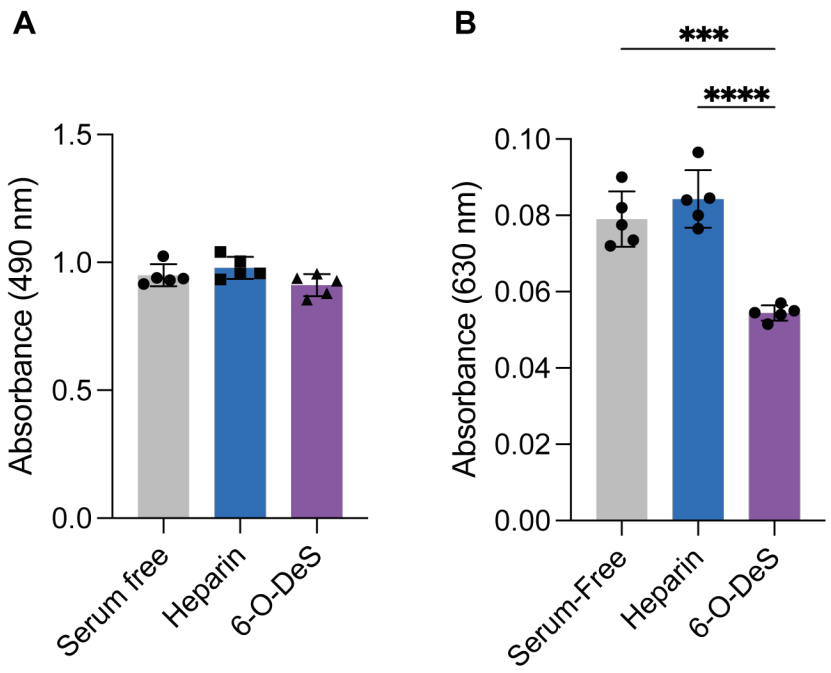

Figure 4.4 6-O-desulfated heparin reduced sGAG accumulation, but not cell viability.

(A) C28/I2 cells ($1x10^4$) were transfected with a mock- or *HS6ST1*-encoding plasmid and cultured in serum-free medium for 5 days with or without heparin- or 6-O-desulfated heparin (100 μg/mL). Viability was assessed using MTT. Data were assessed for normality with Shapiro-Wilks test, analysed with 2-way ANOVA, and corrected for multiple comparisons with Tukey's multiple comparisons test (B) C28/I2 cells ($1x10^5$) were transfected with a mock- or *HS6ST1*-encoding plasmid and cultured in serum-free medium for 5 days with or without heparin- or 6-O-desulfated heparin (100 μg/mL). Cells were fixed with methanol and stained for sGAG content using Alcian blue. The stain was extracted using 6 M Guanidine-HCl and absorbance at 630 nm was measured. Data assessed for normality with Shapiro-Wilks test, ((A, n = 5) (B, n = 5), mean ± SD, analysed with one-way ANOVA with Dunnett's multiple comparison test * $p \leq 0.05$, ** $p \geq 0.001$, *** $p \leq 0.001$).

4.2.2 C28/I2 cells synthesise protease mRNA but their aggrecanase activity was undetectable by western blotting for aggrecan fragments.

A reduction in sGAG content in cartilage is often due to the loss of aggrecan, so aggrecan cleavage in C28/I2 cells was investigated. To optimise detection of

aggrecanase activity with neo-epitope antibodies, porcine cartilage explants were stimulated with IL-1β for 24 h and the conditioned medium western blotted for the ADAMTS-generated ARGSV fragment of aggrecan. As shown in **Figure 4.5 A**, ARGSV fragments were detected in the conditioned medium of porcine cartilage explants. Cleavage of aggrecan by cultured C28/I2 cells was then investigated. C28/I2 cells stimulated with IL-1β showed no detectable release of aggrecan fragments into the conditioned medium (data not shown), potentially because of insufficient endogenous aggrecan synthesis. Therefore, the cleavage of exogenous aggrecan was examined, using a method previously develop to analyse aggrecanase activity in murine chondrocyte cell cultures[273]. As shown in **Figure 4.5 B**, addition of exogenous aggrecan (100 µg*)* did not enable detection of aggrecan cleavage products in IL-1β-stimulated C28/I2 cells.

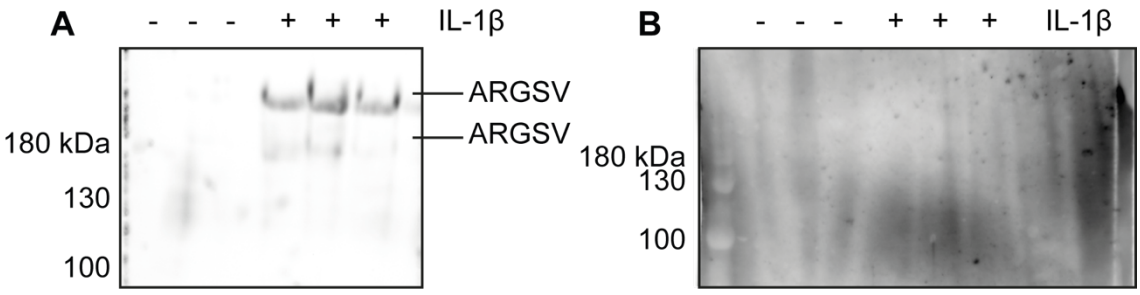

Figure 4.5 Western blotting showed IL-1β-stimulated aggrecan breakdown in porcine cartilage explants, but not in C28/I2 cells.

Porcine cartilage explants and C28/I2 cells ($1x10^6$) were stimulated with IL-1β (10 ng/mL) for 24 h. Conditioned media were deglycosylated, precipitated with acetone, and reconstituted in SDS sample buffer before electrophoresis on 6% polyacrylamide gels. Samples were western blotted for the aggrecan breakdown product ARGSV. (A) The ARGSV breakdown product was detected in IL1 β-stimulated porcine cartilage conditioned medium. (B) ARGSV fragments were not detectable in media of C28/I2 cells treated with IL-1β and 100 µg of aggrecan.

Since aggrecanase activity was not detectable in IL-1β stimulated C28/I2 cells, the expression of *MMP13*, *ADAMTS4* and *ADAMTS5* was investigated. C28/I2 cells expressed moderate amounts of *MMP13*, and lower, but detectable, levels

of *ADAMTS4* and *ADAMTS5*. Expression of these proteases was unchanged by *HS6ST1* overexpression (**Figure 4.6**).

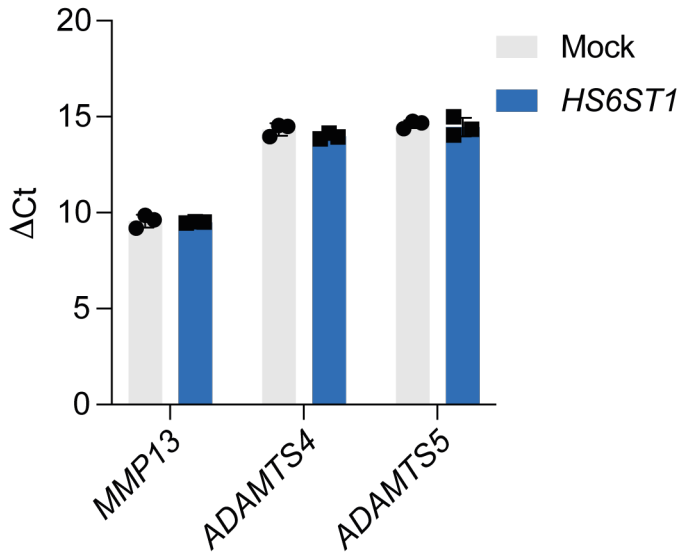

Figure 4.6 RT-qPCR analysis showed *HS6ST1*-transfected C28/I2 cells expressed *MMP13* and low levels of *ADAMTS4* and *ADAMTS5*.

C28/I2 cells ($1x10^6$) were transfected with 2 µg of either mock- or *HS6ST1*-coding plasmid and cultured for 48 h before RNA was isolated and reverse transcribed into cDNA. Expression of *MMP13*, *ADAMTS4* and *ADAMTS5* was measured by RT-qPCR and ΔCt values normalised against *GAPDH* housekeeper. Data were assessed for normality with Shapiro-Wilks test (n = 3, Mean ± SD, analysed with 2-way ANOVA, and corrected for multiple comparisons with Sidak's multiple comparisons test. * $p \leq 0.05$, ** $p \geq 0.001$, *** $p \leq 0.001$).

Expression of *MMP3* was significantly reduced by *HS6ST1* overexpression, whilst expression of *HYAL1*, an enzyme involved in the breakdown of hyaluronan, was significantly increased 24 h post-transfection, but not at 48 h. Expression of *MMP8, MMP9, HYAL2* and *CAPN* (calpain, a protease involved in aggrecan breakdown in intervertebral discs[274]) was unchanged following overexpression (**Figure 4.7**).

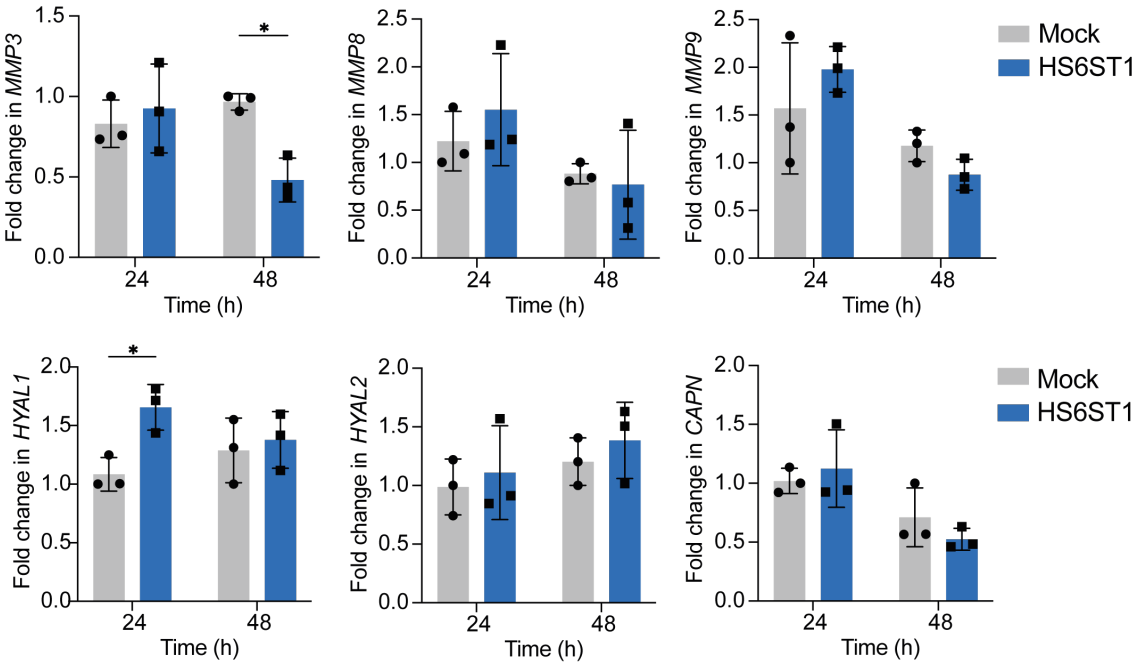

Figure 4.7 RT-qPCR analysis showed reduced *MMP3* and increased *HYAL1* expression in response to *HS6ST1* overexpression.

C28/I2 cells ($1x10^6$) were transfected with 2 ug of a mock- or an *HS6ST1*-encoding plasmid. Cells were cultured in growth medium and lysed after 24 and 48 h. RNA was extracted, cDNA synthesised, and mRNA expression of chosen genes examined using RT-qPCR. Data were normalised against the housekeeper *GAPDH* using the -ΔΔCt method and expressed relative to 24 h mock-transfected cells. Expression of *MMP3*, -8, -9, *HYAL1, -2 and CAPN* was examined. Data were assessed for normality with Shapiro-Wilks test (n = 3, mean ± SD, analysed with 2-way ANOVA, and corrected for multiple comparisons with Sidak's multiple comparisons test * $p \leq 0.05$, ** $p \geq 0.001$, *** $p \leq 0.001$).

The activity of ADAMTS-5 and MMP-13 in the conditioned medium of transfected cells was examined using fluorogenic peptide substrates. These rely on a fluorophore whose fluorescence is quenched by a quencher present on the opposite side of a cleavable bond. Cleavage of the peptide separates the quencher and the fluorophore, enabling fluorescence of the peptide to be detected. Fluorescent substrates have been used by several groups to investigate protease activity[13,26,27] and can be a more sensitive method than traditional overlay assays for quantifying protease activity[275].

As there was reduced sGAG accumulation in *HS6ST1*-transfected C28/I2 cells (**Figure 4.2**), the activity of ADAMTS-5 in the conditioned medium of transfected cells was investigated first. Abz-TESE~SRGAIY-Dpa-KK, henceforth called ADAMTS-5 substrate, was incubated with purified ADAMTS-5 as a positive control, or with conditioned medium from HS6ST1-transfected cells. Incubation of the ADAMTS-5 substrate with ADAMTS-5 significantly increased end-point fluorescence compared to a buffer control (**Figure 4.8 A**). The activity of endogenous ADAMTS-5 in the conditioned medium of transfected cells was then measured. There was very low levels of activity in media collected 48 and 72 h post transfection. Low levels of activity were detectable in media collected 96 h after transfection, but there was no significant difference in cleavage between the two samples at 96 h (**Figure 4.8 B**).

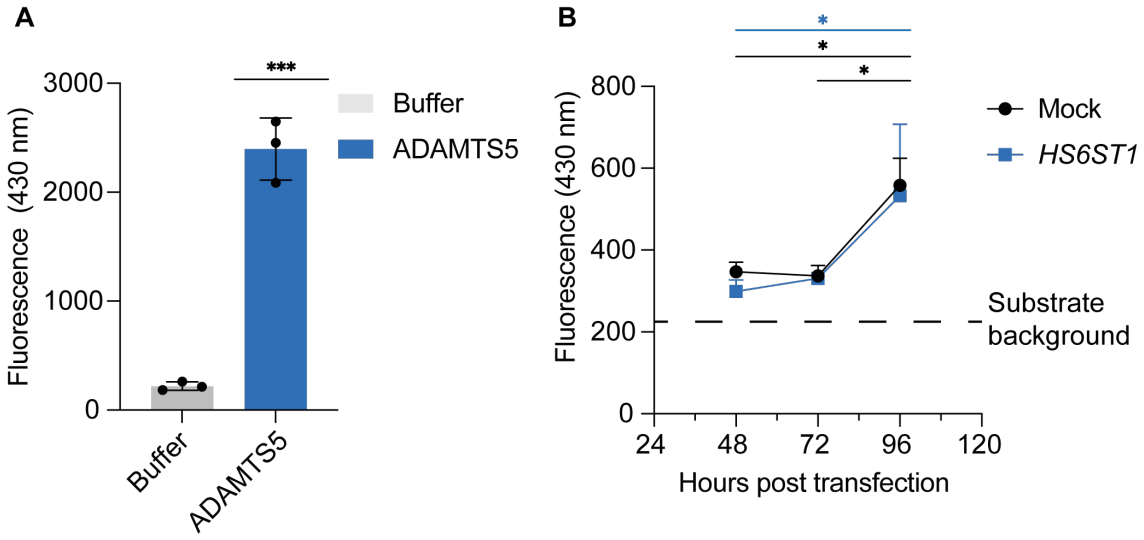

Figure 4.8 ADAMTS-5 activity was increased in the conditioned media of both mock- and HS6ST1-transfected cells 96 h post-transfection.

(A) ADAMTS-5 substrate (20 µM) was incubated with assay buffer or ADAMTS-5 (10 nM) for 24 h at 37 ºC. Endpoint fluorescence was measured. (B) 90 µL of conditioned medium from mock- or HS6ST1-transfected cells (collected 48 – 96 h after transfection) was mixed 1:1 with TNC buffer and incubated with 20 µM ADAMTS-5 substrate for 24 h before endpoint fluorescence was measured. Data assessed for normality with Shapiro-Wilks test (n = 3, mean ± SD, analysed with 2-way ANOVA, and corrected for multiple comparisons with Tukey's multiple comparisons test * $p \leq 0.05$, ** $p \geq 0.001$, *** $p \leq 0.001$. Excitation 300 nm, Emission 430 nm).

Knight substrate[229] was used to measure MMP activity in the conditioned medium of *HS6ST1*-transfected C28/I2 cells. First, Knight substrate was shown to be cleaved by recombinant MMP-13 compared to a buffer control (**Figure 4.9 A**). Next, Knight substrate was incubated with conditioned media from C28/I2 cells transfected with a mock- or *HS6ST1*-encoding plasmid. Cleavage of Knight substrate was significantly increased in mock-transfected samples collected 96 h after transfection compared to those collected after 48 h, but there was no significant difference in *HS6ST1*-transfected samples (**Figure 4.9 B**). There was also no significant difference in substrate cleavage between mock- and *HS6ST1*-transfected samples.

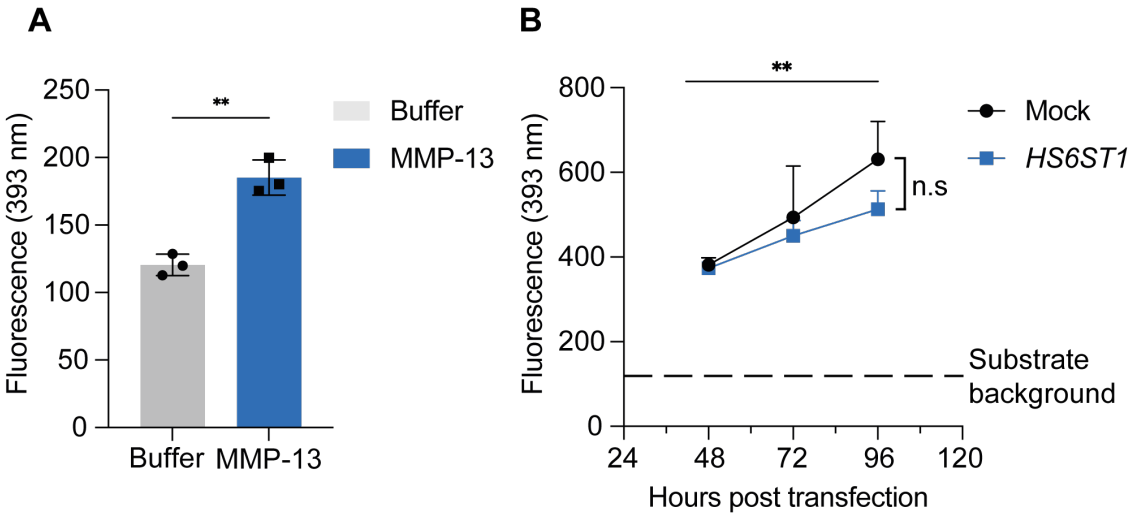

Figure 4.9 Cleavage of Knight fluorescent peptide significantly increased in mock-transfected cells 96 h post-transfection with a mock-encoding plasmid, but not with an HS6ST1-encoding plasmid.

(A) MMP-13 (3 nM) was incubated (16 h, 37 ºC) with Knight substrate (1.5 µM). (B) 100 µL of conditioned media from C28/I2 cells transfected (for 48 – 96 h) with a mock- or *HS6ST1*-coding vector were incubated with 1.5 µM Knight substrate (16 h, 37 ºC) and endpoint fluorescence measured after 16 h of incubation. Data assessed for normality with Shapiro-Wilks test (n = 3, Mean ± SD, analysed with 2-way ANOVA, and corrected for multiple comparisons with Tukey's multiple comparisons test * $p \leq 0.05$, ** $p \geq 0.001$, *** $p \leq 0.001$. Excitation 325 nm, emission 393 nm).

As there was no detectable change in cleavage of aggrecan or fluorescent protease substrates between mock- and HS6ST1-transfected samples, changes in expression of genes associated with chondrocyte phenotype were investigated.

4.2.3 HS6ST1 overexpression causes subtle but significant changes to the expression of GAG-related genes.

Changes to a particular sulfation (e.g. 6-O-sulfation) on the HS chain are often accompanied by compensatory changes in sulfation of other positions (2-, N-) on the HS chain[190], so expression of several HS biosynthesis genes was profiled

using RT-qPCR. Of the 7 genes investigated, only expression of *HS6ST2* and *GLCE* was significantly changed by HS6ST1 overexpression. *B3GALT6* expression, a gene that codes for a protein involved in both HS and CS chain synthesis, was unchanged by overexpression of *HS6ST1* (**Figure 4.10**). Similarly, expression of *HS2ST1, SULF1, SULF2* and *XYLT1* were unchanged by *HS6ST1* overexpression (data not shown).

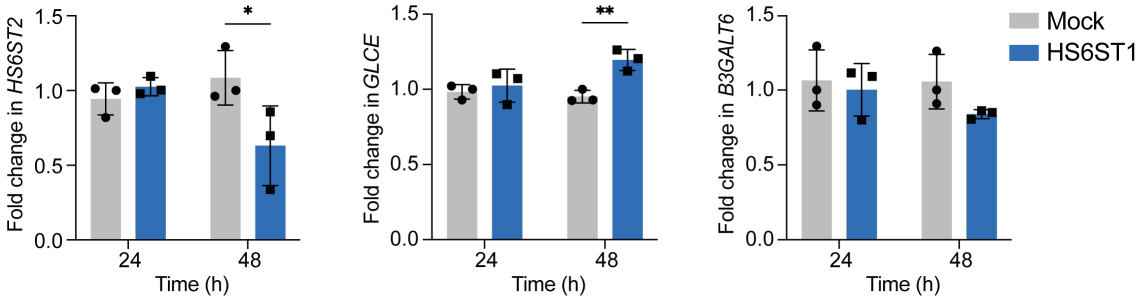

Figure 4.10 *HS6ST1* overexpression augmented expression of heparan sulfate biosynthesis genes.

C28/I2 cells ($1x10^6$) were transfected with 2 μg of either a mock- or an *HS6ST1*-encoding plasmid. Cells were cultured in growth medium and lysed after 24 and 48 h. RNA was extracted, cDNA synthesised, and mRNA expression of chosen genes examined using RT-qPCR. Data were normalised against the housekeeper *GAPDH* using the -ΔΔCt method and expressed relative to 24 h mock-transfected cells. Expression of *HS6ST2, GLCE and B3GALT7* was examined. Data were assessed for normality with Shapiro-Wilks test (n = 3, mean ± SD, analysed with 2-way ANOVA, and corrected for multiple comparisons with Sidak's multiple comparisons test * $p \leq 0.05$, ** $p \geq 0.001$, *** $p \leq 0.001$).

Finally, as there was a change in sGAG accumulation following *HS6ST1* overexpression, I investigated the expression of genes involved in chondroitin sulfate biosynthesis, as well as expression of three prototypic cartilage genes (*ACAN, SOX9 and COL2A1*) and the endocytic receptor *LRP1*. mRNA expression of the chondroitin sulfate biosynthesis genes *CHPF, CHPF2, CSGALNACT1* and expression of the chondroitin sulfate sulfotransferases

CHST3, CHST11 and CHST15 was unchanged following overexpression (**Figure 4.11**).

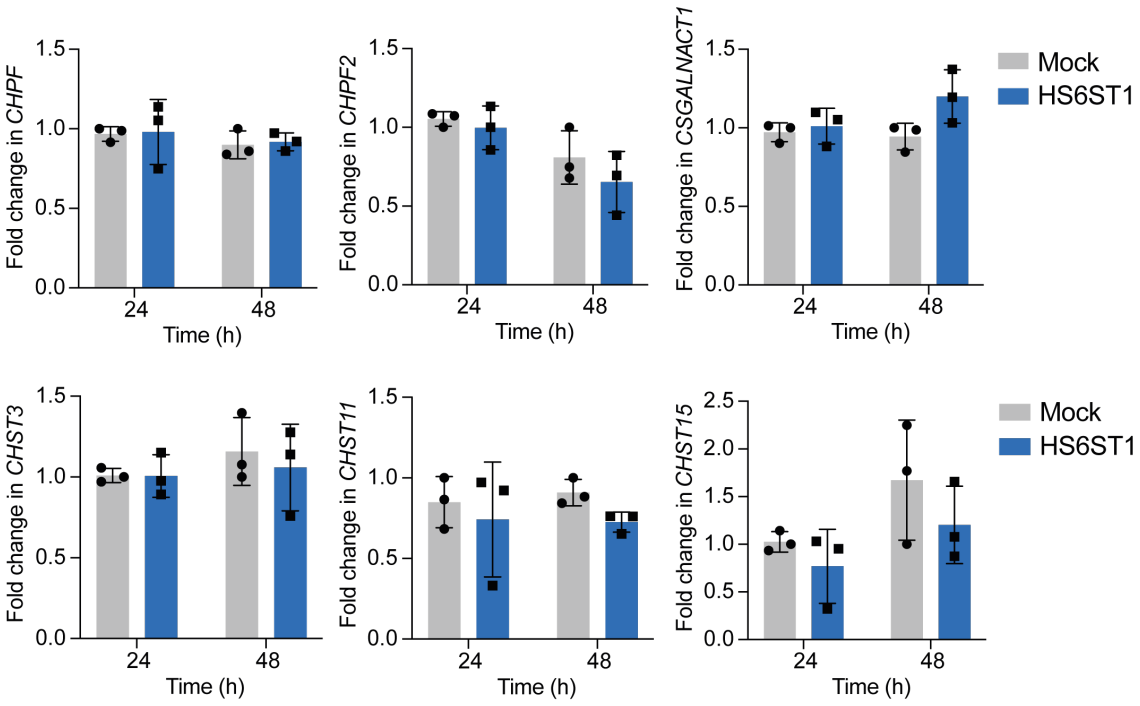

Figure 4.11 RT-qPCR analysis showed expression of chondroitin sulfate biosynthesis genes were unchanged by overexpression of HS6ST1.

C28/I2 cells ($1x10^6$) were transfected with 2 μg of either a mock- or an *HS6ST1*-encoding plasmid. Cells were cultured in growth medium and lysed after 24 and 48 h. RNA was extracted, cDNA synthesised, and mRNA expression of chosen genes examined using RT-qPCR. Data were normalised against the housekeeper *GAPDH* using the -ΔΔCt method and expressed relative to 24 h mock-transfected cells. Expression of *CHPF, CHPF2, CSGALNACT1, CHST3, CHST11* and CHST15 was examined. Data were assessed for normality with Shapiro-Wilks test (n = 3, mean ± SD, analysed with 2-way ANOVA, and corrected for multiple comparisons with Sidak's multiple comparisons test * $p \leq 0.05$, ** $p \geq 0.001$, *** $p \leq 0.001$).

Expression of *ACAN, SOX9* and *LRP1* was unchanged following HS6ST1 transfection, whereas expression of *COL2A1* was significantly reduced 48 h post-transfection (**Figure 4.12**).

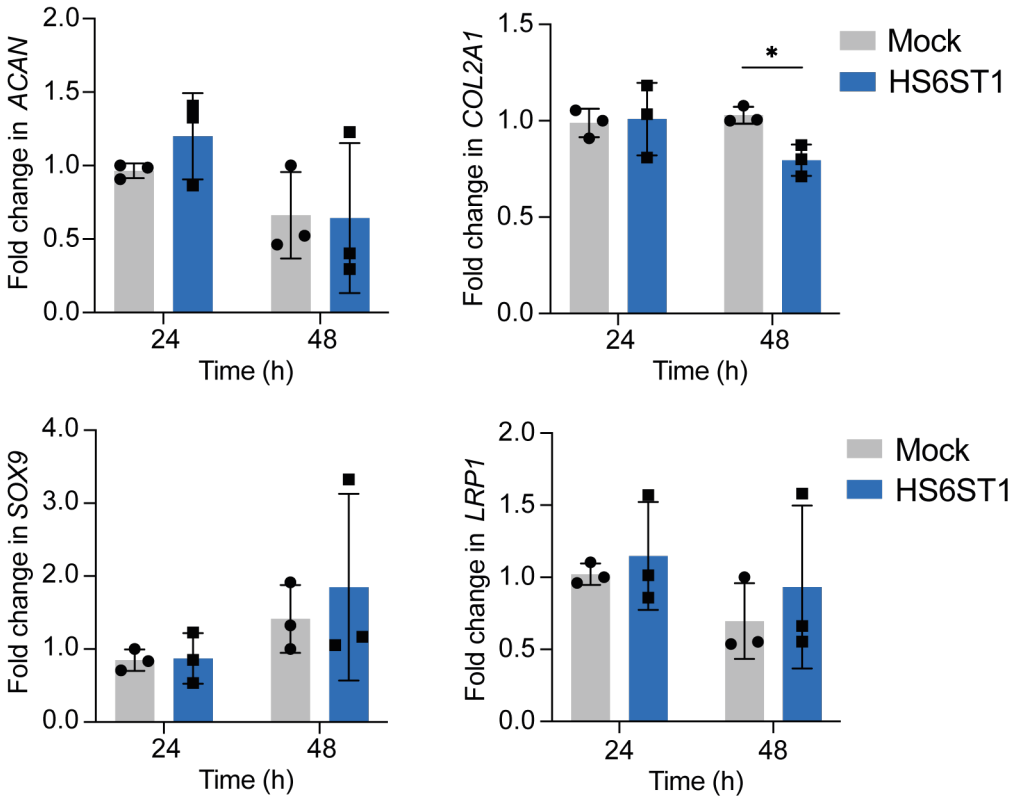

Figure 4.12 RT-qPCR analysis showed expression of *COL2A1* was significantly reduced by overexpression of *HS6ST1*.

C28/I2 cells ($1x10^6$) were transfected with 2 ug of either a mock- or an *HS6ST1*-encoding plasmid. Cells were cultured in growth medium and lysed after 24 and 48 h. RNA was extracted, cDNA synthesised, and mRNA expression of chosen genes examined using RT-qPCR. Data were normalised against the housekeeper *GAPDH* using the -ΔΔCt method and expressed relative to mock-transfected cells at 24 h. Expression of *ACAN, COL2A1, SOX9 and LRP1* was examined. Data were assessed for normality with Shapiro-Wilks test (n = 3, mean ± SD, analysed with 2-way ANOVA, and corrected for multiple comparisons with Sidak's multiple comparisons test * $p \leq 0.05$, ** $p \geq 0.001$, *** $p \leq 0.001$).

As there were no changes in basal gene expression that would explain the reduction in sGAG content in HS6ST1-transfected cells, I went on to investigate whether gene expression was altered in transfected cultures treated with an inflammatory stimulus.

4.2.4 Absence of heparan sulfate impairs IL-1β signalling

Interleukin-1β (IL-1β) is a well-studied cytokine in OA pathology. Historically, it was thought that IL-1 signalling was driven solely through protein-protein interactions, but there is some evidence that IL-1 binds to a heparan sulfate proteoglycan when the signalling complex is established[276,277]. Recently, more evidence emerged about a role for syndecan-4 in IL-1β signalling and IL1 receptor trafficking[278]. So before investigating the impact of HS6ST1 transfection on IL-1-induced changes in gene expression, the effect(s) of inhibiting HS sulfation or binding were investigated.

As shown previously, sodium chlorate can inhibit the synthesis of sulfated glycosaminoglycans (**Figure 4.1**). Therefore, to initially investigate whether IL-1 β requires sulfated GAGs to signal, C28/I2 cells were treated with sodium chlorate for 72 h and their response to IL-1β quantified. As shown in **Figure 4.13 A, B**, IL-1β significantly induced expression of *MMP13* and *IL1B*, and this induction was significantly inhibited by addition of sodium chlorate. Expression of *SULF1* was not significantly induced by IL-1β but was significantly induced by addition of sodium chlorate and sodium chlorate plus heparin.

To further investigate the impact of HS on IL-1β signalling, the small molecule heparan sulfate competitive inhibitor surfen[131] was utilised. Previous work by Schuksz *et al.*[131] showed that surfen dose-dependently inhibited FGF2-induced ERK phosphorylation with an IC_{50} of 5 μM, through competitively binding to the negatively charged sulfated groups on HS. As a confounding variable, surfen will, in sufficient quantities (75% inhibition at 7.5 μM) also inhibit the sulfation of the GAG chain[131]. To avoid this, C28/I2 cells were treated with a low concentration

of surfen (5 μM) for 16 h during serum-starvation to competitively displace endogenous heparan sulfate-binding proteins, and cells were then treated with IL-1β plus surfen (5 μM) for 6 h. Using these conditions, IL-1β significantly induced expression of *MMP13, IL1B* and *SULF1*, and this was significantly reduced by surfen treatment (**Figure 4.13 A**).

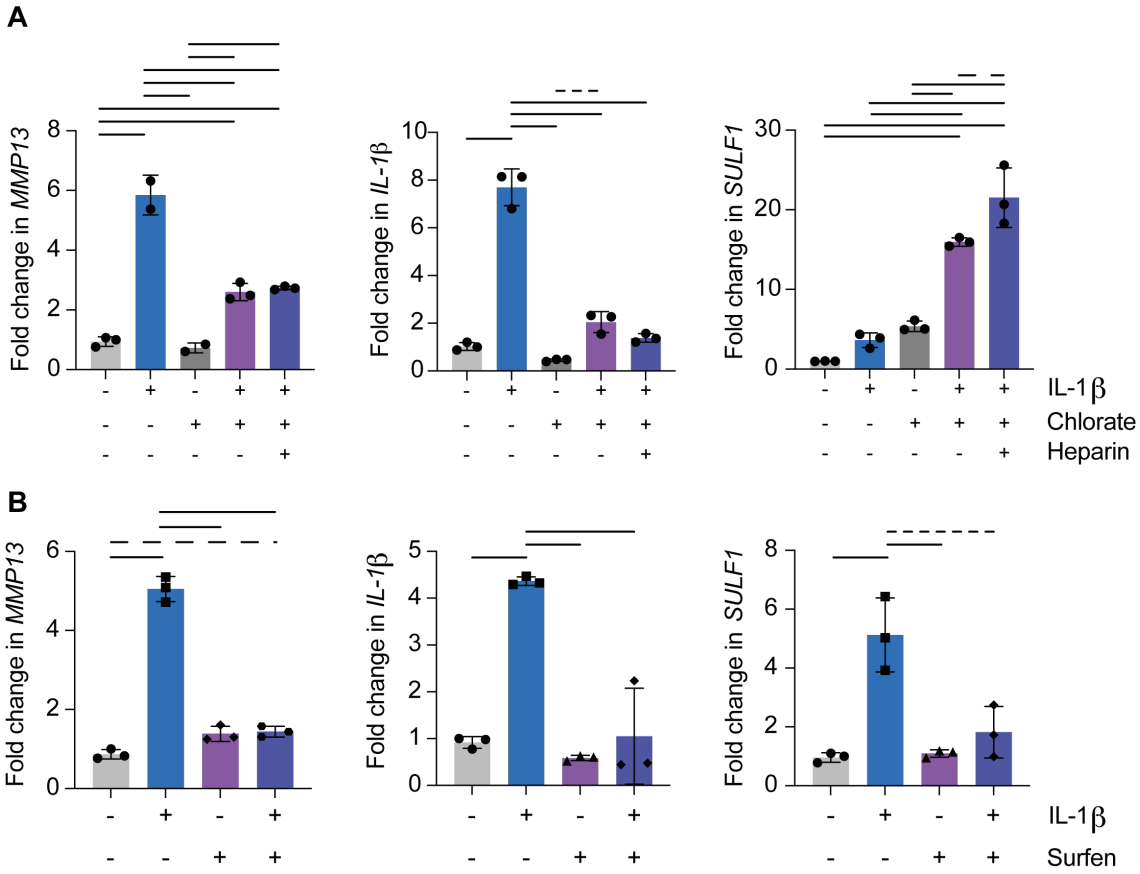

Figure 4.13 RT-qPCR showed that IL-1β-induced gene expression was dependent on heparan sulfate.

(A) C28/I2 cells ($3x10^5$) were cultured in growth medium supplemented with 30 mM sodium chlorate for 48 h. Cells were serum-starved overnight in the presence of sodium chlorate and stimulated for 6 h with IL-1β (5 ng/mL) + sodium chlorate .(B) C28/I2 cells ($3x10^5$) were cultured for 48 h in growth medium. Cells were serum-starved overnight in the presence of surfen (5 μM), and then stimulated for 6 h with IL-1β + surfen. RNA was extracted, cDNA synthesised and mRNA expression of the IL-1β-response genes *MMP13, IL1β* and *SULF1* quantified using RT-qPCR. Data were normalised against the housekeeper *GAPDH* and expressed relative to untreated cells. Data were assessed for normality with Shapiro-Wilks test ((A, n = 5) (B, n = 8) mean ± SD, analysed with 2-way ANOVA, and corrected for multiple comparisons with Tukey's multiple comparisons test)). - - - $p < 0.05$ ····· $p > 0.001$ —— $p < 0.001$

To confirm that these effects were due to modulation of IL-1β signalling and not just off-target toxic effects of sodium chlorate or surfen, mRNA expression of non-IL-1β response genes were investigated. Expression of the housekeeper *GAPDH* was unaffected by treatment with sodium chlorate or surfen (data not shown) and additionally expression of *XYLT1, B3GALT6* and *CHPF2* was unchanged by IL-1β or sodium chlorate treatment (**Figure 4.14 A**). Expression of *B3GALT6* was significantly increased when cells were treated with both IL-1β and surfen, however the effect was minimal (**Figure 4.14 B**).

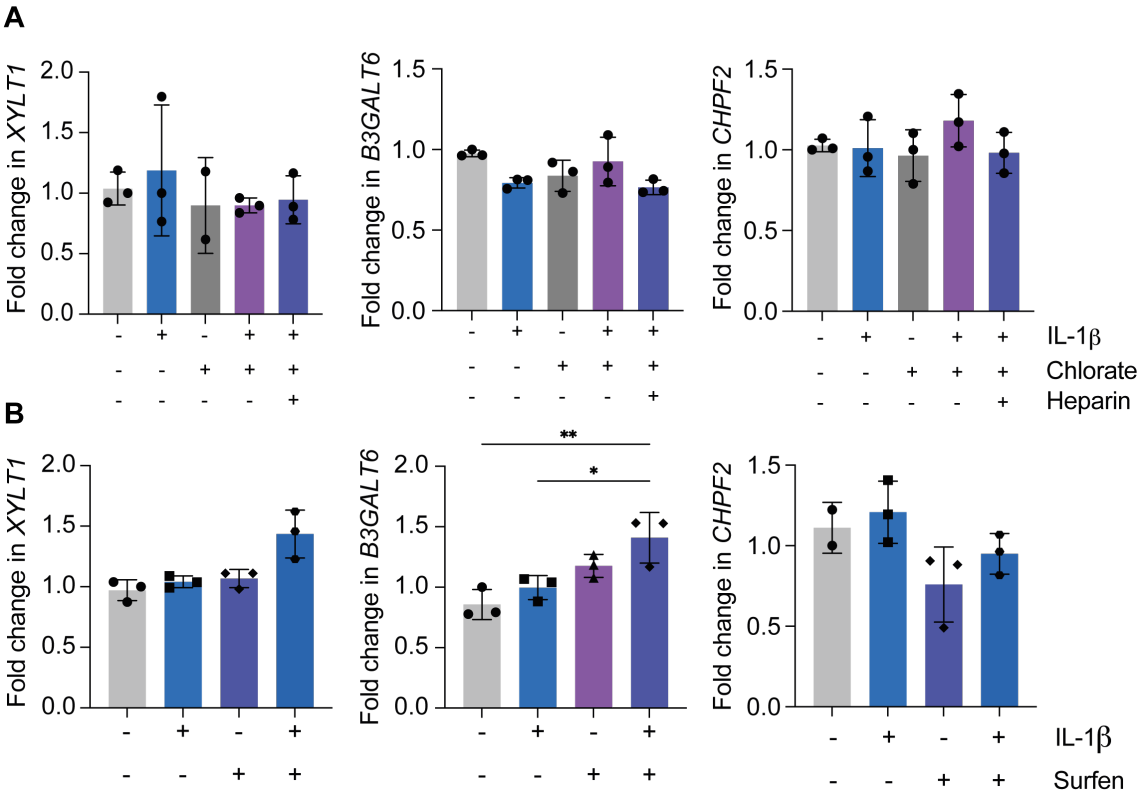

Figure 4.14 The effects of sodium chlorate and surfen are IL-1β dependent as shown by RT-qPCR.

C28/I2 cells were cultured in growth medium for 48 h before being serum-starved overnight. During culturing cells were treated with (A) sodium chlorate (30 mM) and heparin (100 μg/mL) or (B) surfen (5 uM). Cells were stimulated with 5 ng/mL IL-1β for 6 h before being lysed. RNA was extracted, cDNA synthesised, and gene expression quantified using RT-qPCR normalised against the housekeeper *GAPDH*. Data expressed relative to untreated cells. mRNA expression of *XYLT1, B3GALT6* and *CHPF2* was quantified. Data were assessed for normality with Shapiro-Wilks test ((A, n = 5) (B, n = 8) mean ± SD, analysed with 2-way ANOVA, and corrected for multiple comparisons with Tukey's multiple comparisons test. * $p \leq 0.05$, ** $p \geq 0.001$, *** $p \leq 0.001$).

4.2.5 IL-1β signals independent of HS 6-O-sulfation.

As IL-1β induction of its response genes was shown to be dependent on heparan sulfate, the role of heparan sulfate 6-O-sulfation was then investigated. C28/I2 cells were transfected with an *HS6ST1*-encoding plasmid and stimulated with IL-1β before expression of *MMP13, IL1B* and *SULF1* was examined. Compared to mock-transfected cells, there was no difference in the induction of *MMP13* and *IL1B* in response to IL-1β in the *HS6ST1*-transfected cells. There was a significant reduction in *SULF1* mRNA in IL-1β-treated *HS6ST1*-transfected cells compared to mock-transfected cells (**Figure 4.15**). Expression of *ACAN, SOX9* and *COL2A1* was unchanged by IL-1β-treatment (data not shown).

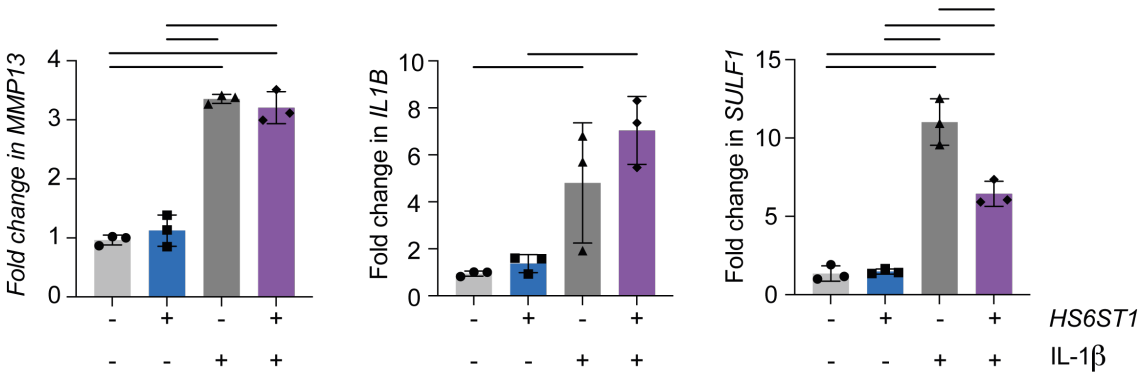

Figure 4.15 IL-1β-induced gene expression was not regulated by HS 6-O-sulfation.

C28/I2 cells ($1x10^6$) were transfected with 2 µg of either a mock- or HS6ST1-encoding plasmid. Cells were cultured for 48 h and serum-starved overnight. Cells were stimulated with IL-1β (5 ng/mL) for 6 h. RNA was extracted, cDNA synthesised, and mRNA expression of the IL-1β response genes *MMP13, IL1*β and *SULF1* quantified using RT-qPCR. Data were normalised against the housekeeper *GAPDH* and expressed relative to untreated mock-transfected cells. Data were assessed for normality with Shapiro-Wilks test. (n = 5, mean ± SD. Data analysed with 2-way ANOVA, and corrected for multiple comparisons with Tukey's multiple comparisons test)
– – – $p < 0.05$ – – $p > 0.001$ —— $p < 0.001$

The effect of IL-1β on sGAG accumulation in C28/I2 cultures was also investigated, with and without HS6ST1 overexpression. As shown previously, overexpression of HS6ST1 reduced sGAG accumulation compared to untreated mock-transfected cells (**Figure 4.16 A**). Addition of IL-1β also significantly reduced sGAG accumulation in mock-transfected cells, but this effect was lost when cells were also transfected with HS6ST1.

The observed reductions in sGAG accumulation were not due to reduced cell growth, because *HS6ST1*-transfected cells had significantly increased viability compared to mock-transfected cells, and IL-1β treatment had no significant effect on viability of mock-transfected cells (**Figure 4.16 B**).

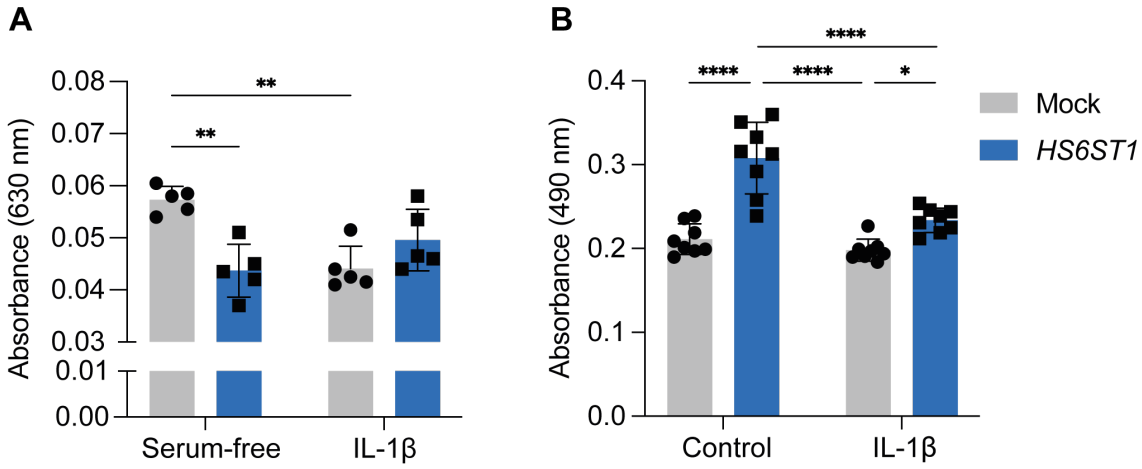

Figure 4.16 IL-1β treatment significantly reduced sGAG accumulation in mock-transfected cells, but not *HS6ST1*-transfected cells.

(A) C28/I2 cells ($1x10^5$) were transfected with a mock- or *HS6ST1*-encoding plasmid and cultured in serum-free medium for 5 days with or without IL-1β. Cells were fixed with methanol and stained for sGAG content using Alcian blue. The stain was extracted using 6 M Guanidine-HCL and absorbance at 630 nm was measured. (B) To assess effects on cell viability, C28/I2 cells ($1x10^4$) were transfected with a mock- or *HS6ST1*-encoding plasmid and cultured in serum-free medium for 5 days with or without IL-1β. Viability was assessed using MTT. Data were assessed for normality with Shapiro-Wilks test. ((A, n = 5) (B, n = 8) mean ± SD. Data analysed with 2-way ANOVA and corrected for multiple comparisons with Tukey's multiple comparisons test. * $p \leq 0.05$, ** $p \geq 0.001$, *** $p \leq 0.001$).

4.3 Discussion

In this chapter, I investigated whether overexpression of *HS6ST1* altered the phenotype of C28/I2 cells. Using Alcian blue staining to quantify sGAG accumulation (**Figure 4.1**), *HS6ST1* overexpression was shown to significantly reduce sGAG accumulation (**Figure 4.2**)., and this effect was reversed by addition of recombinant SULF2 (**Figure 4.2 B**). The reduced sGAG accumulation was not caused by cytotoxic effects of *HS6ST1* overexpression, as *HS6ST1*-transfected cells had increased viability compared to mock-transfected cells (**Figure 4.3**). Together with previous reports of increased 6-O-sulfation in OA[68] and Sulfs being protective in murine OA models[151,191] these data suggest that 6-O-sulfation has a deleterious effect in cartilage. Confoundingly, addition of a heparin oligosaccharide lacking 6-O-sulfation also significantly reduced sGAG accumulation, although a sulfated version of the oligosaccharide had no effect (**Figure 4.4**). It is unclear why there was this discrepancy in the effects of cell-associated HS and exogenously added 6-O-sulfated heparin, but it is difficult to directly compare the two experiments as heparin was added at concentrations that are likely to far exceed that of cell-associated HS, and it is additionally more highly sulfated throughout than HS.

Otsuki *et al.*[151,191] found that knockout of *Sulf1*/*2* led to spontaneous degeneration of murine articular cartilage, along with elevated *Mmp13* and *Adamts5* mRNA and protein expression, as well as reduced mRNA expression of *Col2a1* and *Acan*[151]*.* Reduced expression of *Acan* and increased protease expression provides a compelling mechanism for the spontaneous cartilage degeneration

observed in a double *Sulf1/2*$^{-/-}$ knockout mice. Others have also shown that protease expression can be altered by changes in HS structure e.g. *NDST1* knockdown or heparinase treatment reduced *MMP13* expression in smooth muscle cells[279]. Such supporting changes in expression of *ACAN*, *COL2A1* and proteases regulating their turnover were not observed here in HS6ST1-transfected C28/I2 cells. 48 h after transfection with *HS6ST1, COL2A1* expression was significantly reduced (**Figure 4.12**) but expression of *ACAN, MMP13, ADAMTS4, ADAMTS5* (**Figure 4.6**, **Figure 4.12**) was unchanged. However, there are important differences between the two studies. Primarily, the work by Otsuki *et al.*[151] involves *in vivo* analysis of global *Sulf1/2* knockout mice, whereas the experiments here were conducted *in vitro* on a cartilage-like cell line. Heparan sulfate structures *in vivo* are likely to be altered in multiple joint tissues from early foetal development, potentially altering signalling and protein expression in cells other than chondrocytes. It is tempting to speculate that such changes also contribute to the phenotype observed in their study and is an explanation for why they were not observed in this work. Secondly, overexpression of HS6ST1 and deletion of SULF2 are not entirely equivalent, as the HS domains targeted by SULFs and HS6ST1 differ. SULFs preferentially target the highly sulfated NS domains of HS (i.e. [IdoA(2S)-GlcNS(6S)][37] to form di-sulfated [IdoA(2S)-GlcNS])[75], whereas *HS6ST1* increases 6-O-sulfation on [IdoA-GlcNAc] to form [IdoA-GlcNAc(6S)] and [IdoA-GlcNS(6S)][264]. High levels of HS6ST1 expression can also cause changes in N-sulfation patterns and the domain structure of HS[280] which would not be seen in SULF-deficient conditions.

HS6ST1 overexpression led to a significant reduction in expression of *MMP3* (**Figure 4.7**), which has limited aggrecan-degrading activity and has been

proposed to contribute to ADAMTS-5 activation[267]. This observation is however inconsistent with the reported increase in both HS 6-O-sulfation[68] and *MMP3* expression in OA cartilage. Shamdani *et al*.[281] recently showed that GAGs purified from both normal and osteoarthritic cartilage significantly increased expression of MMP-3 and MMP-13 in murine chondrocytes. Interestingly, GAGs from normal and OA cartilage induced expression by different amounts, indicating altered HS structures in OA cartilage, as has been reported by others[68].

Altered activity of catabolic proteases was investigated as a possible mechanism for the reduced sGAG content in HS6ST1-overexpressing cells. Expression of *MMP13, ADAMTS4, ADAMTS5* were not altered at the mRNA level by HS6ST1-overexpression, but these proteases and their endogenous inhibitor TIMP-3 all bind to HS[62,63], and their LRP1-mediated endocytic clearance is inhibited by heparin[53], providing a potential mechanism by which altered HS 6-O-sulfation could alter their activity post-translationally. Activity of MMP-13, ADAMTS-4, ADAMTS-5 was low in C28/I2 cells, in line with a comprehensive analysis by Finger *et al.*[237] who showed that most chondrocytic cell lines express proteases at a markedly lower level than primary human chondrocytes, with protease expression in C28/I2 cells correlating best with primary chondrocytes. ADAMTS-mediated degradation of aggrecan was undetectable in conditioned media from C28/I2 cells (**Figure 4.5**) and the low levels of activity detected using a fluorescent ADAMTS-5 substrate were not significantly different in media from *HS6ST1*-transfected compared to mock-transfected cells. Similarly, low levels of MMP-13 activity in media were not significantly altered by transfection with *HS6ST1* (**Figure 4.9**). Given the low levels of activity and lack of an effect with HS6ST1 transfection, experiments with diagnostic protease inhibitors were not

conducted. One possibility for future study would be to analyse protease activity in the cell layer, since binding of MMP-13 and ADAMTS-4/-5 to HS could facilitate cell surface localisation. Concentration of the enzymes in conditioned media could be increased by treating cells with sodium chlorate, to inhibit sulfation of cell surface glycosaminoglycans. Alternatively, transfection of primary chondrocytes could be explored.

To further probe how HS6ST1 overexpression could lead to reduced sGAG accumulation, the expression of several genes involved in GAG synthesis was examined using RT-qPCR (**Figure 4.10**). HS6ST1 overexpression led to a significant reduction in *HS6ST2* expression and a significant increase in *GLCE* expression, with no significant effect on expression of the other HS biosynthesis and modifying enzymes examined (*B3GALT6, HS2ST1, XYLT1, SULF1* and *SULF2).* Furthermore, there were no changes to the expression of chondroitin sulfate biosynthesis genes (**Figure 4.11**). Changes to the expression of one HS biosynthesis enzyme can lead to changes to the abundance of sulfate groups added by other enzymes. For example, in some murine studies knockout of *Hs2st1* has been observed to increase N- and 6-O-sulfation[282], and in others to reduce total, 2-O-, and 6-O-sulfation[283]. In *HS6ST1-, HS6ST2*- or *HS6ST3*-overexpressing HEK293 cells, abundance of UA2S-GlcNS and UA2S-GlcNS(6S) disaccharides was reduced. However, Bachvarova *et al*.[283] observed no significant changes to the mRNA expression of non-2-O-sulfate modifying enzymes in *Hs2st1*$^{-/-}$ chondrocytes, despite extensive modification to 6- and N-sulfate groups. It is likely that such changes represent a regulatory mechanism to maintain the charge state of the glycosaminoglycan, but how this is regulated is unknown. A potential alternative way to investigate whether HS6ST1 reduces

synthesis of sGAG would be to analyse [^{35}S] sulfate incorporation into newly synthesised GAG chains. These Pulse-chase studies would enable monitoring of [^{35}S]-labelled sGAG incorporation into the cell layer and subsequent release into the conditioned media. This would allow conclusions to be drawn on whether HS6ST1 increases breakdown of GAG chains, or decreases synthesis of GAG, and/or their respective core proteins.

From the experiments shown here, the most likely explanation for the reduced sGAG accumulation observed with HS6ST1 overexpression is an increase in hyaluronidase activity. HYAL1 expression was significantly increased in HS6ST1-overexpressing cells at 24 h compared to mock-transfected cells (**Figure 4.10**), and this could cause loss of hyaluronan that links aggrecan core proteins in the ECM together[238]. Increased expression of *HYAL2*, but not *HYAL1*, in OA cartilage has previously been reported, but the reduced HA levels in synovium fluid of OA patients was at least partially explained by reduced *HAS2* expression in OA cartilage[284]. Further research is required to confirm the effect of HS6ST1 on HYAL1 expression at the mRNA and protein level, and to extend these findings by quantifying HA concentration and fragmentation in the conditioned medium of transfected cells[48].

Finally, the impact of inflammatory signalling on the phenotype of HS6ST1-overexpresssing C28/I2 cells was assessed. This unexpectedly showed that IL-1β-dependent changes in gene expression required sulfated HS (**Figure 4.13**), although 6-O-sulfation appeared to be dispensable (**Figure 4.15**). Although very limited, there is evidence that IL-1β is a heparan sulfate-binding protein[276] and that formation of its signalling complex requires heparan sulfate, since ligand

blotting with radiolabelled IL-1α showed the presence of a heparinase-digestible high-molecular weight form of IL-1 receptor[276,285]. More recent work showed that blocking SDC4 dimerization with a blocking antibody targeted against the SDC4 dimerization motif reduced IL1R1 trafficking and IL-1β-induced ERK phosphorylation[278].

The surface of the IL-1β/IL-1R1/IL-1RAcP signalling complex, solved by Thomas *et al*.[286] reveals potential HS-binding sites. As shown in **Figure 4.17 (A, D)** the ectodomain of IL-1R1 has a 27.9 Å basic patch located on the D1 domain, at the furthest distal point from the cell surface. IL-1β binding (**Figure 4.17 B, E**) enlarges the basic patch further to 40 Å. On the reverse side of the signalling complex, the D1 domain of IL-1RAcP contains a similar basic patch 30 Å across (**Figure 4.17 C, F**). The presence of these basic regions suggests that HS could potentially bind to the IL-1β/IL-1R1/IL-1RAcP complex, and that HS could help form or stabilise the complex.

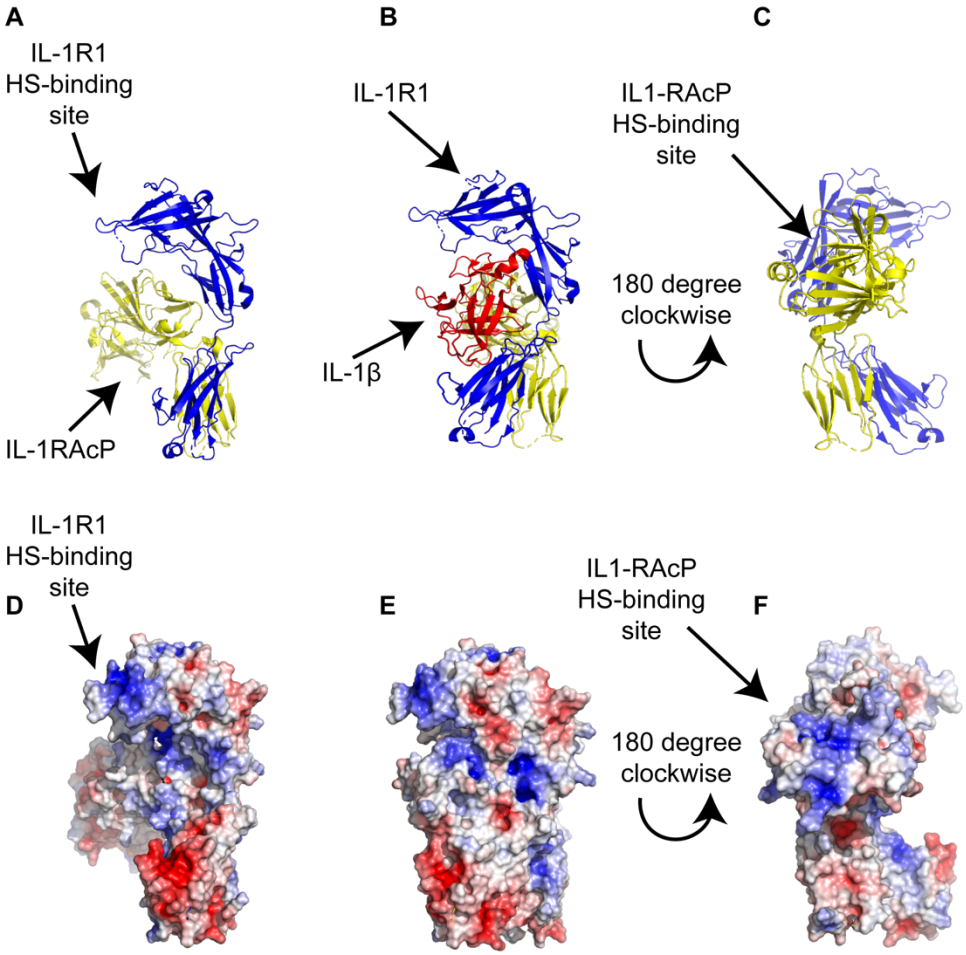

Figure 4.17 Basic patches present on the surface of IL-1R1 and IL-1RAcP are indicative of HS-binding sites.

Structure (4DEP) of the IL-1 signalling complex[287] (IL-1β (red) / IL-1R1 (blue) / IL-1RAcP (yellow)) showing ribbon structure (A, B, C) and surface charge (D, E, F) visualised in PyMOL using APBS Electrostatics plug-in [288]. (A, D) IL-1R and IL-1RAcP. Surface charge shows potential HS binding site on D1 domain of IL-1R1. (B, E) Full signalling complex of IL-1β/IL-1R/IL-1RAcP. (C, F) 180° rotation of IL-1R1 and IL-1RAcP shows potential HS binding site on the D1 domain of IL-1RAcP.

Addition of exogenous heparin to sodium chlorate-treated cells did not restore IL-1β signalling, indicating that the regulatory role for HS requires it to be bound to a core protein on the cell surface. Therefore, I propose a model for IL-1β signalling that requires endogenous HS attached to a core protein to promote receptor-cytokine interactions. Firstly, in the basal state, IL-1R1 is bound to the HS side chains of SDC4, preventing its endocytosis. This is supported by the observation that cell surface abundance of IL-1R1 is reduced in *Sdc4*$^{-/-}$ cells,

without changes in mRNA expresion[278]. I propose that IL-1β forms a trimolecular complex with the IL-1R1 and the HS chain, because IL-1β has been shown to bind to HS[278], and the IL-1R1/ IL-1β complex has a bigger basic patch than the IL-1R1 alone (27.9 to 40 Å). Interleukin-1 receptor accessory protein (IL-1RAcP) may be retained on the cell surface in a similar manner to IL-1R1, given their structural similarity and a basic patch located on the D1 domain of IL-1RAcP, similar in size (30 Å) to the basic patch located on the D1 domain of IL-1R1. Binding of IL-1β to IL-1R1 would then recruit IL-1RAcP, in a manner that may be HS-dependent. Complex formation would bring the TIR domains of IL-1R1 and IL-1RAcP into contact, enabling phosphorylation and subsequent downstream signalling through internalisation of the IL-1 receptor complex[289,290].

Lack of HS on the cell surface would lead to internalisation of the IL-1R1, and potentially IL-1RAcP, preventing IL-1β signalling. This model explains why Sdc4$^{-/-}$ mice show reduced response to IL-1β stimulation and reduced IL-1R1 expression on their cell surface[278]. It also explains how sodium chlorate and surfen inhibit IL-1β signalling. A summary of the model is shown in **Figure 4.18.**

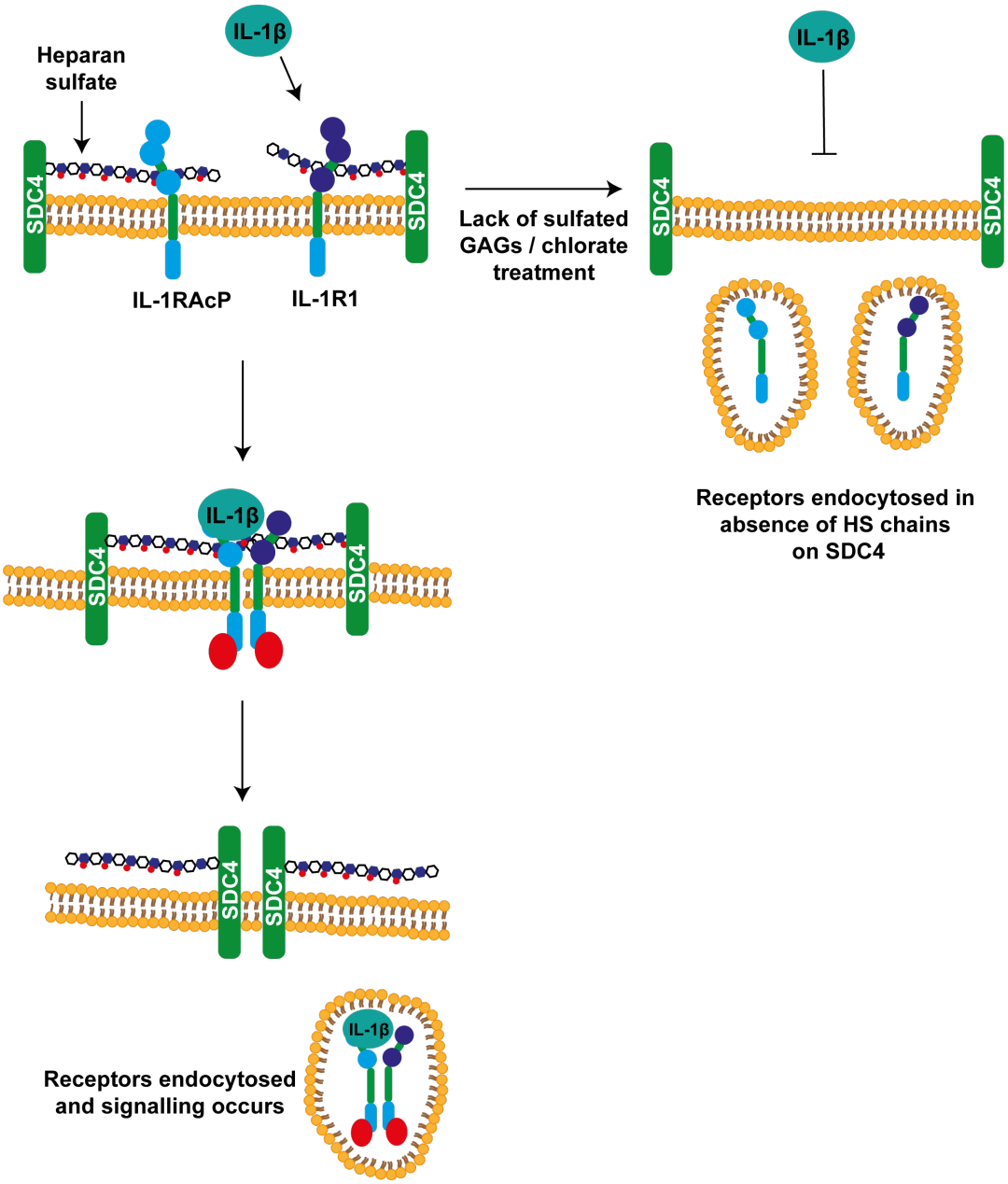

Figure 4.18 Heparan sulfate promotes IL-1R1 localisation on the cell surface and promotes IL-1β signalling.

Heparan sulfate binding retains IL-1 receptor components on the cell surface, preventing their endocytosis and promoting signalling. In the absence of HS, receptor components are endocytosed and signalling is impaired.

This model has several caveats. Primarily, there is little evidence that IL1-RAcP binds to HS, except a predicted basic patch on the surface of the protein (**Figure 4.17**). However, prevention of SDC4 dimerization using a blocking antibody inhibited IL-1β-induced signalling[278] therefore it is probable that the accessory

protein is bound to an HS chain of a second SDC4. Binding of IL-1β to the IL-1R1 and subsequent enlargement of the basic patch on the complex surface may provide sufficient charge to recruit the second HS chain that carries IL-1RAcP. It is possible that higher order complexes of the IL-1R1 form and use of a SDC4 blocking antibody prevents multiple IL-1R1 proteins, bound to SDC4 side chains, being recruited to form a higher order complex, and thus prevents signalling.

However, none of the many crystal structure of IL-1R1 and their intracellular Toll-Interleukin-like receptor domains indicates higher level oligomerisation, as all of the resolved structures in the Toll receptor superfamily show only two clustered Toll-interleukin-like receptor domains[287,291]. Furthermore, IL-1R complexes may bind to GAGs other than heparan sulfate. Many proteins that bind HS also have partial affinity for CS[292]. Therefore, as SDC4 can be substituted with CS rather than HS[293], it could be possible that CS is involved in IL-1R complex formation. A role for CS in IL-1 signalling may explain why strong IL-1β responses can be observed in tissues where CS is the predominant GAG species, such as neuronal tissue[294]. Finally, this model does not explain how addition of exogenous heparin fails to restore signalling in sodium chlorate-treated cells, as addition of exogenous heparin should prevent endocytosis in a similar manner to that observed for TIMP-3, as discussed earlier.

To further investigate how HS6ST1 overexpression caused a reduction in sGAG content, I decided to investigate proteins that preferentially bind the 6-O-sulfate group on HS using heparin chromatography and quantitative mass spectrometry, and then investigated how these proteins effect cartilage anabolism.

Chapter 5. Purification of 6-O-sulfate binding proteins from cartilage.

5.1 Introduction

In the previous chapter, I showed that *HS6ST1*-overexpressing cells accumulate fewer sGAGs. I was unable to determine whether this was due to increased protease activity, and mRNA expression of the HS- and CS-biosynthesis enzymes and *ACAN* were not reduced. Therefore, in this chapter I investigate what proteins preferentially bind the 6-O-sulfate group of HS, and whether these proteins have a role in sGAG accumulation.

A plethora of studies have shown that proteins can preferentially bind to sulfate groups of HS and that protein affinity for HS is altered by changing the abundance of particular kinds of HS sulfate groups. The most well-studied example is antithrombin III, which binds with significantly greater affinity to 3-O-sulfated HS than non-3-O-sulfated HS[295]. Some growth factors, such as FGF2, have been shown to have preference for 2-O and N-sulfated HS over 6-O-sulfated HS[133], however the influence on affinity is not as great as that for antithrombin III. The use of heparin conjugated to Sepharose beads has long been employed to purify heparin-binding proteins[134]. A basic schematic for purification of heparin-binding proteins is shown in **Figure 5.1**. Briefly, heparin is conjugated to Sepharose beads that are packed into a column. After equilibration with a suitable equilibration buffer, samples are incubated on the column and heparin-binding proteins will bind the heparin resin. These heparin-bound proteins can then be competed off the resin by applying increasing concentrations of NaCl[296]. The heparin resin can then be re-equilibrated for future usage.

Therefore, using Sepharose resins conjugated to differentially sulfated (6-O-sulfated / 6-O-desulfated) heparins is a suitable approach for purifying proteins with higher affinity for a particular kind of sulfate group. Following purification, protein abundances can be quantified using LfQ MS/MS[297] and therefore proteins with higher affinity for 6-O-sulfate groups can be identified as they are more abundant in fractions eluted from heparin-Sepharose than from 6-O-desulfated heparin-Sepharose. A similar approach has been used previously to identify novel HS-binding proteins with high affinity for 3-O-sulfate groups[135].

As a first step, I optimised protein extraction from both porcine and human cartilage extracts. Affinity chromatography was then conducted in parallel on custom-synthesised Sepharose resins coupled to heparin or selectively 6-O-desulfated heparin (IntelliHep). LfQ MS was then performed on eluted samples by collaborators (Matteo Calligaris and Simone Scilabra, RiMED, Palermo, Italy), and enabling identification of proteins with increased affinity for 6-O-sulfated heparin (ie proteins more abundant in eluates from heparin-Sepharose than from 6-O-desulfated Sepharose). Following this, the effect of two candidate 6-O-sulfate binding proteins on C28/I2 sGAG accumulation was investigated, along with assessment of how exogenous heparins modulated their activity.

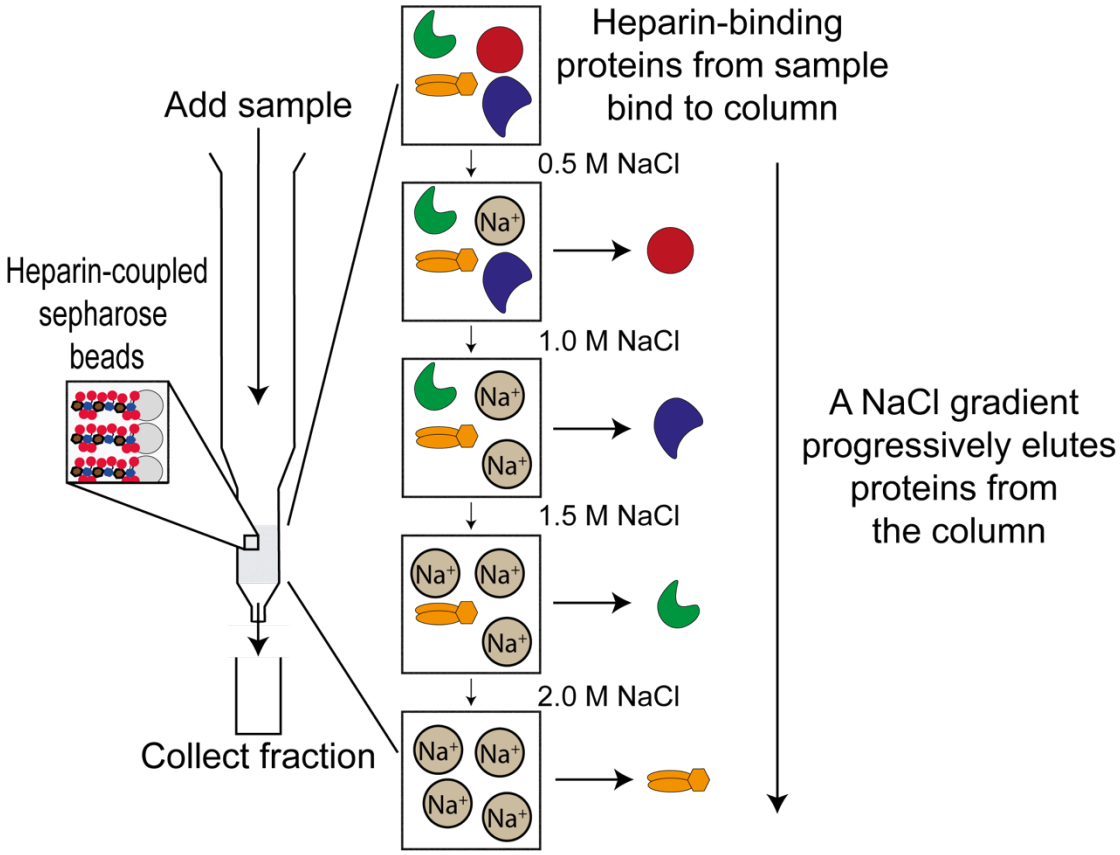

Figure 5.1 Schematic diagram showing heparin affinity chromatography workflow

1 mL of heparin-Sepharose beads were added to a Poly-Prep chromatography column reservoir and washed into equilibration buffer (50 mM Tris-HCl pH 7.4, 150 mM NaCl). Resin was removed from the column and incubated overnight at 4 °C with protein extracts from 120 mg of porcine cartilage in a 15 mL Falcon tube on a rocking platform. The resin was reloaded into the chromatography column and the flow-through was collected. The column was washed using equilibration buffer (20x column volume). Proteins were eluted from the column using a sequential concentration gradient of 0.5, 1, 1.5, 2 M of NaCl (3x1 mL fractions per NaCl concentration) in equilibration buffer. Columns were extensively washed with 2 M NaCl in equilibration buffer (20x column volume), before being re-equilibrated with equilibration buffer (20x column volume).

5.2 Results

5.2.1 Heparin affinity chromatography purifies heparin-binding proteins from cartilage extracts.

Extraction of heparan sulfate-binding proteins from cartilage was compared using four buffers: radio-immunoprecipitation assay (RIPA) buffer, Tris-HCl (0.15 M, pH 7.4), non-reducing SDS sample buffer and guanidine hydrochloride (Gdn-HCl) (**Table 2.5**). Porcine cartilage explants (120 mg) were incubated in the respective buffers, dialysed if necessary (**2.4.1**) and extracts analysed by western blotting for TIMP-3. As shown in **Figure 5.2 A**, Gdn-HCl extracted TIMP-3 most efficiently from porcine cartilage, followed by RIPA, Tris and then non-reducing SDS sample buffer. Thus, Gdn-HCl was used to extract proteins from cartilage for future experiments.

Next, purification of heparin-binding proteins on heparin-Sepharose was optimised using porcine cartilage. The efficiency of purification was again assessed by comparing purification of TIMP-3 by the two methods. Equal volumes of cartilage extract were loaded onto a heparin-Sepharose resin and incubated for 5 min (**Figure 5.2 B**) or overnight (**Figure 5.2 C**) at 4 °C. Overnight incubation of protein extracts with the resin greatly improved protein recovery. The amount of TIMP-3 in the unbound fraction reduced markedly when protein extracts were incubated with the resin overnight and this corresponded with an increase in TIMP-3 eluted from the resin by NaCl. Moderate amounts of TIMP-3 were detected in the 0.5 M NaCl fraction from samples incubated on the column for 5 min, with insubstantial amounts of TIMP-3 eluted from the column by 1 M

NaCl (**Figure 5.2 B**). Similar amounts of TIMP-3 were detected in the 0.5 M fraction of samples incubated overnight with the resin, but there was greater enrichment of TIMP-3 in the 1 M NaCl fraction after overnight incubation (**Figure 5.2 C**). Overnight incubation with resin was thus used for future experiments.

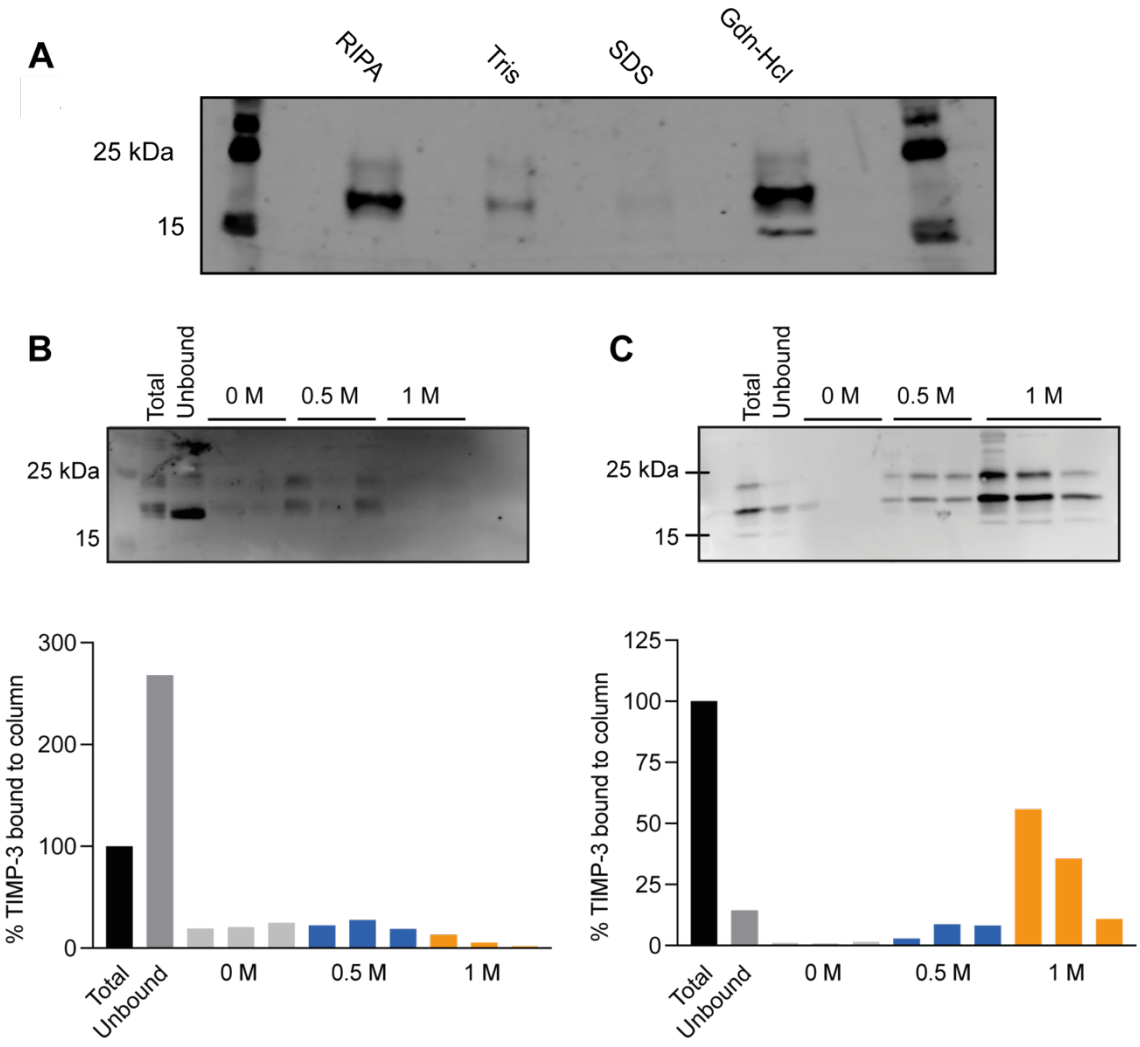

Figure 5.2 Guanidine hydrochloride and overnight column incubation most efficiently extracted and purified TIMP-3 from porcine cartilage.

(A) 120 mg of porcine cartilage was incubated overnight at 4 °C in 3 mLs of either RIPA, Tris-HCl, SDS sample buffer or guanidine hydrochloride (Gdn-HCl). Following sample clean-up by dialysis, extraction efficiency was assessed by western blotting for a known HS-binding protein, TIMP-3. Blot representative of 2 independent experiments. (B, C) Following Gdn-HCl protein extraction and clean-up, protein extracts were loaded onto heparin-Sepharose resins. Extracts were incubated for (B) 5 min or (C) overnight. Following incubation, proteins were eluted using increasing concentrations of NaCl. 10 µL of each fraction was mixed 1:1 with SDS sample buffer and electrophoresed on a 12% SDS-polyacrylamide gel, transferred to a PVDF membrane and western blotted for TIMP-3. Data were quantified by ImageJ (v1.53a)

5.2.2 De-6-O-sulfated heparin-Sepharose resins differentially purify heparin-binding proteins.

As shown in **Figure 5.2**, the use of heparin-Sepharose resin enabled efficient purification of heparin-binding proteins. Therefore, differentially sulfated heparin oligosaccharides (average mass of 14 kDa) conjugated to Sepharose beads should be able to effectively purify proteins with preferential affinity for a particular kind of sulfate group. For example, a similar approach of using differentially sulfated heparins was used by Thacker *et al.*[135], who applied conditioned media from HEK293 cells to heparin-Sepharose and 3-O-desulfated heparin-Sepharose. By comparing which proteins bound to each resin, they were able to identify novel 3-O-sulfate-binding ligands.

Here, a similar workflow was developed using heparin-, and 6-O-desulfated heparin-Sepharose resins, as shown in **Figure 5.3.** These resins were custom-synthesised by our commercial collaborators, IntelliHep. Cartilage protein extracts were loaded onto respective resins and eluted using 0.5, 1, 1.5 and 2 M NaCl in equilibration buffer. Comparison of column eluates allowed identification of proteins whose affinity for heparin was altered by the absence of 6-O-sulfation, as shown in **Figure 5.4** as indicated by white stars. Several bands were observed in samples eluted by 0.5 M NaCl from the heparin-Sepharose resin but not the 6-O-desulfated heparin-Sepharose resin. These proteins have higher affinity for 6-O-sulfated heparin.

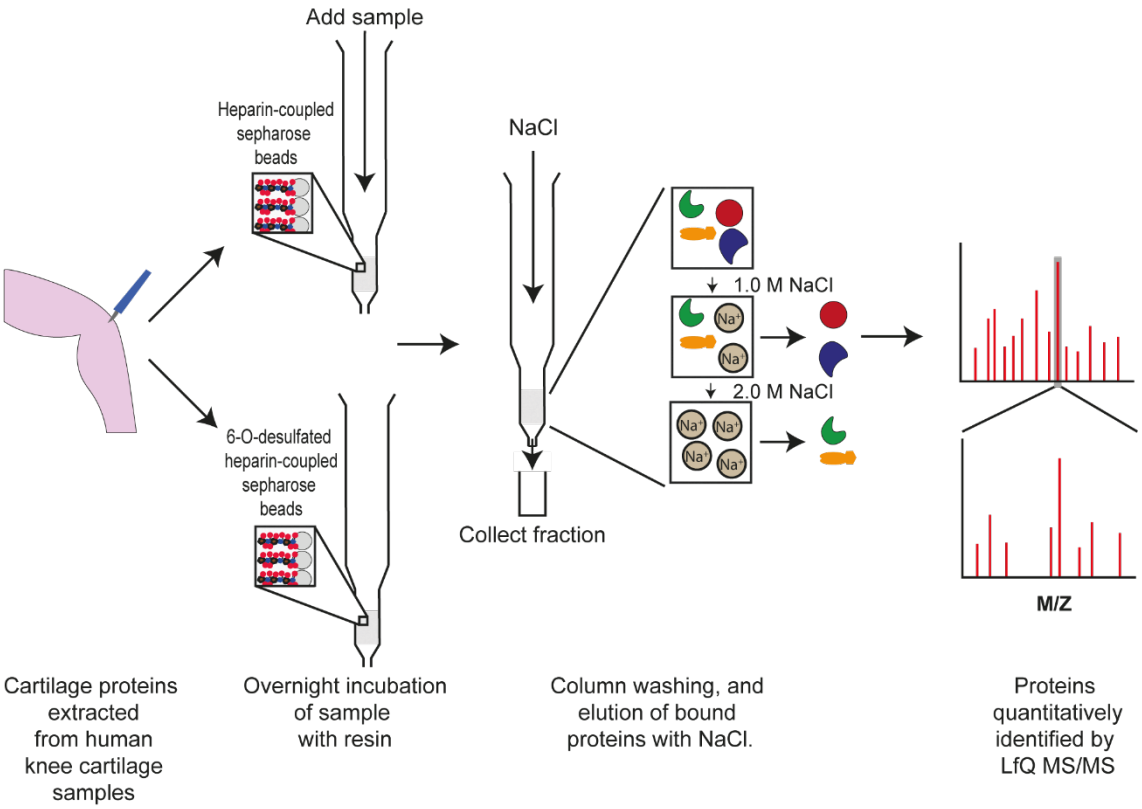

Figure 5.3 Sample workflow for mass spectrometry sample preparation.

Proteins were extracted from human cartilage extracts (120 mg) using Gdn-HCl (**2.4.1**) and incubated overnight on custom heparin-, or 6-O-desulfated heparin-Sepharose resins. Following column washing, proteins were eluted with 1 and 2 M NaCl in equilibration buffer. Proteins eluted in the 1 M NaCl fraction were analysed by LfQ MS.

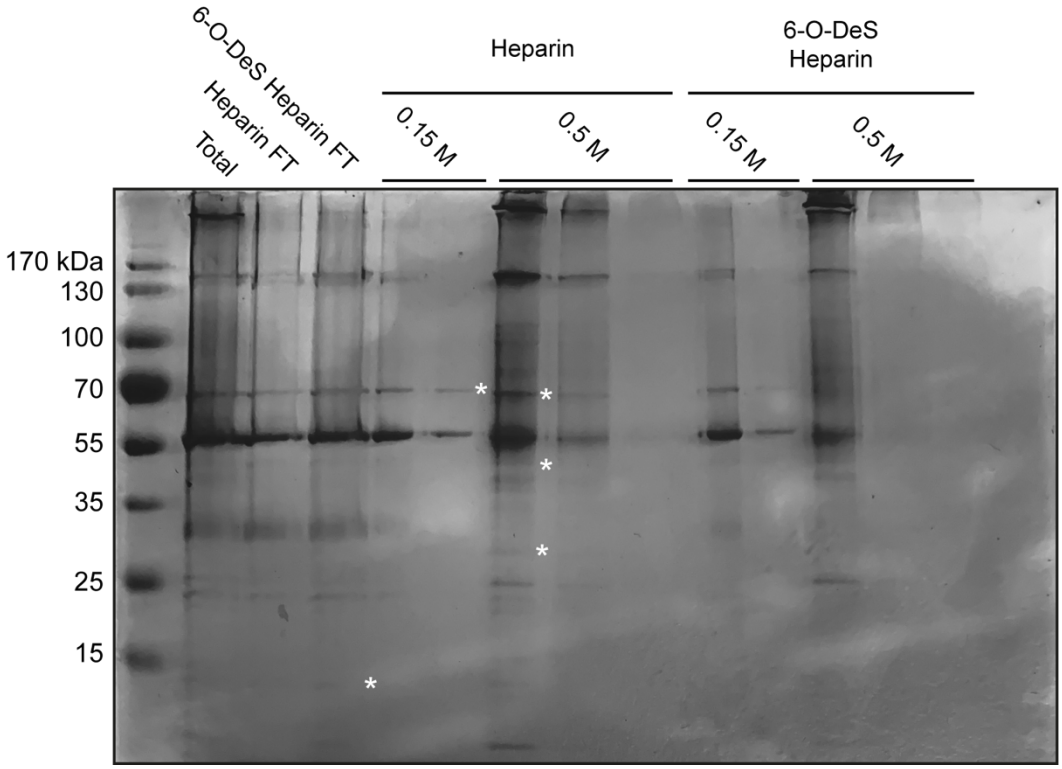

Figure 5.4 Comparison of eluates from heparin- and 6-O-desulfated heparin-Sepharose resins using Coomassie blue staining.

Porcine cartilage (120 mg) extracts were incubated overnight on heparin or 6-O-desulfated heparin-Sepharose resins. Flow through fractions were collected, and columns were washed with 50 mM Tris-HCl, 150 mM NaCl. Proteins were then sequentially eluted using a 0.5, 1 and 2 M NaCl gradient in equilibration buffer. The flow through, 0.15 M and 0.5 M fractions were electrophoresed on a 12% SDS-polyacrylamide gel and stained using Coomassie Blue. White stars indicate bands that are present in the eluates from heparin-Sepharose, but not 6-O-desulfated heparin-Sepharose.

Next, purification of heparin-binding proteins from human cartilage was investigated. Cartilage from only 1 healthy donor (and subsequently one osteoarthritic donor) was used for this hypothesis generating experiment, as discussed in the chapter Discussion.

An extract from knee cartilage (960 mg) from 1 healthy donor (68, male, cause of death reported as cardiopulmonary arrest, no clinical history of joint disease or arthritis, see **2.1.2**) was prepared by incubation in Gdn-HCl overnight and

dialysed as described in **2.4.1**. The extract was split into 8 aliquots (i.e. from 120 mg of cartilage each), with 4 aliquots applied to parallel heparin-Sepharose resins and 4 aliquots to 6-O-desulfated heparin-Sepharose resins (n=4 technical replicates for each resin). Proteins were eluted as described in **Figure 5.3**.

As an initial quality control step, eluates were analysed for two (TIMP-3 and FGF2) well-studied cartilage-relevant proteins by western blotting. Both TIMP-3 and FGF2 are known to bind HS[53,199] and play important roles within the joint. As shown in

A, the heparin-Sepharose resin bound significantly more TIMP-3 than the 6-O-desulfated heparin-Sepharose resin, as shown by western blotting indicating more TIMP-3 in the heparin-Sepharose eluates than the 6-O-desulfated eluates. FGF2 was not expected to bind significantly differently to 6-O-desulfated HS[96] and there was no significant difference in elution of FGF2 from the columns (

B).

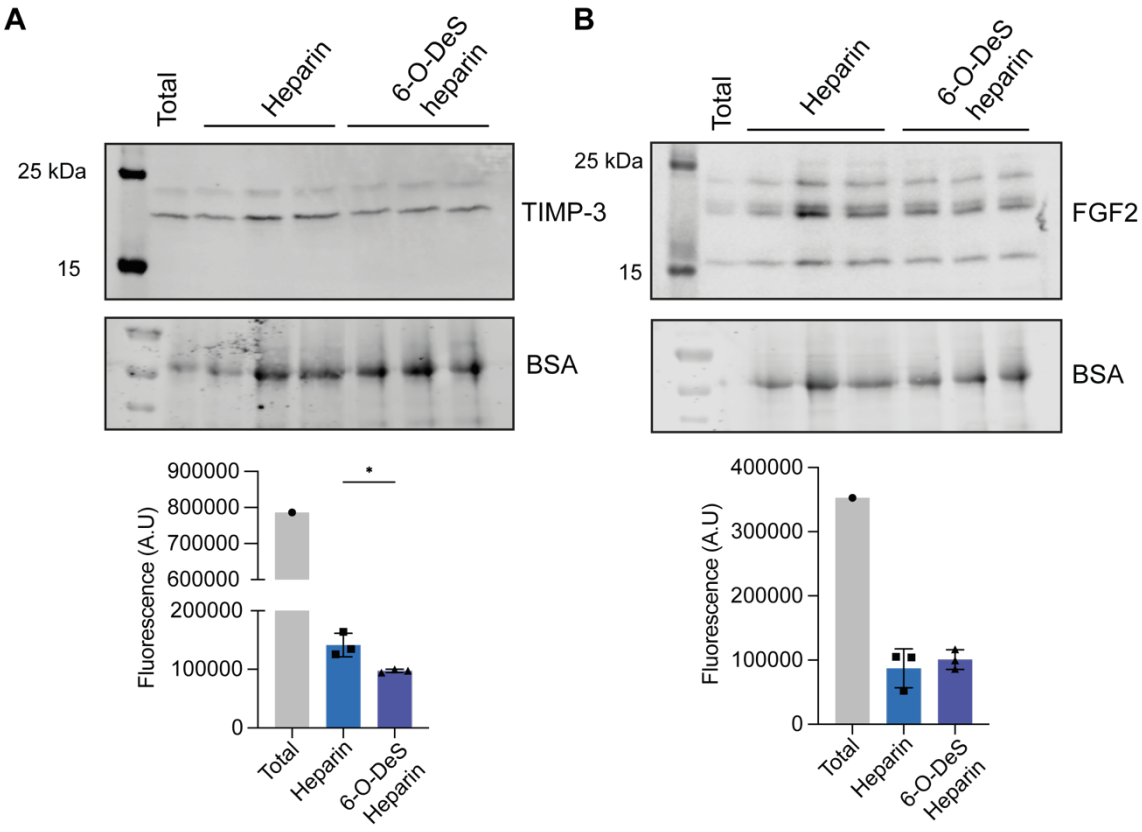

Figure 5.5 Heparin and 6-O-desulfated heparin resins differentially bound TIMP-3 but not FGF2.

960 mg of human normal knee cartilage extracts were incubated overnight with Gdn-HCl (6 M, 7 mL). and the extract dialysed against 50 mM Tris-HCl, 150 mM NaCl (pH 7.4). Dialysed extracts were split into 8 equal volumes and incubated with equilibrated heparin-Sepharose and 6-O-desulfated heparin-Sepharose resins, and bound proteins were eluted with 1 M NaCl in equilibration buffer. Fractions were electrophoresed on a 12% SDS-polyacrylamide gel, transferred to PVDF and analysed for (A) TIMP-3 or (B) FGF2. (n = 3, mean ± SD, analysed using paired t-test. * $p < 0.05$, ** $p < 0.001$, *** $p < 0.001$).

Having shown differential protein binding to the heparin- and 6-O-desulfated heparin-Sepharose as expected, the experiment was repeated on cartilage from one donor with osteoarthritis (68, male, case of death reported as cardiopulmanory embolism, clinical history of OA, see **2.1.2**) as described in **2.4.1.** Normal and osteoarthritic eluates (1 M) were sent to our collaborators, Matteo Calligaris and Simone Scilabra (RiMED, Palermo, Sicily) for LfQ MS analysis to compare protein abundance in the eluates and so identify proteins that preferentially bound 6O-sulfated heparin.

5.2.3 Label-free quantitative mass spectrometry identifies proteins that preferentially bind to 6-O-sulfated heparin-Sepharose in healthy and osteoarthritic cartilage.

The use of mass spectrometry to identify novel heparin binding proteins has previously been employed by numerous research groups[70,135,298,299]. Here, proteins from healthy (n=1) and osteoarthritic (n=1) human cartilage samples that bound to heparin- and 6-O-desulfated heparin-Sepharose were analysed by LfQ MS.

From the healthy cartilage sample, 641 unique proteins were identified and quantified (**Figure 5.6**). Of these, 88 were identified to be of significantly different abundance in the 2 eluates After applying an FDR of 1% (**Figure 5.6**, black lines), 9 proteins retained significance (**Table 5.1**), with 3 proteins binding more strongly to 6-O-desulfated heparin-Sepharose, and 6 proteins binding more strongly to the heparin-Sepharose, thus have higher affinity for 6-O-sulfated heparin. According to Uniprot (2022_02), of the 9 proteins, 3 are secreted type XVIII collagen (COLXVIII), latent TGF-β binding protein 2 (LTBP2) and C-X-C motif chemokine 10 (CXCL10) and the remaining proteins are RNA/DNA binding proteins. COLXVIII had the largest change in abundance of the three secreted proteins with a Log_2fold (heparin/6-O-desulfated heparin) change of 1.16 equating to a fold change of 2.23 vs a Log2fold change of 1.12 for LTBP2 (2.17) and 1.05 (2.07) for CXCL10. Interestingly, COLXVIII is itself an HSPG with three isoforms [300].

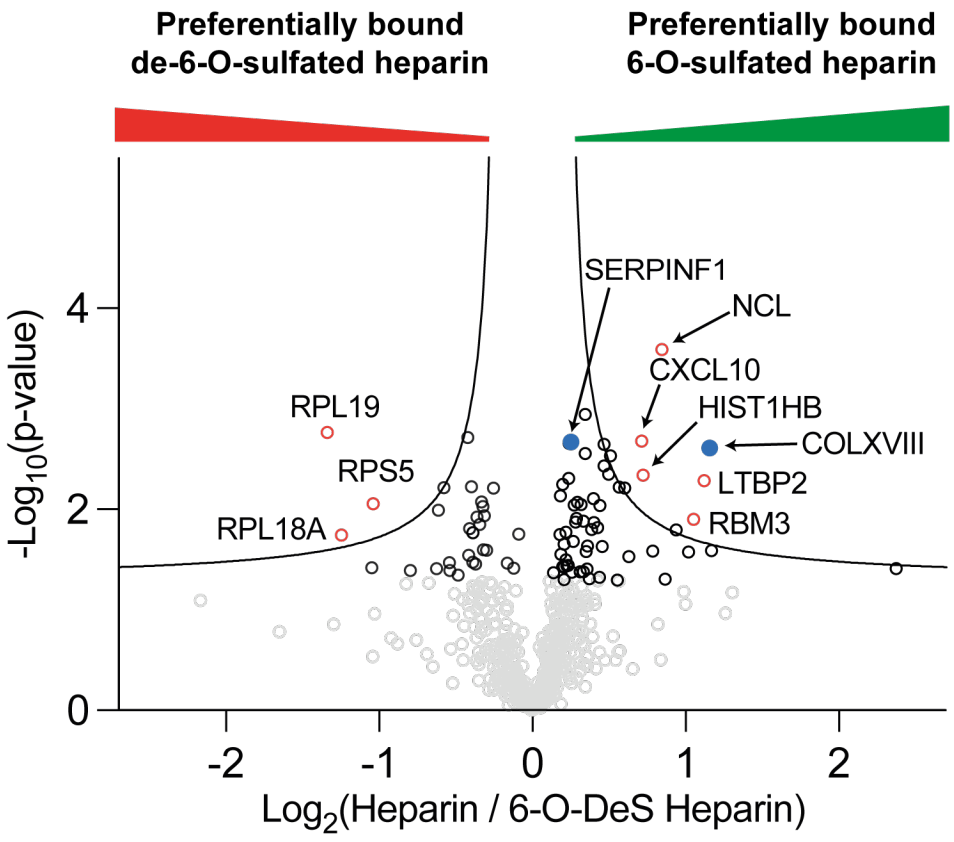

Figure 5.6 Volcano plot showing LfQ MS of proteins from healthy human articular cartilage affinity purified on heparin- and 6-O-desulfated heparin-Sepharose.

Proteins eluting from heparin- and 6-O-desulfated heparin-Sepharose resins were analysed using LfQ MS. Data were analysed with MaxQuant against a *Homo sapiens* reference proteome. FDR was set at 1% (n = 4 technical replicates from 1 donor with no clinical history of OA, statistical analysis was performed as described in **2.4.4**).

Table 5.1 LfQ MS identified 9 proteins from human normal cartilage with significantly(FDR > 1%) different abundance in eluates from heparin- and 6-O-desulfated heparin-Sepharose.

Protein	Log_2 (abundance in heparin/6-O-desulfated heparin)	Localisation (UniProt)	p-value
Type XVIII collagen	1.16	Extracellular	0.0024547
Latent TGF-β binding protein	1.12	Extracellular	0.0051404
RNA binding motif protein 3	1.05	Nucleus, Cytoplasm, Cell surface	0.0124092
Nucleolin	0.85	Nucleolus	0.0002547
Histone gene cluster 1, H1	0.72	Nucleus	0.0045175
C-X-C motif chemokine ligand 10	0.71	Extracellular	0.0020816
Ribosomal protein S5	-1.03	Nucleus, Cytoplasm	0.0087796
Ribosomal protein L18a	-1.24	Ribosome	0.0180301
Ribosomal protein L19	-1.33	Ribosome	0.0017143

As the abundance of numerous proteins changes in osteoarthritic cartilage[301], a similar analysis was also conducted using osteoarthritic cartilage (**Figure 5.7**). 622 proteins were identified in the osteoarthritic cartilage samples, of which 69 proteins were significantly changed ($p < 0.05$), and 9 proteins were below the FDR threshold (1%). Of the 9 proteins (**Table 5.2**), 5 proteins bound more strongly to the heparin-Sepharose resin, and 4 proteins bound more strongly to the 6-O-desulfated heparin-Sepharose resin. 3 of the 9 proteins are secreted

[COLXVIII, LTBP2 and Gelsolin (GSN), which bound more strongly to heparin-Sepharose] and the remaining 6 are RNA/DNA-binding proteins.

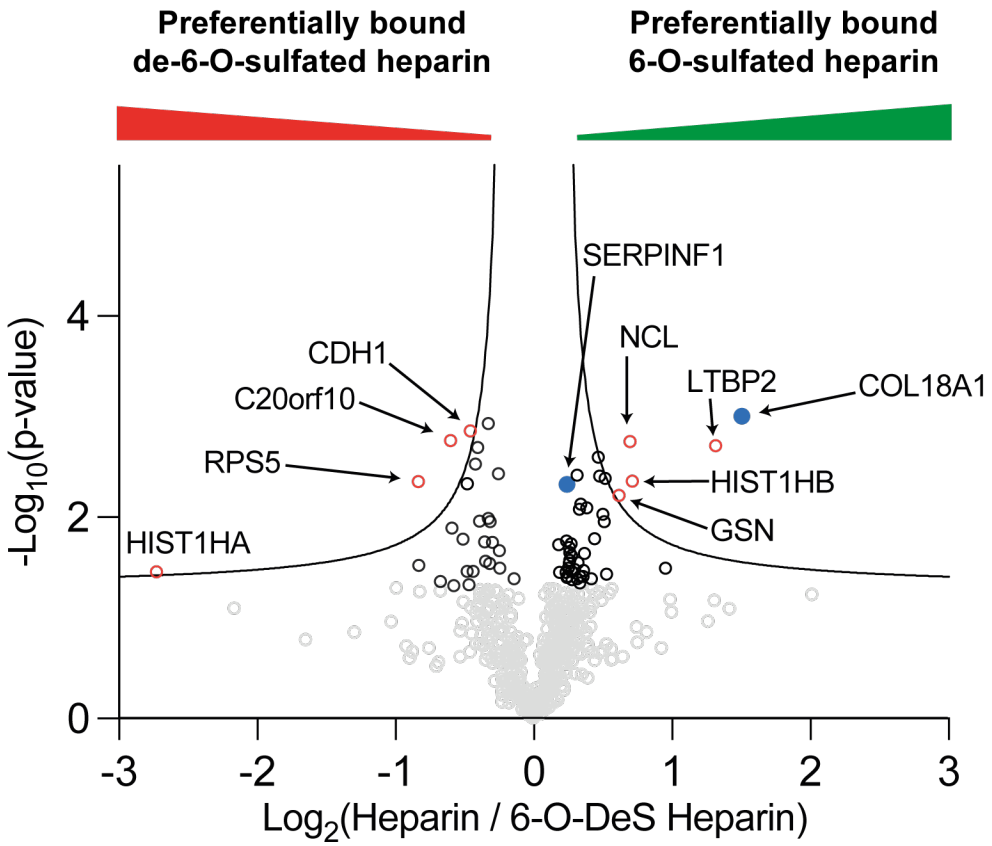

Figure 5.7 Volcano plot showing LfQ MS of proteins from osteoarthritic human articular cartilage affinity purified on heparin- and 6-O-desulfated heparin-Sepharose.

Proteins eluting from heparin- and 6-O-desulfated heparin-Sepharose resins were analysed using LfQ MS. Data were analysed with MaxQuant against a *Homo sapiens* reference proteome. FDR was set at 1% (n = 4 technical replicates from 1 donor with clinical history of OA, statistical analysis was performed as described in **2.4.4**).

COLXVIII was, again, the protein with largest fold change (Log2fold change (heparin/6-O-desulfated heparin) of 1.16, equating to a fold change of 2.23) in abundance in the two eluates. LTBP2, Nucleolin, Histone 1 Gene Cluster 1 B and

Gelsolin were also significantly more abundant in the heparin-Sepharose eluates than the 6-O-desulfated heparin-Sepharose elutions. Proteins that preferentially bound 6-O-desulfated heparin-Sepharose included intracellular proteins E-cadherin (CDH1), Tumour Promotor 53 Target 5 (C20orf10 or TP53 target 5), Ribosomal protein S5 (RPS5), Histone H2A type 1-H (HIST1HA) .

Table 5.2 LfQ MS identified 9 proteins from human osteoarthritic cartilage with significantly (FDR > 1%) different abundance from heparin- and 6-O-desulfated heparin-Sepharose.

Protein	Log_2 (abundance in heparin/6-O-desulfated heparin)	Localisation (Uniprot)	p-value
Type XVIII collagen	1.16	Extracellular	0.0009900
Latent TGF-β binding protein	1.12	Extracellular	0.0019454
Histone gene cluster 1, H1 B	1.05	Nucleus, Cytoplasm	0.0043700
Nucleolin	0.85	Nucleolus, Plasma membrane	0.00176088
Gelsolin	0.72	Cytoplasm, Cytoskeletal, Secreted	0.0060622
E-cadherin	0.71	Nucleus, Cytoplasm	0.00139374
Tumour protein 53-inducible gene 5 protein (C20orf10)	-1.03	Nucleus, Cytoplasm	0.00173466
Ribosomal protein S5	-1.24	Ribosome	0.00444769
Histone gene cluster 1, H1	-1.33	Ribosome	0.00187025

Given the low number of proteins identified above the FDR, I then considered proteins which were significantly altered (-log p-value > 1.3) before the FDR was applied in both normal and OA cartilage (**Figure 5.8**). In total, 47 proteins were detected in both the healthy and osteoarthritic cartilage samples. Of those 47 proteins, 29 were labelled as secreted or present on the cell surface (UniProt). This list included cartilage-relevant proteins such as MMP-2, FGF2, COL11A2, PCOLCE2, HTRA3 and SOST.

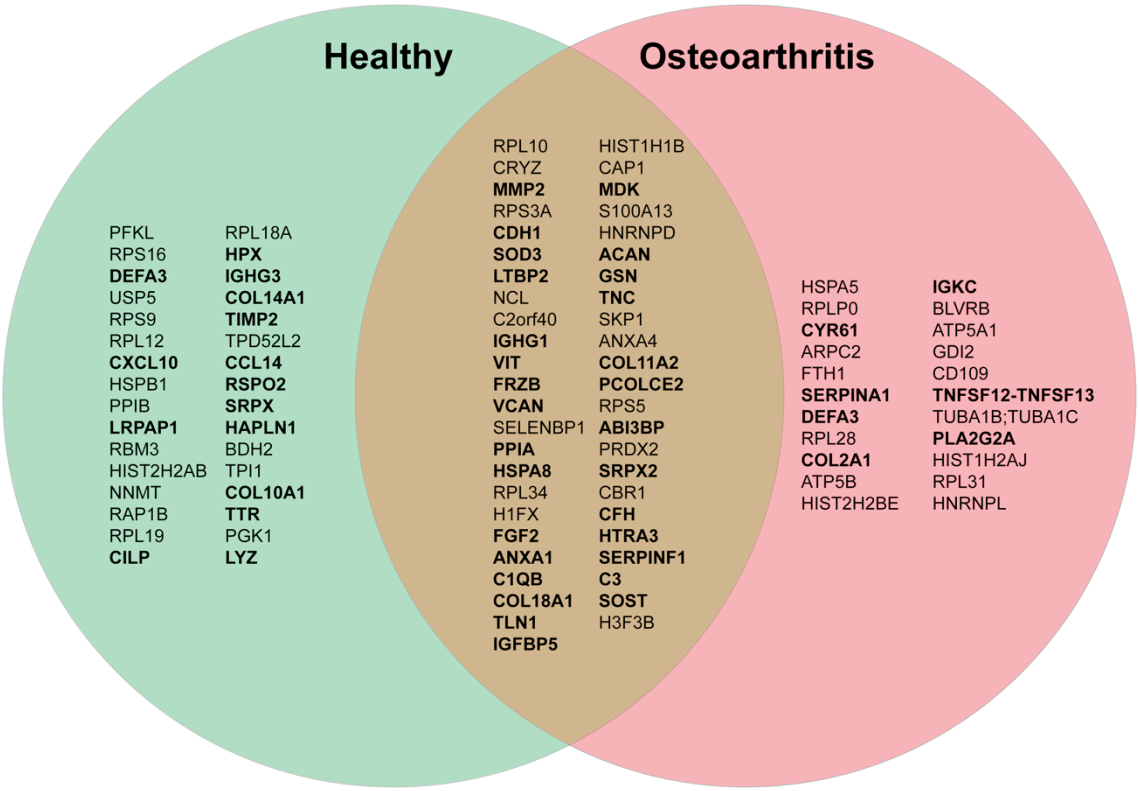

Figure 5.8 47 significantly altered proteins were detected in both the normal and osteoarthritic cartilage samples.

LfQ MS identified 89 and 69 proteins that were significantly changed (-log p-value >1.3) in abundance in heparin affinity chromatography eluates from healthy and osteoarthritic cartilage respectively. Of these proteins, 47 were shared between the healthy and osteoarthritic cartilage samples. COLXVIII was detected in both samples. Proteins in bold are annotated as secreted or localised on the cell surface (UniProt).

From the analyses of normal and osteoarthritic cartilage, two proteins were chosen for further study. COLXVIII was selected as it was the most significantly changed protein in both data sets above the FDR (**Figure 5.6**, **Figure 5.7**). The second, SERPIN F1 (otherwise known as pigment epithelium-derived factor, PEDF) was not above the FDR but was significantly changed before FDR application, and was detected in both the healthy and OA cartilage extracts (**Figure 5.8**). SERPINF1 is a member of the serpin family that has no detectable inhibitory activity against serpin proteases. Previously, SERPINF1 was detected in the cartilaginous zone of the osteophyte[302] and treatment of chondrocytes with SERPINF1 (250 ng/mL) resulted in significant changes in the expression of genes involved in catabolic inflammatory signalling[302]. Furthermore, Nakamura *et al.*[303] showed that recombinant SERPINF1 reduced cartilage loss in a murine surgically-induced OA mice model. Therefore, I decided that SERPINF1, despite not being above the FDR, could potentially be of interest to investigate.

COLXVIII is a non-fibrillar collagen typically found in basement membranes. It assembles to form homotrimers and contains multiple non-collagenous interruptions in their central triple-helix. COLXVIII is a heparan sulfate proteogylcan that can occur as three isoforms, depending on the length of its N-terminal domain, with isoform expression appearing to be tissue-specific[300,304]. A schematic of the COLXVIII sequence is shown in **Figure 5.9**. The C-terminal non-collagenous domain 1 (NC1) of COLXVIII can be cleaved to release a fragment called endostatin[305] which has previously been shown to have moderate affinity for both immobilised heparin- and heparan sulfate (K_D of 1.96 μM and 2.2 μM)[306]. Looking at the LfQ MS data for COLXVIII in more detail, 6 of the 7 peptides identified mapped to the endostatin region of COLXVIII (**Figure 5.9**), indicating

that endostatin rather than full length type XVIII collagen was likely to have been purified by affinity chromatography.

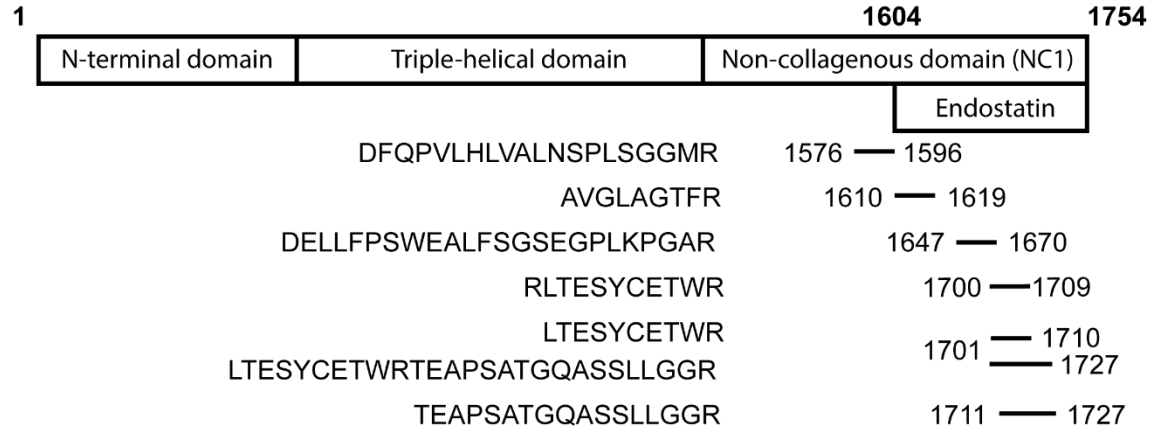

Figure 5.9 COLXVIII peptides detected by LfQ MS analyses map to the endostatin region of COLXVIII.

COLXVIII contains three regions, the N-terminal domain, the triple helical domain, and the non-collagenous domain. The N-terminal domain can be cleaved to release endostatin. The peptides identified in the LfQ mass spectrometry analyses of heparin-binding proteins map to the endostatin domain of COLXVIII.

To confirm that endostatin was being differentially bound to the heparin- and 6-O-desulfated heparin-Sepharose resins, I western blotted the 1 M NaCl eluates from the normal cartilage sample. As shown in **Figure 5.10,** significantly more endostatin was present in the eluates from the heparin-Sepharose resin than from the 6-O-desulfated heparin-Sepharose resin, validating the LfQ MS data and indicating that endostatin is likely to have higher affinity for 6-O-sulfated heparin.

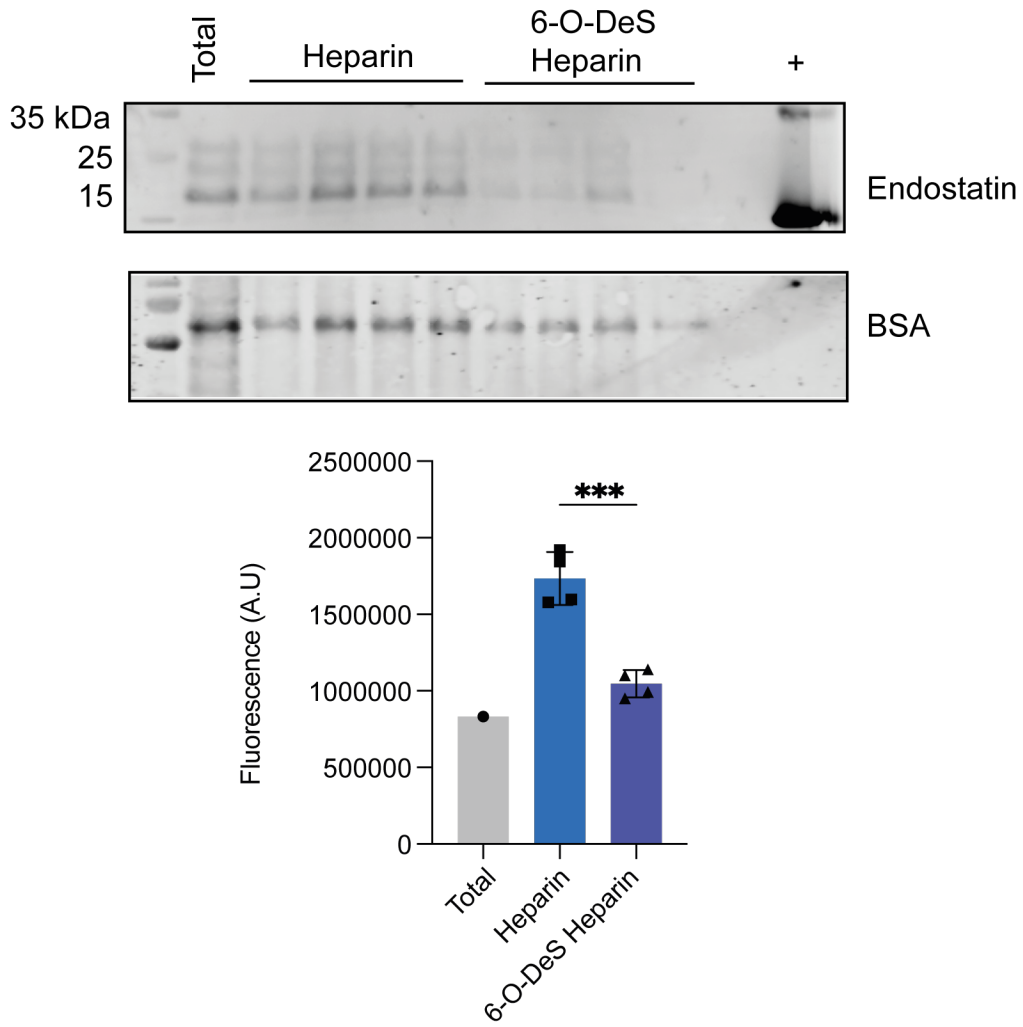

Figure 5.10 More endostatin was recovered from heparin- than 6-O-desulfated heparin-Sepharose resin.

960 mg of human normal knee cartilage extract was incubated overnight with Gdn-HCl (6 M, 7 mL). and the extract dialysed against 50 mM Tris-HCl, 150 mM NaCl (pH 7.4). Dialysed extracts were split into 8 equal volumes and incubated with equilibrated heparin-Sepharose and 6-O-desulfated heparin-Sepharose resins (n=4 technical replicates per resin), and bound proteins were eluted with 1 M NaCl in equilibration buffer. Fractions were electrophoresed on a 12% SDS-polyacrylamide gel, transferred to PVDF and analysed for (A) endostatin or (B) BSA as a loading control. Data analysed form normality using Shapiro-Wilks test (n = 4, mean ± SD, analysed using unpaired t-test. * $p < 0.05$, ** $p < 0.001$, *** $p < 0.001$).

To gain further insight, potential heparin-binding regions of type XVIII collagen were considered. The electrostatic surface charge of murine endostatin was calculated, since human endostatin has not been crystallised to date, but shares high sequence similarity with murine endostatin[307]. In agreement with the findings

of Ricard-Blum *et al.*[306] there is a large basic patch, 27 Å across, on the surface of murine endostatin[308] (**Figure 5.11 A**). Large basic patches such as this are common in heparin-binding proteins[309], where these positively-charged residues drive binding to the negatively charged sulfate groups of heparin. Taken together, both the peptide mapping and surface charge indicate that endostatin, rather than full-length type XVIII collagen was isolated by the heparin-Sepharose resin.

SERPIN F1, the other heparin-binding protein selected for further study, has a negatively-charged surface across one entire side of the protein (**Figure 5.11 B**). with a smaller highly positively-charged patch on the opposite face of the protein. The positively-charged surface of SERPIN F1 contains the heparin-binding site, with binding of heparin shown to induce a conformational change that promotes either signalling or cleavage by trypsin[310,311] .

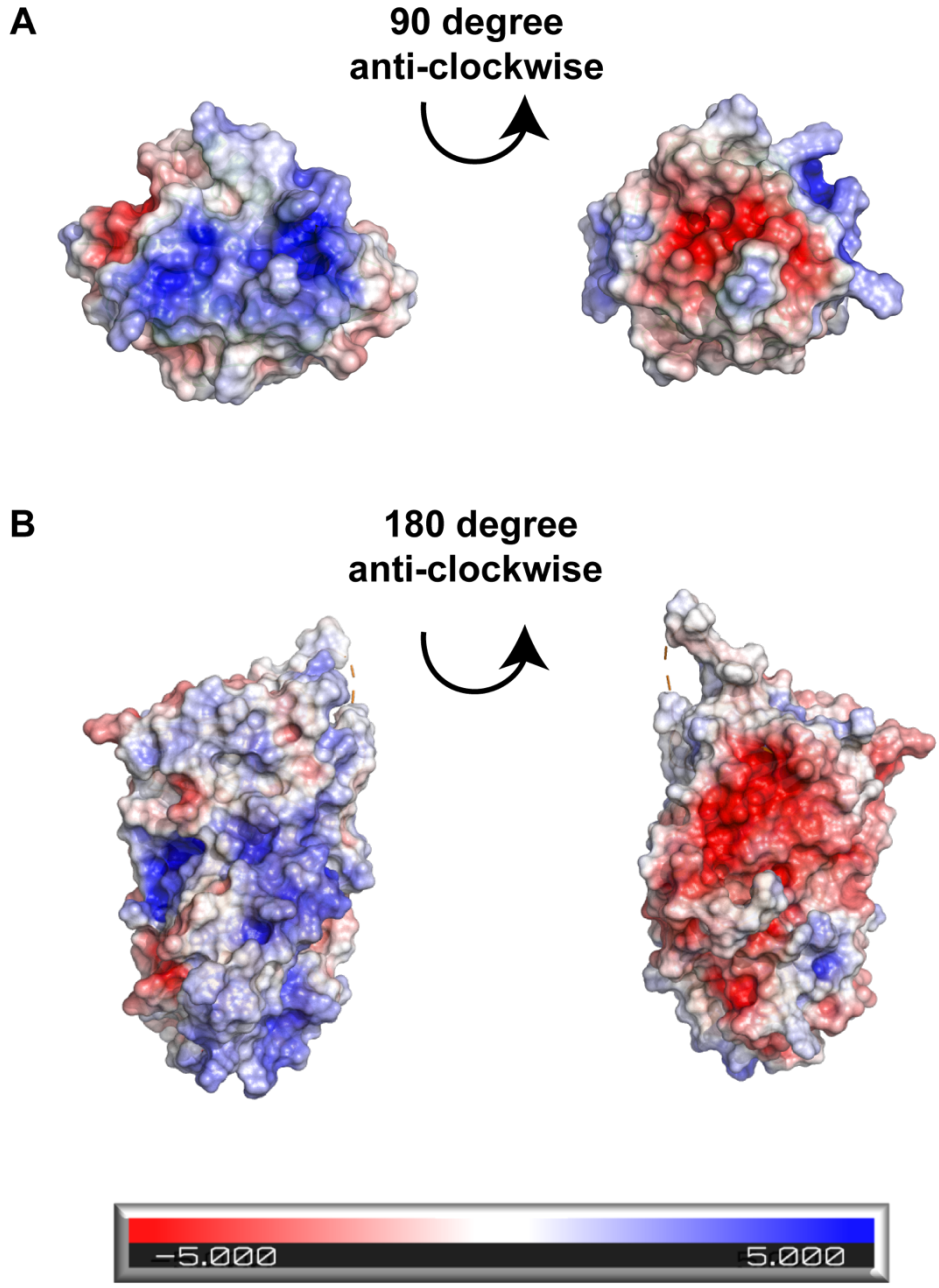

Figure 5.11 Endostatin and SERPINF1 are predicted to contain large basic patches on their protein surface.

The structure of murine endostatin (1KOE[308]), and SERPINF1 (1IMV[312]) and were analysed using PyMOL with surface electrostatic potential visualised using the APBS electrostatics plug-in. Positively charged regions are coloured blue, negatively charged regions are coloured red. (A) Endostatin has a large basic patch (27 Å across) covering one face that measured. (B) SERPIN F1 has a basic patch that covering the majority of one side of the protein, and a negatively-charged surface on the opposite side of the protein face.

5.2.4 Neither endostatin nor SERPIN F1 increases sGAG accumulation

Endostatin is known to be an angiogenesis inhibitor, and those antiangiogenic properties are dependent upon heparan sulfate[313], however little is known about its role in articular cartilage. The limited literature available indicates it is expressed at higher levels foetal and fibrocartilage, with low, but detectable levels in adult articular cartilage[314]. There is some evidence to suggest that endostatin promotes anabolic activity in rabbit articular chondrocytes[315], and that its expression by MSCs does not alter their chondrogenic potential [316].

As discussed, Nakamura *et al.*[303] showed that SERPIN F1 reduced cartilage loss in surgically-induced OA in mice, however other research by Klinger *et al*.[302] found recombinant SERPINF1 induced overexpression of proteases (*MMP13*, *MMP3*, *SAA1*) and downregulated *COL2A1* and cartilage oligomeric protein expression.

Due to the potential roles of both endostatin and SERPINF1 in cartilage, their effect on sGAG accumulation was investigated, to determine whether their differential binding to 6-O-sulfated heparin could be the cause of the reduced sGAG accumulation observed in HS6ST1-overexpressing cells (**Figure 4.2**). Neither endostatin, nor SERPINF1, had a significant effect on sGAG accumulation (**Figure 5.12**). Addition of a heparin oligosaccharide similarly had no effect on sGAG accumulation, in both control, endostatin- and SERPINF1-supplemented cultures. As shown in **Figure 4.4**, addition of a 6-O-desulfated heparin oligosaccharide reduced sGAG accumulation, but this effect was

unchanged by addition of endostatin or SERPINF1. There was no significant effect with addition of a heparin oligosaccharide.

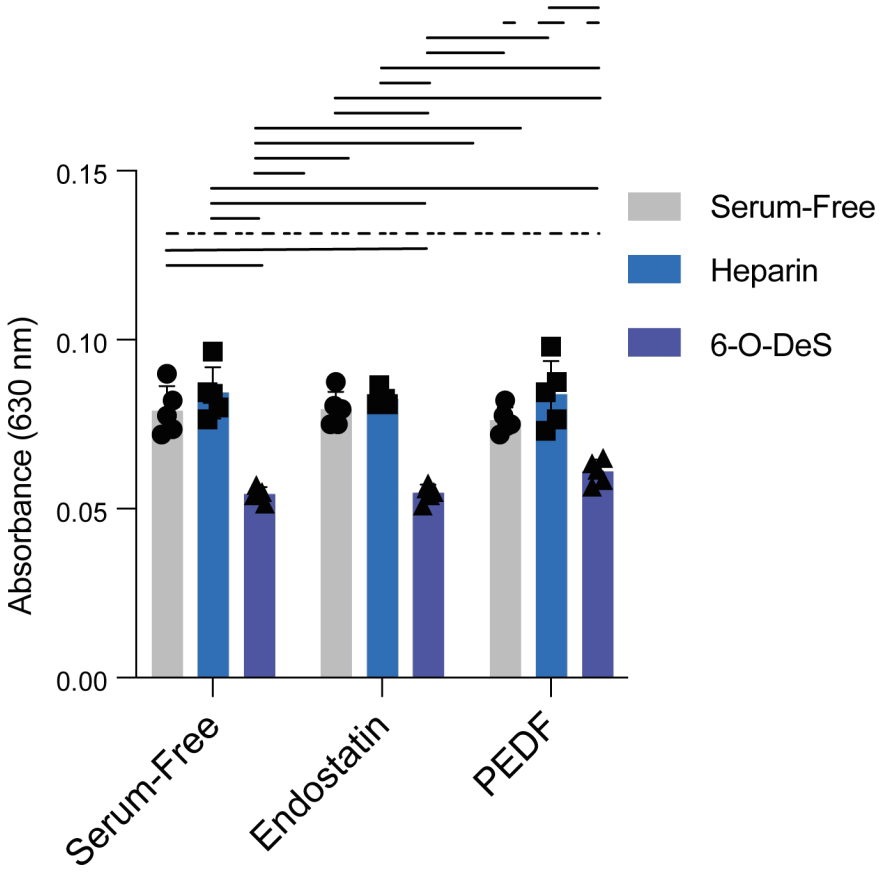

Figure 5.12 Neither endostatin nor SERPINF1 altered sGAG accumulation, measured using Alcian blue staining.

C28/I2 cells ($1x10^5$) were cultured in serum free media, or in serum-free media supplemented with endostatin (100 ng/mL) or SERPINF1(225 ng/mL), heparin or 6-O-desulfated heparin (100 μg/mL) oligosaccharides as indicated. After 4 days cells were fixed and stained for sGAG accumulation using Alcian blue. Alcian blue stain was extracted with 6 M Gdn-HCl and absorbance measured at 630 nm (n = 5, mean ± SD Data analysed using 2-way ANOVA with Tukey's multiple comparisons test). – – – $p < 0.05$ – – – – $p < 0.01$ —— $p < 0.001$

5.3 Discussion

In this chapter I sought to identify proteins from healthy and osteoarthritic human cartilage that differentially bound heparin- and 6-O-desulfated heparin-Sepharose resins. To do this, I first had to extract proteins from cartilage samples using an appropriate buffer. Extracting proteins from tissues for bench side assays, e.g. western blotting, can be a relatively trivial matter. Harsh detergents, or chaotropic agents, such as urea and guanidine hydrochloride, can extract large quantities of proteins from tissue (100 μg/mg of tissue in neuronal samples[317]) This agents break the hydrogen bonds between amino acid residues, thereby increasing the aqueous solubility of the protein. As shown in **Figure 5.2**, I examined four different buffers and observed that guanidine hydrochloride most efficiently extracted the HS-binding protein TIMP-3 from porcine cartilage. 600 mg of cartilage protein was extracted per gram of cartilage, comparable to other studies on cartilaginous tissue[318]. This is broadly comparable to other tissues, e.g. neurological tissues, where extraction of 100-300 mg of protein per gram of tissue has been reported[319,320].

A potential disadvantage of using Gdn-HCl is that it denatures proteins and so can impair their ability to bind to heparin-Sepharose resins. I thus dialysed the extracts against a large excess of buffer to remove the Gdn-HCl and promote refolding of the protein. This method has been widely used for refolding of recombinant proteins expressed in *E.coli*, which commonly require solubilisation from inclusion body aggregates[321]. The dialysis membranes selected must allow movement of solutes but not proteins through the pores of the membrane. As many heparin binding proteins are small (e.g. TIMP-3 ~20 kDa, FGF2 ~20 kDa,

TGF-β1 ~25 kDa), a low molecular weight (3.5 kDa) cut-off dialysis membrane value was chosen. Subsequent analysis of porcine extracts showed that TIMP-3 was purified from extracts using heparin-Sepharose, indicated this approach was suitable for isolating heparin-binding proteins from cartilage. Binding to the resin was increased by increasing the length of incubation (from 5 min to 16 h **Figure 5.2 B,C**). In human cartilage extracts, lower binding to the resins was observed ( ), most likely due to lower coupling density of heparin/6-O-desulfated heparin to the custom Sepharose beads than to commercial heparin-Sepharose used for optimisation with porcine cartilage.

I then investigated protein binding to the heparin- and 6-O-desulfated heparin-Sepharose resins. Coomassie staining (**Figure 5.4**) revealed subtle differences in the elution profile from these resins, with some proteins being present in the 0.5 M NaCl fraction from the heparin column, but not the 6-O-desulfated heparin column (**Figure 5.4 white stars**). Western blotting for TIMP-3 and FGF2, two proteins with known differences in affinity for 6-O-sulfated heparin, confirmed differential protein binding to the resins. There was significantly less TIMP-3 in eluates from the 6-O-desulfated heparin-Sepharose compared to the heparin-Sepharose, whereas there was no significant difference in FGF2 elution between the two columns (

). TIMP-3 binds heparin with high affinity (K_D 19 ± 4 nM for dp 36 heparin) and this binding is dependent on 6-O-sulfation, with K_D to low to determine for dp36 6-O-desulfated heparin[53]. The smaller difference in binding observed here may be due to differences in oligosaccharide length between the two experiments, or the difference in experimental approaches. Troeberg *et al.*[53] analysed binding of purified TIMP-3 using GAG-binding ELISA plates, whereas I analysed binding of

a cartilage extract to Sepharose resins derivatised with 14 kDa heparin (dp 14). In cartilage, TIMP-3 is likely to be bound to proteins and/or glycosaminoglycans (such as ADAMTS-5 and/or HS) but these are likely to dissociate during extraction with Gdn-HCl and so not impair binding to heparin resins. Encouragingly, I observed no difference in FGF2 elution from the heparin and 6-O-desulfated heparin-Sepharose resins, in agreement with studies showing that FGF2-HS binding is not preferentially driven by the 6-O-sulfate group[133,322,323].

LfQ MS was used to identify and quantify proteins eluting from heparin- and 6-O-desulfated heparin-Sepharose. In healthy cartilage, 641 heparin-binding proteins were identified, in line with recent reports which identified between 175 (neurological) and 700 (prostate) heparin binding-proteins respectively[70,135]. As proteomic analysis often involves numerous multiple comparisons, there is an increased probability of false positive significant results. Therefore, proteomic (and other -omic) analyses apply a False Discovery Rate (FDR) to account for these multiple comparisons[324]. Of the 641 heparin-binding proteins identified by LfQ MS, 88 were significantly changed before FDR was applied, and this was reduced to 9 proteins after application of a 1% FDR (**Figure 5.6**). I observed a similar trend in protein extracts from an osteoarthritic cartilage sample: 622 heparin-binding proteins were identified by LfQ MS, of which 69 proteins were significantly changed before FDR application and 9 proteins significantly changed after application of a 1% FDR (**Figure 5.7**). This apparently low number agrees with similar published research using 3-O-sulfated oligosaccharides - Thacker *et al*.[135] identified 43-175 (depending on whether they analysed bovine, murine or human tissue) distinct 3-O-sulfate binding proteins, which was reduced to 12 novel 3-O-sulfate binding proteins when stricter statistical criteria were applied. A

larger number of technical replicates (e.g. 1 x biological replicate, 6-8 technical replicates) or significantly more biological replicates (6-8) would have greatly improved the statistical power. Furthermore, an increased number of replicates would have enabled greater identification (and quantification) of low-abundance proteins. Despite this, validation of endostatin as being more abundant in eluates from heparin-Sepharose than 6-O-desulfated heparin-Sepharose resins (**Figure 5.10**) by western blotting gave me confidence that the proteins identified below the 1% FDR were differentially bound by the respective resins.

In both the healthy and osteoarthritic samples, several DNA/RNA binding proteins were identified. A recent study investigating RNA-binding proteins found that of the proteins investigated, only 30% bound to structurally-defined motifs, whereas 70% bound to short linear non-specific sequences[325]. This is indicative of non-specific, charge-driven binding and therefore offers a potential explanation for the detection of nucleic acid-binding proteins from heparin affinity chromatography. Indeed, heparin can be used to prevent non-specific protein-DNA interactions to improve the clarity of homomeric ribopolymer pull-down experiments[326].

Whilst not directly comparable, due to the lack of biological replicates, and different times at which experiments were performed, it is striking that in both the healthy and OA cartilage sample, COLXVIII was the protein with the greatest fold change in eluates once a 1% FDR was applied (**Figure 5.6, Figure 5.7**). This was validated by western blotting (**Figure 5.10**) which indicated that endostatin bound more strongly to 6-O-sulfated heparin. Alternative approaches to confirm affinity for 6-O-sulfated heparin and HS could include biophysical assays such as SPR or DSF.

As discussed, COLXVIII is a non-fibrillar heterotrimeric collagen that is itself an HSPG. At its C-terminal region it contains a non-collagenous 1 region with a proteolytic site that releases a fragment called endostatin, which is a potent angiogenesis inhibitor[327,328]. Therefore, I analysed whether the MS data indicated detection of full length COLXVIII or endostatin. The peptides identified by the MS map to the c-terminal region of full length COLXVIII, with 6 out of 7 of the peptides mapping to the endostatin region of NC1 (**Figure 5.9**). As such, the mass spec analyses were likely detecting endostatin, and not full-length COLXVIII. The binding of endostatin to heparin is supported by both its crystal structure[308] (**Figure 5.11 A**) and the literature where it has been observed to colocalise with HSPG2[313,329]. The binding to HS has also been shown to be dependent on 6-O-sulfation[330]. COLXVIII is known to be expressed in both cartilage and fibrocartilage[331], but literature on endostatin in cartilage is sparse. For example, a PubMed search of 'endostatin AND cartilage' yielded only 21 results. The limited studies available indicate that endostatin can reportedly alter expression of several genes (*ColX, Col2a1, Mmp13*) involved in chondrocyte phenotype[315].

As I had identified that endostatin bound more strongly to 6-O-sulfated heparin- than 6-O-desulfated heparin-Sepharose resins (**Figure 5.10**), I hypothesized that endostatin may be responsible for the reduced sGAG content observed for *HS6ST1*-overexpressing cells. To test this experimentally, I stimulated wild type C28/I2 cells with endostatin and measured sGAG accumulation. As shown in **Figure 5.12** endostatin had no effect on sGAG accumulation. There is some evidence that endostatin can regulate MMP-3, -9 and -13 activity[332], but I observed no reduction in activity of MMP-13 activity against Knight substrate when incubated with endostatin (data not shown). The role of endostatin, or

COLXVIII, in cartilage may therefore be relevant in late-stage OA where cartilage regions with elevated protease activity would be more likely to liberate endostatin from COLXVIII, leading to inhibition of vascular invasion. Alternatively, endostatin may be involved in regulating blood vessel formation during endochondral ossification. This could be further investigated using inducible-COLXVIII knockout mice to investigate what effect, if any, COLXVIII has on cartilage homeostasis in surgically induced OA.

While not above the 1% FDR, SERPINF1 was also identified as a 6-O-sulfation dependent heparin-binding protein in both the healthy- and osteoarthritic cartilage samples (**Figure 5.8**). As with endostatin, SERPINF1 was found to have no effect on sGAG accumulation of C28/I2 cells (**Figure 5.12**) indicating that SERPINF1-dependent signalling cannot be the cause of the reduced sGAG accumulation observed in *HS6ST1*-overexpressing cells. SERPINF1 is known to be expressed in cartilage and osteophytes[302], and to bind to heparin, which protects it against proteolytic cleavage[311]. Interestingly, Nakamura *et* al.[303] Observed that lentiviral overexpression of SERPINF1 increased IL-1β-induced protease expression (*Mmp1, Mmp3, Mmp13)* in chondrocytes. I observed no difference in IL-1β-induced gene expression of *MMP13, IL1B or SULF1* in the presence of recombinant SERPINF1, both with and without heparin or 6-O-desulfated heparin oligosaccharides (data not shown). Differences in experimental approach are most likely to explain these differences. I investigated how SERPINF1 inhibited IL-1β signalling in over 6 h, which would enable detection of SERPINF1 induced-signalling or competitive inhibition of IL-1β-induced signalling, through binding of SERPINF1 to either the cytokine or receptor. In contrast, Nakamura *et al.*[15] analysed ectopic expression over several days. As exposure to SERPINF1 (>48

h) and IL-1β (4-days) was significantly longer in their experiment, it would allow time for SERPINF1-induced signalling to cause changes in protein expression that could negatively regulate IL-1β-induced protease expression. It may be useful to treat C28/I2 cells with endostatin or SERPINF1 at high doses or for longer times. However, given that these proteins were incubated with C28/I2 cells for 5 days, I think increased time is unlikely to alter my observations.

One possible explanation for the lack of activity of recombinant endostatin and recombinant SERPINF1 could be the organism they were expressed in, as both proteins were expressed in *E. coli.* Bacterial expression systems are useful for producing large quantities of protein, however recombinant proteins from these systems may not be folded properly and generally lack N- (and sometimes O-) glycosylation[333]. Loss of glycosylation has been shown to cause loss of protein activity (e.g. Notch[334]), and may be crucial for the activity of these proteins.

Although these experiments were preliminary and aimed to identify candidates for further study, their biggest limiting factor is the lack of replicates, both biological and technical. Biological replicates were limited to 1 OA and 1 normal due, in part, to the low availability of normal cartilage and also the low availability of OA samples from elective surgery during the COVID19 pandemic. However, there would also have been challenges with using multiple biological replicates, as the considerable variation in primary human cartilage samples would significantly hamper the statistical analysis on which LfQ MS relies.

The relatively low number of proteins identified above the 1% FDR is likely a direct result of analysing insufficient technical replicates. A comprehensive

analysis of phosphopeptides by Ham *et al.*[335] observed that optimal proteome coverage per biological replicate was 6 technical replicates, however, total proteome analysis likely requires fewer replicates for optimal coverage as loss of labile phosphate groups is not as significant an issue. I used 4 technical replicates for each analysis group (heparin- and 6-O-desulfated heparin resin) from one biological sample – while there are limitations on the number of samples that can be processed in parallel for LfQ MS, it is feasible to analyse at least 16 samples in parallel. However, the number of technical replicates was limited by the amount of cartilage available per donor and the amount of protein required for LfQ MS – with the ~ 1g of cartilage available, only 4 technical replicates per analysis group was achievable. Given these challenges and the low number of proteins identified by LFQ MS, it was decided to focus on alternative approaches, such as RNA sequencing (**Chapter 6**).

There were a number of proteins that are known to have an anabolic roles in the joint (e.g. FGF2, MDK, FRZB) were found to be significantly changed but were not above the FDR. Given that this experiment aimed to identify proteins for further study, analysing these candidates may be fruitful.

The aim of this chapter was to identify cartilage proteins with high affinity for 6-O-sulfated heparin and to investigate whether they could be responsible for the reduced sGAG accumulation observed in *HS6ST1*-overexpressing cells. Since neither of the two candidates chosen was found to have a role in sGAG accumulation *in vitro,* I decided that further agnostic interrogation of the transcriptional landscape following *HS6ST1* overexpression was required.

Chapter 6. *HS6ST1* overexpression reduced C28/I2 cells response to their environment.

6.1 Introduction

As LfQ mass spectrometry of 6-O-sulfate binding proteins generated limited leads to explain the reduced sGAG accumulation in *HS6ST1*-overexpressing cells, I decided to investigate changes to the transcriptomic profile of mock- and *HS6ST1*-overexpressing cells using bulk mRNA-sequencing to identify regulated pathways that may explain the observed phenotype.

The core aspects of RNA-sequencing (RNA-seq) have not changed since its first inception; mRNA (of sufficient quality) is enriched, cDNA is synthesised, and adaptors are ligated to the sequencing library. Sample libraries are then sequenced on a high-throughput platform and data is aligned to a reference genome (*Homo sapiens* in this case). Statistical analyses of the reads from samples being compared then determines the extent of differential gene expression. The use of RNA-seq to investigate transcriptomic changes is now widespread[336], with many laboratories extending its usage to single cell[337] and spatial transcriptomics[338]. As shown in Chapter 4, overexpression of *HS6ST1* did not alter the mRNA expression of several candidate genes of relevance to heparan sulfate biosynthesis and cartilage homeostasis but given that it reduced sGAG content *HS6ST1* overexpression is likely to have altered the transcriptomic profile of cells. RNA-sequencing was thus a practical and agnostic method of investigating these changes.

To interrogate -omic data fully, enrichment analyses are used to give insight into which pathways are regulated by the identified differentially-expressed genes (DEGs). Several different enrichment analyses that can be performed, including

Kyoto Encyclopedia of Genes and Genomes (KEGG)[339], REACTOME[340] and the gene ontology (GO) database[341,342]. GO is divided into three distinct ontologies: cellular component (CC), biological process (BP) and molecular function (MF), with overlap often seen in the enriched pathways identified within each ontological group. Multiple enrichment analyses are often performed on each dataset, as each uses different statistical tests to calculate enrichment and so can corroborate identification of regulated pathways. Performing multiple enrichment analyses across each database can be time consuming, so currently a host of software is available to simplify this process. To perform functional enrichment analyses, I used the software Cytoscape[343] which piggybacks on the online web-service g:Profiler[231].

Following RNA-seq analysis, I investigated how *HS6ST1* overexpression impacted a number of signalling pathways using phospho-immunoblotting. Phosphokinase arrays allow simultaneous investigation of multiple phosphorylated proteins on a single set of membranes[344,345]. Membranes dotted with antibodies against 39 phosphorylation sites were purchased and incubated with lysates or medium from treated cells. Phosphorylated proteins are then detected in a similar manner to a western blot. Finally, the response of *HS6ST1*-overexpressing cells to a well-known heparin-binding protein, FGF2, was investigated by quantifying activation of the ERK signalling pathway, and the responses to TGF-β1 and BMP4 were investigated by quantifying the activation of SMAD2/3 and SMAD1/5/8 respectively.

6.2 Results

6.2.1 ERK phosphorylation is constitutively active in C28/I2 cells.

As a first step to investigate how signalling in C28/I2 cells is altered in response to *HS6ST1* overexpression, I investigated whether I could detect changes in ERK phosphorylation in response to treatment with FGF2 as FGF2-induced ERK phosphorylation is highly dependent upon heparan sulfate 6-O-sulfation[92].

Initial experiments showed unexpectedly high basal ERK phosphorylation, independent of the extraction buffer used (data not shown). Therefore, different cell densities were tested. Cell density was increased (from $3x10^5$ to $1x10^6$ / 9.6 cm^2) which is in line with higher densities reported by some other researchers examining FGF2 signalling in chondrocytes[34,68]. Cells were cultured for 48 h and serum-starved overnight before stimulation with a concentration gradient of FGF2 ranging from 0 – 50 ng/mL for 10 min. Higher concentrations did not induce substantially more ERK phosphorylation than that observed under non-stimulated conditions at either cell density tested (**Figure 6.1 A**).

To investigate whether the high basal ERK phosphorylation was an artefact of experimental protocol, basal and FGF2-induced ERK phosphorylation was investigated in porcine chondrocytes. Chondrocytes were isolated and grown for 4 days in growth medium, serum starved overnight and stimulated with 20 ng/mL FGF2. Porcine chondrocytes responded robustly to FGF2, with increased ERK phosphorylation 10 min post stimulation (**Figure 6.1 B**). Next, the inhibition of

FGF2-induced ERK phosphorylation through the addition of exogenous heparin was confirmed. As show in in **Figure 6.1 C**, FGF2-induced ERK phosphorylation was markedly reduced in the presence of both heparin and 6-O-desulfated heparin.

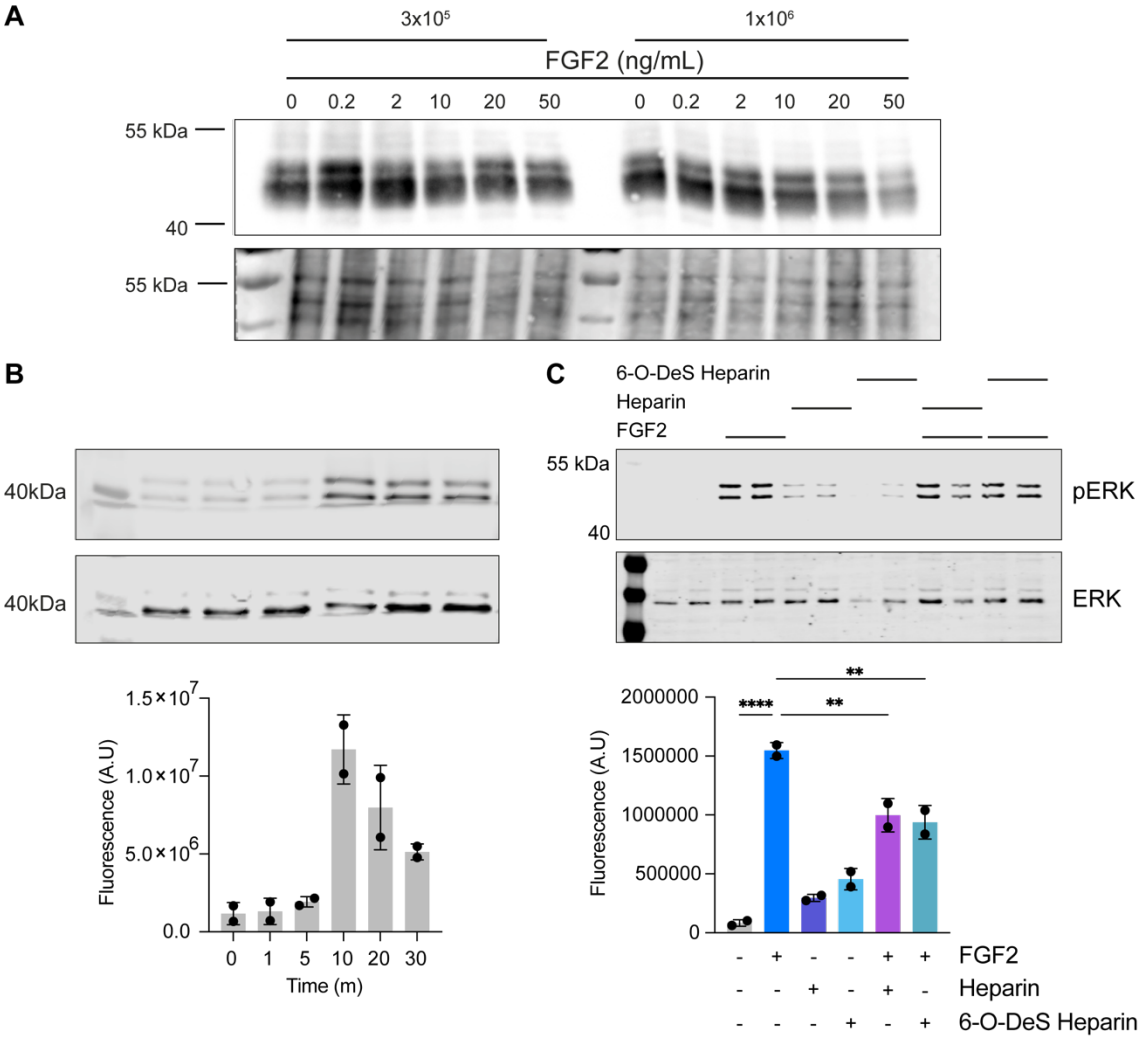

Figure 6.1 High basal ERK phosphorylation was observed in C28/I2 cells but not porcine chondrocytes.

Cells were grown for 48 h, serum-starved overnight and stimulated with FGF2. Cell were washed in PBS and lysed in SDS sample buffer supplemented with protease and phosphatase inhibitors. Equal volumes of cell lysate per well were electrophoresed on a 12% SDS polyacrylamide gel and western blotted for ERK and pERK. (A) C28/I2 ($3x10^5$ or $1x10^6$ cells/9.6 cm^2) were stimulated with a concentration gradient of FGF2 ranging from 0 – 50 ng/mL for 10 min (n=1). (B) Porcine chondrocytes ($1x10^6$) were stimulated with 20 ng/mL FGF2 in a reverse time course from 0 – 30 min (n=2). (C) Porcine chondrocytes ($1x10^6$) stimulated with 20 ng/mL FGF2 with or without

heparin or 6-O-desulfated heparin (100 μg/mL) oligosaccharides (n=2). Images were quantified using ImageStudioLite.

The clear response of porcine chondrocytes to FGF2 indicated that the experimental procedure was working as expected, and that the high basal ERK phosphorylation observed in C28/I2 cells was an intrinsic feature of these cells in, thus rendering them unsuitable for analysing activation of ERK phosphorylation in response to exogenous stimuli. Therefore, phospho-SMAD activation, which is known to be important for chondrocyte development and matrix production[253,346], was investigated by transfecting cells with mock- or *HS6ST1*-encoding plasmids and investigating phospho-SMAD2/3 and SMAD1/5/8 induction.

6.2.2 BMP4-induced SMAD1/5 phosphorylation is reduced following *HS6ST1* overexpression, but not TGF-β1-induced SMAD2/3 phosphorylation.

SMAD phosphorylation, and TGF-β family signalling, is well known to play a role in development of OA and mutations of asporin, a TGF-β pathway inhibitor, is associated with increased susceptibility to OA[347]. TGF-β family members can signal by inducing phosphorylation of SMAD2/3 or SMAD1/5/8 by activating the receptors ALK5 or ALK1 respectively. Constitutive activation of *Alk5*-induced *Smad2/3* phosphorylation has been shown to induce aggrecan expression, whereas constitutive *Alk1* expression induced SMAD1/5/8 phosphorylation and expression of *Mmp13*[348]. Given that European cohorts with a *SMAD3* single nucleotide polymorphism, that reduces SMAD3 phosphorylation, have increased susceptibility for OA[349], SMAD2/3 phosphorylation is generally considered to be

anabolic for cartilage, and SMAD1/5/8 phosphorylation to be catabolic. In OA, there is a shift in the balance of these receptors resulting in an increased ratio of ALK1/ALK5 receptor expression, and therefore a greater potential for SMAD1/5/8 phosphorylation. TGF-β family members have affinity for HS, however BMPs generally have higher affinity than TGF-β proteins[350,351]. The exact role of HS in TGF-β1 signalling is still debated, as TGF-β1 binds to betaglycan (TGF-βR3) in an HS-independent manner, yet treatment of chondrocytes with heparanase reduces SMAD2/3 phosphorylation in response to TGF-β1 treatment[51]. The activation of these pathways in response to *HS6ST1* expression was investigated.

Published TGF-β1 concentrations used to stimulate chondrocytes range from 0.1-10 ng/mL[352,353] so TGF-β1-induced SMAD2/3 phosphorylation in C28/I2 cells was investigated at 0.1, 1 and 10 ng/mL for up to 60 min in a reverse time course. 1 ng/mL TGF-β1-induced the largest increase in SMAD2/3 phosphorylation (**Figure 6.2 A**). TGF-β1 (1 ng/mL) strongly induced SMAD2/3 phosphorylation in mock and *HS6ST1*-overexpressing cells, and this was not significantly between the 2 groups (**Figure 6.2 B**). TGF-β1 did not induce a strong phospho-SMAD1/5/8 response in C28/I2 cells (**Figure 6.2 C**), in contrast to what has previously been observed in primary bovine chondrocytes[353], nor was this significantly different between mock- and *HS6ST1*-overexpressing samples (**Figure 6.2 C**).

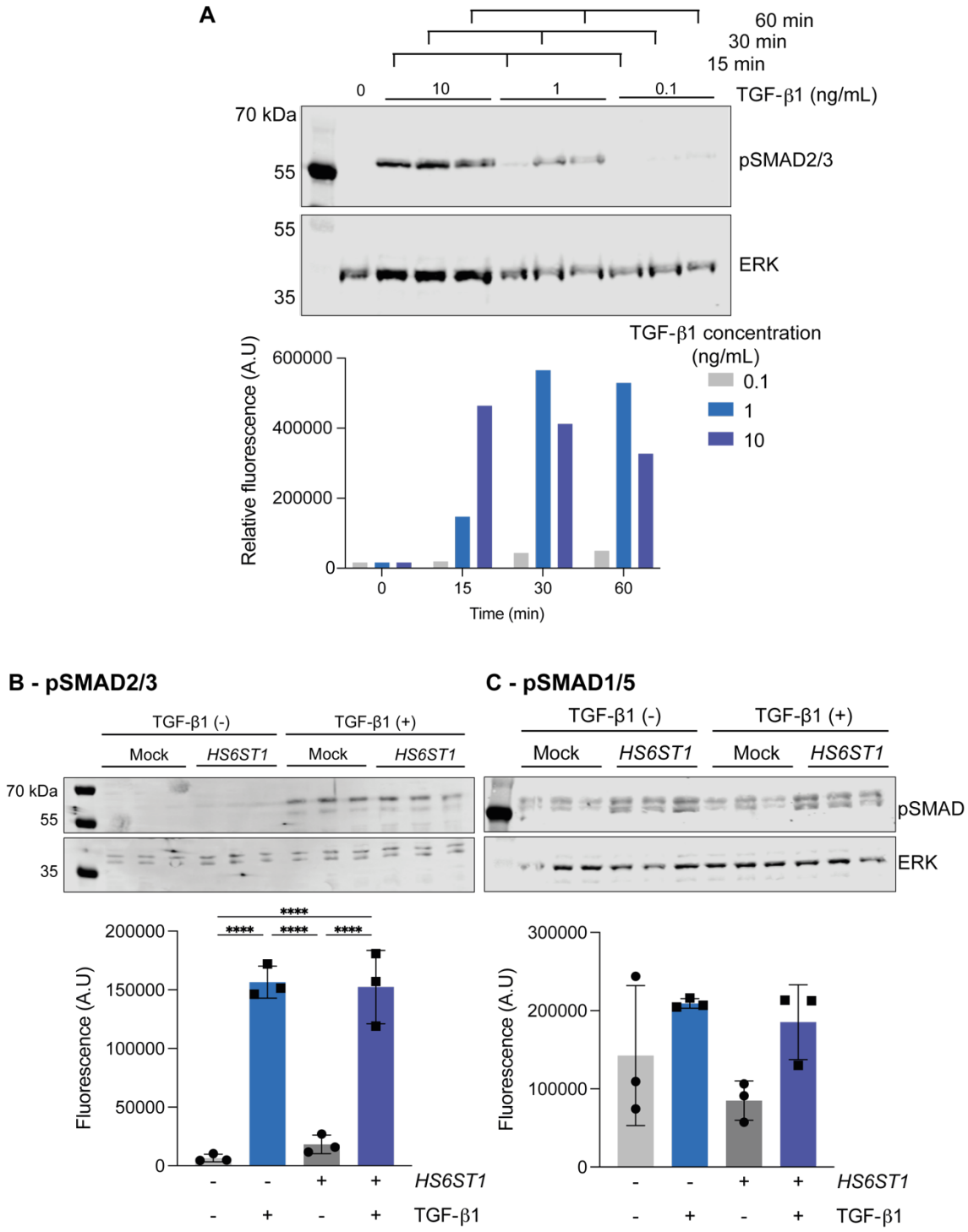

Figure 6.2 Western blotting showed TGF-β1-induced SMAD2/3 phosphorylation was unchanged by HS6ST1 overexpression.

(A) C28/I2 ($1x10^5$) cells were grown for 48 h in growth medium, serum-starved overnight, and stimulated with 0 – 10 ng/mL TGF- β1 for up to 60 min (37 °C, 5% CO_2) in a reverse time course. (B,C) C28/I2 cells were transfected with 2 μg of mock or HS6ST1-encoding plasmid seeded ($3.3x10^5$/well) and grown for 48 h in growth medium. Cells were serum starved overnight and stimulated with TGF- β1 (1 ng/mL, 1h, 37 °C). (A, B, C) Cells were washed twice with ice-cold PBS and cell lysates collected in SDS sample buffer supplemented with protease and phosphatase inhibitors. Equal volumes of cell lysate were electrophoresed on a 10% SDS-

polyacrylamide gel and western blotted for either (A,B) pSMAD2/3 or (C) pSMAD1/5. Phosphorylation was normalised against total ERK. Data assessed for normality with Shapiro-Wilks test (n = 3, mean ± SD, analysed with one-way ANOVA corrected for multiple comparisons using Tukey's multiple comparisons test * $p < 0.05$, ** $p < 0.001$, *** $p < 0.001$).

The effect on TGF-β1 signalling was then investigated using another experimental approach. TGF-β1 was previously observed to cause a small increase in sGAG accumulation in C28/I2 cells (**Figure 4.2**), so the effect of *HS6ST1* overexpression on TGF-β1-induced changes in cell viability and sGAG accumulation were evaluated.

TGF-β1 had no effect on viability of mock-transfected cells, indicating that this was not an appropriate readout for TGF-β1 signalling. However, as observed previously (**Figure 4.3**), transfection with *HS6ST1* increased viability of C28/I2 cells, potentially due to increased signalling by an unidentified HS-binding ligand. The increased viability of *HS6ST1*-overexpressing cells was inhibited by TGF-β1, possibly due to competition with the endogenous ligand (**Figure 6.3 A**).

Next the effect of TGF-β1 on sGAG accumulation was investigated using Alcian blue staining. The previously observed small increase in sGAG accumulation (**Figure 3.3**) was not observed when cells were transfected with the mock plasmid, suggesting that the effect of TGF-β1 treatment on C28/I2 cells is marginal. As detailed on the Discussion of **Chapter 3**, this may be due to differences in culture conditions, but under the culture conditions used this is also not an appropriate readout for TGF-β1 signalling. As observed previously, *HS6ST1* overexpression reduced sGAG accumulation compared to mock transfected cells. This effect was reversed by addition of TGF-β1 (**Figure 6.3 B**).

These data indicate that *HS6ST1* overexpression does not regulate TGF-β1 signalling, as there was no change in TGF-β1 phospho-SMAD induction (**Figure 6.2 B,C**). However, TGF-β1 reversed the HS6ST1-dependent increase in cell viability and decrease in sGAG accumulation. It is likely that exogenous TGF-β1 competitively inhibited the endogenous HS ligand(s) that increased cell viability and reduced sGAG accumulation in an HS6ST1-dependent manner.

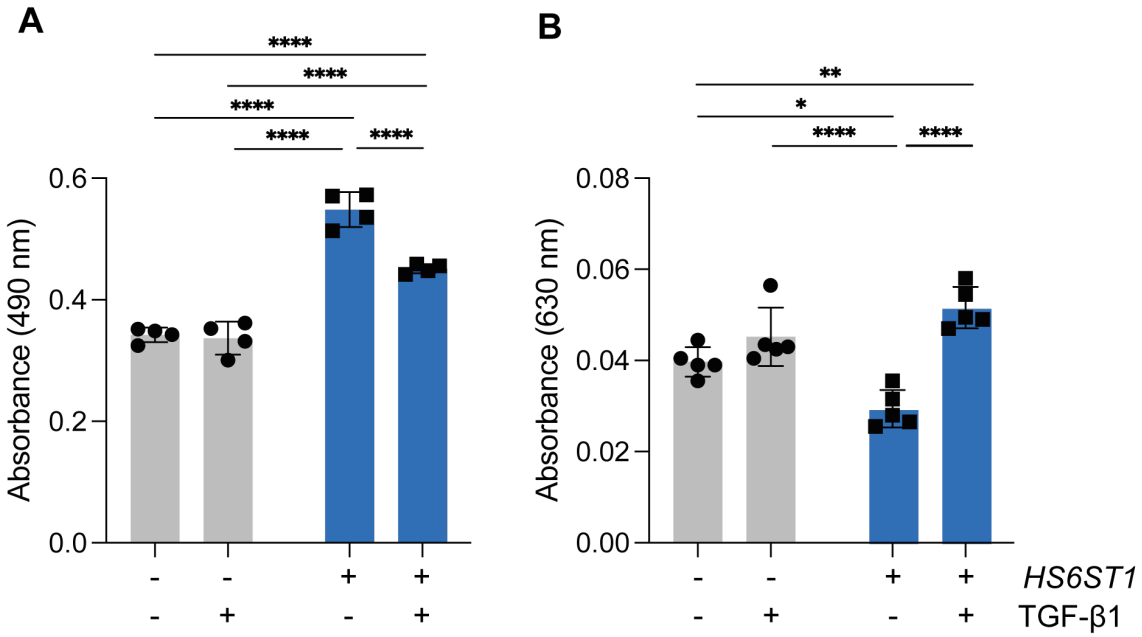

Figure 6.3 TGF-β1 reversed *HS6ST1*-dependent changes in cell viability and sGAG accumulation.

(A) C28/I2 cells ($1x10^6$) cells were transfected with 2 µg of either mock or *HS6ST1*-encoding plasmid and seeded at a density of $3.1x10^5/cm^2$. Cells were grown for 96 h in serum-free medium supplemented with or without TGF-β1 (1 ng/mL). Media were changed to fresh serum-free medium supplemented with MTS reagent, incubated at 37 °C for 1 h, and absorbance at 490 nm measured. B) C28/I2 cells transfected with 2 µg of either mock or *HS6ST*-encoding plasmids were seeded at a density of $1x10^5/cm^2$. Cells were grown for 4 days in serum-free medium supplemented with or without TGF-β1 (1 ng/mL). Cells were fixed with methanol and stained for sGAG using Alcian blue. Stain was extracted using 6 M Guanidine-HCl and absorbance at 630 nm was measured on a plate reader. Data assessed for normality with Shapiro-Wilks test. ((A) n = 4, (B) n=5, mean ± SD analysed with 2-way ANOVA corrected for multiple comparisons with Šídák's multiple comparisons test. * $p \leq 0.05$, ** $p \geq 0.001$, *** $p \leq 0.001$).

Next, as TGF-β1 did not induce SMAD1/5/8 phosphorylation activation of this pathway was investigated using BMP4. BMP2 has previously been shown to induce both SMAD2/3 and SMAD1/5/8 phosphorylation[354], whereas BMP4 selectively activates SMAD1/5/8. BMP4 was thus selected for study of HS6ST1 effects on SMAD1/5/8 phosphorylation.

A concentration gradient and time course was performed, and both 5 and 10 ng/mL of BMP4 gave a strong induction of phospho-SMAD1/5/8 (**Figure 6.4 A**). As with TGF-β1, the lowest concentration of BMP4 tested that still elicited a strong response was selected for further experiments, in which cells were stimulated with 5 ng/mL BMP4 for 60 min. Overexpression of *HS6ST1* had no effect on basal SMAD1/5/8 phosphorylation, but significantly reduced BMP4-induced SMAD1/5/8 phosphorylation (**Figure 6.4 B**)

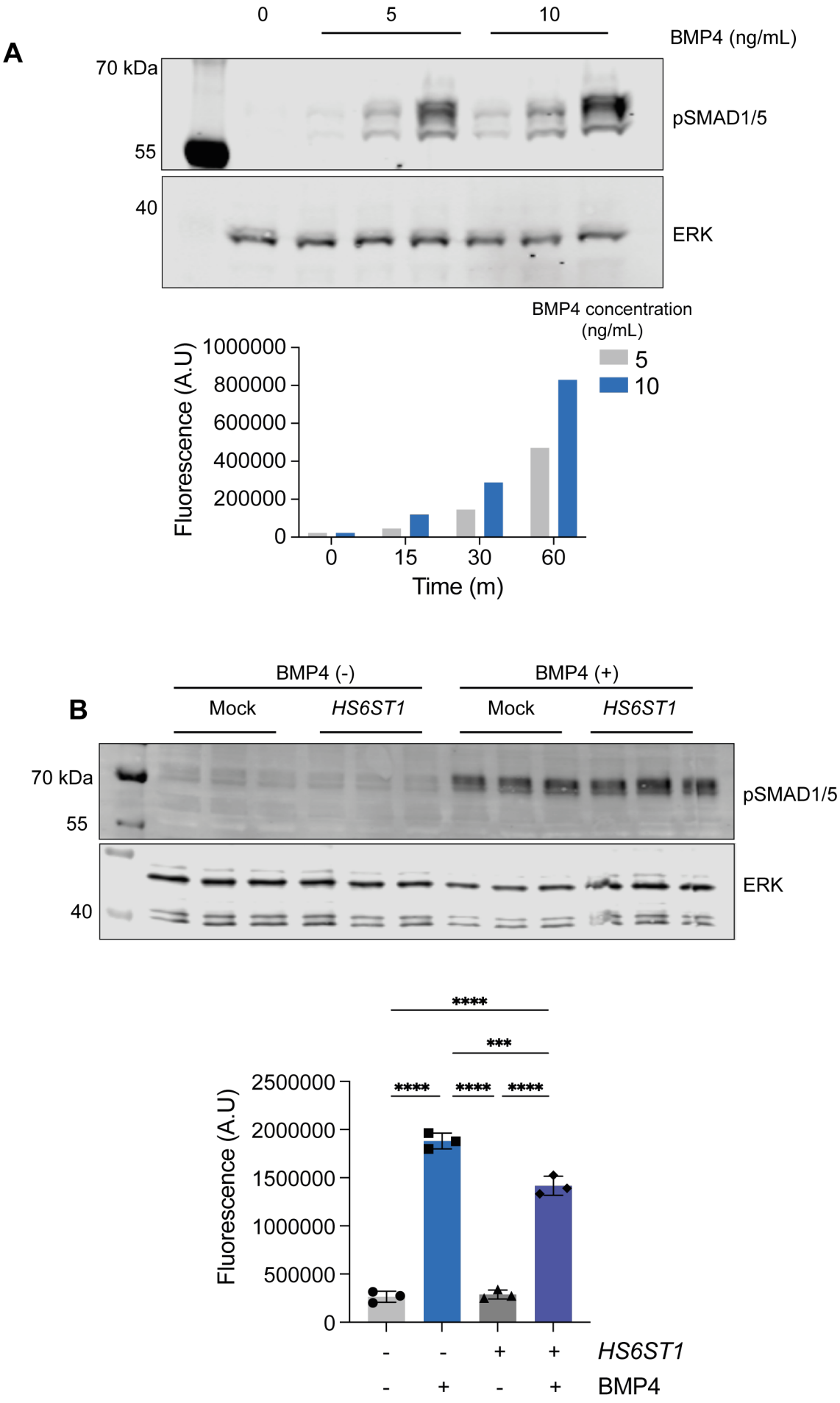
A
0
5
10
BMP4 (ng/mL)
70 kDa
55
pSMAD1/5
40
ERK
BMP4 concentration (ng/mL)
5
10
Fluorescence (A.U)
1000000
800000
600000
400000
200000
0
0
15
30
60
Time (m)
B
BMP4 (-)
BMP4 (+)
Mock
HS6ST1
Mock
HS6ST1
70 kDa
55
pSMAD1/5
40
ERK
****
***
****
****
****
Fluorescence (A.U)
2500000
2000000
1500000
1000000
500000
0
-
-
+
+
HS6ST1
-
+
-
+
BMP4

Figure 6.4 BMP4-induced SMAD1/5 phosphorylation was reduced by overexpression of *HS6ST1*.

Cells were stimulated with BMP4, washed twice with ice-cold PBS and cell lysates collected in SDS sample buffer supplemented with protease and phosphatase inhibitors. Equal volumes of cell lysate were electrophoresed on a 10% SDS polyacrylamide gel and western blotted for phospho-SMAD1/5 and total ERK. (A) C28/I2 ($1x10^5$) cells were cultured for 48 h growth medium. Cells were serum starved overnight before being stimulated with BMP4 (0 – 10 ng/mL) for up to 60 minat 37 °C, 5% CO_2. (B) C28/I2 cells ($1x10^6$) were transfected with 2 ug of mock or HS6ST1-encoding plasmid. Cells were seeded at a final density of $3.3x10^5$ cells per well. Cells were stimulated with 5 ng/mL BMP4 for 60 min at 37 °C. Data assessed for normality using Shapiro-Wilks test (n = 3, mean ± SD, data analysed with one-way ANOVA corrected for multiple comparisons using Tukey's multiple comparisons test. * $p < 0.05$, ** $p < 0.001$, *** $p < 0.001$).

The effects of *HS6ST1* overexpression on BMP4 signalling were also investigated by measuring effects on cell viability and sGAG accumulation. BMP4 had no effect on viability of mock-transfected cells, indicating this is not an appropriate readout for BMP4 signalling. Again, *HS6ST1* overexpression increased viability. The increased viability of *HS6ST1* overexpressing cells was inhibited by BMP4 (**Figure 6.5 A**).

Next the effect of BMP4 on sGAG accumulation was investigated using Alcian blue staining. BMP4 significantly increased sGAG accumulation in both mock-transfected cells, and this effect was not significantly altered by concomitant HS6ST1-transfection (**Figure 6.5 B**). Therefore, despite HS6ST1 reducing BMP4-induced SMAD1/5/8 phosphorylation, it had no effect on the BMP4-induced increase in sGAG accumulation. As with TGF-β1 (**Figure 6.3**), HS6ST1 overexpression reduced sGAG accumulation compared to mock-transfected cells and this effect was reversed by addition of BMP4 (**Figure 6.5 B**).

Using this candidate approach, HS6ST1 was shown to inhibit BMP4-induced SMAD1/5/8 phosphorylation, but not to inhibit BMP4-induced sGAG

accumulation. This indicates that the HS6ST1-dependent reduction in sGAG accumulation is not mediated by effects on BMP4 signalling. Therefore, I used bulk RNA-Seq as an unbiased approach to investigating the transcriptional response of C28/I2 cells to *HS6ST1* overexpression.

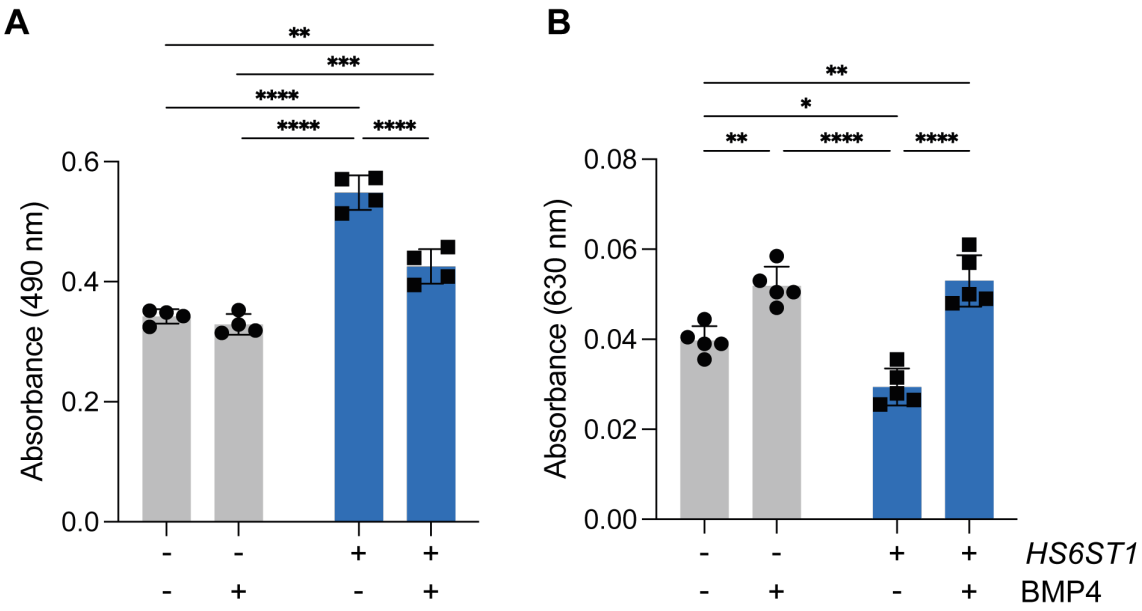

Figure 6.5 *HS6ST1* overexpression had no effect on BMP4-induced sGAG accumulation, but BMP4 reversed *HS6ST1*-dependent changes in cell viability and sGAG accumulation.

(A) C28/I2 cells ($1x10^6$) cells were transfected with 2 µg of either mock or *HS6ST1*-encoding plasmid and seeded at a density of $3.1x10^5/cm^2$. Cells were grown for 96 h in serum-free medium supplemented with or without BMP4 (5 ng/mL). Media were changed to fresh serum-free medium supplemented with MTS reagent, incubated at 37 °C for 1 h, and absorbance at 495 nm measured. B) C28/I2 cells transfected with 2 µg of either mock or *HS6ST*-encoding plasmids were seeded at a density of $1x10^5/cm^2$. Cells were grown for 4 days in serum-free medium supplemented with or without BMP4 (5 ng/mL). Cells were fixed with methanol and stained for sGAG using Alcian blue. Stain was extracted using 6 M Guanidine-HCl and absorbance at 630 nm was measured on a plate reader. Data assessed for normality with Shapiro-Wilks test ((A) n = 4, (B) n=5, mean ± SD analysed with 2-way ANOVA corrected for multiple comparisons with Šídák's multiple comparisons test. * $p \leq 0.05$, ** $p \geq 0.001$, *** $p \leq 0.001$).

6.2.3 *HS6ST1* overexpression modifies the expression of 840 genes.

C28/I2 ($1x10^6$) cells were transfected with 2 µg of *HS6ST1*-encoding plasmid and grown for 48 h in growth medium before cells were lysed and RNA was isolated. Bulk RNA-sequencing off mock- and *HS6ST1*-transfected cells was performed on 4 replicates per treatment group by Novogene as described in **2.3.6**. *HS6ST1* overexpression significantly altered expression of 840 genes, with 441 genes downregulated and 399 upregulated (**Figure 6.6 A**). Hierarchical cluster analysis showed that mock- and *HS6ST1*-transfected samples separated into two discrete groups (**Figure 6.6 B**).

For RNA-seq functional analysis there is no 'gold standard' for functional enrichment analysis. DEG functional enrichment analysis has focused on pooled DEGs[355–357] (both upregulated and downregulated genes) or separate analyses of the upregulated and downregulated genes[358–360]. Hong *et al*.[361] found that singular enrichment analysis of pathways using a separate-DEG strategy was more powerful for finding, biologically relevant, significantly enriched functional pathways. Therefore, I first separately analysed upregulated and downregulated enriched pathways, followed by analysis of the total DEGs to identify as many affected pathways as possible.

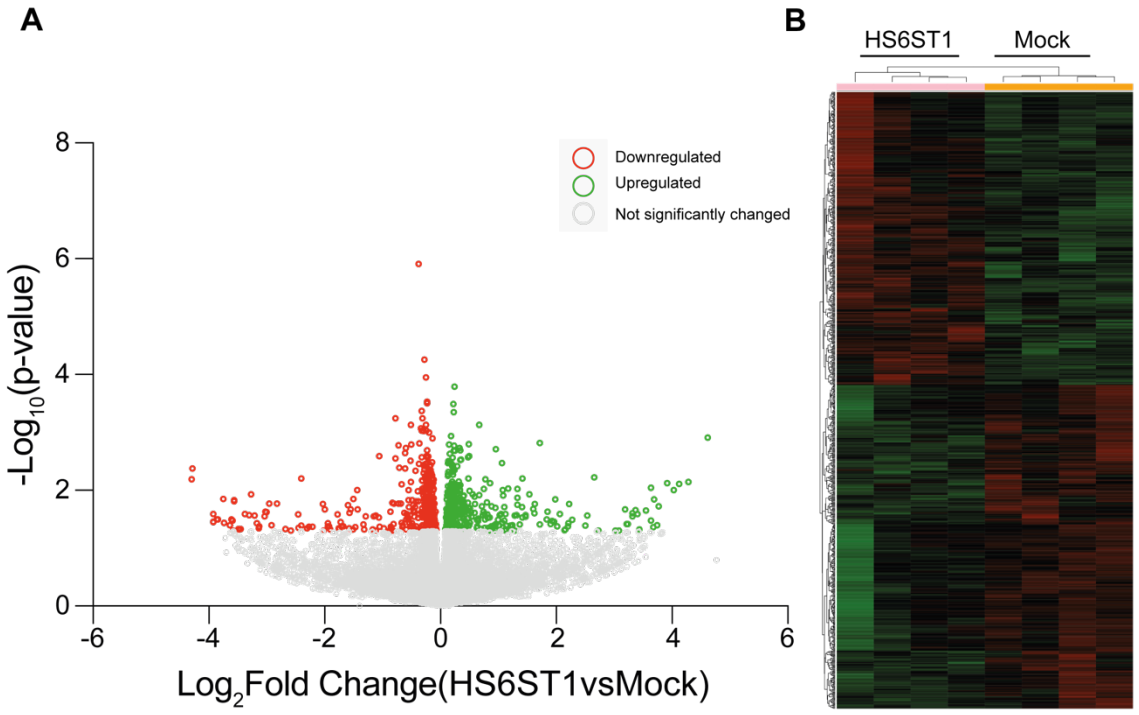

Figure 6.6 Bulk RNA-Seq analysis identified 840 genes differentially expressed in response to *HS6ST1* overexpression.

C28/I2 ($1x10^6$) cells were transfected with 2 µg of a mock- or *HS6ST1*-encoding plasmid. Cells were grown for 48 h in growth medium and cells lysed for RNA isolation. Purity of RNA samples was analysed using a Nanodrop 3000 and bulk RNA-sequencing performed by Novogene (n = 4). (A) Volcano plot of DEGs, where red indicates significantly downregulated genes, and green indicates significantly upregulated genes ($-Log_{10}$(p-value) > 1.3). (B) Hierarchical clustering map of DEGs.

6.2.4 HS6ST1-overexpression upregulates expression of cell cycle genes.

Whilst 399 genes were significantly upregulated, only a small number of functional terms were significantly enriched, and all related to DNA repair and control of the cell cycle. Of the top 10 most significantly enriched GO:BP pathways (**Figure 6.7 A**) control of the cell cycle was most significantly enriched, with the transition into mitosis particularly highlighted (3/10 GO:BP terms: Mitotic cell cycle phase transition, Mitotic cell cycle process, G2/M transition of mitotic

cell cycle). No GO:MF or GO:CC terms were enriched. KEGG enrichment analysis indicated significant changes in 'Cell cycle' pathways. REACTOME pathway analysis returned only cell-cycle related terms (**Figure 6.7 B**).

Increased expression of only 8 genes led to identification of the top 10 terms in the GO:BP analysis as well as the top 10 terms in the REACTOME pathway analysis. Expression of these 8 genes was investigated further, by calculating the frequency with which each gene was present in the top 10 GO:BP (or REACTOME) terms, with 1 indicating that the gene was present in each of the 10 GO:BP (or REACTOME) terms, and 0 indicating it was not present in any of the top 10 (**Figure 6.7 C**). CDC25C was present in all top 10 REACTOME terms, and *CHEK2* was present in all top 10 GO:BP terms. *CDC25C*, *CHEK2*, *IF1*, *PCNA* and *CENPA* were present in both GO:BP and REACTOME terms, while *CDCA3*, *TACC3* and *CCNB2* were present in the GO:BP enriched terms, but not the REACTOME terms.

Overall, this indicates that *HS6ST1* overexpression led to significantly increased expression of a handful of genes that promote mitosis.

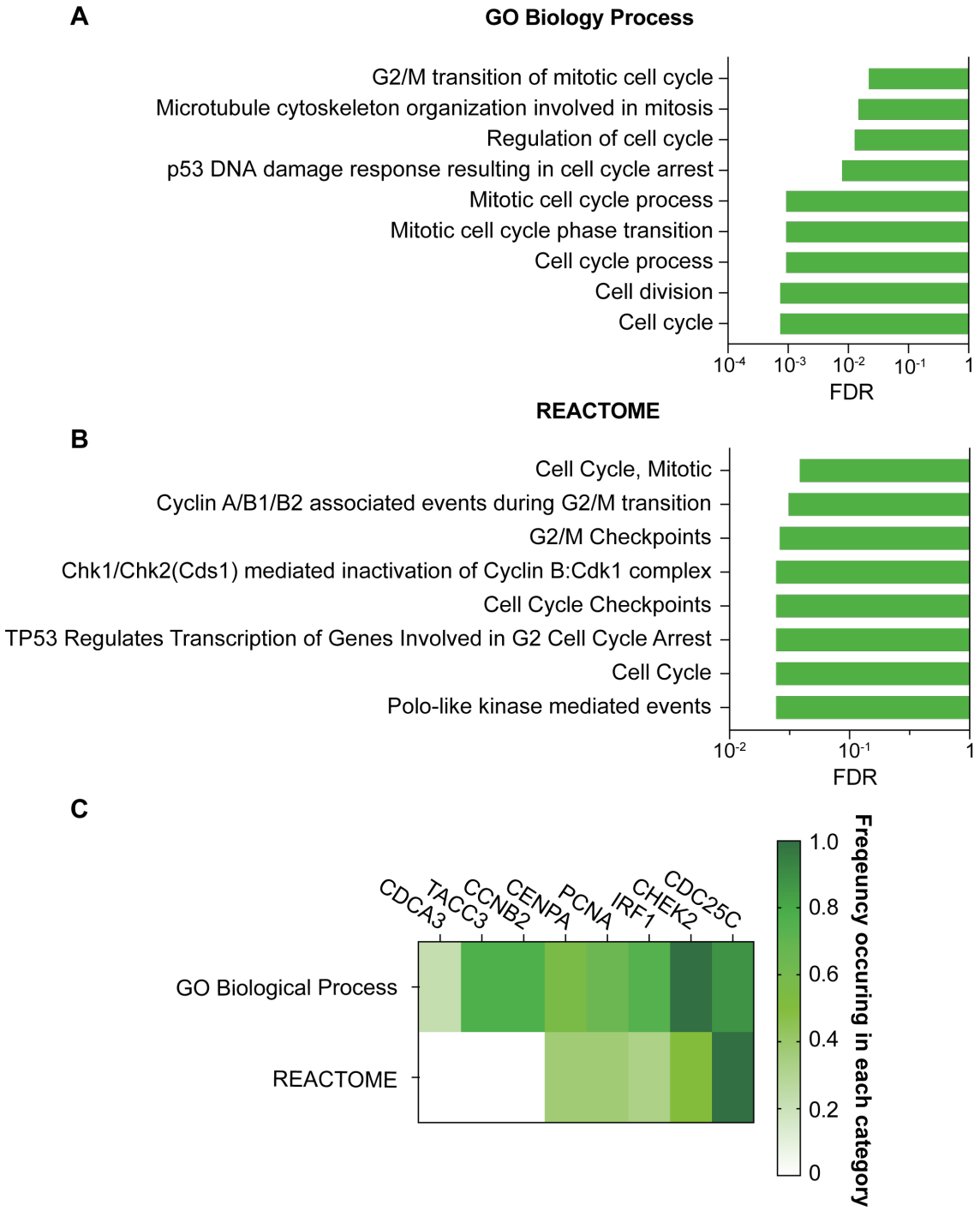

Figure 6.7 *HS6ST1* overexpression upregulated cell cycle-related genes.

Significantly upregulated genes (399 genes with -$\log_{10}$ p-value > 1.3) underwent functional enrichment analysis using g:Profiler. Significantly (FDR <0.05, using g:SCS multiple-testing correction) regulated terms are shown for (A) GO Biology Process and (B) REACTOME analysis. (C) The top 10 identified GO:BP and REACTOME terms reflected increased expression of only 8 genes. The frequency with each gene was present in the top 10 terms identified by GO:BP or REACTOME analysis is shown, with 1 indicating that the gene was present in each of the 10 terms, and 0 indicating it was not present in any of them.

6.2.5 HS6ST1 overexpression downregulates genes involved in cell-ECM interaction

More significantly altered terms were identified from the downregulated gene list than from the upregulated DEGs. The three most significantly enriched terms in the GO Cellular compartment (CC) analysis were 'Focal adhesion', 'Anchoring junction' and 'Cell surface' (**Figure 6.8 A**). Enriched GO Molecular function (GO:MF) terms were all related to cell adhesion and signalling, with 'Integrin binding', 'Adhesion molecule binding' and 'Signalling receptor binding' being the top 3 most enriched terms (**Figure 6.8 B**). Finally, GO:BP enriched terms were more varied, and included 'Cell migration', 'Tube morphogenesis', 'Wound healing' and 'Extracellular matrix organisation' (**Figure 6.8 C**).

KEGG analysis identified that 'Focal adhesion' formation was most significantly regulated, followed by 'Proteoglycans in cancer' and 'ECM-receptor interaction' (**Figure 6.9 A**). REACTOME identified that 'Integrin cell surface interactions' was the most significantly regulated term, however 'Signalling by receptor tyrosine kinases', 'Extracellular matrix organization', 'Non-integrin membrane-ECM interactions' and 'Syndecan interactions' were all similar in FDR value (between 10^{-8} and 10^{-6}) (**Figure 6.9 B**).

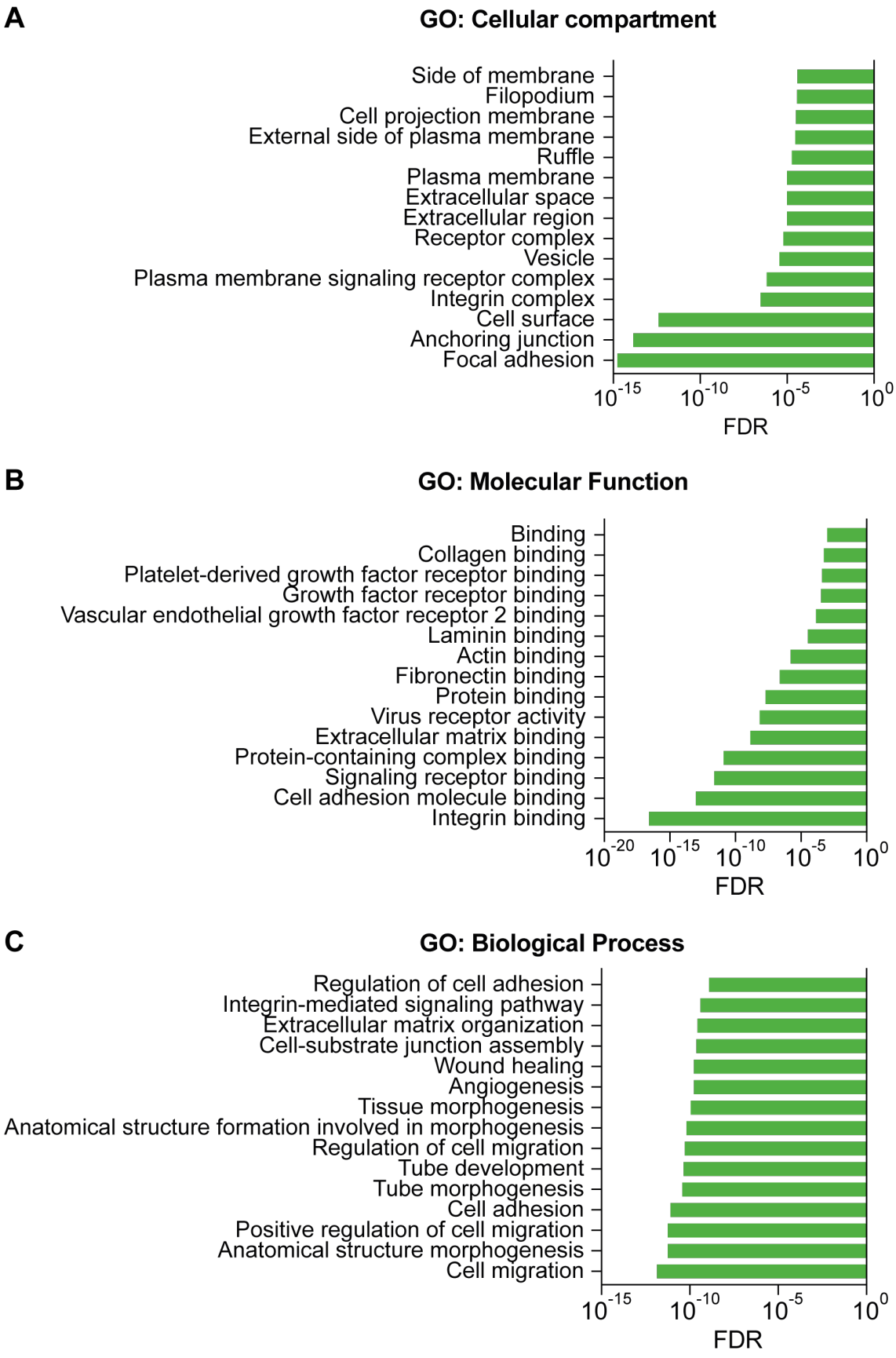

Figure 6.8 Cell-ECM association terms were enriched in GO functional analysis of genes downregulated by *HS6ST1* overexpression.

Significantly downregulated genes (441 DEGs with -log$_{10}$ p-value > 1.3) underwent GO functional enrichment analysis using g:Profiler. The top 15 significantly (FDR <0.05, using g:SCS multiple-testing correction) regulated terms are shown for (A) Top 15 GO cellular compartment terms (B) Top 15 GO molecular function terms (C) Top 15 GO Biological processes terms.

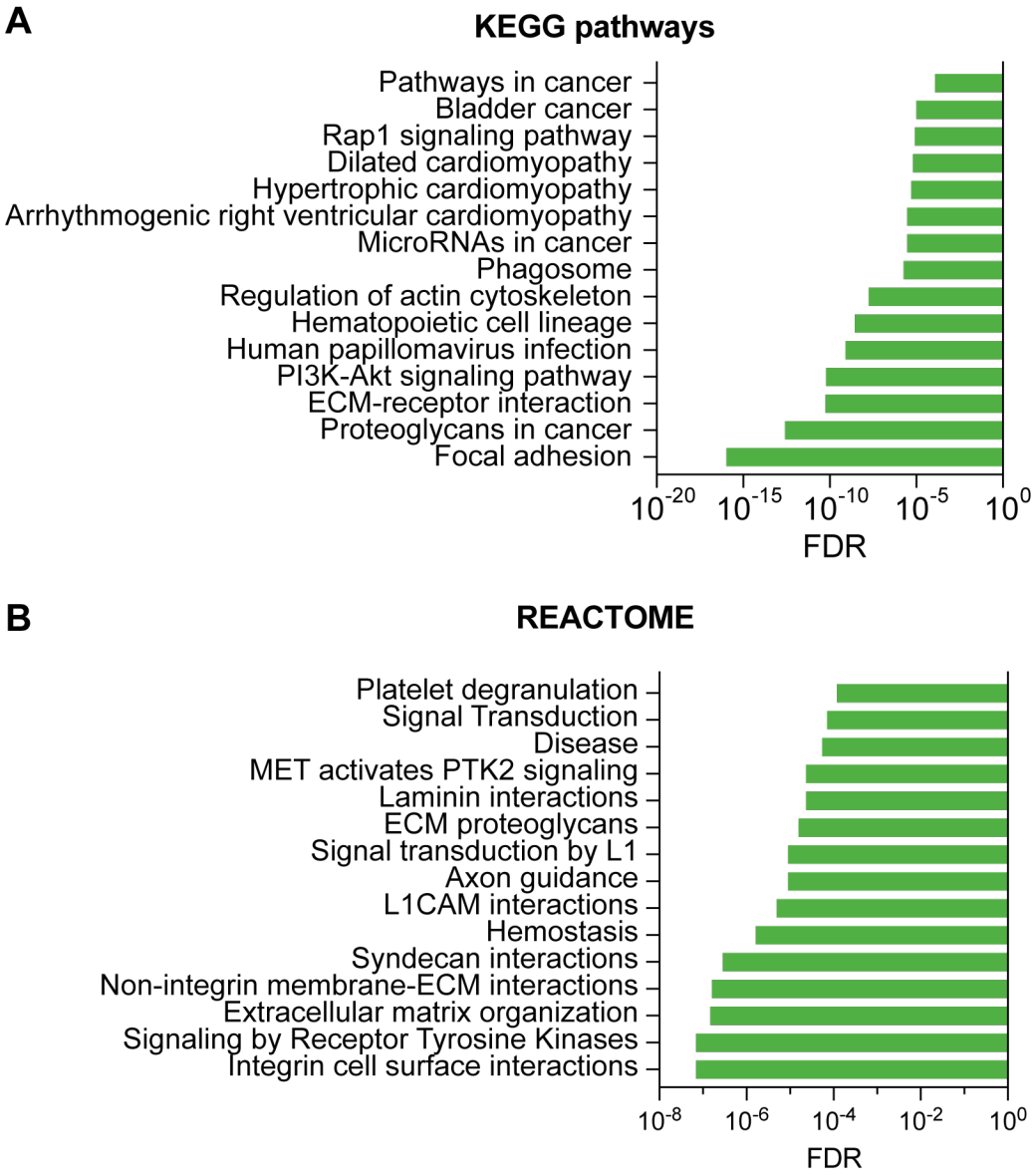

Figure 6.9 KEGG and REACTOME functional enrichment analysis of downregulated genes identified integrin structures to be most significantly regulated by *HS6ST1* overexpression.

Significantly downregulated genes (441 DEGs with -log$_{10}$ p-value > 1.3) underwent GO functional enrichment analysis using g:Profiler. The top 15 significantly (FDR <0.05, using g:SCS multiple-testing correction) regulated terms are shown for (A) KEGG and (B) REACTOME analysis.

Reduced expression of 24 genes led to identification of the top 15 terms in the

GO, KEGG and REACTOME analyses. These 24 genes were investigated further, by calculating the frequency with which each gene was present in the top 15 GO, KEGG or REACTOME analyses, with 1 indicating that the gene was present in each of the top 15 GO (or KEGG or REACTOME) terms, and 0 indicating it was not present in any of the top 15 terms. As shown in **Figure 6.10**, integrin genes were most consistently identified in the terms calculated to be enriched by the GO, KEGG and REACTOME analyses. There are over 26 integrin genes, but *ITGA2*, *ITGA3*, *ITGA5*, *ITGB1* and *ITGB3* were the only integrin genes that were differentially regulated. *EGFR*, *THBS1* and *VEGFA* were also identified in at least 4/5 of the enrichment analyses, however they were generally identified to be in fewer than 50% of each of the 15 categories for each analysis method. As integrins are known to be important for connecting chondrocytes to the pericellular matrix through interactions with type VI collagen, reduced expression of these genes indicates that increased expression of HS6ST1 is likely to inhibit cell-ECM interactions.

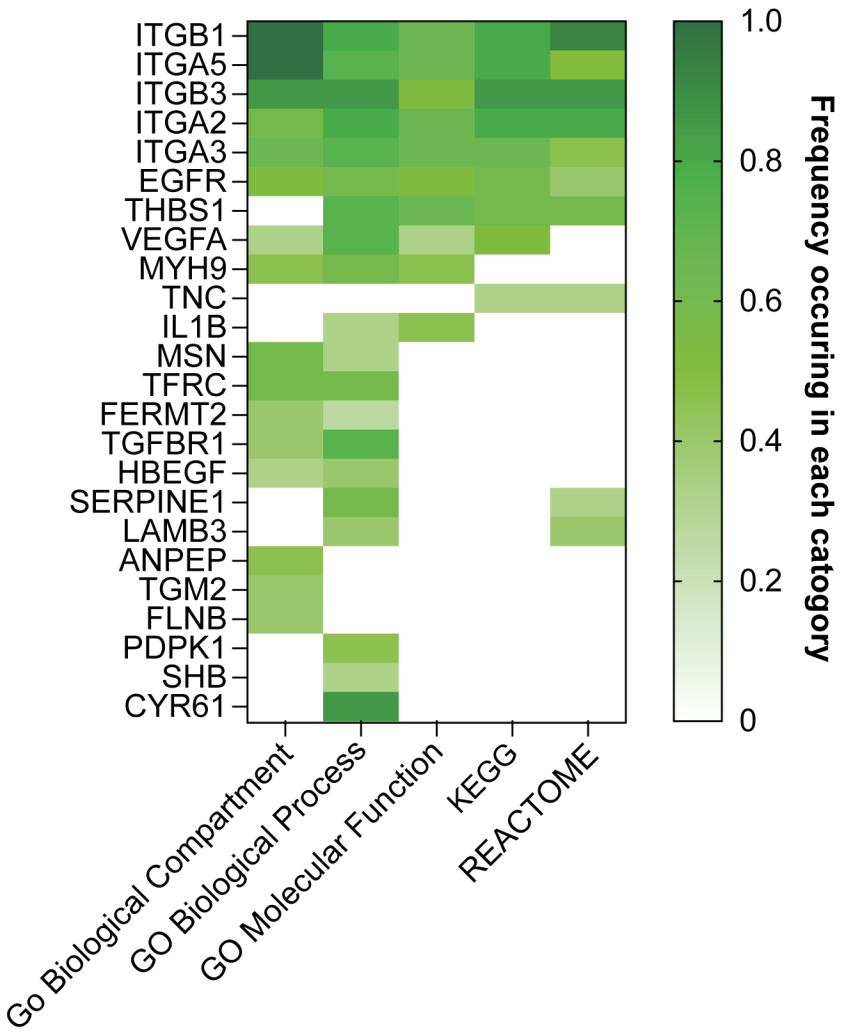

Figure 6.10 Integrin-related genes were most significantly regulated across functional enrichment analysis in *HS6ST1*-overexpressing transcripts.

The top 15 identified GO, KEGG and REACTOME terms reglected changes in expression of 24 genes. The frequency with which each gene was identified in the top 15 enriched GO:CC, GO:BP, GO:MF, KEGG or REACTOME terms is shown, with 1 indicating that the gene was represented in each of the terms of a particular analysis method, and 0 indicating it was not represented.

Finally, functional enrichment analysis of the pool of both upregulated and downregulated genes was carried out, to determine the overall effect of *HS6ST1* overexpression on C28/I2 phenotype.

6.2.6 *HS6ST1* overexpression alters cell-ECM responses

Functional enrichment analysis was performed on the pool of upregulated and downregulated genes. Compared to enrichment analysis of the downregulated genes (**Figure 6.8**) analysis of both up- and downregulated genes identified fewer significantly altered terms. This agrees with previous research where DEGs have been separated by expression. For example, in a gastric cancer data set, Hong *et al.*[361] identified 36 significantly regulated KEGG pathways in a separate analysis strategy (17 upregulated pathways, 19 downregulated pathways) but only 5 KEGG pathways in an all-enrichment strategy (which were all identified in the separated upregulated KEGG pathways).

The most significantly enriched GO:CC terms included 'Intracellular', 'Cytoplasm' and 'Focal adhesions' (**Figure 6.11 A**), in contrast with the 'Focal adhesion', 'Anchoring junctions' and 'Cell surface' GO:CC terms identified from analysis of the downregulated DEGs (**Figure 6.8**). The most significantly enriched GO:MF terms were all related to protein binding (**Figure 6.11 B**) in agreement with analysis of the downregulated DEGs (**Figure 6.8**). Indeed, some of the most significantly altered terms, such as 'Integrin binding', 'Extracellular matrix binding' and 'Protein binding' are present in both analyses.

Several (4/10) of the significantly enriched GO:BP terms identified from the pool of up- and downregulated DEGs related to (negative) regulation of cell signalling (**Figure 6.11 C**), with the remainder enriched for developmental processes (such as 'Anatomical structure morphogenesis', 'Developmental process' and 'Tube morphogenesis'). This differed slightly from terms identified by analysis of

downregulated DEGs only, which identified terms related to ‘Cellular migration’, ‘Morphogenesis’ and ‘ECM-interactions’ (**Figure 6.8**).

No REACTOME pathways were significantly enriched in the pool of up and downregulated DEGs. Finally, only 3 KEGG terms were enriched in the total pool of DEGs, with these relating to ‘TGF-β signalling pathway’, ‘Tight junctions’, and ‘microRNAs in cancer’.

The data indicate that *HS6ST1* overexpression is to negatively regulates cell signalling and the integration of signals from the ECM into a cell. This enrichment of developmental processes (‘Multicellular organism development’, ‘Anatomical structure development’ and ‘Developmental process’) in the GO:BP analyses is likely to be due to the fact that these processes are highly reliant upon growth factor signalling. integration of signals into cells is highly dependent upon membrane components and cytoskeletal components. This is reflected in the enriched GO:CC terms, with ‘Focal adhesion’, ‘Membrane-bounded organelle’, ‘Intracellular membrane-bounded organelle’ and ‘Actin filament bundle’ are all significantly enriched.

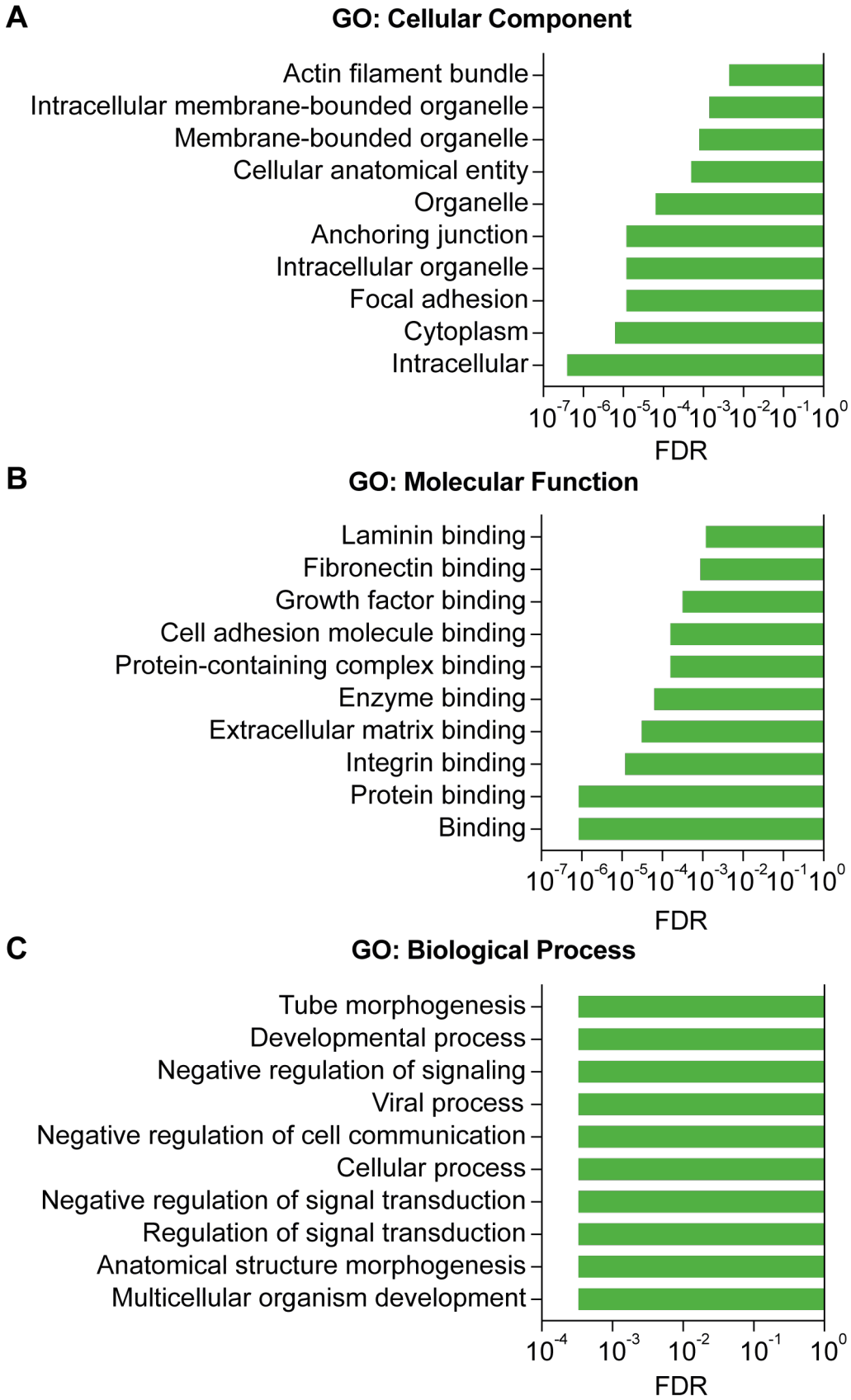

Figure 6.11 GO functional enrichment showed that ell-ECM interactions are regulated by *HS6ST1*-overexpression.

Top 10 pathways returned by GO functional enrichment analysis of all the DEGs (840 genes, Log p-value > 1.3) (A) Top 15 GO cellular component terms (B) Top 15 GO molecular function terms

(C) Top 15 GO Biological processes terms. (Functional enrichment performed using g;Profiler, p-value cut of 0.05 using g:SCS multiple-testing correction)

Functional enrichment analyses identified two key points: 1) *HS6ST1* overexpression resulted in the downregulation of integrins, which have previously been shown to control the activation of intracellular phosphorylation pathways. For example, silencing of *ITGA5* using lentiviral plasmids has been shown to significantly reduce AKT phosphorylation[362] and ITGB1 deficient mice show dysregulated ERK and JNK signalling[363] and, 2) protein interactions were particularly impacted by *HS6ST1* overexpression, in particular protein binding terms were significantly enriched in the downregulated DEGs (and, consequently, in the total pool of DEGs). Therefore, I hypothesised that the cellular responses to stimuli would be reduced.

To test this, mock- and *HS6ST1*-overexpressing cells were stimulated with growth medium for 30 min (37 ºC, 5% CO_2) and the change in phosphorylation of 39 proteins was investigated using a phosphokinase array. Due to its cost, this analysis was performed to screen for potentially altered pathways, and thus was not analysed for statistical significance. As shown in **Figure 6.12**, the response of *HS6ST1*-overexpressing cells to stimulation trended towards reduced phosphorylation of most signalling pathways compared to mock-transfected cells. Of note, phosphorylation of multiple SRC family member proteins (LCK, YES, SRC and FGR) was reduced – these tyrosine kinases bind to the cytoplasmic tail of integrin β[364], supporting the RNA-Seq data which indicated that integrin expression was reduced. This indicated that, as predicted by the RNA-seq, *HS6ST1* overexpressing cells cannot respond to their environment as robustly as mock-transfected cells. It is likely the reduced expression of integrins and matrix-

associated components inhibited the integration of extracellular signals.

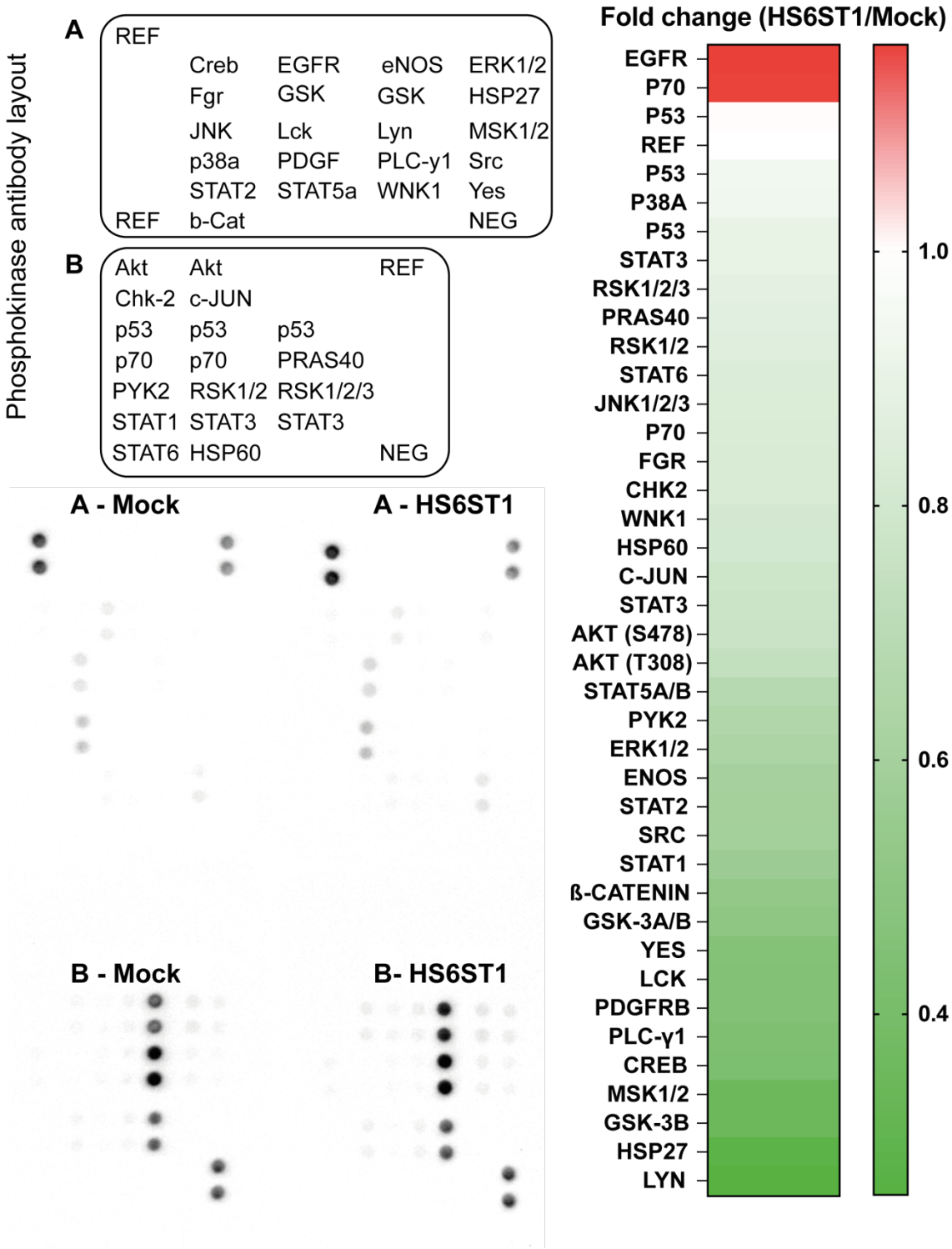

Figure 6.12 Phosphoarray showed that HS6ST1 overexpressing cells had a reduced response to serum stimulation.

C28/I2 cells ($1x10^6$) were transfected with 2 µg of mock or HS6ST1-encoding plasmid and cultured for 48 h. Cells were serum starved for 24 h and stimulated with growth medium for 30 min (37 ºC, 5% CO_2). Cells were washed twice in ice-cold PBS and cell lysates were collected in SDS sample buffer supplemented with protease and phosphatase inhibitors. Cell lysates (400 µg)

were incubated with membranes as per the manufacturer's instructions to quantify phosphorylation of the indicated proteins. Reference spots on each membrane were used to control for signal between membranes. Data analysed using ImageJ (v1.53a), and phosphorylation is shown as a fold change (signal in *HS6ST1* overexpressing cells relative to mock overexpressing cells).

6.3 Discussion

In this Chapter, I set out to identify proteins that could be responsible for the reduction in sGAG content observed when *HS6ST1* was overexpressed in C28/I2 cells. I expected responsible protein(s) to bind to heparin with an affinity that was impacted by 6-O-sulfation. Therefore, I investigated FGF-ERK signalling which is a known HS-dependent signalling pathway, and then investigated how overexpression of *HS6ST1* effected SMAD2/3 and SMAD1/5/8 phosphorylation.

As FGF2-induced ERK phosphorylation is known to be dependent upon heparan sulfate for signalling, since it promotes receptor complex formation[365] and stabilises FGF2 from denaturation/proteolysis[93], so I initially investigated this pathway as the cause of the phenotype observed. However, ERK phosphorylation was unexpectedly high in unstimulated C28/I2 cells (**Figure 6.1 A**). Both high[124,366] and low[367,368] basal ERK phosphorylation has been reported for C28/I2 cells, indicating that phospho-ERK induction in these cells is likely to be highly responsive to the culturing conditions. To eliminate the possibility that experimental protocol was responsible for the high basal activation, a published protocol[52] was followed to stimulate porcine chondrocytes with FGF2. These showed a robust induction of phospho-ERK (**Figure 6.1 B**) that was inhibited by addition of heparin or 6-O-desulfated heparin (**Figure 6.1 C**). Therefore, I decided that these cells were unsuitable for investigating ERK phosphorylation.

Equivalent inhibition of FGF2 signalling in porcine chondrocytes by heparin and 6-O-desulfated heparin oligosaccharides was not unexpected given the known effects of heparin on FGF2 signalling, with 6-O-sulfate groups being important for formation of the ternary receptor complex[92], but not for initial interactions of FGF2 with cell surface HS[133]. Both forms of exogenously added heparin oligosaccharides thus compete with endogenous HS for FGF2 binding displace FGF2 from the cell surface, therefore inhibiting FGF2-induced ERK phosphorylation. As this competitive inhibition is directed against FGF2 and not the receptor complex, the 6-O-sulfate group is largely dispensable. Indeed, my observations agree with previous literature, which found that loss of the 2-O-sulfate group most strongly inhibited heparin-FGF2-binding[369].

TGF-β-induced SMAD phosphorylation has previously been implicated in increased cartilage formation of chick limb buds[370], stimulation of undifferentiated mesenchymal cells into chondrocytes[370], and inhibition of hypertrophic differentiation of cultured chondrocytes[371]. Therefore, I investigated how overexpression of *HS6ST1* changed SMAD2/3 and SMAD1/5/8 phosphorylation. Overexpression of *HS6ST1* had no effect on TGF-β1-induced SMAD2/3 phosphorylation or TGF-β1-induced SMAD1/5/8 phosphorylation (**Figure 6.3 B**). Then, I investigated the effect of *HS6ST1* on SMAD1/5/8 signalling using BMP4. In agreement with Otsuki *et al.*[151] who observed reduced BMP7-induced SMAD1/5/8 phosphorylation in *Sulf* deficient mice, overexpression of *HS6ST1* significantly reduced BMP4-induced SMAD1/5/8 phosphorylation (**Figure 6.4 B**) but unexpectedly had no significant effect on BMP4-induced sGAG accumulation (**Figure 6.5**).

The reduction in BMP4-induced SMAD1/5/8 phosphorylation may have been insufficient to feed through to a change in sGAG accumulation, or sGAG accumulation may not be a sufficiently robust readout of SMAD signalling. Other biological consequences of BMP4 signalling may be useful in this context. For example, BMP4 strongly induces expression of ID1-3[372], so future experiments could utilise RT-qPCR analysis to investigate the induction of ID1-3 (or their target genes). Alternatively, as ID proteins function by binding to transcription factors to inhibit signalling, a pulldown assay of ID1-3 would elucidate which transcription factors are being targeted. Altered pulldown of these transcription factors in HS6ST1-overexpressing cells would indicate that HS6ST1 regulates BMP4-induced ID activity. As these are direct effects of SMAD1/5/8 phosphorylation they could offer a more reliable readout for BMP4 signalling than sGAG accumulation, which is the result of multiple signalling, transcriptional and translational events.

Interestingly, *HS6ST1*-overexpressing cells had significantly reduced viability when treated with TGF-β1 (**Figure 6.3 A**) or BMP4 (**Figure 6.5 A**) compared to *HS6ST1*-overexpressing cells. Furthermore, treatment with either TGF-β1 or BMP4 restored the sGAG content of *HS6ST1*-overexpressing cells to levels in mock-transfected cultures, despite these growth factors having no significant effect on sGAG accumulation in the absence of *HS6ST1* overexpression (**Figure 6.3 B**, **Figure 6.5 B**). The increased viability and reduced sGAG content of *HS6ST1*-overexpressing cells may be caused by endogenous ligand(s) that bind to (highly 6-O-sulfated) HS and are competitively displaced from HS by addition of these two growth factors. In support of this interpretation, TGF-β1 and BMP4 did not reduce the sGAG content of mock overexpressing cells, where

endogenous ligands were not impacted by HS6ST1 overexpression. This will be further discussed in **Chapter 7**.

RNA-sequencing of C28/I2 cells overexpressing *HS6ST1* identified that 840 genes were significantly regulated by *HS6ST1* overexpression, and the expression of these genes could be used to identified which treatment group a sample belonged to (**Figure 6.6**). *HS6ST1* overexpression upregulated genes controlling the cell cycle and downregulated genes controlling cellular responses to their environment. Specifically, integrin genes were found to be abundant in pathways identified among the downregulated genes.

Intriguingly, the upregulated genes all converge on control of the transition from G2 into mitosis. CDC25A initiates mitosis after activation of CDK1 during G2[373], CHEK2 is an inhibitor of CDC25C, and controls entry into mitosis[374], CENPA and TACC3 are both involved in formation and stabilization of the kinetochores[375,376], which establish a physical connection between chromosomes and the mitotic spindle and are thereby crucial for proper mitosis. PCNA is involved in lagging-strand DNA synthesis[377] and TACC3 has previously been shown to promote mitosis of MSCs [378]. Increased cell division may underlie the increased signal in the MTS assay, which can be used as a measure of cell viability and of cell number. However, increased expression of these genes is however not necessarily indicative of increased cell growth. Overexpression of *CDC25A* has been observed to reduce cell growth, marked by mitotic aberrations and replication stress in RPE-1 cells[379]. Increased *CHEK2* expression in hepatocellular carcinoma cells caused chromosomal segregation deficiencies that were reversible by CHEK2 knockdown[380]. In chondrocytes, *CENPA* was

found to be highly expressed in 'proliferating chondrocytes' [381], but both increased and reduced expression has previously been shown to promote mitotic defects and chromosomal instability in various cell types [382,383], suggesting that effective control of *CENPA* expression is crucial for cell cycle control and DNA integrity. Altered expression of cell cycle genes may thus indicate that *HS6ST1* overexpression induces changes in gene expression that may cause chromosomal instability and thus, DNA damage in C28/I2 cells. This is likely to lead to dysregulated expression of numerous genes, as is seen in OA chondrocytes[384]. Indeed, upregulation of cell-cycle related genes in OA chondrocytes has been demonstrated[385]. *HS6ST1*-overexpression may therefore push C28/I2 cells towards an OA phenotype through upregulation of these genes. This stands at odds with a report from Sun *et al.*[386], who concluded that cell-cycle related pathways were enriched among downregulated genes from OA chondrocytes. However, this data was a reanalysis of microarray data first published by Chou *et al.*[387], who specify that the samples analysed are isolated from total joints. The samples are thus likely to contain more subchondral bone than cartilage, and so our findings are not directly comparable, due to the difference in tissue origin. This does however raise interesting questions as to whether bone and articular cartilage gene expression does indeed move in opposite directions in OA, and why cell cycle related gene expression is reduced in bone given the osteophyte formation observed in OA. Further research must be done on this question, as the results are seemingly paradoxical with clinical observations.

Genes downregulated by *HS6ST1* overexpression were enriched for terms relating to cell-ECM interactions, such as integrins. Enriched GO:CC and GO:MF

terms both related to how cells attach to the ECM (Figure 6.8). KEGG and REACTOME analysis agreed with this, as both analyses indicated enrichment of terms related to focal adhesion, and ECM organisation and interaction (Figure 6.9). When I analysed the frequency with which genes were present in the 15 most significant terms of each functional analysis, integrin genes, specifically *ITGA2, 3, 5* and *ITGB1* and *-3*, were most commonly found. This reflects the integrin expression pattern of chondrocytes, which are known to express integrin α1, 2, 3 and 5 subunits, alongside β1 and 3[43]. This expression pattern allows chondrocytes to interact with several ligands commonly found in cartilage, such as type II and VI collagen (via α2β1)[388], chondroadherin (via α2β1)[389] and fibronectin (via α3β1, α4β1 and α5β1)[390,391]. Surprisingly, integrins have previously been suggested to promote OA pathogenesis. Integrin β3-deficient mice showed reduced cartilage degeneration following DMM surgery[392] and *α5* conditional knockout mice had reduced OA progression following DMM surgery[45]. Chondrocytes isolated from OA cartilage failed to respond to cyclic compression in the α5β1-dependent manner seen in normal chondrocytes [393]. As control of integrin expression has been shown to be regulated at the transcriptional, translational, and post-translational level, further work is required to determine whether *HS6ST1*-overexpression reduces cell surface integrin levels. This could be investigated using flow cytometry, immunocytochemistry, and immunohistochemistry. However, it is notable that the phosphorylation of a number of kinases that are downstream of the integrin receptors, such as the SRC kinases[394] LYN, LCK, YES, SRC and FGR was reduced in stimulated *HS6ST1*-overexpressing C28/I2 cells (**Figure 6.12**) possibly suggesting reduced integrin signalling. Given the phosphoarray is a single replicate, and there is inherent variability with the quantity of antibodies spotted onto each membrane,

the reduced phosphorylation of these kinases in response to stimulation must be further validated, such as by western blotting, or using an approach such as phosphoproteomics. If further investigation shows HS6ST1-dependent downregulation of SRC kinase phosphorylation is a direct result of reduced integrin expression, then using siRNA (or CRISPR) against each individual integrin predicted to be downregulated could elucidate how phosphorylation of these kinases is being regulated by *HS6ST1* overexpression.

Finally, I looked at which pathways were enriched by all DEGs. Overall, the effect of the downregulated genes contributed more to the enriched pathways in this analysis than the upregulated genes. The enriched GO:MF terms were similar to the downregulated GO:MF enriched terms as all involved protein binding. Intriguingly, GO:CC enriched terms (**Figure 6.11 A**) included both intracellular terms (Intracellular, Cytoplasm), with genes contributing to enrichment having roles in diverse processes such as metabolism, cell cycle control and protein-protein interactions, and terms related to cell-ECM interactions ('Focal adhesion', 'Anchoring junction'). As with the downregulated genes, integrin-related genes were identified in these enriched ECM-related terms. In contrast to this, the GO:BP (**Figure 6.11 C**) enriched terms were more varied than for the downregulated genes. It is unsurprising that many developmental processes were enriched, given the known role for HS in development (**1.3**). The other major categories of enriched terms related to negative regulation of cell signalling and communication. Therefore, in conjunction with the reduced sGAG accumulation observed, I hypothesised that *HS6ST1* overexpression reduced cellular signalling in response to stimuli. Using a commercially available phosphokinase array, I tested the activation of 39 phosphoproteins in response to *HS6ST1*

overexpression. This showed that phosphorylation of 37 out of 39 of the phosphoproteins on the array was reduced when *HS6ST1* was overexpressed in C28/I2 cells (**Figure 6.12**).

As there was no reduced cell viability (**Figure 4.3**) this indicates that overexpression of *HS6ST1* had an inhibitory effect on cellular signalling in response to a broad stimulus such a serum. This is supported by the reduced response to BMP4 (**Figure 6.4**) and the reduced sGAG-accumulation of *HS6ST1* overexpressing cells (**Figure 4.2**).

Whilst not identified, it is possible that a single or group of ligand(s) is responsible for the changes in gene expression observed. A growth factor is most likely to be responsible, as *HS6ST1*-overexpressing cells had not only increased viability (**Figure 4.3**) and altered sGAG accumulation over time (**Figure 4.2**) indicating some form of positive feedback cycle. Finally, integrin expression is known to be tightly regulated by many growth factors[395–397]

Chapter 7. Discussion

Sulfated glycosaminoglycans are critical for cartilage function as they confer the mechanoproperties of cartilage through the chondroitin sulfate side chains of aggrecan and enable a response to biochemical stimuli through the heparan sulfate side chains of proteoglycans located in the pericellular matrix (**1.2**). sGAG content has been shown to decrease significantly with age in femoral head articular cartilage of both aged male and female rats[398] and *in vitro* examination of chondrocytes from young and old healthy human donors showed loss of *SOX9* expression and increased expression of *MMP13* and *p21* with age[399]. In OA, CS is lost from the joint as aggrecan undergoes proteolysis[238], and HSPG content is changed as chondrocyte gene synthesis is dysregulated[68]. Loss of CS from the joint is likely both a natural feature of ageing, and a process that is dysregulated in OA, potentiated by increased activity of proteases that cause a dramatic decrease in sGAG content. Interestingly, sGAG recovery following IL-1β treatment of young bovine cartilage explants was markedly lower in regions with greater sGAG loss, whereas regions with 'mild' sGAG loss recovered well[400]. This implies that for mild to moderate damage there is a robust recovery mechanism. This is further supported by the fact that moderate cyclic loading (stimulating aerobic exercise) of chondrocytes stimulates the expression of anabolic genes, whereas for more serious damage this recovery mechanism is impaired. Given these loading experiments were conducted on chondrocytes isolated from young cows, a possible explanation for the lack of repair in aged cartilage may be the loss of repair in response to 'light' loading. Furthermore, this repair is most likely

a response to growth factor-mediated signalling, which can stimulate anabolic gene expression and the synthesis of new matrix components. The signalling of growth factors, as discussed in Chapter 1, is largely (although not exclusively) regulated by the heparan sulfate side chains of proteoglycans in the pericellular matrix and the cell surface. Strict control of heparan sulfate biosynthesis is therefore crucial for cartilage phenotype. This is highlighted by the fact that many HS knockout mice show chondrogenic and skeletal defects (**Table 1.1**). It was perhaps unsurprising then that HS structure and functions were found to be altered in OA. First, an important role for 6-O-sulfation of HS in cartilage homeostasis was observed by Otsuki *et al.*[151], who showed that *Sulf1*$^{-/-}$ and *Sulf2*$^{-/-}$ mice had greater spontaneous and surgically-induced cartilage loss. Then, HS from OA cartilage was identified to have increased 6-O-sulfation, driven by increased expression of the 6-O-sulfotransferase *HS6ST1*[68] and finally HS from OA cartilage was observed to have reduced affinity for FGF2 and VEGF[401].

Therefore, I set out to determine what the effect of increased 6-O-sulfation was on the phenotype of a cartilage cell line. In this thesis, I investigated the phenotype of C28/I2 cells in response to *HS6ST1* overexpression, characterizing how increased 6-O-sulfation altered the 'ligandome' of HS, and how the signalling and transcriptional landscape of C28/I2 cells changed in response to *HS6ST1* overexpression.

7.1 C28/I2 cells were a viable choice for investigating chondrocyte biochemistry.

I used an immortalised chondrocyte cell line, C28/I2, to investigate the effect of *HS6ST1* on chondrocyte phenotype. A murine model with *HS6ST1* expression either 'knocked out' or 'knocked in' would likely have yielded more physiologically-relevant information but would have had several drawbacks. Knockout of *HS6ST1* would have necessitated using a Cre-lox method utilising a Cre recombinase driven by the promoter of a prototypic cartilage gene, such as *Prg4, Col2* or *Acan*, given the embryonic (and post-embryonic) lethality observed in *HS6ST1*$^{-/-}$ mice[145,402]. A knock-in model would have best matched the observed increase in 6-O-sulfation observed in OA cartilage. To date, there are no published models of mice overexpressing *HS6ST1*. The generation of such a transgenic animal and investigation of its susceptibility to OA can be prohibitively expensive, necessitating the use of alternative models. Primary chondrocytes would have been the next-best model to use, but these show high donor-to donor variability and low transfection efficiency. Additionally, COVID19 impacts on elective surgery meant that I was unable to obtain any fresh healthy or OA cartilage samples from which I could have isolated viable chondrocytes for further study.

Therefore, a cell line was used to investigate the role of *HS6ST1* in chondrocytes. I compared two different cell lines for their expression of HS-related and anabolic cartilage genes (**Figure 3.1**). I selected the immortalised chondrocyte cell line C28/I2 for further study as it expressed the chosen anabolic cartilage genes and expressed detectable levels of relevant HS biosynthesis genes (**Figure 3.2** and

Figure 3.3). Next, I optimised transfection with an *HS6ST1*-encoding plasmid using a transient transfection system and detected expression of FLAG-tagged *HS6ST1* at the mRNA and protein level for up to 96 h (**Figure 3.5**). The effect of this overexpression is likely to have significantly altered the 6-O-sulfation levels of the HS chain[403]. I would have liked to have conducted quantitative HS disaccharide analysis to confirm the extent of 6-O-sulfation achieved by HS6ST1 overexpression; however, this analysis is restricted to specialised laboratories, and we have been unable to establish this in-house. Future work would benefit greatly from this analysis, as an understanding of how and when the disaccharide composition changes in response to overexpression would help answer many of the biological questions that were raised by this research. Work by Do *et al.*[403] can partially answer this question, as they observed a dose-dependent decrease in 2-O-sulfated UA(2S)-GlcNS and UA(2S)-GlcNS(6S) disaccharides, together with an increase in UA-GlcNS(6S) disaccharides following *HS6ST1* overexpression in HEK293 cells. It is likely that C28/I2 cells may follow a similar change in disaccharide composition following *HS6ST1* overexpression, however HS composition can vary dramatically between tissues and cell types. Importantly, HEK293 cells are embryonic in origin, and during the transition from embryonic stem cells to neural progenitor cells HS becomes more highly sulfated[404], and induced-pluripotent stem cell commitment to the ectoderm lineage reduces FGF2 binding to neural cell HS[405], most likely due to reduced 2-O-sulfated iduronic acid-containing disaccharides (see **1.2.3**). Therefore, it is not possible to draw firm conclusions on the change in HS structure following *HS6ST1* overexpression in C28/I2 cells from studies in HEK293 cells. Additionally, one caveat of quantitative disaccharide analysis is that any change in domain architecture following *HS6ST1* overexpression may not be detected.

Chanalaris *et al.*[68] identified increased total 6-O-sulfation, but there were no significant differences in the abundance of individual disaccharides between healthy and OA cartilage. Furthermore, despite having a robust phenotype, *Sulf2*-null exhibit no differences in their levels of HS 6-O-sulfation, whereas such changes are observed in *Sulf1*-null mice[406]. This likely represents compensatory mechanisms by other biosynthesis enzymes, or localization of the changes to distinct, biologically-important areas of the HS chain.

7.2 *HS6ST1* overexpression reduced sGAG content.

As OA is characterised by the loss of sGAG from the joint, I investigated how overexpression of *HS6ST1* changed the sGAG content of C28/I2 cells. I observed a significant, time-dependent decrease in sGAG content following *HS6ST1* overexpression which could be reversed by addition of recombinant SULF2 (**Figure 4.2**). This was in line with observations made using *Sulf*-null mice, which also had reduced sGAG content[151]. In general, increased sulfation of GAGs within the PCM appears to have a catabolic effect on chondrocytes, since loss of *Hspg2*[185]*, Ext1* or *Ndst1* in mice reduced either reduced surgically-induced OA or protease activity[189]. Furthermore, knockdown of decorin (a small CSPG) in C28/I2 cells increased sGAG content[407].

As discussed previously, the major GAG observed in the joint is the CSPG aggrecan which composes 50% of the dry weight of the joint. In C28/I2 cells, expression of aggrecan (ACAN) was similar to that of the HS biosynthesis enzymes (**Figure 3.1**) and it was not as highly expressed as *SOX9.* However, this may be explained by the relatively long half-life of structural ECM molecules

like aggrecan compared to transcription factors such as *SOX9.* It is known the major sGAG signal (Alcian blue staining) of cartilage comes from aggrecan, and the same is expected of C28/I2 cells – that is, CS is expected to make up the majority of the sGAG signal detected by the Alcian blue stain. Given that cells *in vitro* tend to accumulate less ECM than cells *in vivo,* it is possible that the ratio of CS:HS in C28/I2 cultures is not representative of that which may be observed *in vivo,* however it is most likely that the changes in sGAG content observed here are due to reductions in CS content, and not due to reduced HS content. This would support the observations made in this thesis where few changes in gene expression were detected, since changes in HS would have been expected to change expression of many genes given the relative importance HS has in protein signalling compared to CS.

This reduction in sGAG content in HS6ST1-overexpressing C28/I2 cells was initially hypothesised to be due to a reduction in the amount of aggrecan. Expression of *ACAN* mRNA was not changed by *HS6ST1* overexpression (**Figure 4.12**), so I investigated whether protease expression and activity were altered. mRNA expression of *ADAMTS4*, *ADAMTS5* and several *MMPs* was unchanged (**Figure 4.7**), and their expression levels were too low for reliable detection of activity using aggrecan or fluorescent substrates until at least 96 h post-transfection (**Figure 4.5, Figure 4.8, Figure 4.9**). I am thus unable to decisively conclude whether the observed reduction in sGAG content was due to a change in the activities of aggrecan-degrading proteases following *HS6ST1* overexpression. Future work to address this important question could utilise transgenic mouse cartilage, where higher levels of protease activity can be quantified by ELISA[23], immunohistochemistry and immunoblotting[408].

I observed a significant increase in the expression of *HYAL1* (**Figure 4.9**), a hyaluronidase that breaks down hyaluronan, and a decrease in the expression of *HAS2* (RNA-seq, **Figure 6.6**). HA enables the aggregation of aggrecan molecules within cartilage, and treatment of cartilage with hyaluronidase results in a significant loss of the hyaline architecture[17]. The combination of these two changes may reduce aggrecan retention by *HS6ST1*-overexpressing cells. Further work will be needed to confirm this. It would be interesting to quantify changes to HA with the use of HA-binding protein in cultures of mock and *HS6ST1*-overexpressing cells using confocal microscopy, or culture cells in the presence of a HYAL inhibitor, such as poly(styrene-4-sulfonate)[409], to investigate whether sGAG content can be recovered.

IGFBP-5 was among the proteins detected to bind with higher affinity to 6-O-sulfated heparin by LfQ MS (**Figure 5.6, Figure 5.7, Figure 5.8**). As increased binding was not significant once FDR was applied, IGFBP-5 was not studied further, but based on previous studies, the IGF axis may be worth investigating further as a possible explanation of the reduced sGAG content of HS6ST1-overexpressing cells. IGF-1 has potent anabolic effects on chondrocytes, promoting chondrogenesis and preventing cartilage damage[410,411]. However, the anabolic activity of IGF-1 is regulated by a negative feedback loop, which I propose is dysregulated in *HS6ST1*-overexpressing cells, as outlined in **Figure 7.1**. IGF-1 activation of insulin-like growth factor receptor 1 (IGFR1) stimulates phosphorylation of Src homology 2 domain-containing protein tyrosine phosphatase substrate 1 (SHPS1), which attenuates IGF-1-IGFR1 signalling by recruiting Src homology 2 domain-containing protein tyrosine phosphatase 2

(SHP2) to IGFR1. Integrin-associated protein (IAP) promotes SHPS1 recruitment of SHP2 to IGFR1, thus IAP also inhibits IGF-1 signalling[412].

Thrombospondin-1 (TS-1) inhibits IAP/SHPS1 interactions, by competing with SHPS1 for IAP binding, thus TS-1 promotes IGF-1 signalling[413]. Insulin-like growth factor binding protein 5 (IGFBP5) directly binds TS-1 to prevent TS-1/IAP binding and therefore has an overall inhibitory effect on IGF-1 signalling. Interestingly, the interaction between IGFBP-5 and TS-1 is promoted by heparin but inhibited by HS[414]. Although not above the FDR, IGFBP5 was identified to be significantly more abundant in eluates from heparin- than 6-O-desulfated heparin-Sepharose in my MS screen, indicating its binding to HS is promoted by 6-O-sulfation. IGFBP5 interactions with TS-1 may thus be promoted in *HS6ST1*-overexpressing cells, leading to inhibition of IGF-1 signalling through reduced inhibition of IAP/SHPS1 recruitment of SHP2 to IGFR1. This in turn inhibits the anabolic activity of IGF-1. Therefore, *HS6ST1* overexpression is predicted to reduce IGF-1 signalling, leading to a reduction in sGAG accumulation in C28/I2 cells. Investigating IGFR1 phosphorylation dynamics in *HS6ST1* overexpressing cells could be a potential next step in identifying the mechanism of reduced sGAG accumulation observed in these cells, as this model proposes IGFR1 phosphorylation in response to IGF-1 stimulation would be more transient. One possible way to investigate this would be by western blotting for phospho-IGFR. Alternatively, expression of IGF-1 response genes could be determined using RT-qPCR. If IGF-1 signalling is reduced due to more transient phosphorylation of the receptor, then overexpression of IGFR1 could be one possible avenue to attenuate the effects of *HS6ST1*. Despite extensive efforts, there are currently no

clinically available SHP2-targetting drugs[415,416], meaning that directly targeting SHP2 as a modulator of IGF-1 signalling in OA is currently unviable.

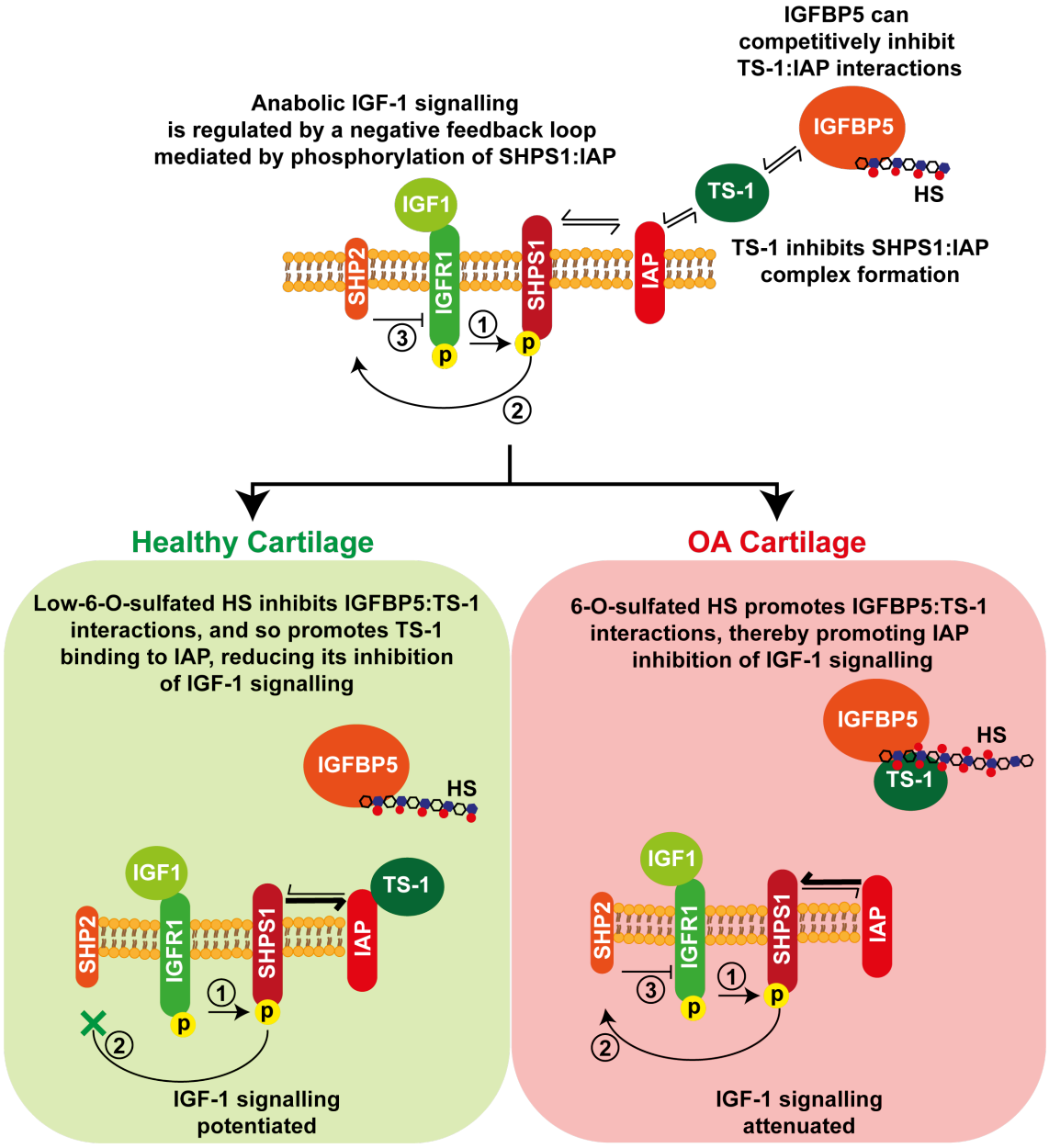

Figure 7.1 6-O-sulfated HS promotes IGFBP5 inhibition of IGF-1 signalling

IGF-1 signalling is regulated by a negative feedback loop where phosphorylation of SHPS1:IAP complexes recruits SHP2 to IGFR1, causing dephosphorylation of the receptor and inhibiting signalling. TS-1 inhibits IAP:SHPS1 interactions, TS-1 can in turn be inhibited by IGFBP5. In healthy cartilage, lowly-sulfated HS is proposed to bind to IGFBP5, preventing IGFBP5:TS-1 binding, and thereby promoting IAP:TS-1 interactions and reducing IAP inhibition of IGF-1 signalling. In OA cartilage, 6-O-sulfated HS would promote IGFBP5:TS-1 interactions, reducing IAP:TS-1 interactions, and thus promoting IAP-induced inhibition of IGF-1 signalling.

7.3 COLXVIII may have a role in the joint not involving GAG synthesis.

A key aspect of this thesis was to identify which proteins differentially bound 6-O-sulfated HS. To achieve this, I extracted proteins from cartilage and quantified the heparin- and 6-O-desulfated heparin-binding proteins using differentially sulfated heparin-Sepharose chromatography resins and LfQ MS. This was performed on cartilage extracts from both healthy (**Figure 5.6**) and OA (**Figure 5.7**) cartilage samples. In both experiments COLXVIII was identified to be most significantly changed in the eluates from the 2 resins, and the identified protein was then identified to be the cleaved version of COLXVIII, namely endostatin (**Figure 5.9**). Despite having only a single biological replicate, and a low number of technical replicates, COLXVIII was identified as the top hit in both the normal and OA samples. Therefore, I am confident that the protein is present in adult articular cartilage, and that it preferentially binds 6-O-sulfated HS. By western blotting for endostatin, the C-terminally cleaved version of COLXVIII, I confirmed that the abundance of endostatin in 6-O-desulfated heparin-Sepharose eluates was reduced compared to heparin-Sepharose eluates (**Figure 5.11**).

The role of COLXVIII in cartilage is unclear. My experiments showed that endostatin had no effect on sGAG synthesis in C28/I2 cells. Previous studies have shown that endostatin increased the expression of *Col2a1* and decrease expression of *Mmp* genes in rat chondrocytes[315], and interestingly endostatin levels are reduced in OA cartilage compared to healthy[331]. Endostatin may have an anti-catabolic role, as it has been suggested to block the activation of MMP-2 -9 and -13[417] and to inhibit the activity of MMP-2 by binding to its catalytic site[332].

In preliminary experiments, I did not observe similar effects on MMP-13 (data not shown). Endostatin inhibits endochondral ossification[418], but is not required for proper skeletal formation[419], suggesting it may have a role in preventing the premature ossification of articular cartilage in healthy tissues. As endostatin is lost from the joint in OA, its proposed protective activities, such as preventing MMP activation and/or activity and inhibiting ossification of cartilage should be further investigated. COLXVIII-null mice show no apparent differences in body size[420] but no skeletal and/or cartilage-focused studies have been published. Interestingly, COLXVIII-null mice developed more severe glomerulonephritis than wild-type mice, which could not be recovered by addition of exogenous endostatin. The activity of COLXVIII in protecting basement membranes is therefore either endostatin-independent or exogenous endostatin does not function in a similar manner as endogenously produced endostatin. The reason for this is unclear but may relate to differences in proteolytic cleavage or glycosylation dependence of endogenous endostatin. Finally, while I propose that aberrant *HS6ST1* expression is detrimental for cartilage, endostatin – the cartilage protein most strongly predicted to bind to 6-O-sulfated HS – is proposed to be anabolic. It is confounding that the protein that was most strongly predicted to bind to this 6-O-sulfated HS is endostatin, which is proposed to be anabolic. It may be that binding of the endostatin region of full-length type XVIII collagen to HS is what promotes its cleavage, or that binding of endostatin to HS brings it into proximity with proteases that cleave it into a non-functional protein. This binding may be increased in OA where there is an increase in 6-O-sulfated HS, any this may be an explanation for the reduced levels of endostatin in OA joints. Alternatively, binding of endostatin to 6-O-sulfated HS may inhibit its proposed anabolic activities. Future experiments could investigate how incubation of

differentially-sulfated heparins and endostatin alongside pro-MMPs alter MMP activation or activity of MMPs against Knight substrate.

A significant disadvantage to LfQ MS analysis of conditioned medium is it provides no information on cell surface proteins that are not shed. This is especially pronounced when investigating heparan sulfate-related proteins, as cell surface HSPGs (syndecans and glypicans) are involved in retaining proteins on the cell surface. An alternative approach may therefore involve investigating the conditioned medium and 'cell surfaceome' of C28/I2 cells transfected with *HS6ST1*. This could be achieved using a method such as Cell Surface Capture (CSC)[421,422], which enables quantification of transmembrane proteins such as G-protein coupled receptors, receptor tyrosine kinases and integrins. Coupled with quantification of the conditioned medium this would give a more comprehensive view of the effect of HS6ST1 on receptor growth factor and protease expressions, and potentially enable identification of factors that may be responsible for reduced sGAG accumulation. Furthermore, due to the ease of culturing cell lines, this would also enable a greater number of replicates to be analysed, therefore increasing statistical power.

7.4 *HS6ST1* overexpression reduced cell-matrix interactions.

I observed a significant downregulation of genes involved in cell-matrix adhesion following *HS6ST1* overexpression. Interestingly, a specific subset of genes that influenced many of the analyses were integrins, which were downregulated in response to *HS6ST1* overexpression (**Figure 6.10**). Integrins are crucial for cell adherence to the matrix and can cooperatively activate several signalling

pathways, such as IGF-1 and Yes-associated protein (YAP) signalling. Canonical IGF-1 signalling occurs solely through IGFR1, but recent work indicates integrins associate with IGF:IGFR signalling complexes to promote their signalling[423]. Interaction of integrins with the matrix controls the activity of YAP[424], which was shown to be chondroprotective in a surgically-induced OA model[425]. Interestingly, IGF-1 signalling directly increased YAP expression[424], potentially leading to a positive feedback cycle where IGF-1 signalling induces YAP expression and activity. *HS6ST1* overexpression therefore may inhibit both IGF-1 signalling (through downregulation of integrins) and YAP activity (by downregulating IGF-1 signalling). In OA cartilage, YAP expression reduces as cartilage damage increases[425]. OA cartilage has reduced Youngs moduli compared to healthy cartilage[426]. Reductions in ECM stiffness can in turn reduce YAP activity[427]. As HA contributes to ECM stiffness it is possible that early reductions in HA content, as discussed in **7.2**, in *HS6ST1*-overexpressing cells may downregulate integrin expression and focal adhesion formation, due to a reduction in matrix stiffness[428,429], and therefore reduce YAP activity. YAP activity in *HS6ST1*-overexpressing cells was not investigated in this thesis, but a reduction in YAP activity is supported by the observation of reduced phosphorylation of SRC-family kinases (YES, LYN, LCK **Figure 6.12**) that subsequently activate YAP. Recent work suggest they can have a catabolic role in embryonic chondrocytes, inhibiting chondrogenic phenotype in chondrocytes isolated from embryonic long bones[430], but their role in adult chondrocytes requires further investigation.

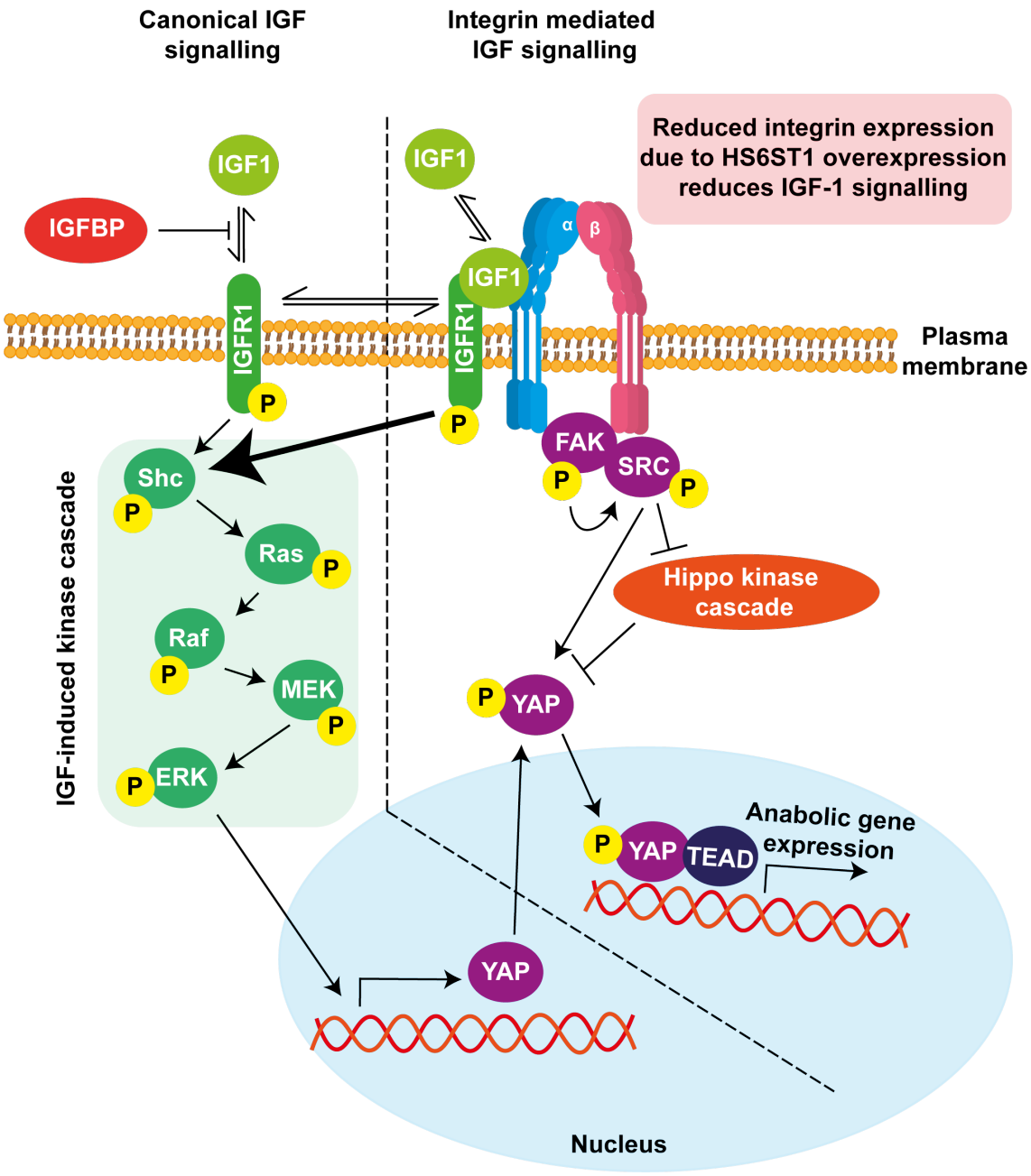

Figure 7.2 Proposed model showing HS6ST1-induced reduction in integrin expression leading to reduced IGF-1/integrin pathway crosstalk.

IGF-1-induced phosphorylation of IGFR1 initiates a signalling cascade that causes expression of IGF-1 target genes, including YAP. IGF-1 signalling is potentiated when IGF-1/IGFR1 are associated with integrins. IGF-1-induced YAP expression then promotes integrin-mediated signalling following focal adhesion formation. YAP translocates to the nucleus where it induces expression of target genes. Reduced integrin expression in response to *HS6ST1* overexpression reduces both IGF-1 signalling and YAP activity, inhibiting anabolic gene expression.

While reduced integrin expression is the most likely explanation for the reduced

signalling observed in HS6ST1-overexpressing C28/I2 cells (**Figure 6.12**) it is possible however that this is due to altered signalling by unknown growth factor(s). A key question not answered in this thesis is which protein(s) interact with 6-O-sulfated HS to induce downregulation of genes involved in matrix adhesion. I was unable to interrogate FGF2-induced signalling inC28/I2 cells due to basally high ERK phosphorylation, and did not observe any effect of HS6ST1 on TGF-β1-induced SMAD2/3 phosphorylation (**Figure 6.2**), but did observe moderate differences in BMP4-induced SMAD1/5 phosphorylation (**Figure 6.4**) following overexpression of HS6ST1. Further work should aim to clarify whether *HS6ST1* overexpression is involved in TGF-β1/BMP4 regulation of integrin expression, as both have been shown previously to induce integrin expression[431,432]. However, a candidate approach such as this to identify ligands that regulate integrin expression is challenging, as integrins are regulated by numerous growth factors and ECM composition[433,434]. The observation that TGF-β1 and BMP4 could reverse the HS6ST1-dependent reduction in sGAG content (**Figure 6.3, Figure 6.5**) is a strong indication that this cellular phenotype is caused by an endogenous HS-binding protein, whose signalling is modulated by the HS6ST1-modified HS and is competitively displaced by addition of exogenous HS-binding proteins, or potentially by proteins that bind with higher affinity for 6-O-sulfated heparin, such as those identified by the LfQ MS screen performed here. A possible approach to identifying this 6-O-sulfate-binding protein would be to treat cells with surfen, which could compete this protein(s) off HS and enable its identification by LfQ-MS.

Broader implications

Given the consistent reduction in sGAG content following *HS6ST1* overexpression (**Figure 4.2**), and the observations made by *Otsuki et al.*[151,191] it must be concluded that increased 6-O-sulfation of HS is detrimental for cartilage. As recombinant SULF2 could reverse the loss of sGAG content, a potential therapeutic option may be intra-articular injections of SULFatases in OA patients, although this is a challenging protein to express recombinantly. Inhibition of HS6ST1 could be a potential therapeutic avenue, however there are no published specific inhibitors for HS6ST1, and targeting drugs to either HS6ST1 or SULFs in cartilage could be difficult given most drugs would diffuse across the synovial membrane and may result enzyme inhibition in non-joint tissues. Optimisation of delivery methods would therefore be required, such as fusion with a targeting peptide[435], as non-specific inhibition of HS6ST1 in other tissues may lead to disease or other disorders (see **1.4**). Targeting drugs to HS6ST1 may also be difficult given the high sequence and structural similarity between HS6ST1, -2 and -3.

The cause of increased *HS6ST1* expression in OA cartilage is unknown. One possible explanation is that age-induced cellular stress may cause dysregulation of gene expression. Endoplasmic and Golgi apparatus stress have been linked to OA[436], other age-related diseases such as Alzheimers and Parkinson's Disease[437,438], and increased expression of HS biosynthesis genes, including *HS6ST1,* in HeLa cells[439]. As the prevalence of clinically-diagnosed OA is known to increase with age, age-related Golgi stress may induce HS6ST1 overexpression and thus leading to dysregulated cartilage homeostasis.

Therefore, drugs targeting Golgi stress may therefore be potential future therapeutic options following further research.

6-O-sulfation likely has a nuanced role across tissues in the body. Whilst this thesis proposes that increased 6-O-sulfation is detrimental for cartilage and dysregulation has a pathogenic role (see **1.4**), increased expression of SULF2 (indicating reduced 6-O-sulfation) has been detected in cirrhotic patients[440], squamous cell carcinoma tumours[440], and is associated with cervical cancer progression[441]. As each cell type has different signalling demands depending on its localisation, 6-O-sulfation is thus tightly regulated. It is possible that any disruption of this homeostasis (either by increased of decreased 6-O-sulfation) is detrimental for a tissue. Therefore, it is difficult to claim a globally protective or detrimental role for HS 6-O-sulfation, as its role is tissue-specific, and detailed studies must be done to determine its role in homeostasis of individual tissues.

Conclusion

In my PhD, I set out to investigate the effect of *HS6ST1* on cartilage homeostasis. I established that overexpression of *HS6ST1* reduced sGAG content of C28/I2 cells. RNASeq analysis revealed that *HS6ST1* transfection significantly-downregulated genes involved in cell-ECM interactions, with integrins abundant in these downregulated terms. Therefore, I propose that overexpression of *HS6ST1* results in downregulation of integrin expression, with subsequent downregulation of integrin signalling and integrin-cross talking signal pathways, disrupting cartilage homeostasis and contributing to a loss of sGAG. Increased *HS6ST1* expression reduced the ability of chondrocytes to respond to changes

in their environment, and so potentially contributes to a deterioration of cartilage homeostasis that predisposes the joint to osteoarthritis.

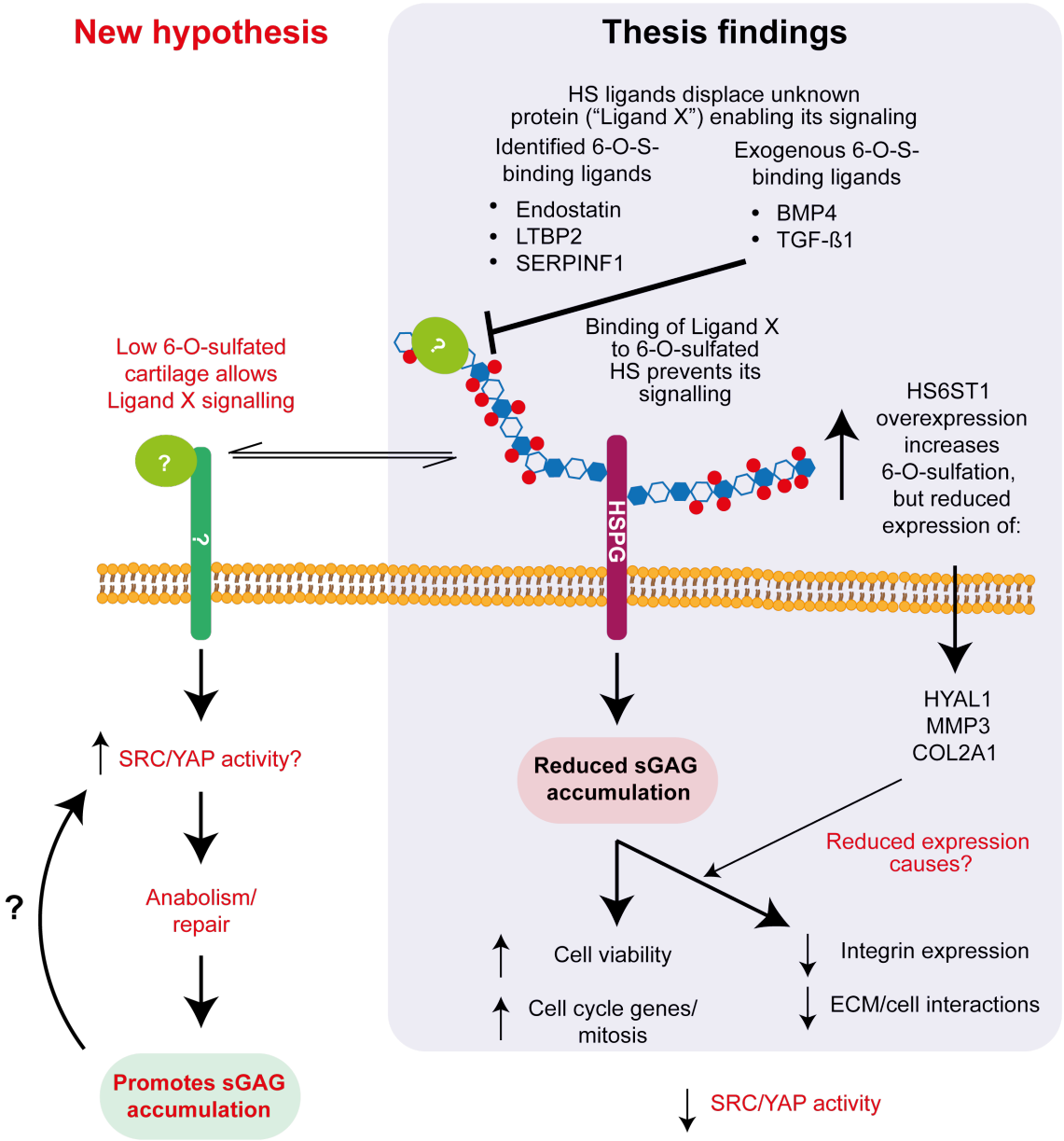

Figure 7.3 Proposed model showing that signaling of an unknown anabolic ligand is prevented by binding to 6-O-sulfated HS.

The data in this thesis support a model in which a currently unknown ligand (Ligand X) supports cartilage homeostasis by promoting sGAG accumulation in C28/I2 cells. This unknown ligand binds to 6-O-sulfated HS, which inhibits its signalling. HS6ST1 overexpression increases HS 6-O-sulfation, resulting in reduced signalling of Ligand X. This results in reduced sGAG content, and changes in cell viability and expression of ECM-cell adhesion molecules. When exogenous HS-binding proteins are added (e.g. TGF-β1, BMP4), Ligand X is competed off the HS and this promotes recovery of sGAG levels. Any 6-O-sulfate binding ligands identified by the LfQ MS screen would have a similar effect.

Chapter 8. Appendix

Table 8.1 Proteins identified from healthy cartilage by LfQ MS as having significantly (Log10 p-value > 1.3) different abundance in 1 M NaCl eluates from heparin and 6-O-desulfated heparin-Sepharose resins.

Protein names	Log_{10}p-value	Log_2 Fold Change
TPD52L2	1.300149549	-0.559889476
PGK1	1.304921275	-0.211153984
SKP1	1.308367009	-0.871304989
C3	1.326432567	-0.443182945
LRPAP1	1.331595236	0.6678346
CBR1	1.370612122	-0.141763687
TLN1	1.376688631	-0.26279068
TNC	1.380286977	-0.336122036
DEFA3;DEFA1	1.39255594	0.794175148

RPL10	1.407705624	0.621654987
RPL12	1.411410569	-0.360095978
BDH2	1.415397866	-2.379028956
C1QB	1.416110361	0.119467735
LYZ	1.417572312	1.046256065
SOD3	1.434404208	-0.211462021
IGHG1	1.442458967	-0.228919506
HSPA8	1.445225989	-0.238347054
RPS16	1.455402345	0.366650581
HAPLN1	1.465803311	0.161970139
HSPB1	1.467600629	0.538476944
RSPO2	1.471286842	0.385211945
TTR	1.479852182	-0.333021164
SOST	1.501447792	-0.2222085
HPX	1.53253458	-0.633333683

PRDX2	1.556015831	-0.191906929
S100A13	1.58159739	-0.355735302
PPIB	1.587879656	-0.789360523
FRZB	1.593804956	0.296918392
HIST2H2AB	1.598300152	0.317148685
RAP1B;RAP1A	1.635218762	-0.460323652
VIT	1.640415262	-0.363469601
COL10A1	1.686294995	-0.272766113
CILP	1.754079767	0.086005211
SELENBP1	1.754656553	-0.184006691
HTRA3	1.77432996	-0.22253561
IGFBP5	1.784963299	0.368405819
CCL14	1.797159345	-0.943582058
C2orf40	1.807251694	0.407461166
PPIA	1.821230886	-0.429371834

CRYZ	1.849003567	0.339399338
COL14A1	1.872531597	-0.407146931
ANXA4	1.875426502	-0.286241531
ABI3BP	1.887741575	-0.336949825
RBM3	1.906255	-1.056004047
ANXA1	1.914858444	-0.291595936
VCAN	1.922688224	0.357133865
RPS9	1.936881988	0.310799599
MDK	1.991405171	0.61111784
H3F3B;H3F3A;HIST3H3;H3F3C	2.025923337	0.318323135
SRPX	2.043910256	-0.446960449
SRPX2	2.046591448	-0.277524471
RPS5	2.056524251	1.037473043
GSN	2.074930809	-0.298079967
RPL34	2.07557799	0.328299522

NNMT	2.137264525	-0.18623654
H1FX	2.211339648	0.249642372
FGF2	2.214623484	0.574148655
GSN	2.217369174	-0.608202934
CDH1	2.223602155	0.39426136
CAP1	2.253600193	-0.201253891
LTBP2	2.289125299	-1.126170158
TPI1	2.311292443	-0.240682602
HIST1H1B	2.345101569	-0.728731791
PCOLCE2	2.351328353	-0.501450539
CFH	2.435408017	-0.47296524
COL11A2	2.537663664	-0.515054703
MMP2	2.561953116	-0.348753452
COL18A1	2.612734869	-1.161761761
IGHG3	2.658457061	-0.243233681

SERPINF1	2.675926641	-0.255355358
CXCL10	2.681601158	-0.717194557
ACAN	2.714013765	0.418978691
RPL19	2.765902007	1.335858663
HNRNPD	2.949885539	-0.350056648
RPS3A	3.506385719	0.378677368
NCL	3.593898583	-0.85159874

Table 8.2 Proteins identified from osteoarthritic cartilage by LfQ MS as having significantly (Log10 p-value > 1.3) different abundance in 1 M NaCl eluates from heparin and 6-O-desulfated heparin-Sepharose resins.

Protein names	Log_{10}p-value	Log_2 Fold Change
RPL10	1.317394402	-0.573551178
TNFSF12-TNFSF13	1.326227258	-0.465936661
ATP5A1	1.347128603	0.337237358
RPL28	1.358170773	-0.671120644
IGKC	1.37611175	0.281812668
ABI3BP	1.384632423	0.317949772
SERPINA1	1.386532614	0.42130661
C1QB	1.387459776	-0.139689922
RPLP0	1.402360644	0.244520664
HSPA8	1.410675291	0.249042511
COL2A1	1.411019146	0.362796783

PRDX2	1.411233123	0.336714268
C3	1.433684557	0.53013134
TUBA1B	1.449754509	0.237402916
SELENBP1	1.450833846	0.192286015
HIST1H2AJ	1.455559906	-2.728107135
GSN	1.459601872	0.277869701
RPL34	1.461205158	-0.479491711
FTH1	1.461586162	-0.434452057
TNC	1.468268775	0.364753246
SOST	1.476595063	0.303153038
GDI2	1.493696198	0.253387451
SKP1	1.493823196	0.957439899
HNRNPL	1.493986112	-0.240712166
DEFA3	1.518448853	-0.82818079
VCAN	1.537057017	-0.316339016

ARPC2	1.543162829	0.261763573
ATP5B	1.547569456	0.323748589
CYR61	1.561041598	-0.343987942
HSPA5	1.56812072	0.264716625
SOD3	1.617099184	0.279524326
CD109	1.640322255	0.372808456
SRPX2	1.648823859	0.266484737
HIST2H2BE	1.667855456	-0.244672298
CAP1	1.695835964	0.261277199
CBR1	1.723468385	0.185550213
ANXA4	1.735999333	0.276016712
BLVRB	1.749574109	-0.295829296
CRYZ	1.751655001	-0.351490498
HTRA3	1.762083552	0.240774155
MDK	1.781423887	-0.506775856

S100A13	1.783896399	0.444535255
FGF2	1.890329805	-0.587615967
H1FX	1.953240557	-0.310508728
PPIA	1.955288428	0.514546871
H3F3B	1.960560182	-0.387846947
FRZB	1.986480246	-0.325917721
VIT	2.028127779	0.503641129
MMP2	2.076829507	0.33601141
ANXA1	2.094310258	0.387804031
IGHG1	2.130936425	0.34457159
GSN	2.216831477	0.622905731
SERPINF1	2.326543509	0.24399519
RPS5	2.351865432	-0.833174706
IGFBP5	2.357942604	-0.459489346
HIST1H1B	2.359509555	0.717475096

PCOLCE2	2.387648615	0.52309227
COL11A2	2.408081261	0.480122566
TLN1	2.417241954	0.319907665
PLA2G2A	2.431220173	-0.250864983
ACAN	2.527482726	-0.416770935
CFH	2.596603032	0.473005772
RPS3A	2.693922816	-0.400965214
LTBP2	2.710973472	1.322029114
NCL	2.754268876	0.700726986
C2orf40	2.760783689	-0.597288609
CDH1	2.855815611	-0.454163551
RPL31	2.93105672	-0.323482037
COL18A1	3.004346927	1.512600422
HNRNPD	3.044761146	0.360271931

Table 8.3 Genes identified to be significantly differentially (p-value < 0.05) expressed by RNASeq following overexpression of *HS6ST1* for 48 h using 1 µg of *HS6ST1*-encoding plasmid in C28/I2 cells.

Gene	Gene ID	P-value	Log_2 Fold Change	HS6ST1 read count	Mock read count
PTX3	ENSG00000163661	1.23E-06	-0.375782346	1293.89	1678.162
HAS2	ENSG00000170961	5.54E-05	-0.27995125	873.0278	1059.789
TFPI2	ENSG00000105825	0.000113	-0.252292237	5095.394	6068.229
PBXIP1	ENSG00000163346	0.000161	0.240884491	916.7925	776.155
SIPA1L1	ENSG00000197555	0.000296	-0.232077227	761.5623	894.6261
JUN	ENSG00000177606	0.000318	-0.232473782	1930.657	2266.791
CLEC11A	ENSG00000105472	0.000323	0.223394504	1435.799	1229.125
ADAMTS1	ENSG00000154734	0.000431	-0.321078679	523.136	653.6358
PAX2	ENSG00000075891	0.000449	0.228016802	956.1793	815.607
IL1B	ENSG00000125538	0.000574	-0.312302753	470.4448	582.4605
MIR3176	ENSG00000266235	0.000575	-0.774134598	45.09014	77.79243

NAV3	ENSG00000067798	0.00074	-0.512771226	179.1745	256.1195
SEMA7A	ENSG00000138623	0.000741	-0.251974727	1864.409	2219.855
CSDC2	ENSG00000172346	0.000744	0.667597015	76.52353	48.10894
TNFAIP3	ENSG00000118503	0.000851	-0.335272035	322.0704	406.2833
ADAM19	ENSG00000135074	0.00094	-0.321133505	1358.196	1697.389
MGLL	ENSG00000074416	0.000942	-0.242342689	1113.267	1316.225
GLIPR1	ENSG00000139278	0.000947	-0.293301693	320.2725	392.9837
STK4	ENSG00000101109	0.000997	-0.19624979	2836.009	3250.847
CYTH2	ENSG00000105443	0.001148	0.185748487	1727.951	1517.424
EEF1A1P3	ENSG00000232587	0.001236	4.617167087	4.516144	0
GFPT2	ENSG00000131459	0.001254	-0.137999495	3973.275	4371.796
RGPD6	ENSG00000183054	0.001525	1.713753463	42.31767	13.02057
ESM1	ENSG00000164283	0.001561	-0.365290366	706.8979	909.7317
AL121832.3	ENSG00000275437	0.001575	0.488286835	151.4907	108.5445
NOMO3	ENSG00000103226	0.001614	-0.505216311	230.0812	325.6911

FADS2	ENSG00000134824	0.001637	0.147586579	2780.624	2510.913
STS	ENSG00000101846	0.001656	-0.721934923	44.38875	73.63356
UBE2L6	ENSG00000156587	0.001706	0.233364064	905.6543	771.185
APLN	ENSG00000171388	0.001867	-0.595862366	56.84161	85.93426
HCFC1R1	ENSG00000103145	0.001881	0.328831169	551.7924	438.9645
LINC01711	ENSG00000268941	0.001933	0.9577034	37.0492	18.91849
HPF1	ENSG00000056050	0.002042	0.340185591	413.516	326.6495
SOWAHC	ENSG00000198142	0.00206	-0.229986087	598.0732	701.2891
Mar-04	ENSG00000144583	0.002092	-0.417842686	282.9218	378.3706
SULF2	ENSG00000196562	0.002102	0.227028128	824.0063	705.3141
PCOLCE	ENSG00000106333	0.002103	0.247102981	1628.812	1372.484
LCP1	ENSG00000136167	0.002296	-0.609912505	60.38564	92.5225
NMT2	ENSG00000152465	0.002333	0.160574808	1418.631	1269.38
HIST2H2BF	ENSG00000203814	0.002542	-1.0580867	15.38492	31.54843
SLC27A5	ENSG00000083807	0.002556	0.498611901	118.8663	83.96912

SH2B3	ENSG00000111252	0.002591	-0.246398519	2165.127	2568.684
SERPINE1	ENSG00000106366	0.002621	-0.207683027	3019.851	3487.222
RBM24	ENSG00000112183	0.002666	-0.325814503	245.5717	308.2954
TMEM99	ENSG00000167920	0.002679	0.474833643	144.1146	103.1665
FUZ	ENSG00000010361	0.002731	0.207550149	705.3224	610.3254
HS3ST3A1	ENSG00000153976	0.002759	-0.221155078	535.7529	624.2933
GTF2IP1	ENSG00000277053	0.002849	-0.77915977	231.0448	396.741
ZDHHC1	ENSG00000159714	0.002945	0.355196066	258.8975	202.6254
ARHGDIG	ENSG00000242173	0.002988	0.344016732	363.0357	285.6125
RAD54B	ENSG00000197275	0.003116	-0.517926229	77.44589	110.709
SAMHD1	ENSG00000101347	0.003136	0.138361776	2055.246	1866.154
SLC20A1	ENSG00000144136	0.003324	-0.145480173	2684.491	2969.002
LUC7L3	ENSG00000108848	0.003353	0.131055958	3095.977	2826.171
MAP4K3	ENSG00000011566	0.003364	-0.222289877	524.1299	611.7723
MYL6	ENSG00000092841	0.003411	0.185119798	10180.2	8952.498

AP004609.3	ENSG00000278376	0.003412	1.062113596	30.51688	14.70887
TBX1	ENSG00000184058	0.003421	0.159265096	2377.001	2128.507
ENC1	ENSG00000171617	0.003445	-0.25568582	556.1287	664.5407
ITGA2	ENSG00000164171	0.003463	-0.370213988	645.9229	835.4936
SLC36A1	ENSG00000123643	0.003614	-0.293717067	405.4278	497.4204
CYLD	ENSG00000083799	0.003647	-0.168216991	1076.102	1209.946
IFT81	ENSG00000122970	0.003716	0.213899553	629.2875	542.8644
INAFM2	ENSG00000259330	0.003773	-0.263715713	353.4129	424.9272
GRAMD2B	ENSG00000155324	0.003804	0.289827561	309.8589	253.3662
STRA6	ENSG00000137868	0.003836	0.20628174	630.4977	546.6585
ANPEP	ENSG00000166825	0.003906	-0.183147703	3485.981	3957.211
H2AFJ	ENSG00000246705	0.003963	0.219909479	1426.273	1223.885
TNS1	ENSG00000079308	0.0041	-0.707111756	36.98135	60.39321
PDCD1LG2	ENSG00000197646	0.004168	-0.612532439	44.23366	67.51945
AP001020.2	ENSG00000264635	0.004179	-4.282140596	0	3.576834

ZNF580	ENSG00000213015	0.004272	0.232188284	891.9475	758.2334
RGS4	ENSG00000117152	0.004319	-0.27542039	416.2055	503.8209
RPAIN	ENSG00000129197	0.004394	0.223898946	550.2731	470.5834
GNPNAT1	ENSG00000100522	0.004442	-0.170974264	1215.472	1369.666
TMEM160	ENSG00000130748	0.004477	0.245476525	575.5454	485.0038
GCLM	ENSG00000023909	0.004479	-0.176229286	2002.412	2263.512
ZNF585B	ENSG00000245680	0.004535	-0.430048606	127.5702	171.5742
INHBA	ENSG00000122641	0.004573	-0.196052349	6390.98	7321.398
EMP1	ENSG00000134531	0.004708	-0.206179652	1221.294	1409.527
MYL6B	ENSG00000196465	0.004768	0.200309945	939.0907	816.8878
SNHG16	ENSG00000163597	0.00479	-0.219047335	865.2063	1007.917
MAP2K2	ENSG00000126934	0.004804	0.138032892	4558.37	4140.79
DUSP7	ENSG00000164086	0.005007	-0.189249139	1470.908	1677.254
ADCY1	ENSG00000164742	0.005012	-0.290294209	356.6069	436.8776
PHLDA1	ENSG00000139289	0.005067	-0.153772218	2720.414	3026.237

DDX56	ENSG00000136271	0.005281	0.129557377	3234.286	2955.299
IGFBP6	ENSG00000167779	0.005394	0.218361352	987.0775	847.9681
HIVEP1	ENSG00000095951	0.005474	-0.24597421	603.7598	717.2076
TFRC	ENSG00000072274	0.005478	-0.143997092	6979.508	7713.316
MYO10	ENSG00000145555	0.005547	-0.186599057	4532.229	5159.083
ANTXR2	ENSG00000163297	0.005637	-0.192064404	1862.505	2127.865
H1F0	ENSG00000189060	0.005643	0.129997818	5705.646	5213.221
B4GALT6	ENSG00000118276	0.005799	-0.260511859	294.4475	352.978
AL590652.1	ENSG00000227885	0.006041	2.658398177	7.704919	1.161322
SUCO	ENSG00000094975	0.006166	-0.222884363	570.5245	665.9038
CEMIP2	ENSG00000135048	0.00626	-0.263889735	458.3073	550.5964
ITGA3	ENSG00000005884	0.006266	-0.144154418	3958.668	4375.969
SEC22B2	ENSG00000274423	0.00627	1.416073397	22.32156	8.525489
DUSP1	ENSG00000120129	0.006279	-0.230524568	718.0094	842.3825
RPSAP19	ENSG00000183298	0.006366	0.480538234	117.9241	84.9942

AC008894.2	ENSG00000269243	0.006381	-2.402646096	1.546641	7.985934
AC005330.1	ENSG00000267372	0.006392	0.776352558	50.44039	29.35012
AL358472.1	ENSG00000231416	0.006446	-4.298569889	0	3.620604
UTP4	ENSG00000141076	0.006547	-0.1136011	3399.805	3679.161
MMP1	ENSG00000196611	0.00664	-0.151999112	22253.2	24723.69
GLIS3	ENSG00000107249	0.006689	-0.31570432	214.4625	267.305
CDK17	ENSG00000059758	0.00676	-0.194852149	964.3205	1104.27
POLK	ENSG00000122008	0.006856	-0.307328698	211.6835	262.2819
HBEGF	ENSG00000113070	0.006884	-0.240055247	495.1833	583.7637
BRICD5	ENSG00000182685	0.007052	0.315239377	232.9327	186.8552
IGF2R	ENSG00000197081	0.007057	-0.207136443	3574.531	4127.698
PHLDB2	ENSG00000144824	0.007101	-0.190635713	3144.318	3589.297
POLR2F	ENSG00000100142	0.007126	0.20172343	1246.592	1083.509
HIST1H4L	ENSG00000275126	0.007196	4.282846104	3.598058	0
GPAT3	ENSG00000138678	0.00727	-0.511776289	89.92653	127.8291

DUSP4	ENSG00000120875	0.007288	-0.173367975	1927.921	2174.537
UAP1	ENSG00000117143	0.007339	-0.144826906	1963.897	2170.22
EGFR	ENSG00000146648	0.00743	-0.221969564	2736.458	3192.631
PRNP	ENSG00000171867	0.007478	-0.124680656	6919.386	7544.045
ALG1L6P	ENSG00000238278	0.007546	0.855674858	41.76366	23.06718
TGM2	ENSG00000198959	0.007565	-0.162510233	12772.41	14295.19
MTREX	ENSG00000039123	0.007576	-0.136771935	1694.305	1863.427
CHADL	ENSG00000100399	0.007582	3.918916769	4.603422	0.264179
PLEKHO1	ENSG00000023902	0.007678	0.18753503	1125.604	987.6657
RPS3AP34	ENSG00000242607	0.007683	4.122656229	3.192145	0
ID3	ENSG00000117318	0.007829	0.22515385	1035.851	885.428
CHCHD10	ENSG00000250479	0.007857	0.183579931	1659.756	1461.268
KCNS1	ENSG00000124134	0.007891	-0.667348442	37.94174	60.1708
FOXD1	ENSG00000251493	0.008011	-0.185090177	992.9726	1127.94
SDR39U1	ENSG00000100445	0.00808	0.307252921	221.8121	179.5171

SH3RF1	ENSG00000154447	0.008172	-0.238790698	689.269	813.2184
ZSCAN9	ENSG00000137185	0.008191	0.344341837	189.2339	148.8756
PLEC	ENSG00000178209	0.008193	-0.203042431	17328.79	19948.48
ITPRIP	ENSG00000148841	0.008301	-0.163896681	2036.701	2282.316
NOMO1	ENSG00000103512	0.008383	-0.142600459	2486.167	2745.219
KAT8	ENSG00000103510	0.008455	0.171530277	800.1552	710.0731
CTBP1	ENSG00000159692	0.008481	0.127913631	1875.659	1716.291
RHPN1	ENSG00000158106	0.008501	0.282044325	325.7307	267.3645
PSMB8	ENSG00000204264	0.008568	0.226001539	830.8976	709.3752
WDR36	ENSG00000134987	0.008636	-0.187286531	1005.72	1145.221
AMIGO2	ENSG00000139211	0.008656	-0.135729423	4887.088	5368.568
TMEM200A	ENSG00000164484	0.008724	-0.207612142	1338.637	1546.198
RNF111	ENSG00000157450	0.008752	-0.236020133	596.3353	703.3268
PPP1R15A	ENSG00000087074	0.008805	-0.146254219	2128.786	2354.035
CLMP	ENSG00000166250	0.009098	-0.233958658	530.6308	624.0897

C17orf99	ENSG00000187997	0.009199	3.635980918	3.780901	0.264179
KLF4	ENSG00000136826	0.009215	-0.289984358	289.4247	352.9956
MRAP2	ENSG00000135324	0.009273	1.170781351	18.36486	8.189277
TEDC2	ENSG00000162062	0.009283	0.24466714	641.3175	540.6962
ZKSCAN2-DT	ENSG00000274925	0.009492	0.748289278	42.52623	25.25429
CUL2	ENSG00000108094	0.009529	-0.116117444	2231.216	2418.296
HIPK2	ENSG00000064393	0.009543	-0.2598286	989.3243	1185.451
BSN	ENSG00000164061	0.009548	-0.319854519	209.8667	262.1938
AC022211.1	ENSG00000263786	0.009596	1.328305381	15.55835	6.148149
AC025171.1	ENSG00000177738	0.009721	0.335297346	209.3541	165.6662
C9orf3	ENSG00000148120	0.009907	0.20792314	701.1375	606.8721
DUSP18	ENSG00000167065	0.009942	-0.551538949	47.05907	69.30301
LRIG1	ENSG00000144749	0.009983	-0.214838325	1126.97	1308.236
MFAP1	ENSG00000140259	0.009984	0.171386779	972.5646	863.1838
PPRC1	ENSG00000148840	0.010047	-0.123493933	3760.65	4097.889

LINC01176	ENSG00000281404	0.010091	1.077972519	21.8472	10.19975
HAR1B	ENSG00000231133	0.010098	-1.439419255	5.178302	13.95643
LRRD1	ENSG00000240720	0.010102	4.027689787	3.001708	0
HIRIP3	ENSG00000149929	0.010128	0.236983243	402.4833	340.6536
PAAF1	ENSG00000175575	0.010132	0.334381773	219.2057	173.3824
AF131215.5	ENSG00000255310	0.010307	0.505861327	89.21531	62.63283
GEMIN5	ENSG00000082516	0.010427	-0.179620964	1204.352	1364.025
DTNBP1	ENSG00000047579	0.010475	0.282003858	332.471	273.7719
SPCS2	ENSG00000118363	0.010499	0.287727033	596.9836	488.5859
AC138969.1	ENSG00000227827	0.010586	-0.388901883	131.1524	172.6194
RPL39	ENSG00000198918	0.010676	0.176414473	7606.03	6729.965
PHGDH	ENSG00000092621	0.010727	0.122221247	6333.802	5819.121
MPDZ	ENSG00000107186	0.010743	-0.306208301	465.6678	576.3284
RGMB	ENSG00000174136	0.01075	-0.31416031	227.4918	282.4532
OLMALINC	ENSG00000235823	0.010958	0.205983714	473.8441	410.657

CHEK2	ENSG00000183765	0.011193	0.241358879	602.1738	509.277
PRKRIP1	ENSG00000128563	0.011276	0.197876253	804.9362	700.3303
HDAC3	ENSG00000171720	0.011284	0.145919507	1249.973	1128.903
LPGAT1	ENSG00000123684	0.011442	-0.147640101	2075.684	2301.217
RIN2	ENSG00000132669	0.011589	-0.145171921	1008.658	1115.875
TEAD2	ENSG00000074219	0.011679	0.180477732	697.2997	614.2256
AL591623.2	ENSG00000228955	0.011731	-3.269773075	0.538684	4.793394
IL10RA	ENSG00000110324	0.011743	0.554464712	74.32476	50.61832
LMTK2	ENSG00000164715	0.011852	-0.232482687	646.7786	761.0332
REPS2	ENSG00000169891	0.011858	-0.22836612	334.6823	392.5931
TMEM231P1	ENSG00000262583	0.011862	1.534831732	12.49386	4.22824
BNIPL	ENSG00000163141	0.012078	0.668370844	50.36047	31.91879
ARID5B	ENSG00000150347	0.012135	-0.297750192	231.5376	284.2563
AC004057.1	ENSG00000196656	0.012203	0.405767998	232.5362	175.0649
NAPA-AS1	ENSG00000268061	0.012231	1.084267092	20.25153	9.453919

CALCOCO2	ENSG00000136436	0.01234	0.113474598	2335.4	2159.457
ALKBH6	ENSG00000239382	0.012518	0.398789876	137.936	104.2076
TAF15	ENSG00000270647	0.012523	0.129629781	2829.854	2586.493
RPL36AL	ENSG00000165502	0.012582	0.176973607	2358.618	2085.923
PPFIBP1	ENSG00000110841	0.012611	-0.179299522	1225.198	1387.557
BACH1	ENSG00000156273	0.012621	-0.185046551	974.0104	1107.955
MVB12B	ENSG00000196814	0.012835	-0.171084979	849.3805	957.8133
CDCP1	ENSG00000163814	0.012866	-0.167974326	2620.691	2944.706
WDR43	ENSG00000163811	0.012919	-0.163452258	2108.882	2362.759
METRNL	ENSG00000176845	0.012968	0.230977281	479.3901	407.6957
OLFML2B	ENSG00000162745	0.012969	0.59186333	53.71573	35.77998
FNBP1L	ENSG00000137942	0.013016	-0.239195282	330.8135	390.6736
SOX12	ENSG00000177732	0.013038	0.172333349	892.2068	792.1889
PDLIM5	ENSG00000163110	0.013047	-0.163654686	2609.641	2924.281
DHRSX	ENSG00000169084	0.013048	0.32690367	201.8326	160.6933

LDLRAD3	ENSG00000179241	0.013078	-0.228516934	316.2689	370.4659
STARD13	ENSG00000133121	0.013217	-0.183462975	1271.753	1444.171
DOCK4	ENSG00000128512	0.013257	-0.263462905	1254.365	1506.049
NEK7	ENSG00000151414	0.013335	-0.179382926	2021.737	2290.114
SESN2	ENSG00000130766	0.013371	-0.221196041	428.756	500.5677
SLC4A7	ENSG00000033867	0.013394	-0.217411786	2693.674	3132.772
UBA7	ENSG00000182179	0.013459	0.181515605	612.0541	539.2932
AC245452.2	ENSG00000225544	0.013502	1.33103017	14.15354	5.54216
JAG1	ENSG00000101384	0.013601	-0.188025854	4844.383	5519.157
FNDC3B	ENSG00000075420	0.013608	-0.181124034	1496.833	1698.298
IL11	ENSG00000095752	0.013662	-0.170892207	907.9509	1020.28
SLC25A28	ENSG00000155287	0.013767	0.17686928	796.1194	703.9038
ODC1	ENSG00000115758	0.013818	-0.116174041	10341.8	11206.97
PHTF2	ENSG00000006576	0.013958	-0.210367584	673.7953	779.9331
HIST1H2BF	ENSG00000277224	0.014029	-1.504567751	3.750169	10.54156

TPGS1	ENSG00000141933	0.01411	0.305282215	262.3412	211.9687
SLC7A2	ENSG00000003989	0.014137	-0.283910805	553.3787	674.5203
FBXW4	ENSG00000107829	0.014183	0.218975809	935.5293	804.09
LINC00654	ENSG00000205181	0.014254	-3.753138619	0.271241	4.037652
URB2	ENSG00000135763	0.014294	-0.17736745	878.3442	993.1576
TCEAL3	ENSG00000196507	0.014328	0.203402305	672.1015	583.805
PVALEF	ENSG00000225180	0.014382	3.690877853	3.897278	0.206278
LYPLA1	ENSG00000120992	0.014498	-0.140567945	1398.065	1542.302
AC096887.1	ENSG00000272305	0.014543	1.983562897	7.693915	1.92826
SP100	ENSG00000067066	0.014601	-0.197974005	497.7283	570.3976
HSPA1A	ENSG00000204389	0.014619	0.112391633	2984.988	2760.523
SSTR1	ENSG00000139874	0.014624	-0.548114053	56.73144	83.0391
RPS7P11	ENSG00000213326	0.014652	0.346817547	424.1115	333.1093
SFT2D1	ENSG00000198818	0.014679	0.17723441	968.3793	856.288
MZT2B	ENSG00000152082	0.01468	0.214247547	1263.957	1088.875

PIR	ENSG00000087842	0.014732	0.235902251	592.3945	502.8747
APBB1	ENSG00000166313	0.014813	0.187965393	840.9051	738.1627
AC104596.1	ENSG00000250326	0.014862	-3.561772932	0.244306	3.516269
RABGEF1	ENSG00000154710	0.014901	-0.491850598	60.54166	84.89756
MPP5	ENSG00000072415	0.014925	-0.180956126	929.4727	1054.09
ZNF142	ENSG00000115568	0.014936	-0.20810296	734.2946	849.0221
FLYWCH2	ENSG00000162076	0.01524	0.218141592	708.3589	607.9827
CPEB4	ENSG00000113742	0.015242	-0.24138467	613.211	725.3246
COMMD7	ENSG00000149600	0.015256	0.211800677	623.9199	538.1866
NBPF14	ENSG00000270629	0.01527	-0.258364407	433.6835	518.0985
PPIAP22	ENSG00000198618	0.015346	0.372719712	167.994	129.601
NRIP1	ENSG00000180530	0.015398	-0.244832523	1047.343	1241.642
AL390719.1	ENSG00000217801	0.015432	0.285480354	220.5081	180.6214
MRPS17P1	ENSG00000268949	0.015496	-3.565647301	0.215048	3.598121
CENPA	ENSG00000115163	0.01554	0.157978739	926.385	829.2068

PMAIP1	ENSG00000141682	0.015548	-0.155815704	899.7538	1003.043
ABI3BP	ENSG00000154175	0.015558	-0.380793359	138.8161	180.4552
BACE1	ENSG00000186318	0.015588	-0.421768057	77.33152	103.9685
BICD2	ENSG00000185963	0.015649	-0.158893402	1198.163	1337.318
PKD1P6	ENSG00000250251	0.015753	-0.264762402	624.2738	751.1404
DUSP5	ENSG00000138166	0.015762	-0.262294916	406.5638	487.2158
GAMT	ENSG00000130005	0.015831	0.400938087	119.8761	90.44568
RIC1	ENSG00000107036	0.015907	-0.231472463	411.9649	484.9181
LTBP1	ENSG00000049323	0.016138	-0.205390666	832.2154	959.5174
AC097468.3	ENSG00000272644	0.016183	0.800401359	33.36057	19.16037
KLF6	ENSG00000067082	0.016292	-0.178785367	1532.514	1734.788
RAB3IL1	ENSG00000167994	0.01643	0.229312866	398.661	340.4348
TIGD3	ENSG00000173825	0.016503	0.474811927	80.21914	57.34273
NUDT4	ENSG00000173598	0.016505	-0.149214101	964.749	1070.712
USP15	ENSG00000135655	0.016596	-0.170668422	826.1031	930.8001

SIK1	ENSG00000142178	0.01661	-0.224631267	306.3692	358.4264
APLP1	ENSG00000105290	0.016622	0.134167114	1372.327	1250.486
UBXN1	ENSG00000162191	0.016648	0.19041071	1972.035	1727.155
SNORA71A	ENSG00000225091	0.016707	-0.829876046	18.1376	31.9897
LYPD3	ENSG00000124466	0.016872	-0.720543649	26.65756	43.96595
UBE2MP1	ENSG00000261461	0.01689	-0.803158383	17.72367	30.81481
AL353708.1	ENSG00000260360	0.016907	-2.822853616	0.674401	5.080237
CYR61	ENSG00000142871	0.016931	-0.100028953	3872.718	4149.248
AANAT	ENSG00000129673	0.016947	-2.958169699	0.756056	5.73302
STT3B	ENSG00000163527	0.01696	-0.111810675	4325.932	4676.46
EPG5	ENSG00000152223	0.017003	-0.205832812	1065.417	1229.359
CENPT	ENSG00000102901	0.017034	0.137567454	1853.902	1683.456
TRIM23	ENSG00000113595	0.017064	-0.277563442	226.7506	275.2582
IPO7	ENSG00000205339	0.017113	-0.151879464	4523.975	5027.753
SLC6A11	ENSG00000132164	0.017176	-0.683174045	22.88313	36.6283

FAM83A	ENSG00000147689	0.017269	-2.032925578	2.152606	8.908676
IKBKGP1	ENSG00000275882	0.017395	2.224134248	83.54867	17.85306
LINC00705	ENSG00000225269	0.017433	1.626707569	10.02537	3.28999
HOOK2	ENSG00000095066	0.017438	0.182214015	1447.342	1274.565
AC015922.3	ENSG00000276855	0.017492	0.595280215	49.4563	32.65708
DYNC2LI1	ENSG00000138036	0.017583	0.332712823	257.9423	204.972
DHX36	ENSG00000174953	0.017618	-0.137605389	1346.486	1482.085
GCSH	ENSG00000140905	0.017624	0.314257555	183.7258	147.1275
ATP13A3	ENSG00000133657	0.017651	-0.204970854	3987.082	4596.908
UNC13A	ENSG00000130477	0.017688	-0.210377699	594.5412	689.0515
ZBTB8B	ENSG00000273274	0.017707	1.331543726	13.17582	5.24385
EPOP	ENSG00000273604	0.017766	0.187448796	639.0847	561.0391
ARPP19	ENSG00000128989	0.017842	-0.128244307	3270.122	3575.991
SNHG20	ENSG00000234912	0.017909	0.411217808	124.089	93.92719
BCAR3	ENSG00000137936	0.018052	-0.157599159	1661.717	1852.29

TIRAP	ENSG00000150455	0.018164	-0.470480626	58.46258	80.49029
VWCE	ENSG00000167992	0.018359	-1.598362276	3.55148	11.0133
BVES	ENSG00000112276	0.018448	-0.22269747	384.1447	447.8136
ANKRD40	ENSG00000154945	0.018541	-0.144302707	1113.3	1231.39
RPL38	ENSG00000172809	0.018565	0.186215202	5306.528	4663.18
FAM173A	ENSG00000103254	0.018692	0.196512902	609.4848	532.556
ZNF468	ENSG00000204604	0.018847	-0.275232673	182.5434	221.1993
RBBP4P5	ENSG00000256737	0.018887	3.769163847	2.511622	0
TRIM45	ENSG00000134253	0.018915	0.300417409	224.883	182.0507
AC007969.1	ENSG00000233762	0.018918	0.216113929	385.8395	331.405
HES7	ENSG00000179111	0.018979	0.882755831	39.26549	21.08366
STON1	ENSG00000243244	0.01899	0.719882019	34.07129	20.5956
MBD4	ENSG00000129071	0.019005	0.139678909	983.375	892.8524
NPAS2	ENSG00000170485	0.019169	-0.217206094	408.8998	474.1537
HILPDA	ENSG00000135245	0.019216	0.394766895	119.2096	90.97874

VEGFA	ENSG00000112715	0.019258	-0.138211057	2620.063	2883.008
PMVK	ENSG00000163344	0.019271	0.232075201	608.4907	516.511
BPHL	ENSG00000137274	0.019455	0.385232918	154.9137	118.4566
AC126755.1	ENSG00000205746	0.019508	-0.4364145	160.9854	218.0535
YRDC	ENSG00000196449	0.019521	-0.153261449	712.7457	791.6912
PKDREJ	ENSG00000130943	0.019526	1.406735157	13.17485	4.970033
HS1BP3	ENSG00000118960	0.019599	0.18967898	498.254	436.4971
SAPCD1	ENSG00000228727	0.019604	1.106587724	19.23078	9.079174
RPL4P4	ENSG00000229638	0.01962	0.373978017	138.5128	107.0126
CRLF1	ENSG00000006016	0.019701	0.178685167	523.6913	462.6862
POMK	ENSG00000185900	0.019704	-0.542482746	66.27166	97.01427
AL031729.1	ENSG00000235912	0.019784	0.947375149	22.08213	11.46514
THBS1	ENSG00000137801	0.019839	-0.172364944	12675.43	14284.7
ABCE1	ENSG00000164163	0.019926	-0.117976215	3191.037	3463.724
FAR1	ENSG00000197601	0.019974	-0.128915791	1511.787	1653.625

HK2	ENSG00000159399	0.020045	-0.255181416	453.8165	541.215
SLC9A3-AS1	ENSG00000225138	0.020187	0.143479768	2468.534	2234.14
B4GALNT3	ENSG00000139044	0.020215	0.507819378	72.13939	51.05997
FOXK1	ENSG00000164916	0.020241	-0.17771107	1726.721	1955.18
HHIP	ENSG00000164161	0.020313	-0.148406623	1944.47	2154.977
PREX1	ENSG00000124126	0.020417	-0.174752944	2009.604	2268.214
TMEM218	ENSG00000150433	0.02045	0.37696493	184.8327	142.6473
PGAP1	ENSG00000197121	0.020559	-0.314138044	159.5789	198.5582
LHPP	ENSG00000107902	0.020585	0.489083729	84.96011	60.36359
CAMSAP3	ENSG00000076826	0.02078	0.286057837	202.8831	166.2547
CLIC4P1	ENSG00000236739	0.020801	1.603879316	9.062715	3.013238
OSMR	ENSG00000145623	0.020855	-0.204074026	1048.655	1208.616
SLC48A1	ENSG00000211584	0.020888	0.144289848	937.3078	848.6004
TRMT2A	ENSG00000099899	0.020889	0.113908813	2037.359	1882.773
PDXK	ENSG00000160209	0.021049	0.104269912	3100.769	2884.361

DCAF4L1	ENSG00000182308	0.021147	-1.549424309	4.086367	12.09837
CXCL8	ENSG00000169429	0.021225	-0.234648413	634.7971	746.3591
METTL15P1	ENSG00000174912	0.021251	-1.431728858	4.620278	12.70244
GSK3B	ENSG00000082701	0.021449	-0.139377077	1782.583	1964.48
AC096540.1	ENSG00000227527	0.021569	3.192580166	4.509525	0.461924
PAQR9-AS1	ENSG00000241570	0.0216	-1.997832663	1.676236	6.783594
UBASH3B	ENSG00000154127	0.021615	-0.155698012	1396.634	1556.355
AL391834.1	ENSG00000272842	0.021671	3.369737619	3.100572	0.255646
DGLUCY	ENSG00000133943	0.021671	0.262817565	260.4811	217.1901
PANX1	ENSG00000110218	0.021694	-0.195024661	538.3668	617.4314
KLF5	ENSG00000102554	0.021728	-0.23989636	251.6509	297.3977
ADGRB2	ENSG00000121753	0.02197	0.166013283	784.4077	698.7626
PC	ENSG00000173599	0.022152	0.279481206	250.7252	205.5784
EPAS1	ENSG00000116016	0.022176	-0.184434658	1738.424	1975.866
TNC	ENSG00000041982	0.022195	-0.21971399	509.5243	594.0954

GPR87	ENSG00000138271	0.02223	3.547425202	3.499935	0.206278
RASA1	ENSG00000145715	0.02229	-0.231246656	416.9518	490.5946
AKAP12	ENSG00000131016	0.022294	-0.163923066	6149.934	6890.125
TENM2	ENSG00000145934	0.022467	-0.462306617	58.324	80.88111
URB1	ENSG00000142207	0.02247	-0.170208812	2163.186	2434.81
ZNF345	ENSG00000251247	0.022472	0.475805327	77.97252	56.24885
FNDC3A	ENSG00000102531	0.022595	-0.224070972	755.5784	882.898
EHD4	ENSG00000103966	0.022851	-0.136281085	1114.402	1224.773
TNRC18	ENSG00000182095	0.022938	-0.169241869	3951.734	4444.807
PID1	ENSG00000153823	0.023219	-0.180318589	570.1083	646.8291
ZDHHC20	ENSG00000180776	0.023235	-0.145035677	1505.13	1665.241
DLL4	ENSG00000128917	0.023407	-0.86386868	18.23243	32.82877
LINC01089	ENSG00000212694	0.023432	0.254632738	317.7576	265.3033
GOLIM4	ENSG00000173905	0.023447	-0.144228386	941.351	1041.579
SPATA13	ENSG00000182957	0.023463	-0.254572198	210.9482	251.9781

AC145422.1	ENSG00000256742	0.023554	1.851536751	8.796745	2.410185
AL133338.1	ENSG00000260000	0.023556	0.742170818	38.01794	22.61948
IPO5	ENSG00000065150	0.023564	-0.08463771	7945.48	8426.325
RPS6KA2-IT1	ENSG00000232082	0.023643	-3.025514378	0.515547	4.112348
PNKD	ENSG00000127838	0.023694	0.181096747	515.0086	453.6277
KCNH1	ENSG00000143473	0.023726	-0.441431123	69.40809	94.64878
AC019257.1	ENSG00000253764	0.023727	-3.003262434	0.515547	4.026184
GATD3A	ENSG00000160221	0.023828	-0.33189051	238.7234	301.0464
TRIAP1	ENSG00000170855	0.023877	0.201075671	624.5448	542.7118
YPEL3	ENSG00000090238	0.024003	0.389862894	94.04715	71.54857
KDSR	ENSG00000119537	0.024006	-0.12180812	1517.916	1652.785
NPTX2	ENSG00000106236	0.024073	-0.228484899	280.6221	329.1159
CNTNAP3	ENSG00000106714	0.024118	-0.303529289	198.4181	244.7078
ERRFI1	ENSG00000116285	0.024143	-0.166382487	1642.58	1843.701
PCNA	ENSG00000132646	0.024147	0.154576511	6446.456	5790.755

SNRPEP4	ENSG00000233270	0.024168	0.526684265	62.75688	43.51862
ARL4C	ENSG00000188042	0.02424	-0.142503699	1239.902	1368.582
RBM41	ENSG00000089682	0.024265	-0.242953123	289.5402	343.5624
MICAL3	ENSG00000243156	0.024277	-0.278467032	424.0028	515.2656
ISYNA1	ENSG00000105655	0.024413	0.389817189	121.0778	92.13324
ZNF547	ENSG00000152433	0.024413	0.592407012	47.23773	31.31536
AC087501.4	ENSG00000271851	0.024413	-0.62243751	27.77318	42.6367
MMAB	ENSG00000139428	0.024415	0.153738803	796.9859	715.642
AGAP12P	ENSG00000265018	0.024448	-1.572712358	3.284694	9.751597
NFS1	ENSG00000244005	0.024578	0.166814082	690.4909	615.0695
HSBP1L1	ENSG00000226742	0.024624	0.307582322	241.8732	195.5843
TROAP	ENSG00000135451	0.024638	0.110756427	1931.433	1788.208
ZNF652	ENSG00000198740	0.024736	0.180360655	553.4343	488.0385
CRIM1	ENSG00000150938	0.024928	-0.21435834	2556.418	2966.642
MIR4768	ENSG00000265465	0.024955	1.621621475	9.032412	2.863575

FAM229A	ENSG00000225828	0.025002	0.484341311	92.76279	66.12286
AC006511.3	ENSG00000279865	0.025075	3.315218273	3.027169	0.206278
UHMK1	ENSG00000152332	0.025125	-0.172019355	2704.554	3048.249
GK5	ENSG00000175066	0.025217	-0.164069738	667.68	748.7344
HMG20B	ENSG00000064961	0.025321	0.154281742	1184.729	1064.131
CDCA3	ENSG00000111665	0.025344	0.13945908	1849.554	1678.365
AL021154.1	ENSG00000235052	0.025501	1.122463237	15.93071	7.335904
CORO1C	ENSG00000110880	0.02558	-0.10363719	7147.142	7679.079
TLK2P1	ENSG00000226049	0.025646	-0.584712701	33.28369	50.15953
UBXN11	ENSG00000158062	0.025657	0.211396644	731.0943	630.708
ONECUT3	ENSG00000205922	0.025681	0.762255022	30.85837	18.01557
AC136443.3	ENSG00000257264	0.0257	-3.375057441	0.267443	3.171435
CDK2AP2	ENSG00000167797	0.025716	0.191493211	731.2985	638.88
LINC00471	ENSG00000181798	0.025743	1.049991534	19.07817	9.290868
AC008013.1	ENSG00000226472	0.025763	3.402748322	3.194469	0.255646

ABCA1	ENSG00000165029	0.025767	-0.23531414	1051	1238.607
EML1	ENSG00000066629	0.025815	-0.189131778	491.1362	560.4101
HES4	ENSG00000188290	0.025877	0.181895866	769.672	676.9262
AL353803.4	ENSG00000261334	0.025905	-3.921831132	0	2.7352
SCAND2P	ENSG00000176700	0.025925	0.498465964	61.44065	43.31666
TAS1R1	ENSG00000173662	0.02597	2.060874564	6.158473	1.460738
AF228730.4	ENSG00000284614	0.026219	-2.459729056	1.077368	5.608141
SHF	ENSG00000138606	0.026255	0.372391928	108.9182	84.30689
POM121	ENSG00000196313	0.026281	-0.20921222	1899.997	2197.494
SPSB1	ENSG00000171621	0.026351	-0.156587806	882.7412	982.7103
ITGA5	ENSG00000161638	0.026352	-0.104072718	3453.709	3712.239
SERINC5	ENSG00000164300	0.026468	-0.367490267	130.6165	168.4959
CEP170	ENSG00000143702	0.026481	-0.220147158	2766.77	3223.495
SERF1B	ENSG00000205572	0.026492	-1.775510095	30.78709	105.1761
CDKN2B	ENSG00000147883	0.026553	0.250993328	325.4476	273.6021

LRRC58	ENSG00000163428	0.026574	-0.158531195	2273.808	2538.945
KCTD4	ENSG00000180332	0.026591	0.806917513	28.20422	15.97462
NHLH2	ENSG00000177551	0.026609	-0.521845551	42.88842	62.18192
AC010435.1	ENSG00000279557	0.026678	-3.306525698	0.267443	2.986534
ADGRL2	ENSG00000117114	0.026708	-0.568583468	58.33683	85.97038
PMEL	ENSG00000185664	0.026803	0.728284858	31.27285	18.77754
AC083862.2	ENSG00000272941	0.026852	1.471443294	9.838539	3.58803
MYH9	ENSG00000100345	0.026869	-0.109404457	21514.84	23211.02
AL451085.2	ENSG00000271380	0.026875	1.315749176	12.43941	4.974254
SMAD6	ENSG00000137834	0.026894	0.296873426	266.4335	217.8887
CYTH1	ENSG00000108669	0.026925	0.123618448	1934.832	1776.019
FRMD6	ENSG00000139926	0.027022	-0.180523243	2733.612	3099.001
TMEM128	ENSG00000132406	0.027039	0.279830634	187.7949	154.4102
MET	ENSG00000105976	0.027047	-0.222700583	1028.537	1200.472
SPATA18	ENSG00000163071	0.02707	1.021434973	16.46896	8.004376

QTRT1	ENSG00000213339	0.027365	0.175616081	1048.832	927.4962
KPNA5	ENSG00000196911	0.027456	-0.31416821	126.9858	158.1388
KLHDC8B	ENSG00000185909	0.027471	0.202471869	605.9063	525.4326
EYA2	ENSG00000064655	0.027533	0.111216888	1776.301	1643.815
AC009078.2	ENSG00000240338	0.027578	2.537261406	5.557668	0.940913
AC008735.4	ENSG00000276488	0.02767	-1.116242648	8.420055	18.6321
U73166.1	ENSG00000230454	0.027679	1.280122934	13.53995	5.482701
CYBA	ENSG00000051523	0.027779	0.208648481	1754.256	1517.173
INPP4B	ENSG00000109452	0.027799	-0.207000632	484.395	560.1977
SCN1B	ENSG00000105711	0.027805	0.200776153	494.5733	430.5624
RNA5SP311	ENSG00000238405	0.027829	-3.212161828	0.459354	4.562622
SHB	ENSG00000107338	0.027956	-0.175005257	431.3083	487.374
ABAT	ENSG00000183044	0.028083	-1.291638639	4.978797	12.25199
EDF1	ENSG00000107223	0.028098	0.190229512	4255.004	3728.258
CINP	ENSG00000100865	0.028231	0.171444156	832.1653	738.3476

ACTBP7	ENSG00000185607	0.028245	3.317019443	3.030966	0.206278
STX5	ENSG00000162236	0.028327	0.140003622	1130.485	1024.78
DCBLD2	ENSG00000057019	0.028337	-0.148892879	9683.208	10736.4
BRD8	ENSG00000112983	0.028339	0.109336828	1680.365	1557.02
WIPI1	ENSG00000070540	0.028417	-0.267808458	173.2179	208.4055
C1orf100	ENSG00000173728	0.02846	-3.035362078	0.488612	4.130519
FP565260.3	ENSG00000277117	0.028471	-1.149209011	6.594689	14.75531
NUP188	ENSG00000095319	0.028471	-0.112773361	5416.859	5859.114
SSH1	ENSG00000084112	0.028553	-0.178813881	2638.429	2987.296
AC233968.1	ENSG00000274615	0.02858	1.469474288	15.24071	5.516562
DGKD	ENSG00000077044	0.028732	-0.149939249	1236.98	1372.32
RPL10P9	ENSG00000233913	0.028828	0.191855629	2376.995	2080.61
ARNTL2	ENSG00000029153	0.028933	-0.140743637	1084.81	1195.529
ID2	ENSG00000115738	0.029017	0.537086544	48.83476	33.76152
CUTA	ENSG00000112514	0.029048	0.14948274	3951.614	3561.462

RHOT1	ENSG00000126858	0.029055	0.202648561	418.4036	363.9525
TRIO	ENSG00000038382	0.029059	-0.194805861	12151.62	13909.53
ITGB3	ENSG00000259207	0.029065	-0.451627728	90.96883	124.8344
TLN1	ENSG00000137076	0.029068	-0.150983268	11057.24	12278.5
TXLNG	ENSG00000086712	0.029176	-0.128918367	2755.108	3013.95
HTR7P1	ENSG00000183935	0.029253	-0.308772952	131.2013	162.7595
SOX21-AS1	ENSG00000227640	0.029282	0.851822863	21.32707	11.72105
AC073861.1	ENSG00000242299	0.029302	0.227081362	435.3976	371.2715
IL6ST	ENSG00000134352	0.029493	-0.177138498	3617.197	4091.192
LHX1	ENSG00000273706	0.029554	-0.195759457	536.085	614.3098
NIT2	ENSG00000114021	0.029609	0.160465162	1210.716	1082.672
AC004854.2	ENSG00000272768	0.029631	-0.565153135	34.57017	51.25881
PTPA	ENSG00000119383	0.029691	0.098127169	6976.38	6517.692
METTL26	ENSG00000130731	0.029721	0.144698926	1346.729	1217.765
TM2D1	ENSG00000162604	0.029731	0.328986065	168.2326	134.253

BRD3OS	ENSG00000235106	0.029811	-0.138671747	941.9549	1037.905
SCRN1	ENSG00000136193	0.029813	-0.133828686	4656.151	5109.61
CYP2W1	ENSG00000073067	0.029844	1.418053991	9.231916	3.411663
AC000078.1	ENSG00000232926	0.029846	-1.06579749	7.354045	15.38387
CBWD4P	ENSG00000204778	0.029908	0.819754488	25.6166	14.46341
TMEM91	ENSG00000142046	0.029989	0.484126729	72.21484	51.48684
MRPL28	ENSG00000086504	0.030017	0.167741747	2317.017	2061.988
RPL28	ENSG00000108107	0.030077	0.168757295	12473.27	11095.06
CCDC124	ENSG00000007080	0.030108	0.17576299	1921.767	1700.193
OTUD4	ENSG00000164164	0.030257	-0.160966909	1119.55	1252.983
LSM3	ENSG00000170860	0.030268	0.169223299	2330.256	2072.144
HMGB2	ENSG00000164104	0.03027	0.147371484	3788.916	3420.416
GNG2	ENSG00000186469	0.030379	0.227915998	300.7577	257.1539
ACTRT3	ENSG00000184378	0.030418	0.395524969	100.034	76.19285
TGFBR3	ENSG00000069702	0.030525	-0.384077758	73.55491	95.99381

ARHGEF2	ENSG00000116584	0.030594	-0.103976498	2483.508	2668.762
GPAM	ENSG00000119927	0.030637	-0.138840497	1159.273	1276.774
TMEM59	ENSG00000116209	0.030644	0.132762666	1295.907	1181.445
RPL12	ENSG00000197958	0.030647	0.17532464	15318.17	13564.7
PHC3	ENSG00000173889	0.030735	-0.186362514	1045.603	1190.807
KATNAL1	ENSG00000102781	0.030841	-0.241987188	703.0382	832.2676
MELTF-AS1	ENSG00000228109	0.030845	0.388593566	133.6652	101.5747
TRBJ2-4	ENSG00000211768	0.030858	0.651404393	40.12795	25.47617
FLNB	ENSG00000136068	0.031023	-0.167770898	7033.728	7902.361
NEAT1	ENSG00000245532	0.031156	0.21190021	1869.335	1613.19
CFDP1	ENSG00000153774	0.031371	0.220095916	1199.223	1028.809
NDUFB10	ENSG00000140990	0.031414	0.125131471	1861.019	1705.651
AL157911.1	ENSG00000258553	0.03143	-3.844803073	0	2.652987
AC004540.2	ENSG00000225792	0.031468	-3.611985844	0	2.237768
XKR5	ENSG00000275591	0.031545	1.838225471	7.013392	1.954964

PCDHA11	ENSG00000249158	0.031576	-0.587266339	28.55234	43.0332
CBLN1	ENSG00000102924	0.031643	0.769724309	28.64833	16.72761
NUDC	ENSG00000090273	0.031708	0.151120148	5069.995	4564.533
EMD	ENSG00000102119	0.031777	0.118344121	1832.68	1687.787
FAM53B-AS1	ENSG00000233334	0.03178	-3.861613068	0	2.689782
AL121845.3	ENSG00000273154	0.031972	-0.553198518	33.69475	49.21934
AC116667.1	ENSG00000271009	0.032012	0.999857659	20.1057	10.06661
PPP1R15B	ENSG00000158615	0.032047	-0.155710246	1253.057	1396.392
UQCC2	ENSG00000137288	0.032077	0.192360004	563.1965	492.5725
MYEOV	ENSG00000172927	0.03208	0.630613163	43.18938	27.65685
HSPB1	ENSG00000106211	0.032117	0.163637033	5826.978	5200.938
CTGF	ENSG00000118523	0.032269	-0.132619002	3478.674	3812.755
BCKDHA	ENSG00000248098	0.032297	2.274580408	4.74968	0.955045
SIPA1L3	ENSG00000105738	0.032413	-0.192460622	1782.25	2037.536
RBM5	ENSG00000003756	0.032423	0.129313828	1535.288	1402.55

COX7B	ENSG00000131174	0.032454	0.168771945	1430.597	1271.754
SLC25A1	ENSG00000100075	0.032544	0.109491214	4699.048	4355.398
DNAJC8	ENSG00000126698	0.032585	0.109499233	2651.118	2457.047
SMIM10L1	ENSG00000256537	0.032591	0.176429292	664.7087	587.8611
KIAA1549L	ENSG00000110427	0.032916	-0.194917146	641.1441	734.4544
AC100793.3	ENSG00000267765	0.032933	-3.590053865	0	2.192439
RAP1GAP2	ENSG00000132359	0.033031	-0.180737209	421.6411	477.5829
NALT1	ENSG00000237886	0.03311	0.416671845	83.03472	62.33874
SPAG9	ENSG00000008294	0.033135	-0.145114559	1922.235	2126.475
COMMD5	ENSG00000170619	0.033155	0.170454054	642.0831	570.4871
AC069213.1	ENSG00000223711	0.033204	3.637768568	2.300372	0
SPRY2	ENSG00000136158	0.033293	-0.191088684	339.8834	387.1577
DNMBP	ENSG00000107554	0.033449	-0.134429021	3166.371	3476.67
GPR83	ENSG00000123901	0.033469	1.106126922	14.01845	6.523637
NEDD4L	ENSG00000049759	0.033601	-0.162403419	1034.338	1157.693

MTPN	ENSG00000105887	0.033781	-0.143252467	3075.091	3397.554
MCL1	ENSG00000143384	0.033952	-0.098187405	9222.294	9872.048
LINC01106	ENSG00000175772	0.034055	0.652130541	31.81676	20.33004
ZNF428	ENSG00000131116	0.034082	0.177701464	793.9985	702.3515
AKAP8L	ENSG00000011243	0.034124	0.130976118	1406.71	1283.217
AC068946.2	ENSG00000284820	0.034219	1.92892604	6.93135	1.883114
BMP4	ENSG00000125378	0.034304	0.155876004	752.1258	676.3402
RHOB	ENSG00000143878	0.034417	-0.119287033	992.9169	1078.75
RPS28	ENSG00000233927	0.034427	0.13548771	8532.749	7766.03
RN7SL521P	ENSG00000240877	0.034671	1.965490482	5.742447	1.439632
NDUFB3	ENSG00000119013	0.034787	0.211956819	600.9738	518.1357
AC084757.1	ENSG00000259216	0.034794	-3.926600598	0	2.785401
FASTKD3	ENSG00000124279	0.034853	-0.207119823	382.9116	442.3862
ACSL3	ENSG00000123983	0.034861	-0.112395899	1446.055	1564.607
KLHDC3	ENSG00000124702	0.034877	0.135386582	1881.05	1712.279

MSN	ENSG00000147065	0.034918	-0.134430456	13614.44	14944.68
PCGF2	ENSG00000277258	0.034957	0.142934669	752.5778	681.1992
UTP18	ENSG00000011260	0.035014	-0.128579823	1199.692	1310.76
PHF23	ENSG00000040633	0.035024	0.12927289	1508.427	1379.598
BARX1	ENSG00000131668	0.035189	0.145148478	1259.12	1137.184
PITPNM2-AS1	ENSG00000251497	0.035201	-3.920450667	0	2.77127
MRPS15	ENSG00000116898	0.035217	0.184887091	1666.642	1464.94
CNIH4	ENSG00000143771	0.035232	0.127278957	1061.037	971.6054
ASPH	ENSG00000198363	0.035265	-0.12123791	4622.489	5028.868
NNMT	ENSG00000166741	0.035285	0.155964904	3709.091	3328.442
ANAPC2	ENSG00000176248	0.035329	0.108643811	1879.136	1742.684
WTAPP1	ENSG00000255282	0.035361	-1.724530879	2.162524	7.282042
TET3	ENSG00000187605	0.03553	-0.237356252	849.867	1002.641
RND3	ENSG00000115963	0.03556	-0.132618191	1195.982	1310.494
NAT10	ENSG00000135372	0.035715	-0.137847631	1237.375	1362.576

MRPL24	ENSG00000143314	0.035811	0.168662489	1167.556	1038.106
FSD1L	ENSG00000106701	0.035866	-0.2387787	248.3427	293.3507
TANK	ENSG00000136560	0.035951	0.208858538	351.9591	304.6558
ARHGAP5-AS1	ENSG00000258655	0.036138	-0.671107258	18.60455	29.49529
IMPA1	ENSG00000133731	0.036163	-0.175787891	381.9213	431.8553
ORMDL3	ENSG00000172057	0.036251	0.167676305	642.4549	573.0366
LIMA1	ENSG00000050405	0.036373	-0.134117918	3515.741	3859.134
TECR	ENSG00000099797	0.036453	0.117141921	3829.73	3529.76
MTCO1P27	ENSG00000232579	0.036561	-3.736106379	0	2.42542
ZNF324	ENSG00000083812	0.03658	-0.21964456	295.0478	344.1798
LMTK3	ENSG00000142235	0.036603	1.072716473	14.70033	7.129626
AC019205.1	ENSG00000229852	0.036607	0.506698043	57.28125	40.37096
NTSR1	ENSG00000101188	0.036776	-0.487333715	65.03407	91.92266
WBP1	ENSG00000239779	0.036803	0.289747216	171.7304	140.196
PLB1	ENSG00000163803	0.036826	2.21229118	5.594487	1.147191

DPM2	ENSG00000136908	0.03687	0.150843544	1578.515	1421.101
LINC01511	ENSG00000250584	0.03718	0.418912533	70.8412	53.02392
AL022344.2	ENSG00000259869	0.037236	-0.534416522	38.1125	55.63691
NEDD8	ENSG00000129559	0.037363	0.200928989	1396.936	1214.896
NSFP1	ENSG00000260075	0.037466	-1.942377392	3.246014	12.4636
ANGPTL7	ENSG00000171819	0.03749	-3.169348153	0.215048	2.708224
TNNT1	ENSG00000105048	0.037531	0.204166882	906.112	785.604
HBP1	ENSG00000105856	0.037539	0.234157907	224.4417	191.0807
TRIM60P18	ENSG00000227986	0.037608	0.954287876	18.08374	9.2615
ITGB1	ENSG00000150093	0.037711	-0.131572088	20894.81	22891.04
DPP3	ENSG00000254986	0.037766	-0.115647677	1218.212	1319.315
EXOC5	ENSG00000070367	0.037799	-0.134182555	2021.648	2219.954
AC009303.2	ENSG00000235066	0.037831	3.214079944	2.836732	0.27831
ARMC4P1	ENSG00000238021	0.037876	3.233922695	2.885331	0.264179
STC2	ENSG00000113739	0.037892	-0.075180384	17305.83	18231.7

PTMS	ENSG00000159335	0.03805	0.166893741	5888.488	5244.313
SHISA8	ENSG00000234965	0.038075	0.18686788	493.5725	433.698
ABHD14B	ENSG00000114779	0.03812	0.147735434	752.3037	678.3867
SLC26A4-AS1	ENSG00000233705	0.038147	1.904302929	5.475004	1.416968
KPNA3	ENSG00000102753	0.038189	-0.142929846	1481.977	1637.925
TGFBR1	ENSG00000106799	0.038227	-0.113039283	3641.412	3939.849
AC002350.1	ENSG00000278993	0.038329	-0.808060741	13.74213	24.07462
CGB5	ENSG00000189052	0.038475	1.716670193	6.584577	1.994694
SLC7A1	ENSG00000139514	0.03858	-0.150242332	3901.113	4330.383
ELL2	ENSG00000118985	0.03871	-0.164477843	554.4543	622.5554
TMSB10	ENSG00000034510	0.038749	0.161936292	12144.71	10854.12
DDX21	ENSG00000165732	0.03879	-0.15494353	10298.35	11466.61
PRKACB	ENSG00000142875	0.038851	-0.168262017	740.9988	834.4585
ECT2	ENSG00000114346	0.038891	-0.092932704	3059.101	3263.872
AL596325.2	ENSG00000272574	0.039019	1.371314803	8.39126	3.277417

COMTD1	ENSG00000165644	0.039108	0.164817979	653.3646	581.4975
PDCD11	ENSG00000148843	0.039184	-0.104686606	3692.075	3971.063
KCNG2	ENSG00000178342	0.039186	-1.328015551	5.237441	13.22401
FERMT2	ENSG00000073712	0.039408	-0.143773234	1796.929	1986.459
AC231657.1	ENSG00000279422	0.039464	-3.637490024	0	2.282642
PDE10A	ENSG00000112541	0.039501	-0.161208979	581.6831	651.0343
ZDHHC21	ENSG00000175893	0.039524	-0.187028145	362.5216	413.2361
CEP192	ENSG00000101639	0.039535	-0.201072051	794.3951	914.3741
ACD	ENSG00000102977	0.039572	0.119858474	2071.338	1905.061
PMM2	ENSG00000140650	0.039594	-0.247240812	202.8561	240.6163
CD96	ENSG00000153283	0.039629	3.745136017	2.460699	0
ACSL4	ENSG00000068366	0.039914	-0.116599657	2327.278	2523.659
WWTR1	ENSG00000018408	0.039916	-0.095044071	3890.196	4155.338
SLFN13	ENSG00000154760	0.039924	0.927770663	21.80913	11.40164
AC009120.2	ENSG00000259972	0.039935	0.496245452	57.84578	41.18937

ASIC1	ENSG00000110881	0.039952	0.201278672	345.0118	299.8459
ASAP3	ENSG00000088280	0.039993	0.198347039	376.7347	328.7867
ZEB2	ENSG00000169554	0.040008	-0.183755679	525.597	596.8477
KHK	ENSG00000138030	0.040066	0.312275888	149.3688	120.0016
CDC25C	ENSG00000158402	0.040087	0.163725616	660.3255	589.4531
COL8A2	ENSG00000171812	0.040093	-0.650874533	21.33816	33.81988
ACAT2	ENSG00000120437	0.040101	0.101170953	2654.471	2473.903
COX5B	ENSG00000135940	0.040108	0.165213769	3259.792	2906.391
PPP1R32	ENSG00000162148	0.040112	1.244975246	11.15134	4.689892
AL353704.1	ENSG00000285856	0.040189	-2.918103664	0.482491	3.644916
GPR137	ENSG00000173264	0.040201	0.110925272	1998.235	1848.857
CYP51A1	ENSG00000001630	0.040226	-0.311333454	147.8714	183.4524
H1FX	ENSG00000184897	0.040376	0.127349711	4157.223	3805.989
SART1	ENSG00000175467	0.040386	0.121912431	2627.389	2412.303
C3orf58	ENSG00000181744	0.040448	-0.295473678	153.3113	188.3351

COL27A1	ENSG00000196739	0.040501	-0.133374963	1681.159	1844.2
CNPY4	ENSG00000166997	0.040661	0.245696352	247.8971	208.5129
DHRS3	ENSG00000162496	0.040665	0.203145079	654.4587	568.1421
API5	ENSG00000166181	0.040781	-0.1104431	2135.783	2306.579
SMTNL2	ENSG00000188176	0.040791	1.24269417	14.86313	6.149797
PRDX3P2	ENSG00000231468	0.040793	2.501120672	4.167046	0.726103
PGM1	ENSG00000079739	0.040797	0.195943382	451.0887	393.4816
MTX1P1	ENSG00000236675	0.040807	1.016151215	143.6129	70.90533
CACNA1I	ENSG00000100346	0.040823	1.208695359	11.10091	4.910483
ACHE	ENSG00000087085	0.040839	-0.50070355	35.32967	49.97903
C2	ENSG00000166278	0.040888	1.133486321	12.94097	5.957379
SACS	ENSG00000151835	0.040897	-0.168337769	2037.031	2289.86
PHF24	ENSG00000122733	0.040939	-2.404735992	1.017378	5.330195
ELK4	ENSG00000158711	0.041002	-0.152625296	1064.44	1184.346
NDUFAF8	ENSG00000224877	0.041101	0.259774723	755.2014	630.7426

RPL29P11	ENSG00000224858	0.041232	0.877665947	45.80896	24.97698
KMT5A	ENSG00000183955	0.041331	0.100588152	2138.211	1995.317
SH3RF3	ENSG00000172985	0.041354	-0.248251334	280.5395	333.4108
BDNF-AS	ENSG00000245573	0.041355	-3.13138582	0.271241	2.613527
EXOC3L1	ENSG00000179044	0.041362	0.634765379	41.87917	26.976
RARRES2P2	ENSG00000213543	0.041403	2.014922809	5.944704	1.416968
RALGAPA1	ENSG00000174373	0.041439	-0.209106669	563.4286	651.7338
SH3BP4	ENSG00000130147	0.041501	-0.164840718	2802.508	3142.504
ZNF849P	ENSG00000198153	0.041525	-0.525047906	34.83579	50.18448
COL24A1	ENSG00000171502	0.041549	-1.921510289	1.45127	5.519496
C9orf84	ENSG00000165181	0.041585	-1.711874805	1.966817	6.371311
ABCC3	ENSG00000108846	0.041597	0.326734021	116.4426	92.49487
SLC25A24	ENSG00000085491	0.0417	-0.134424271	1710.15	1877.463
MCFD2	ENSG00000180398	0.041707	-0.110627234	4517.271	4877.607
AC013472.1	ENSG00000205500	0.041737	2.203793275	4.591019	1.027077

ELOF1	ENSG00000130165	0.041801	0.144321992	1155.653	1044.778
PDPK1	ENSG00000140992	0.041863	-0.160363355	1077.123	1203.621
ZNF485	ENSG00000198298	0.041888	-0.320236878	95.41509	119.1569
LIPE	ENSG00000079435	0.041953	0.445933638	65.91932	48.35331
AL096677.1	ENSG00000234832	0.041965	-1.945031416	1.430457	5.700085
SPATA6L	ENSG00000106686	0.04204	-1.675980729	2.261195	7.238454
AC004148.2	ENSG00000263272	0.042043	0.4859527	71.46887	50.90123
RAB3B	ENSG00000169213	0.042043	-0.159719863	815.8853	912.4884
PLLP	ENSG00000102934	0.042138	-0.415368755	63.06618	83.91342
POP5	ENSG00000167272	0.042161	0.223754673	703.4103	601.6823
H2AFY2	ENSG00000099284	0.0422	0.115456652	1563.382	1442.432
HMGA2	ENSG00000149948	0.042301	-0.137164514	1952.66	2147.287
MAF1	ENSG00000179632	0.042349	0.106531022	2334.678	2167.474
INA	ENSG00000148798	0.04249	-0.138157701	1111.748	1224.635
SETX	ENSG00000107290	0.042562	-0.141552852	1954.667	2157.34

KIAA1671	ENSG00000197077	0.042619	-0.191754563	645.7448	738.9561
CXCL12	ENSG00000107562	0.042658	0.156051649	573.2924	515.1135
AC113404.3	ENSG00000254893	0.04266	-0.857791261	12.51079	22.40374
HSD17B1	ENSG00000108786	0.04267	0.338830239	105.1235	83.04079
CCNB2	ENSG00000157456	0.042692	0.113108846	2422.87	2239.524
OCLN	ENSG00000197822	0.04275	0.919063544	19.57065	10.29821
RPS16	ENSG00000105193	0.042788	0.126908352	18959.54	17362.18
LBX1-AS1	ENSG00000227128	0.04279	0.282017219	183.3728	150.8625
AC004951.1	ENSG00000228434	0.042811	-1.04762202	7.646789	16.02261
CAPZB	ENSG00000077549	0.042824	0.111356198	3790.02	3507.144
AL133485.2	ENSG00000285747	0.04283	-2.209629842	0.971103	4.581246
PARD6A	ENSG00000102981	0.042899	0.365892671	107.003	83.03666
KLHL20	ENSG00000076321	0.042982	-0.201309575	406.1593	467.5878
AC107959.2	ENSG00000246130	0.04312	-2.268482651	1.021175	4.855063
RDH13	ENSG00000160439	0.043277	0.250924163	205.8991	172.6311

AC021086.1	ENSG00000247877	0.043287	3.67606569	2.321379	0
CLIP1	ENSG00000130779	0.043309	-0.15623679	1543.085	1721.249
SOX1	ENSG00000182968	0.043328	0.185493312	372.287	327.3847
FMO4	ENSG00000076258	0.043335	-1.46777883	2.997911	8.282869
DMXL2	ENSG00000104093	0.04345	-0.228577949	351.1438	412.663
MBTPS2	ENSG00000012174	0.043494	-0.12552913	4629.754	5051.485
AC084033.3	ENSG00000257698	0.043525	0.365063453	157.705	122.428
PHF13	ENSG00000116273	0.043615	0.125632912	939.5535	861.7591
SVBP	ENSG00000177868	0.043681	0.343412535	139.3481	110.1113
ATP5F1E	ENSG00000124172	0.043709	0.180308124	2873.084	2535.238
AL162377.1	ENSG00000231856	0.043753	1.079158566	16.47838	7.834169
SIRT1	ENSG00000096717	0.043764	-0.120380799	1487.114	1618.263
FUT8	ENSG00000033170	0.043826	-0.131626691	893.0056	978.1388
RIMBP3	ENSG00000275793	0.04387	-0.653941516	25.62279	40.23276
FKBP8	ENSG00000105701	0.043886	0.135145628	4906.326	4466.494

IGF2BP2	ENSG00000073792	0.043947	-0.148448787	1981.499	2197.074
LANCL1	ENSG00000115365	0.043997	-0.126599617	1166.453	1274.827
EPSTI1	ENSG00000133106	0.044282	0.451254131	61.73444	45.28438
JARID2-AS1	ENSG00000235488	0.044446	-2.447144865	0.779193	4.085462
S100A5	ENSG00000196420	0.044447	0.760269663	24.21969	14.42607
ZDHHC11	ENSG00000188818	0.044466	-0.349015038	95.44249	121.5663
EDEM3	ENSG00000116406	0.044477	-0.195736386	608.2212	697.1657
EYA4	ENSG00000112319	0.044519	-0.454616059	56.48057	77.92541
ARL8A	ENSG00000143862	0.044811	0.1402087	1026.386	931.6625
MPZ	ENSG00000158887	0.044982	0.823857023	24.78566	13.76832
COLGALT2	ENSG00000198756	0.045002	-0.463737179	50.10185	68.97642
EXOC3	ENSG00000180104	0.045084	0.096505239	1942.129	1816.37
FOXQ1	ENSG00000164379	0.045099	-0.464203047	41.15432	56.81895
NR2F2-AS1	ENSG00000247809	0.045167	0.627484646	32.55181	21.13129
IGBP1	ENSG00000089289	0.045169	0.149027512	658.1605	593.9736

ZBTB38	ENSG00000177311	0.045179	-0.165802805	2714.896	3046.738
LINC01004	ENSG00000228393	0.045183	0.822413468	20.50258	11.55268
TMEM161A	ENSG00000064545	0.045199	0.14663747	678.9695	613.5567
HIVEP2	ENSG00000010818	0.045231	-0.282530725	371.7549	452.8442
AMOTL2	ENSG00000114019	0.04533	-0.149635931	4272.248	4739.291
AC105206.1	ENSG00000177725	0.045334	-3.133904834	0.244306	2.62206
BST2	ENSG00000130303	0.04537	0.149238027	1947.602	1755.179
CLDN14	ENSG00000159261	0.045458	-0.977321861	10.16783	20.14293
DNM1P51	ENSG00000235370	0.045465	-1.741798316	2.829137	9.336741
BSG	ENSG00000172270	0.0455	0.096267729	13724.66	12837.27
TMOD1	ENSG00000136842	0.045522	0.272411411	161.0361	133.7855
ANKRD63	ENSG00000230778	0.045525	-1.755603182	2.056066	6.8459
CTSS	ENSG00000163131	0.045553	-0.162205153	612.8777	684.8679
CCDC130	ENSG00000104957	0.045557	0.172259794	625.9569	554.8533
SEMA6B	ENSG00000167680	0.045622	0.150644584	1772.547	1597.433

SNRNP25	ENSG00000161981	0.045644	0.13476947	1166.514	1061.949
TMEM30A	ENSG00000112697	0.045677	-0.095811711	2568.591	2745.779
TGIF1	ENSG00000177426	0.045745	0.174035453	429.8553	380.7442
RALA	ENSG00000006451	0.04588	-0.104071556	2389.212	2568.091
ADGRG1	ENSG00000205336	0.046016	-0.169264633	654.1588	734.4453
PCDHB13	ENSG00000187372	0.046022	-0.849613578	11.29779	20.64377
AC110079.2	ENSG00000281731	0.04607	-2.305274938	0.947966	4.773664
ETF1	ENSG00000120705	0.046101	-0.074510472	5701.848	6004.018
WWC2	ENSG00000151718	0.046108	-0.188922393	1503.589	1715.057
MEIOB	ENSG00000162039	0.046164	-1.577003451	3.493814	10.71747
CPA4	ENSG00000128510	0.046245	0.081777336	4330.049	4091.338
ACSS2	ENSG00000131069	0.046339	0.156021615	750.3542	672.5013
TMEM179	ENSG00000258986	0.046515	0.328571223	106.5021	84.9061
MIR3177	ENSG00000265820	0.046648	-2.674236507	0.730594	4.756237
MRPS30	ENSG00000112996	0.046692	-0.101426159	2058.823	2207.863

MT-ATP6	ENSG00000198899	0.0467	0.143737693	41105.15	37205.75
DNAJC11	ENSG00000007923	0.046738	-0.12257345	1165.906	1268.829
AC015819.1	ENSG00000273669	0.046751	-3.449249352	0	2.000292
TCTEX1D2	ENSG00000213123	0.046786	0.701546523	33.97201	20.89585
TACC3	ENSG00000013810	0.046941	0.102981446	2979.492	2773.723
LUZP1	ENSG00000169641	0.046971	-0.161480639	1998.65	2236.557
CCDC106	ENSG00000173581	0.046977	0.231593728	391.1179	331.9631
GPR162	ENSG00000250510	0.047091	0.30530197	135.1179	109.1979
ENO3	ENSG00000108515	0.04724	0.177717087	422.6037	373.1388
AC068580.4	ENSG00000250644	0.047269	-3.49181756	0	2.07526
CTPS2	ENSG00000047230	0.047275	0.098009156	2328.037	2173.955
PRR16	ENSG00000184838	0.047297	-0.209216122	228.7593	264.7265
YTHDF3	ENSG00000185728	0.047302	-0.145578768	1065.962	1180.14
GAS6-AS1	ENSG00000233695	0.047359	-0.856857091	11.70963	21.25674
PIN4	ENSG00000102309	0.04737	0.177193934	696.4262	616.0948

DCAF10	ENSG00000122741	0.047391	-0.14015308	746.4052	822.7213
PDE4DIP	ENSG00000178104	0.04744	-0.156693328	1095.042	1220.08
EPHA2	ENSG00000142627	0.047492	-0.118746317	3659.843	3973.88
QSOX1	ENSG00000116260	0.047493	-0.069737519	8671.667	9099.107
AP001189.5	ENSG00000255363	0.047499	-3.474888054	0	2.044063
CAPN15	ENSG00000103326	0.047529	-0.108201652	3779.081	4072.357
SLC22A1	ENSG00000175003	0.047591	-1.313381814	4.598614	11.57663
AF131216.1	ENSG00000246477	0.047626	-1.512664615	2.705857	7.680738
AFAP1L1	ENSG00000157510	0.047657	-0.407979342	61.0176	80.69768
ADCY3	ENSG00000138031	0.047683	-0.142012115	1515.212	1672.444
LINC02182	ENSG00000260420	0.047691	3.437756928	1.992278	0
APOBR	ENSG00000184730	0.047713	2.158481913	4.61249	1.076445
TMEM249	ENSG00000261587	0.047717	-0.590911575	25.8154	38.68347
AC125437.1	ENSG00000267655	0.047756	0.978477181	15.81898	7.971803
CDK12	ENSG00000167258	0.047809	-0.172027855	1596.556	1799.929

CFAP58	ENSG00000120051	0.047839	-1.170848582	4.864584	11.00193
AC004908.3	ENSG00000273402	0.047943	-1.904144681	1.476731	5.571528
PLIN1	ENSG00000166819	0.047948	1.136862806	12.02652	5.445815
MARCKSL1	ENSG00000175130	0.047956	0.10605412	2554.211	2372.937
DDX18	ENSG00000088205	0.047986	-0.103587832	2147.512	2307.957
GNAQ	ENSG00000156052	0.048087	-0.135633809	865.462	951.7366
FBXL15	ENSG00000107872	0.048113	0.221339947	597.2183	512.0809
TGIF2	ENSG00000118707	0.048163	0.131608314	792.3069	723.1489
MARCKS	ENSG00000277443	0.048186	0.105373771	4993.495	4643.192
ZRSR2	ENSG00000169249	0.048355	0.151220466	579.1629	521.2328
AL583810.2	ENSG00000258811	0.048439	2.140075248	4.529362	1.076445
COPS6	ENSG00000168090	0.048486	0.100496876	2518.959	2348.874
SAMD1	ENSG00000141858	0.048496	0.137386493	1870.066	1698.448
LAMB3	ENSG00000196878	0.04852	-0.166031032	403.1223	451.5109
OSBP	ENSG00000110048	0.048672	-0.129964102	1017.102	1113.946

MIGA1	ENSG00000180488	0.048687	-0.182348497	430.1483	488.6257
MTERF2	ENSG00000120832	0.048755	0.304294378	127.7865	103.1568
ENOX2	ENSG00000165675	0.048866	-0.205084822	258.3889	298.4166
RTN4	ENSG00000115310	0.048871	-0.091010557	6548.019	6974.633
UBE2T	ENSG00000077152	0.049008	0.130881764	1333.231	1217.934
C2orf74	ENSG00000237651	0.049164	-0.870504815	9.736923	17.78543
HOXC13-AS	ENSG00000249641	0.049186	0.429677028	85.65835	63.67268
AC004846.1	ENSG00000258376	0.049214	-0.261292017	144.9201	173.152
B4GALT4	ENSG00000121578	0.04926	0.161238092	467.6744	418.2762
STMN1	ENSG00000117632	0.049359	0.144404987	7190.949	6505.629
AC018529.2	ENSG00000278330	0.049362	1.112409465	11.27659	5.17448
RERG	ENSG00000134533	0.049551	0.835341617	25.39069	14.54224
IRF1	ENSG00000125347	0.04958	0.140552405	653.2928	592.077
SULF1	ENSG00000137573	0.049669	-2.581781709	0.749934	4.455352
AL020997.2	ENSG00000269971	0.049683	2.732640677	3.292288	0.461924

MAGED4	ENSG00000154545	0.049781	-1.114512818	10.77891	23.34823
ATG4B	ENSG00000168397	0.049793	0.11109529	2405.629	2226.853
DAAM1	ENSG00000100592	0.049798	-0.172886964	450.7034	509.2285
AC027088.3	ENSG00000259265	0.049992	3.083366141	2.59475	0.206278

Abbreviations

ADAMTS	A disintegrin and metalloproteinase with thrombospondin motif
COLXVIII	Type XVIII collagen
CS	Chondroitin sulfate
CSPG	Chondroitin sulfate proteoglycan
CXCL10	C-X-C motif chemokine 10
DEG	Differentially expressed gene
DMEM	Dulbecco's Modified Eagle medium
DMOAD	Disease modifying osteoarthritis drug
DSF	Differential scanning fluorimetry
FBS	Foetal bovine serum
GAG	Glycosaminoglycan
GLCE	D-glucuronyl C5-epimerase
GLCNAc	N-acetyl glucosamine
GSN	Gelsolin
HA	Hyaluronan
HEPES	4-(2-hydroxyethyl)-1-piperazineethanesulfonic acid
HS	Heparan sulfate
HS2ST	Heparan sulfate 2-O-sulfotransferase
HS3ST	Heparan sulfate 3-O-sulfotransferase
HS6ST	Heparan sulfate 6-O-sulfotransferase
HSBP	Heparan sulfate binding protein
HSPG	Heparan sulfate proteoglycan

HSPG2	Heparan sulfate proteoglycan 2
IAP	Integrin-associated protein
IdoA	Iduronic acid
IGF-1	Insulin-like growth factor-1
IGFBP5	Insulin-like growth factor binding protein-5
IGFR1	Insulin-like growth factor receptor 1
Ihh	Indian hedgehog
IL-1	Interleukin-1
IPF	Idiopathic pulmonary fibrosis
KO	Knock out
LFQ MS	Label-free quantitative mass spectrometry
LTBP2	Latent TGF-β binding protein 2
MMP	Matrix metalloprotease
MSK	Musculoskeletal
NC1	Non-collagenous 1
NDST	N-deacetylase/N-sulfotransferase
OA	Osteoarthritis
P/S	Penicillin/Streptomycin
PEDF	Pigment epithelium-derived factor
SERPINF1	Serpin family F member 1
SHP2	Src homology 2 domain-containing protein tyrosine-phosphatase 2
SHPS1	Src homology 2 domain-containing protein tyrosine-phosphatase substrate 1
SPR	Surface plasma resonance
SULF	Sulfatase

TGF	Transforming growth factor
TNC	Tris/sodium/calcium assay buffer
TS-1	Thrombospondin-1
YAP	Yes-associated protein

Bibliography

1. *The State of Muscoloskeletal Health 2023*. (2023).
2. Hunter, D. J. *et al.* Osteoarthritis. *The Lancet* **393**, 1745–1759 (2019).
3. Shedd, K. M. *et al.* Quantifying leisure physical activity and its relation to bone density and strength. *Med Sci Sports Exerc* **39**, 2189–2198 (2007).
4. Semanik, P. A. *et al.* Aerobic Activity in Prevention & Symptom Control of Osteoarthritis. *PM R* **4**, S37 (2012).
5. Swain, S. *et al.* Trends in incidence and prevalence of osteoarthritis in the United Kingdom: findings from the Clinical Practice Research Datalink (CPRD). *Osteoarthritis Cartilage* **28**, 792–801 (2020).
6. Mcclurg, O. *et al.* Targeting Cartilage Degradation in Osteoarthritis. (2021) doi:10.3390/ph14020126.
7. van der Kraan, P. M. *et al.* Osteophytes: relevance and biology. *Osteoarthritis Cartilage* **15**, 237–244 (2007).
8. Sanchez-Lopez, E. *et al.* Synovial inflammation in osteoarthritis progression. *Nat Rev Rheumatol* **18**, 258 (2022).
9. Mapp, P. I. *et al.* Mechanisms and targets of angiogenesis and nerve growth in osteoarthritis. *Nat Rev Rheumatol* **8**, 390–398 (2012).
10. Eyre, D. R. *et al.* Cross linking in collagen and elastin. *Annual Reviews Biochemistry* **53**, 717–748 (1984).
11. Siegel, R. C. Biosynthesis of Collagen Crosslinks: Increased Activity of Purified Lysyl Oxidase with Reconstituted Collagen Fibrils. *PNAS* **71**, 4826–4830 (1974).
12. Myllyharju, J. Prolyl 4-hydroxylases: the key enzymes of collagen biosynthesis. *Matrix Biology* **22**, 15–24 (2003).

13. Kannu, P. *et al.* Premature arthritis is a distinct type II collagen phenotype. *Arthritis Rheum* **62**, 1421–1430 (2010).

14. Mier, R. J. *et al.* Osteoarthritis in children associated with a mutation in the type II procollagen gene (COL2A1). *Mol Genet Metab* **74**, 338–341 (2001).

15. Zheng, J. *et al.* Aggrecan Synthesis and Secretion: A paradigm for molecular and cellular coordination of multiglobular protein folding and intracellular trafficking. *J. Biol. Chem* **273**, 12999–13006 (1998).

16. Ishida, O. *et al.* Chondrocytes are regulated by cellular adhesion through CD44 and hyaluronic acid pathway. *Journal of Bone and Mineral Research* **12**, 1657–1663 (1997).

17. Knudson, W. *et al.* CD44-anchored hyaluronan-rich pericellular matrices: an ultrastructural and biochemical analysis. *Exp Cell Res* **228**, 216–228 (1996).

18. Koziel, L. *et al.* Ext1-dependent heparan sulfate regulates the range of Ihh signaling during endochondral ossification. *Dev Cell* **6**, 801–813 (2004).

19. St-Jacques, B. *et al.* Indian hedgehog signaling regulates proliferation and differentiation of chondrocytes and is essential for bone formation. *Genes Dev* **13**, 2072–2086 (1999).

20. Mackie, E. J. *et al.* Endochondral ossification: How cartilage is converted into bone in the developing skeleton. *Int J Biochem Cell Biol* **40**, 46–62 (2008).

21. Maroudas, A. *et al.* Racemization of Aspartic Acid in Human Articular Cartilage. *Connect Tissue Research* **28**, 161–169 (2009).

22. Troeberg, L. *et al.* Proteases involved in cartilage matrix degradation in osteoarthritis. *Biochim Biophys Acta* **1824**, 133–145 (2012).

23. Stanton, H. *et al.* ADAMTS5 is the major aggrecanase in mouse cartilage in vivo and in vitro. *Nature* **434**, 648–652 (2005).

24. Glasson, S. S. *et al.* Deletion of active ADAMTS5 prevents cartilage degradation in a murine model of osteoarthritis. *Nature* **434**, 644–648 (2005).

25. Glasson, S. S. *et al.* Characterization of and osteoarthritis susceptibility in ADAMTS-4-knockout mice. *Arthritis Rheum* **50**, 2547–2558 (2004).

26. Durigova, M. *et al.* MMPs are less efficient than ADAMTS5 in cleaving aggrecan core protein. *Matrix Biology* **30**, 145–153 (2011).

27. Struglics, A. *et al.* MMP proteolysis of the human extracellular matrix protein aggrecan is mainly a process of normal turnover. *Biochem. J* **446**, 213–223 (2012).

28. Bau, B. *et al.* Relative messenger RNA expression profiling of collagenases and aggrecanases in human articular chondrocytes in vivo and in vitro. *Arthritis Rheum* **46**, 2648–2657 (2002).

29. Neuhold, L. A. *et al.* Postnatal expression in hyaline cartilage of constitutively active human collagenase-3 (MMP-13) induces osteoarthritis in mice. *J Clin Invest* 35–44 (2001).

30. Little, C. B. *et al.* Matrix metalloproteinase-13 deficient mice are resistant to osteoarthritic cartilage erosion but not chondrocyte hypertrophy or osteophyte development. *Arthritis Rheum* **60**, 3723 (2009).

31. Kevorkian, L. *et al.* Expression profiling of metalloproteinases and their inhibitors in cartilage. *Arthritis Rheum* **50**, 131–141 (2004).

32. Clements, K. M. *et al.* Gene Deletion of Either Interleukin-1β, Interleukin-1β -Converting Enzyme, Inducible Nitric Oxide Synthase, or Stromelysin 1 Accelerates the Development of Knee Osteoarthritis in Mice after Surgical

Transection of the Medial Collateral Ligament and Partial Medial Meniscectomy. *Arthritis Rheum* **48**, 3452–3463 (2003).

33. Meurs, J. Van *et al.* Cleavage of aggrecan at the Asn341–Phe342 site coincides with the initiation of collagen damage in murine antigen-induced arthritis: A pivotal role for stromelysin 1 in matrix metalloproteinase activity. *Arthritis and Rheumatology* **42**, 2074–2084 (2001).
34. Vincent, T. L. *et al.* FGF-2 is bound to perlecan in the pericellular matrix of articular cartilage, where it acts as a chondrocyte mechanotransducer. *Osteoarthritis Cartilage* **15**, 752–763 (2007).
35. Kvist, A. J. *et al.* The major basement membrane components localize to the chondrocyte pericellular matrix - A cartilage basement membrane equivalent? *Matrix Biology* **27**, 22–33 (2008).
36. Wilusz, R. E. *et al.* A biomechanical role for perlecan in the pericellular matrix of articular cartilage. *Matrix Biology* **31**, 320–327 (2012).
37. Lamandé, S. R. *et al.* A mouse 3T6 fibroblast cell culture model for the study of normal and protein-engineered collagen synthesis and deposition into the extracellular matrix. *Matrix* **13**, 323–330 (1993).
38. Reinboth, B. *et al.* Beta ig-h3 interacts directly with biglycan and decorin, promotes collagen VI aggregation, and participates in ternary complexing with these macromolecules. *J. Biol. Chem* **281**, 7816–7824 (2006).
39. Marcelino, J. *et al.* Attachment of articular cartilage chondrocytes to the tissue form of type VI collagen. *Biochim Biophys Acta* **1249**, 180–188 (1995).
40. Midwood, K. S. *et al.* NG2/HMPG modulation of human articular chondrocyte adhesion to type VI collagen is lost in osteoarthritis. *J Pathol* **195**, 631–635 (2001).

41. Alexopoulos, L. G. *et al.* Developmental and osteoarthritic changes in col6a1 knockout mice: The biomechanics of collagen vi in the cartilage pericellular matrix. *Arthritis Rheum* **60**, 771 (2009).

42. Christensen, S. E. *et al.* Altered trabecular bone structure and delayed cartilage degeneration in the knees of collagen VI null mice. *PLoS One* **7**, (2012).

43. Loeser, R. F. *et al.* Expression of β1 Integrins by Cultured Articular Chondrocytes and in Osteoarthritic Cartilage. *Exp Cell Res* **217**, 248–257 (1995).

44. Pfaff, M. *et al.* Integrin and Arg-Gly-Asp dependence of cell adhesion to the native and unfolded triple helix of collagen type VI. *Exp Cell Res* **206**, 167–176 (1993).

45. Candela, M. E. *et al.* Alpha 5 Integrin Mediates Osteoarthritic Changes in Mouse Knee Joints. *PLoS One* **11**, (2016).

46. Wright, M. O. *et al.* Hyperpolarisation of cultured human chondrocytes following cyclical pressure-induced strain: Evidence of a role for α5β1 integrin as a chondrocyte mechanoreceptor. *Journal of Orthopaedic Research* **15**, 742–747 (1997).

47. Attur, M. G. *et al.* Functional Genomic Analysis in Arthritis-Affected Cartilage: Yin-Yang Regulation of Inflammatory Mediators by 5 1 and V 3 Integrins 1. *The Journal of Immunology* **164**, 2684–2691 (2000).

48. Costell, M. *et al.* Perlecan Maintains the Integrity of Cartilage and Some Basement Membranes. *J Cell Biol* **147**, 1109–1122 (1999).

49. Arikawa-Hirasawa, E. *et al.* Perlecan is essential for cartilage and cephalic development. *Nat Genet* **23**, 354–358 (1999).

50. Keppie, S. J. *et al.* Matrix-Bound Growth Factors are Released upon Cartilage Compression by an Aggrecan-Dependent Sodium Flux that is Lost in Osteoarthritis. *Function* **2**, (2021).

51. Tang, X. *et al.* Connective tissue growth factor contributes to joint homeostasis and osteoarthritis severity by controlling the matrix sequestration and activation of latent TGFβ. *Annals of Rheumatic Disease* **77**, 1372–1380 (2018).

52. Vincent, T. *et al.* Basic FGF mediates an immediate response of articular cartilage to mechanical injury. *PNAS* **99**, 8259–8264 (2002).

53. Troeberg, L. *et al.* Sulfated glycosaminoglycans control the extracellular trafficking and the activity of the metalloprotease inhibitor timp-3. *Chem Biol* **21**, 1300–1309 (2014).

54. Vincent, T. L. Fibroblast growth factor 2: Good or bad guy in the joint? *Arthritis Res Ther* **13**, 1–2 (2011).

55. Sawaji, Y. *et al.* Fibroblast growth factor 2 inhibits induction of aggrecanase activity in human articular cartilage. *Arthritis Rheum* **58**, 3498–3509 (2008).

56. Im, H. J. *et al.* Basic fibroblast growth factor stimulates matrix metalloproteinase-13 via the molecular cross-talk between the mitogen-activated protein kinases and protein kinase Cdelta pathways in human adult articular chondrocytes. *J. Biol. Chem* **282**, 11110–11121 (2007).

57. Yan, D. *et al.* Fibroblast growth factor-2 promotes catabolism via FGFR1-Ras-Raf-MEK1/2- ERK1/2 axis that coordinates with the PKCδ pathway in human articular chondrocytes. *J Cell Biochem* **113**, 2856–2865 (2012).

58. Smith, S. M. L. *et al.* The core protein of growth plate perlecan binds FGF-18 and alters its mitogenic effect on chondrocytes. *Arch Biochem Biophys* **468**, 244–251 (2007).

59. Echtermeyer, F. *et al.* Syndecan-4 regulates ADAMTS-5 activation and cartilage breakdown in osteoarthritis. *Nat Med* **15**, 1072–1076 (2009).

60. Yamamoto, K. *et al.* A top-down approach to uncover the hidden ligandome of low-density lipoprotein receptor-related protein 1 in cartilage. *Matrix Biology* **112**, 190–218 (2022).

61. Ori, A. *et al.* The heparanome and regulation of cell function: structures, functions and challenges. *Frontiers of Biosciences* **1**, 4309–4338 (2008).

62. Zeng, W. *et al.* Glycosaminoglycan-binding properties and aggrecanase activities of truncated ADAMTSs: comparative analyses with ADAMTS-5, -9, -16 and -18. *Biochim Biophys Acta* **1760**, 517–524 (2006).

63. Flannery, C. R. *et al.* Autocatalytic cleavage of ADAMTS-4 (Aggrecanase-1) reveals multiple glycosaminoglycan-binding sites. *J. Biol. Chem* **277**, 42775–42780 (2002).

64. Yu, W.-H. *et al.* Heparan Sulfate Proteoglycans as Extracellular Docking Molecules for Matrilysin (Matrix Metalloproteinase 7)*. *J. Biol. Chem* **275**, 4183–4194 (2000).

65. Embree, M. C. *et al.* Biglycan and Fibromodulin Have Essential Roles in Regulating Chondrogenesis and Extracellular Matrix Turnover in Temporomandibular Joint Osteoarthritis. *Am J Pathol* **176**, 812 (2010).

66. Jamil, N. S. *et al.* NG2/CSPG4 regulates aggrecanase and MMP expression in human chondrocytes. *Osteoarthritis Cartilage* **20**, S44 (2012).

67. Sarrazin, S. *et al.* Heparan Sulfate Proteoglycans. *Cold Spring Harb Perspect Biol* **3**, 1–33 (2011).

68. Chanalaris, A. *et al.* Heparan Sulfate Proteoglycan Synthesis Is Dysregulated in Human Osteoarthritic Cartilage. *Am J Pathol* **189**, 632–647 (2019).

69. Sanchez, C. *et al.* Syndecan-4 Is Increased in Osteoarthritic Knee, but Not Hip or Shoulder, Articular Hypertrophic Chondrocytes. *Cartilage* **13**, 862S (2021).

70. Nunes, Q. M. *et al.* The heparin-binding proteome in normal pancreas and murine experimental acute pancreatitis. *PLoS One* **14**, e0217633 (2019).

71. Qin, Y. *et al.* Structural and Functional Study of d-Glucuronyl C5-epimerase. *J. Biol. Chem* **290**, 4620 (2015).

72. Bethea, H. N. *et al.* Redirecting the substrate specificity of heparan sulfate 2-O-sulfotransferase by structurally guided mutagenesis. *PNAS* **105**, 18724–18729 (2008).

73. Smeds, E. *et al.* Target selection of heparan sulfate hexuronic acid 2-O-sulfotransferase. *Glycobiology* **20**, 1274–1282 (2010).

74. Neelamegham, S. *et al.* Updates to the Symbol Nomenclature for Glycans guidelines. *Glycobiology* **29**, 620–624 (2019).

75. Ai, X. *et al.* QSulf1 remodels the 6-O sulfation states of cell surface heparan sulfate proteoglycans to promote Wnt signaling. *J Cell Biol* **162**, 341 (2003).

76. Morimoto-Tomita, M. *et al.* Cloning and Characterization of Two Extracellular Heparin-degrading Endosulfatases in Mice and Humans. *J. Biol. Chem* **277**, 49175 (2002).

77. Masri, R. El *et al.* Extracellular endosulfatase Sulf-2 harbors a chondroitin/dermatan sulfate chain that modulates its enzyme activity. *Cell Rep* **38**, (2022).

78. Kato, M. *et al.* Physiological degradation converts the soluble syndecan-1 ectodomain from an inhibitor to a potent activator of FGF-2. *Nat Med* **4**, 691–697 (1998).

79. McKenzie, E. *et al.* Cloning and expression profiling of Hpa2, a novel mammalian heparanase family member. *Biochem Biophys Res Commun* **276**, 1170–1177 (2000).

80. Levy-Adam, F. *et al.* Heparanase 2 interacts with heparan sulfate with high affinity and inhibits heparanase activity. *J. Biol. Chem* **285**, 28010–28019 (2010).

81. Shteper, P. J. *et al.* Role of promoter methylation in regulation of the mammalian heparanase gene. *Oncogene* **22**, 7737–7749 (2003).

82. Gibor, G. *et al.* Heparanase is expressed in adult human osteoarthritic cartilage and drives catabolic responses in primary chondrocytes. *Osteoarthritis Cartilage* **26**, 1110–1117 (2018).

83. Muñoz-García, J. C. *et al.* Conformations of the iduronate ring in short heparin fragments described by time-averaged distance restrained molecular dynamics. *Glycobiology* **23**, 1220–1229 (2013).

84. Hsieh, P. H. *et al.* Uncovering the Relationship between Sulphation Patterns and Conformation of Iduronic Acid in Heparan Sulphate. *Sci Rep* **6**, 1–8 (2016).

85. Das, S. K. *et al.* Synthesis of conformationally locked L-iduronic acid derivatives: Direct evidence for a critical role of the skew-boat 2S0 conformer in the activation of antithrombin by heparin. *Chemistry - A European Journal* **7**, 4821–4834 (2001).

86. Zhang, F. *et al.* Comparison of the Interactions of Different Growth Factors and Glycosaminoglycans. *Molecules* **24**, (2019).

87. Loganathan, D. *et al.* Structural Variation in the Antithrombin III Binding Site Region and Its Occurrence in Heparin from Different Sources. *Biochemistry* **29**, 4362–4368 (1990).

88. Matsuo, I. *et al.* Extracellular distribution of diffusible growth factors controlled by heparan sulfate proteoglycans during mammalian embryogenesis. *Philosophical Transactions of the Royal Society* **369**, (2014).

89. Koziel, L. *et al.* Ext1-dependent heparan sulfate regulates the range of Ihh signaling during endochondral ossification. *Dev Cell* **6**, 801–813 (2004).

90. Itakura, E. *et al.* Heparan sulfate is a clearance receptor for aberrant extracellular proteins. *Journal of Cell Biology* **219**, (2020).

91. Innis, C. A. *et al.* Crystal structures of the heparan sulfate-binding domain of follistatin. Insights into ligand binding. *J. Biol. Chem* **278**, 39969–39977 (2003).

92. Schlessinger, J. *et al.* Crystal Structure of a Ternary FGF-FGFR-Heparin Complex Reveals a Dual Role for Heparin in FGFR Binding and Dimerization. *Mol Cell* **6**, 743–750 (2000).

93. Koledova, Z. *et al.* Fibroblast growth factor 2 protein stability provides decreased dependence on heparin for induction of FGFR signaling and alters ERK signaling dynamics. *Front Cell Dev Biol* **7**, 475053 (2019).

94. Plotnikov, A. N. *et al.* Structural Basis for FGF Receptor Dimerization and Activation et al Dimerization of the extracellular domains leads to juxtaposition of the cytoplasmic domains and. *Cell* **98**, 641–650 (1999).

95. Harmer, N. J. *et al.* Towards a Resolution of the Stoichiometry of the Fibroblast Growth Factor (FGF)–FGF Receptor–Heparin Complex. *J Mol Biol* **339**, 821–834 (2004).

96. Delehedde, M. *et al.* Fibroblast growth factor-2 binds to small heparin-derived oligosaccharides and stimulates a sustained phosphorylation of p42/44 mitogen-activated protein kinase and proliferation of rat mammary fibroblasts. *Biochem J* **366**, 235–244 (2002).

97. Ibrahimi, O. A. *et al.* Analysis of mutations in fibroblast growth factor (FGF) and a pathogenic mutation in FGF receptor (FGFR) provides direct evidence for the symmetric two-end model for FGFR dimerization. *Mol Cell Biol* **25**, 671–684 (2005).

98. Gualandris, A. *et al.* Interaction of high-molecular-weight basic fibroblast growth factor with endothelium: biological activity and intracellular fate of human recombinant M(r) 24,000 bFGF. *J Cell Physiol* **161**, 149–159 (1994).

99. Arese, M. *et al.* Nuclear activities of basic fibroblast growth factor: potentiation of low-serum growth mediated by natural or chimeric nuclear localization signals. *Mol Biol Cell* **10**, 1429–1444 (1999).

100. Krejci, P. *et al.* Fibroblast growth factors 1, 2, 17, and 19 are the predominant FGF ligands expressed in human fetal growth plate cartilage. *Pediatr Res* **61**, 267–272 (2007).

101. Montero, A. *et al.* Disruption of the fibroblast growth factor-2 gene results in decreased bone mass and bone formation. *J Clin Invest* **105**, 1085–1093 (2000).

102. Hung, I. H. *et al.* FGF9 regulates early hypertrophic chondrocyte differentiation and skeletal vascularization in the developing stylopod. *Dev Biol* **307**, 300–313 (2007).

103. Liu, Z. *et al.* FGF18 is required for early chondrocyte proliferation, hypertrophy and vascular invasion of the growth plate. *Dev Biol* **302**, 80–91 (2007).

104. Ellman, M. B. *et al.* Fibroblast growth factor control of cartilage homeostasis. *Journal of Cellular Biochemistry* vol. 114 735–742 Preprint at https://doi.org/10.1002/jcb.24418 (2013).

105. Yan, D. *et al.* Fibroblast growth factor receptor 1 is principally responsible for fibroblast growth factor 2-induced catabolic activities in human articular chondrocytes. *Arthritis Res Ther* **13**, (2011).

106. Li, C. *et al.* FGFR1 function at the earliest stages of mouse limb development plays an indispensable role in subsequent autopod morphogenesis. *Development* **132**, 4755–4764 (2005).

107. Verheyden, J. M. *et al.* Conditional inactivation of Fgfr1 in mouse defines its role in limb bud establishment, outgrowth and digit patterning. *Development* **132**, 4235 (2005).

108. Davidson, D. *et al.* Fibroblast growth factor (FGF) 18 signals through FGF receptor 3 to promote chondrogenesis. *J. Biol. Chem* **280**, 20509–20515 (2005).

109. Iijima, H. *et al.* Age-related matrix stiffening epigenetically regulates α-Klotho expression and compromises chondrocyte integrity. *Nat Commun* **14**, 18 (2023).

110. Bianchi, A. *et al.* Fibroblast Growth Factor 23 drives MMP13 expression in human osteoarthritic chondrocytes in a Klotho-independent manner. *Osteoarthritis Cartilage* **24**, 1961–1969 (2016).

111. Orfanidou, T. *et al.* Involvement of SOX-9 and FGF-23 in RUNX-2 regulation in osteoarthritic chondrocytes. *J Cell Mol Med* **13**, 3186–3194 (2009).

112. Yang, L. *et al.* FGF13 Selectively Regulates Heat Nociception by Interacting with Nav1.7. *Neuron* **93**, 806-821.e9 (2017).

113. Fu, W. *et al.* Nav1.7 as a chondrocyte regulator and therapeutic target for osteoarthritis. *Nature* **625**, 557–565 (2024).

114. Duchesne, L. *et al.* Transport of fibroblast growth factor 2 in the pericellular matrix is controlled by the spatial distribution of its binding sites in heparan sulfate. *PLoS Biol* **10**, 16 (2012).

115. Sun, C. *et al.* Selectivity in glycosaminoglycan binding dictates the distribution and diffusion of fibroblast growth factors in the pericellular matrix. *Open Biol* **6**, (2015).

116. Sadir, R. *et al.* Heparan sulfate/heparin oligosaccharides protect stromal cell-derived factor-1 (SDF-1)/CXCL12 against proteolysis induced by CD26/dipeptidyl peptidase IV. *J. Biol. Chem* **279**, 43854–43860 (2004).

117. Ziarek, J. J. *et al.* Heparin oligosaccharides inhibit chemokine (CXC motif) ligand 12 (CXCL12) cardioprotection by binding orthogonal to the dimerization interface, promoting oligomerization, and competing with the chemokine (CXC motif) receptor 4 (CXCR4) N terminus. *J. Biol. Chem* **288**, 737–746 (2013).

118. Yamamoto, K. *et al.* LRP-1-mediated endocytosis regulates extracellular activity of ADAMTS-5 in articular cartilage. *FASEB J.* **27**, 511–521 (2013).

119. Huang, K. *et al.* Heparan Sulfated Glypican-4 Is Released from Astrocytes by Proteolytic Shedding and GPI-Anchor Cleavage Mechanisms. *eNeuro* **8**, 69–90 (2021).

120. Patterson, A. M. *et al.* Differential expression of syndecans and glypicans in chronically inflamed synovium. *Annals of Rheumatic Disease* **67**, 592 (2008).

121. Gardiner, M. D. *et al.* Transcriptional analysis of micro-dissected articular cartilage in post-traumatic murine osteoarthritis. *Osteoarthritis Cartilage* **23**, 616–628 (2015).

122. Appleton, C. T. G. *et al.* Global analyses of gene expression in early experimental osteoarthritis. *Arthritis Rheum* **56**, 1854–1868 (2007).

123. Fitzgerald, M. L. *et al.* Shedding of syndecan-1 and -4 ectodomains is regulated by multiple signaling pathways and mediated by a TIMP-3-sensitive metalloproteinase. *J Cell Biol* **148**, 811–824 (2000).

124. Bollmann, M. *et al.* MMP-9 mediated Syndecan-4 shedding correlates with osteoarthritis severity. *Osteoarthritis Cartilage* **29**, 280–289 (2021).

125. Szajek, A. Y. *et al.* The US regulatory and pharmacopeia response to the global heparin contamination crisis. *Nat Biotechnol* **34**, 625 (2016).

126. Skidmore, M. A. *et al.* Disaccharide compositional analysis of heparan sulfate and heparin polysaccharides using UV or high-sensitivity fluorescence (BODIPY) detection. *Nat Protoc* **5**, 1983–1992 (2010).

127. Shriver, Z. *et al.* Sequencing of 3-O sulfate containing heparin decasaccharides with a partial antithrombin III binding site. *PNAS* **97**, 10359–10364 (2000).

128. Thanawiroon, C. *et al.* Liquid Chromatography/Mass Spectrometry Sequencing Approach for Highly Sulfated Heparin-derived Oligosaccharides. *J. Biol. Chem* **279**, 2608–2615 (2004).

129. Puvirajesinghe, T. M. *et al.* Glycomics Approaches for the Bioassay and Structural Analysis of Heparin/Heparan Sulphates. *Metabolites* **2**, 1060–1089 (2012).

130. Humphries, D. E. *et al.* Chlorate: a reversible inhibitor of proteoglycan sulfation. *Biochem Biophys Res Commun* **154**, 365–371 (1988).

131. Schuksz, M. *et al.* Surfen, a small molecule antagonist of heparan sulfate. *PNAS* **105**, 13075–13080 (2008).

132. Raitman, I. *et al.* Heparin-Fibronectin Interactions in the Development of Extracellular Matrix Insolubility. *Matrix Biology* **67**, 107 (2018).

133. Uniewicz, K. A. *et al.* Differential scanning fluorimetry measurement of protein stability changes upon binding to glycosaminoglycans: A screening test for binding specificity. *Anal Chem* **82**, 3796–3802 (2010).

134. Farooqui, A. A. Purification of enzymes by Heparin-Sepharose affinity chromatography. *J Chromatogr* 335–345 (1980).

135. Thacker, B. E. *et al.* Expanding the 3-O-Sulfate Proteome - Enhanced Binding of Neuropilin-1 to 3-O-Sulfated Heparan Sulfate Modulates Its Activity. *ACS Chem Biol* **11**, 971–980 (2016).

136. Lin, X. *et al.* Disruption of gastrulation and heparan sulfate biosynthesis in EXT1-deficient mice. *Dev Biol* **224**, 299–311 (2000).

137. Sgariglia, F. *et al.* Epiphyseal abnormalities, trabecular bone loss and articular chondrocyte hypertrophy develop in the long bones of postnatal Ext1-deficient mice. *Bone* **57**, 220–231 (2013).

138. Ringvall, M. *et al.* Defective heparan sulfate biosynthesis and neonatal lethality in mice lacking N-deacetylase/N-sulfotransferase-1. *J. Biol. Chem* **275**, 25926–25930 (2000).

139. Grobe, K. *et al.* Cerebral hypoplasia and craniofacial defects in mice lacking heparan sulfate Ndst1 gene function. *Development* **132**, 3777–3786 (2005).

140. Flores, E. B. *et al.* Reduced cellular binding affinity has profoundly different impacts on the spread of distinct poxviruses. *PLoS One* **15**, (2020).

141. Reijmers, R. M. *et al.* Impaired lymphoid organ development in mice lacking the heparan sulfate modifying enzyme glucuronyl C5-epimerase. *Journal of Immunology* **184**, 3656–3664 (2010).

142. Dierker, T. *et al.* Altered heparan sulfate structure in Glce(-/-) mice leads to increased Hedgehog signaling in endochondral bones. *Matrix Biology* **49**, 82–92 (2016).

143. Bullock, S. L. *et al.* Renal agenesis in mice homozygous for a gene trap mutation in the gene encoding heparan sulfate 2-sulfotransferase. *Genes Dev* **12**, 1894–1906 (1998).

144. Shah, M. M. *et al.* Hs2st mediated kidney mesenchyme induction regulates early ureteric bud branching. *Dev Biol* **339**, 354–365 (2010).

145. Habuchi, H. *et al.* Mice Deficient in Heparan Sulfate 6-O-Sulfotransferase-1 Exhibit Defective Heparan Sulfate Biosynthesis, Abnormal Placentation, and Late Embryonic Lethality. *J. Biol. Chem* **282**, 15578–15588 (2007).

146. Smits, N. C. *et al.* HS3ST1 genotype regulates antithrombin's inflammomodulatory tone and associates with atherosclerosis. *Matrix Biology* **63**, 69–90 (2017).

147. HajMohammadi, S. *et al.* Normal levels of anticoagulant heparan sulfate are not essential for normal hemostasis. *J Clin Invest* **111**, 989–999 (2003).

148. Jiang, W. *et al.* Sulfatase 2 Modulates Fate Change from Motor Neurons to Oligodendrocyte Precursor Cells through Coordinated Regulation of Shh Signaling with Sulfatase 1. *Dev Neurosci* **39**, 361–374 (2017).

149. Holst, C. R. *et al.* Secreted sulfatases Sulf1 and Sulf2 have overlapping yet essential roles in mouse neonatal survival. *PLoS One* **2**, (2007).

150. Otsuki, S. *et al.* Role of heparan sulfate 6-0 endosulfatases in intervertebral disc homeostasis. *Histol Histopathol* **34**, 1051 (2019).

151. Otsuki, S. *et al.* Extracellular sulfatases support cartilage homeostasis by regulating BMP and FGF signaling pathways. *PNAS* **107**, 10202–10207 (2010).

152. Izvolsky, K. I. *et al.* Heparan sulfate–FGF10 interactions during lung morphogenesis. *Dev Biol* **258**, 185–200 (2003).

153. Hu, Z. *et al.* NDST1-dependent heparan sulfate regulates BMP signaling and internalization in lung development. *J Cell Sci* **122**, 1145–1154 (2009).

154. Galambos, C. *et al.* Defective pulmonary development in the absence of heparin-binding vascular endothelial growth factor isoforms. *Am J Respir Cell Mol Biol* **27**, 194–203 (2002).

155. Baasanjav, S. *et al.* Faulty initiation of proteoglycan synthesis causes cardiac and joint defects. *Am J Hum Genet* **89**, 15–27 (2011).

156. Pan, Y. *et al.* Heparan Sulfate Expression in the Neural Crest is Essential for Mouse Cardiogenesis. *Matrix Biology* **35**, 253 (2014).

157. Ng, A. *et al.* Loss of glypican-3 function causes growth factor-dependent defects in cardiac and coronary vascular development. *Dev Biol* **335**, 208–215 (2009).

158. Jochmann, K. *et al.* Heparan sulfate as a regulator of endochondral ossification and osteochondroma development. *Matrix Biology* **34**, 55–63 (2014).

159. Ohba, S. Hedgehog Signaling in Endochondral Ossification. *J Dev Biol* **4**, (2016).

160. Matsumoto, Y. *et al.* Conditional ablation of the heparan sulfate-synthesizing enzyme Ext1 leads to dysregulation of bone morphogenic protein signaling and severe skeletal defects. *J. Biol. Chem* **285**, 19227–19234 (2010).

161. Huegel, J. *et al.* Perichondrium phenotype and border function are regulated by Ext1 and heparan sulfate in developing long bones: A mechanism likely deranged in Hereditary Multiple Exostoses. *Dev Biol* **377**, 100 (2013).

162. Mundy, C. *et al.* Synovial joint formation requires local Ext1 expression and heparan sulfate production in developing mouse embryo limbs and spine. (2010) doi:10.1016/j.ydbio.2010.12.022.

163. Tzeng, S.-T. *et al.* NDST4 Is a Novel Candidate Tumor Suppressor Gene at Chromosome 4q26 and Its Genetic Loss Predicts Adverse Prognosis in Colorectal Cancer. *PLoS One* **8**, (2013).

164. Fuster, M. M. *et al.* Genetic alteration of endothelial heparan sulfate selectively inhibits tumor angiogenesis. *Journal of Cell Biology* **177**, 539–549 (2007).

165. Prudnikova, T. Y. *et al.* Antiproliferative effect of D-glucuronyl C5-epimerase in human breast cancer cells. *Cancer Cell Int* **10**, 1–8 (2010).

166. Hwang, J. A. *et al.* Epigenetic inactivation of heparan sulfate (glucosamine) 3-O-sulfotransferase 2 in lung cancer and its role in tumorigenesis. *PLoS One* **8**, (2013).

167. Hatabe, S. *et al.* Overexpression of heparan sulfate 6-O-sulfotransferase-2 in colorectal cancer. *Mol Clin Oncol* **1**, 845–850 (2013).

168. Ferguson, B. W. *et al.* Role of heparan sulfate 2-o-sulfotransferase in prostate cancer cell proliferation, invasion, and growth factor signaling. *Prostate Cancer* **2011**, 1–14 (2011).

169. Takahashi, I. *et al.* Important role of heparan sulfate in postnatal islet growth and insulin secretion. *Biochem Biophys Res Commun* **383**, 113–118 (2009).

170. Ziolkowski, A. F. *et al.* Heparan sulfate and heparanase play key roles in mouse β cell survival and autoimmune diabetes. *J Clin Invest* **122**, 132–141 (2012).

171. Dhounchak, S. *et al.* Heparan sulfate proteoglycans in beta cells provide a critical link between endoplasmic reticulum stress, oxidative stress and type 2 diabetes. *PLoS One* **16**, (2021).

172. Shafat, I. *et al.* Heparanase Levels Are Elevated in the Urine and Plasma of Type 2 Diabetes Patients and Associate with Blood Glucose Levels. *PLoS One* **6**, e17312 (2011).

173. Jiang, D. *et al.* Inhibition of pulmonary fibrosis in mice by CXCL10 requires glycosaminoglycan binding and syndecan-4. *J Clin Invest* **120**, 2049–2057 (2010).

174. Kliment, C. R. *et al.* Oxidative Stress Alters Syndecan-1 Distribution in Lungs with Pulmonary Fibrosis. *J. Biol. Chem* **284**, 3537–3545 (2009).

175. Bjermer, L. *et al.* Increased deposition of glycosaminoglycans and altered structure of heparan sulfate in idiopathic pulmonary fibrosis. *Int J Biochem Cell Biol* **83**, 27–38 (2017).

176. Lu, J. *et al.* Up-Regulation of Heparan Sulfate 6-O-Sulfation in Idiopathic Pulmonary Fibrosis. *Am J Respir Cell Mol Biol* **50**, 106–114 (2014).

177. Yue, X. *et al.* Overexpression of Sulf2 in idiopathic pulmonary fibrosis. *Glycobiology* **23**, 709–719 (2013).

178. Bukowska-Olech, E. *et al.* Hereditary Multiple Exostoses—A Review of the Molecular Background, Diagnostics, and Potential Therapeutic Strategies. *Front Genet* **12**, 759129 (2021).

179. Stickens, D. *et al.* Mice deficient in Ext2 lack heparan sulfate and develop exostoses. *Development* **132**, 5055–5068 (2005).

180. Jones, K. B. *et al.* A mouse model of osteochondromagenesis from clonal inactivation of Ext1 in chondrocytes. *PNAS* **107**, 2054–2059 (2010).

181. Pallerla, S. R. *et al.* Heparan Sulfate Ndst1 Gene Function Variably Regulates Multiple Signaling Pathways During Mouse Development. *Developmental Dynamics* **236**, 556–563 (2006).

182. Grobe, K. *et al.* Cerebral hypoplasia and craniofacial defects in mice lacking heparan sulfate Ndst1 gene function. *Development* **132**, 3777–3786 (2005).

183. Schneider, R. A. *et al.* Local retinoid signaling coordinates forebrain and facial morphogenesis by maintaining FGF8 and SHH. *Development* **128**, 2755–2767 (2001).

184. Yasuda, T. *et al.* Sulfotransferase Ndst1 is Needed for Mandibular and TMJ Development. *J Dent Res* **89**, 1111 (2010).

185. Shu, C. C. *et al.* Ablation of Perlecan Domain 1 Heparan Sulfate Reduces Progressive Cartilage Degradation, Synovitis, and Osteophyte Size in a Preclinical Model of Posttraumatic Osteoarthritis. *Arthritis and Rheumatology* **68**, 868–879 (2016).

186. Kaneko, H. *et al.* Synovial perlecan is required for osteophyte formation in knee osteoarthritis. *Matrix Biology* **32**, 178–187 (2013).

187. Kawashima, K. *et al.* Heparan sulfate deficiency leads to hypertrophic chondrocytes by increasing bone morphogenetic protein signaling. *Osteoarthritis Cartilage* **28**, 1459 (2020).

188. Gerstner, M. *et al.* Heparan Sulfate Deficiency in Cartilage: Enhanced BMP-Sensitivity, Proteoglycan Production and an Anti-Apoptotic Expression Signature after Loading. *International Journal of Molecular Sciences 2021, Vol. 22, Page 3726* **22**, 3726 (2021).

189. Severmann, A. C. *et al.* An altered heparan sulfate structure in the articular cartilage protects against osteoarthritis. *Osteoarthritis Cartilage* **28**, 977–987 (2020).

190. Bachvarova, V. *et al.* Chondrocytes respond to an altered heparan sulfate composition with distinct changes of heparan sulfate structure and increased levels of chondroitin sulfate. *Matrix Biology* **93**, 43–59 (2020).

191. Otsuki, S. *et al.* Expression of novel extracellular sulfatases Sulf-1 and Sulf-2 in normal and osteoarthritic articular cartilage. *Arthritis Res Ther* **10**, (2008).

192. Waaijer, C. J. F. *et al.* Cartilage tumour progression is characterized by an increased expression of heparan sulphate 6O-sulphation-modifying enzymes. *Virchows Arch* **461**, 475–481 (2012).

193. Brickman, Y. G. *et al.* Structural Modification of Fibroblast Growth Factor-binding Heparan Sulfate at a Determinative Stage of Neural Development. *J. Biol. Chem* **273**, 4350–4359 (1998).

194. Kalus, I. *et al.* Differential involvement of the extracellular 6-O-endosulfatases Sulf1 and Sulf2 in brain development and neuronal and behavioural plasticity. *J. Cell. Mol. Med* **13**, 4505–4521 (2009).

195. Kalus, I. *et al.* Sulf1 and Sulf2 Differentially Modulate Heparan Sulfate Proteoglycan Sulfation during Postnatal Cerebellum Development: Evidence for Neuroprotective and Neurite Outgrowth Promoting Functions. (2015) doi:10.1371/journal.pone.0139853.

196. Takashima, Y. *et al.* Heparan sulfate 6-O-endosulfatases, Sulf1 and Sulf2, regulate glomerular integrity by modulating growth factor signaling. *Am J Physiol Renal Physiol* **310**, 395–408 (2016).

197. Gorsi, B. *et al.* The heparan sulfate editing enzyme Sulf1 plays a novel role in zebrafish VegfA mediated arterial venous identity. *Angiogenesis* **17**, 77–91 (2014).

198. Buresh-Stiemke, R. A. *et al.* Distinct Expression Patterns of Sulf1 and Hs6st1 Spatially Regulate Heparan Sulfate Sulfation During Prostate Development. *Developmental Dynamics* **241**, (2012).

199. Ghadiali, R. S. *et al.* Dynamic changes in heparan sulfate during muscle differentiation and ageing regulate myoblast cell fate and FGF2 signalling. *Matrix Biology* **59**, 54–68 (2016).

200. Feyzi, E. *et al.* Age-dependent modulation of heparan sulfate structure and function. *J. Biol. Chem* **273**, 13395–13398 (1998).

201. Yamada, T. *et al.* Heparan sulfate alterations in extracellular matrix structures and fibroblast growth factor-2 signaling impairment in the aged neurogenic niche. *J Neurochem* **142**, 534–544 (2017).

202. Ratzka, A. *et al.* Expression Patterns of Sulfatase Genes in the Developing Mouse Embryo. *Developmental Dynamics* **239**, 1779–1788 (2010).

203. Nagamine, S. *et al.* Organ-specific sulfation patterns of heparan sulfate generated by extracellular sulfatases Sulf1 and Sulf2 in mice. *J. Biol. Chem* **287**, 9579–9590 (2012).

204. Kalus, I. *et al.* Sulf1 and Sulf2 Differentially Modulate Heparan Sulfate Proteoglycan Sulfation during Postnatal Cerebellum Development: Evidence for Neuroprotective and Neurite Outgrowth Promoting Functions. *PLoS One* **10**, (2015).

205. Ai, X. *et al.* SULF1 and SULF2 regulate heparan sulfate-mediated GDNF signaling for esophageal innervation. *Development* **134**, 3327–3338 (2007).

206. Ai, X. *et al.* Substrate Specificity and Domain Functions of Extracellular Heparan Sulfate 6-O-Endosulfatases, QSulf1 and QSulf2 *. *J. Biol. Chem* **281**, 4969–4976 (2005).

207. Wyss-Coray, T. Ageing, neurodegeneration and brain rejuvenation. *Nature* **539**, 180 (2016).

208. Motamedi-Shad, N. *et al.* Kinetic Analysis of Amyloid Formation in the Presence of Heparan Sulfate: Faster unfolding and change of pathway. *J. Biol. Chem* **284**, 29921–29934 (2009).

209. Holmes, B. B. *et al.* Heparan sulfate proteoglycans mediate internalization and propagation of specific proteopathic seeds. *PNAS* 3138–3147 (2013) doi:10.1073/pnas.1301440110.

210. Zhao, J. *et al.* Glycan Determinants of Heparin-Tau Interaction. *Biophyisical Journal* **112**, 921–932 (2017).

211. Rauch, J. N. *et al.* Tau Internalization is Regulated by 6-O Sulfation on Heparan Sulfate Proteoglycans (HSPGs). *Sci Rep* **8**, (2018).

212. P Erez-L Opez, N. *et al.* Alterations in the Expression of the Genes Responsible for the Synthesis of Heparan Sulfate in Brains With Alzheimer Disease. *Journal Neuropathological Experimental Neurology* **80**, 446–456 (2021).

213. Hosono-Fukao, T. *et al.* Heparan Sulfate Subdomains that are Degraded by Sulf Accumulate in Cerebral Amyloid ß Plaques of Alzheimer's Disease Evidence from Mouse Models and Patients Address reprint requests to. *Am J Pathol* **180**, 2056–2067 (2012).

214. Miettinen, P. J. *et al.* TGF-beta induced transdifferentiation of mammary epithelial cells to mesenchymal cells: involvement of type I receptors. *Journal of Cell Biology* **127**, 2021–2036 (1994).

215. Alhasan, A. A. *et al.* Role of 6-O-Sulfated Heparan Sulfate in Chronic Renal Fibrosis. *J. Biol. Chem* **289**, 20295 (2014).

216. Yamamoto, K. *et al.* MMP-13 is constitutively produced in human chondrocytes and co-endocytosed with ADAMTS-5 and TIMP-3 by the endocytic receptor LRP1. *Matrix Biology* **56**, 57 (2016).

217. Gao, W. *et al.* Epitope mapping by a Wnt-blocking antibody: evidence of the Wnt binding domain in heparan sulfate. *Sci Rep* **6**, 1–11 (2016).

218. Zhu, M. *et al.* Activation of beta-catenin signaling in articular chondrocytes leads to osteoarthritis-like phenotype in adult beta-catenin conditional activation mice. *Journal of Bone and Mineral Research* **24**, 12–21 (2009).

219. Nalesso, G. *et al.* WNT16 antagonises excessive canonical WNT activation and protects cartilage in osteoarthritis. doi:10.1136/annrheumdis-2015-208577.

220. Liu, S. S. *et al.* Abnormal expression of key genes and proteins in the canonical Wnt/β-catenin pathway of articular cartilage in a rat model of exercise-induced osteoarthritis. *Mol Med Rep* **13**, 1999–2006 (2016).

221. Serra, R. *et al.* Expression of a truncated, kinase-defective TGF-beta type II receptor in mouse skeletal tissue promotes terminal chondrocyte differentiation and osteoarthritis. *J Cell Biol* **139**, 541–552 (1997).

222. Lee, J. *et al.* Structural determinants of heparin-transforming growth factor-β1 interactions and their effects on signaling. *Glycobiology* **25**, 1491–1504 (2015).

223. Kuo, W.-J. *et al.* Heparan Sulfate Acts as a Bone Morphogenetic Protein Coreceptor by Facilitating Ligand-induced Receptor Hetero-oligomerization. *Mol Biol Cell* **21**, 4028–4041 (2010).

224. Denardo, A. *et al.* BMP6 binding to heparin and heparan sulfate is mediated by N-terminal and C-terminal clustered basic residues. *BBA-General Subjects* **1865**, 129799 (2021).

225. Ashikari-Hada, S. *et al.* Characterization of Growth Factor-binding Structures in Heparin/Heparan Sulfate Using an Octasaccharide Library. *J. Biol. Chem* **279**, 12346–12354 (2004).

226. Chuang, C. Y. *et al.* Heparan sulfate dependent signaling of fibroblast growth factor (FGF) 18 by chondrocyte-derived perlecan. *Biochemistry* **49**, 5524 (2010).

227. Froger, A. *et al.* Transformation of plasmid DNA into E. coli using the heat shock method. *Journal of Visualized Experiments* (2007) doi:10.3791/253.

228. Greco, K. V. *et al.* High density micromass cultures of a human chondrocyte cell line: A reliable assay system to reveal the modulatory functions of pharmacological agents. *Biochem Pharmacol* **82**, 1919–1929 (2011).

229. Knight, C. G. *et al.* A novel coumarin-labelled peptide for sensitive continuous assays of the matrix metalloproteinases. *FEBS Lett* **296**, 263–266 (1992).

230. Troeberg, L. *et al.* The C-terminal domains of ADAMTS-4 and ADAMTS-5 promote association with N-TIMP-3. *Matrix Biology* **28**, 463–469 (2009).

231. Raudvere, U. *et al.* g:Profiler: a web server for functional enrichment analysis and conversions of gene lists (2019 update). *Nucleic Acids Res* **47**, W191–W198 (2019).

232. Rappsilber, J. *et al.* Stop and Go Extraction Tips for Matrix-Assisted Laser Desorption/Ionization, Nanoelectrospray, and LC/MS Sample Pretreatment in Proteomics. *Anal Chem* **75**, 663–670 (2002).

233. Calligaris, M. *et al.* Identification of membrane proteins regulated by ADAM15 by SUSPECS proteomics. *Front Mol Biosci* **10**, (2023).

234. Gebauer, M. *et al.* Comparison of the chondrosarcoma cell line SW1353 with primary human adult articular chondrocytes with regard to their gene expression profile and reactivity to IL-1beta. *Osteoarthritis Cartilage* **13**, 697–708 (2005).

235. Eldridge, S. *et al.* Agrin mediates chondrocyte homeostasis and requires both LRP4 and α-dystroglycan to enhance cartilage formation in vitro and in vivo. *Annals of Rheumatic Disease* **75**, 1228–1235 (2016).

236. Finger, F. *et al.* Phenotypic characterization of human chondrocyte cell line C-20/A4: a comparison between monolayer and alginate suspension culture. *Cells Tissues Organs* **178**, 65–77 (2004).

237. Finger, F. *et al.* Molecular phenotyping of human chondrocyte cell lines T/C-28a2, T/C-28a4, and C-28/I2. *Arthritis Rheum* **48**, 3395–3403 (2003).

238. Roughley, P. J. *et al.* The role of aggrecan in normal and osteoarthritic cartilage. *J Exp Orthop* **1**, (2014).

239. Malemud, C. J. *et al.* Enhanced sulfated-proteoglycan core protein synthesis by incubation of rabbit chondrocytes with recombinant transforming growth factor-β1. *J Cell Physiol* **149**, 152–159 (1991).

240. Van Der Kraan, P. *et al.* Differential effect of transforming growth factor beta on freshly isolated and cultured articular chondrocytes. *J Rheumatol* **19**, 140–145 (1992).

241. Yue, X. *et al.* Transforming growth factor-beta1 induces heparan sulfate 6-O-endosulfatase 1 expression in vitro and in vivo. *J Biol Chem* **283**, 20397–20407 (2008).

242. Hodax, J. K. *et al.* Aggrecan is required for chondrocyte differentiation in ATDC5 chondroprogenitor cells. *PLoS One* **14**, (2019).

243. Otero, M. *et al.* Human Chondrocyte Cultures as Models of Cartilage-Specific Gene Regulation. *Methods Mol Med* **107**, 69 (2005).

244. Holtzer, H. *et al.* The loss of phenotypic traits by differentiated cells in vitro: Dedifferentiation of cartilage cells. *PNAS* **46**, 1533 (1960).

245. Ma, B. *et al.* Gene expression profiling of dedifferentiated human articular chondrocytes in monolayer culture. *Osteoarthritis Cartilage* **21**, 599–603 (2013).

246. Chen, Y. *et al.* A high-resolution route map reveals distinct stages of chondrocyte dedifferentiation for cartilage regeneration. *Bone Res* **10**, 1–16 (2022).

247. Tare, R. S. *et al.* Tissue engineering strategies for cartilage generation-Micromass and three dimensional cultures using human chondrocytes and a continuous cell line. (2005) doi:10.1016/j.bbrc.2005.05.117.

248. Dehne, T. *et al.* Gene expression profiling of primary human articular chondrocytes in high-density micromasses reveals patterns of recovery, maintenance, re- and dedifferentiation. *Gene* **462**, 8–17 (2010).

249. Eldridge, S. E. *et al.* Agrin induces long-term osteochondral regeneration by supporting repair morphogenesis. *Sci Transl Med* **12**, (2020).

250. Haseeb, A. *et al.* SOX9 keeps growth plates and articular cartilage healthy by inhibiting chondrocyte dedifferentiation/ osteoblastic redifferentiation. *PNAS* **118**, (2021).

251. Chua, K. H. *et al.* Insulin-Transferrin-Selenium prevent human chondrocyte dedifferentiation and promote the formation of high quality tissue engineered human hyaline cartilage. *Eur Cell Mater* **9**, 58–67 (2005).

252. Morales, T. I. *et al.* Transforming growth factor-beta in calf articular cartilage organ cultures: synthesis and distribution. *Arch Biochem Biophys* **288**, 397–405 (1991).

253. Yang, X. *et al.* TGF-β/Smad3 Signals Repress Chondrocyte Hypertrophic Differentiation and Are Required for Maintaining Articular Cartilage. *J Cell Biol* **153**, 35 (2001).

254. Fischer, B. *et al.* First Characterization of Human Dermal Fibroblasts Showing a Decreased Xylosyltransferase-I Expression Induced by the CRISPR/Cas9 System. *Int J Mol Sci* **23**, 5045 (2022).

255. Zhou, Y. *et al.* Lysophosphatidic acid receptor 5 transactivation of TGFBR1 stimulates the mRNA expression of proteoglycan synthesizing genes XYLT1 and CHST3. *BBA - Molecular Cell Research* **1867**, (2020).

256. Yue, X. *et al.* Transforming Growth Factor-β1 Induces Heparan Sulfate 6-O-Endosulfatase 1 Expression in Vitro and in Vivo. *J. Biol. Chem* **283**, 20397 (2008).

257. Madry, H. *et al.* Efficient lipid-mediated gene transfer to articular chondrocytes. *Gene Ther* **7**, 286–291 (2000).

258. Morrey, M. E. *et al.* Optimizing nonviral-mediated transfection of human intervertebral disc chondrocytes. doi:10.1016/j.spinee.2007.05.010.

259. Welter, J. F. *et al.* High-efficiency nonviral transfection of primary chondrocytes. *Methods Mol Med* **100**, 129–146 (2004).

260. Haag, J. *et al.* Efficient non-viral transfection of primary human adult chondrocytes in a high-throughput format. *Osteoarthritis Cartilage* **17**, 813–817 (2009).

261. Nagai, N. *et al.* Stem domains of heparan sulfate 6-O-sulfotransferase are required for Golgi localization, oligomer formation and enzyme activity. *J Cell Sci* **117**, 3331–3341 (2004).

262. Habuchi, H. *et al.* Purification and Characterization of Heparan Sulfate 6-Sulfotransferase from the Culture Medium of Chinese Hamster Ovary Cells*. *J. Biol. Chem* **270**, 4172–4179 (1995).

263. Nagai, N. *et al.* Regulation of Heparan Sulfate 6-O-Sulfation by β-Secretase Activity. *J. Biol. Chem* **282**, 14942–14951 (2007).

264. Habuchi, H. *et al.* The Occurrence of Three Isoforms of Heparan Sulfate 6-O-Sulfotransferase Having Different Specificities for Hexuronic Acid Adjacent to the Targeted N-Sulfoglucosamine*. *J. Biol. Chem* **275**, 2859–2868 (2000).

265. Severmann, A.-C. *et al.* An altered heparan sulfate structure in the articular cartilage protects against osteoarthritis. (2020) doi:10.1016/j.joca.2020.04.002.

266. Yamamoto, K. *et al.* MMP-13 is constitutively produced in human chondrocytes and co-endocytosed with ADAMTS-5 and TIMP-3 by the endocytic receptor LRP1. *Matrix Biology* **56**, 57 (2016).

267. Echtermeyer, F. *et al.* Syndecan-4 regulates ADAMTS-5 activation and cartilage breakdown in osteoarthritis. *Nat Med* **15**, 1072–1076 (2009).

268. Vincent, T. L. IL-1 in osteoarthritis: time for a critical review of the literature. *F1000Res* **8**, (2019).

269. Saklatvala, J. Tumour necrosis factor alpha stimulates resorption and inhibits synthesis of proteoglycan in cartilage. *Nature* **322**, 547–549 (1986).

270. Morgan, T. G. *et al.* Human nasal cartilage responds to oncostatin M in combination with interleukin 1 or tumour necrosis factor alpha by the release of collagen fragments via collagenases. *Annals of Rheumatic Disease* **65**, 184–190 (2006).

271. Prante, C. *et al.* The Formation of Extracellular Matrix During Chondrogenic Differentiation of Mesenchymal Stem Cells Correlates with Increased Levels of Xylosyltransferase I. *Stem Cells* **24**, 2252–2261 (2006).

272. Ovchinnikov, D. Alcian blue/alizarin red staining of cartilage and bone in mouse. *Cold Spring Harb Protoc* **4**, (2009).

273. Ismail, H. M. *et al.* Interleukin-1 Acts via the JNK-2 Signaling Pathway to Induce Aggrecan Degradation by Human Chondrocytes. *Arthritis and Rheumatology* **67**, 1826–1836 (2015).

274. Fukuta, S. *et al.* Abundance of calpain and aggrecan-cleavage products of calpain in degenerated human intervertebral discs. *Osteoarthritis Cartilage* **19**, 1254–1262 (2011).

275. James, M. L. *et al.* A molecular imaging primer: modalities, imaging agents, and applications. *Physiol Rev* **92**, 897–965 (2012).

276. Ranisden, L. *et al.* Selective and differential binding of interleukin (1L)-la, IL-lp, IL-2 and IL-6 to glycosaminoglycans*. *Eur. J. Immunology* 3027–3031 (1992).

277. Vallé, S. *et al.* Recruitment of a Heparan Sulfate Subunit to the Interleukin-1 Receptor Complex REGULATION BY FIBRONECTIN ATTACHMENT*. *J. Biol. Chem* **274**, 20103–20109 (1999).

278. Godmann, L. *et al.* Antibody-mediated inhibition of syndecan-4 dimerisation reduces interleukin (IL)-1 receptor trafficking and signalling. *Annals of Rheumatic Disease* **79**, 481–489 (2020).

279. Shi, Z. D. *et al.* Heparan Sulfate Proteoglycans Mediate Interstitial Flow Mechanotransduction Regulating MMP-13 Expression and Cell Motility via FAK-ERK in 3D Collagen. *PLoS One* **6**, e15956 (2011).

280. Do, A. T. *et al.* Overexpression of heparan sulfate 6-O-sulfotransferases in human embryonic kidney 293 cells results in increased N-acetylglucosaminyl 6-O-sulfation. *Journal of Biological Chemistry* **281**, 5348–5356 (2006).

281. Shamdani, S. *et al.* Heparan sulfate functions are altered in the osteoarthritic cartilage. *Arthritis Res Ther* **22**, (2020).

282. Merry, C. L. R. *et al.* The Molecular Phenotype of Heparan Sulfate in the Hs2st−/− Mutant Mouse. *J. Biol. Chem* **276**, 35429–35434 (2001).

283. Bachvarova, V. *et al.* Chondrocytes respond to an altered heparan sulfate composition with distinct changes of heparan sulfate structure and increased levels of chondroitin sulfate. *Matrix Biology* **93**, 43–59 (2020).

284. Yoshida, M. *et al.* Expression analysis of three isoforms of hyaluronan synthase and hyaluronidase in the synovium of knees in osteoarthritis and rheumatoid arthritis by quantitative real-time reverse transcriptase polymerase chain reaction. *Arthritis Res Ther* **6**, R514 (2004).

285. Vallés, S. *et al.* Recruitment of a heparan sulfate subunit to the interleukin-1 receptor complex. Regulation by fibronectin attachment. *J. Biol. Chem* **274**, 20103–20109 (1999).

286. Thomas, C. *et al.* Structure of the activating IL-1 receptor signaling complex. *Nat Struct Mol Biol* **19**, (2012).

287. Thomas, C. *et al.* Structure of the activating IL-1 receptor signaling complex. *Nat Struct Mol Biol* **19**, 455 (2012).

288. Jurrus, E. *et al.* Improvements to the APBS biomolecular solvation software suite. *Protein Science* **27**, 112–128 (2018).

289. Lowenthal, J. W. *et al.* Binding and internalization of interleukin 1 by T cells. Direct evidence for high- and low-affinity classes of interleukin 1 receptor. *J Exp Med* **164**, 1060 (1986).

290. Brissoni, B. *et al.* Intracellular Trafficking of Interleukin-1 Receptor I Requires Tollip. *Current Biology* **16**, 2265–2270 (2006).

291. Asami, J. *et al.* Structural and functional understanding of the toll-like receptors. *Protein Science* **30**, 761 (2021).

292. Jan, S. Le *et al.* Functional overlap between chondroitin and heparan sulfate proteoglycans during VEGF-induced sprouting angiogenesis. *Arterioscler Thromb Vasc Biol* **32**, 1255 (2012).

293. Deepa, S. S. *et al.* Chondroitin sulfate chains on syndecan-1 and syndecan-4 from normal murine mammary gland epithelial cells are structurally and functionally distinct and cooperate with heparan sulfate chains to bind growth factors. A novel function to control binding of midkine, pleiotrophin, and basic fibroblast growth factor. *J. Biol. Chem* **279**, 37368–37376 (2004).

294. Nemeth, D. P. *et al.* Modulation of Neural Networks by Interleukin-1. *Brain Plasticity* **7**, 17 (2021).

295. Lindahl, U. *et al.* Evidence for a 3-O-sulfated D-glucosamine residue in the antithrombin-binding sequence of heparin. *PNAS* **77**, 6551–6555 (1980).

296. Karlsson, G. *et al.* Separation of latent, prelatent, and native forms of human antithrombin by heparin affinity high-performance liquid chromatography. *Protein Expr Purif* **33**, 339–345 (2004).

297. Wang, W. *et al.* Quantification of Proteins and Metabolites by Mass Spectrometry without Isotopic Labeling or Spiked Standards. *Anal Chem* **75**, 4818–4826 (2003).

298. Guyot, N. *et al.* Proteomic analysis of egg white heparin-binding proteins: towards the identification of natural antibacterial molecules. *Sci Rep* **6**, 1–11 (2016).

299. Sandoval, D. R. *et al.* Proteomics-based screening of the endothelial heparan sulfate interactome reveals that C-type lectin 14a (CLEC14A) is a heparin-binding protein. *J. Biol. Chem* 2804–2821 (2020) doi:10.1074/jbc.RA119.011639.

300. Aikio, M. *et al.* Specific collagen XVIII isoforms promote adipose tissue accrual via mechanisms determining adipocyte number and affect fat deposition. *PNAS* **111**, E3043 (2014).

301. Folkesson, E. *et al.* Proteomic comparison of osteoarthritic and reference human menisci using data-independent acquisition mass spectrometry. *Osteoarthritis Cartilage* **28**, 1092 (2020).
302. Klinger, P. *et al.* PEDF is associated with the termination of chondrocyte phenotype and catabolism of cartilage tissue. *Biomed Res Int* **2017**, (2017).
303. Nakamura, D. S. *et al.* Pigment Epithelium-Derived Factor (PEDF) mediates cartilage matrix loss in an age-dependent manner under inflammatory conditions. *BMC Musculoskelet Disord* **18**, (2017).
304. Saarela, J. *et al.* The Short and Long Forms of Type XVIII Collagen Show Clear Tissue Specificities in Their Expression and Location in Basement Membrane Zones in Humans. *Am J Pathol* **153**, 611–626 (1998).
305. O'Reilly, M. S. *et al.* Endostatin: an endogenous inhibitor of angiogenesis and tumor growth. *Cell* **88**, 277–285 (1997).
306. Ricard-Blum, S. *et al.* Characterization of endostatin binding to heparin and heparan sulfate by surface plasmon resonance and molecular modeling: Role of divalent cations. *J. Biol. Chem* **279**, 2927–2936 (2004).
307. Ständker, L. *et al.* Isolation and characterization of the circulating form of human endostatin. *FEBS Lett* **420**, 129–133 (1997).
308. Hohenester, E. *et al.* Crystal structure of the angiogenesis inhibitor endostatin at 1.5 A resolution. *EMBO J* **17**, 1656–1664 (1998).
309. Ori, A. *et al.* Identification of Heparin-binding Sites in Proteins by Selective Labeling. *Molecular & Cellular Proteomics* **8**, 2256 (2009).
310. Alberdi, E. M. *et al.* Glycosaminoglycans in human retinoblastoma cells: Heparan sulfate, a modulator of the pigment epithelium-derived factor-receptor interactions. *BMC Biochem* **4**, 1–9 (2003).

311. Valnickova, Z. *et al.* Heparin binding induces a conformational change in pigment epithelium-derived factor. *J. Biol. Chem* **282**, 6661–6667 (2007).

312. Simonovic, M. *et al.* Crystal structure of human PEDF, a potent anti-angiogenic and neurite growth-promoting factor. *PNAS* **98**, 11131–11135 (2001).

313. Kreuger, J. *et al.* Role of heparan sulfate domain organization in endostatin inhibition of endothelial cell function. *EMBO Journal* **21**, 6303–6311 (2002).

314. Pufe, T. *et al.* Endostatin/collagen XVIII - An inhibitor of angiogenesis - Is expressed in cartilage and fibrocartilage. *Matrix Biology* **23**, 267–276 (2004).

315. Feng, Y. *et al.* Endostatin promotes the anabolic program of rabbit chondrocyte. *Cell Res* **15**, 201–206 (2005).

316. Jeng, L. *et al.* Engineering Endostatin-Producing Cartilaginous Constructs for Cartilage Repair Using Nonviral Transfection of Chondrocyte-Seeded and Mesenchymal-Stem-Cell-Seeded Collagen Scaffolds. *Tissue Eng Part A* **16**, 3011 (2010).

317. Ericsson, C. *et al.* Chapter 17 Protein Extraction from Solid Tissue. doi:10.1007/978-1-59745-423-0_17.

318. Vincourt, J. B. *et al.* Establishment of a reliable method for direct proteome characterization of human articular cartilage. *Molecular & cellular proteomics* **5**, 1984–1995 (2006).

319. Hirano, M. *et al.* New Protein Extraction/Solubilization Protocol for Gel-based Proteomics of Rat (Female) Whole Brain and Brain Regions. *Mol. Cells* **22**, 119–125 (2006).

320. Ericsson, C. *et al.* Optimized protein extraction from cryopreserved brain tissue samples. *Connect Tissue Research* **46**, 10–20 (2009).

321. Machuca, M. A. *et al.* Method for Efficient Refolding and Purification of Chemoreceptor Ligand Binding Domain. *Journal of Visualized Experiments* **2017**, 57092 (2017).

322. Digabriele, A. D. *et al.* Structure of a heparin-linked biologically active dimer of fibroblast growth factor. *Nature* **393**, 812–817 (1998).

323. Faham, S. *et al.* Heparin structure and interactions with basic fibroblast growth factor. *Science* **271**, 1116–1120 (1996).

324. Aggarwal, S. *et al.* False Discovery Rate Estimation in Proteomics. *Methods in Molecular Biology* **1362**, 119–128 (2016).

325. Jolma, A. *et al.* Binding specificities of human RNA-binding proteins toward structured and linear RNA sequences. *Genome Res* **30**, 962–973 (2020).

326. Bendak, K. *et al.* A rapid method for assessing the RNA-binding potential of a protein. *Nucleic Acids Res* **40**, e105 (2012).

327. Shichiri, M. *et al. Antiangiogenesis Signals by Endostatin*.

328. Abdollahi, A. *et al.* Endostatin's Antiangiogenic Signaling Network. *Mol Cell* **13**, 649–663 (2004).

329. Miosge, N. *et al.* The Collagen Type XVIII Endostatin Domain Is Co-localized with Perlecan in Basement Membranes In Vivo. *The Journal of Histochemistry & Cytochemistry* **51**, 285–296 (2003).

330. Sasaki, T. *et al.* Structural basis and potential role of heparin/heparan sulfate binding to the angiogenesis inhibitor endostatin. *EMBO Journal* **18**, 6240–6248 (1999).

331. Pufe, T. *et al.* Endostatin/collagen XVIII—an inhibitor of angiogenesis—is expressed in cartilage and fibrocartilage. *Matrix Biology* **23**, 267–276 (2004).

332. Lee, S.-J. *et al.* Endostatin binds to the catalytic domain of matrix metalloproteinase-2. *FEBS J.* 147–152 (2002) doi:10.1016/S0014-5793(02)02742-4.

333. Bhatwa, A. *et al.* Challenges Associated With the Formation of Recombinant Protein Inclusion Bodies in Escherichia coli and Strategies to Address Them for Industrial Applications. *Front Bioeng Biotechnol* **9**, 630551 (2021).

334. Stanley, P. Regulation of Notch signaling by glycosylation. *Curr Opin Struct Biol* **17**, 530–535 (2007).

335. Ham, B. M. *et al.* The Influence of Sample Preparation and Replicate Analyses on HeLa Cell Phosphoproteome Coverage. *J Proteome Res* **7**, 2215 (2008).

336. Wang, Z. *et al.* RNA-Seq: a revolutionary tool for transcriptomics. *Nat Rev Genet* **10**, 57 (2009).

337. Potter, S. S. Single-cell RNA sequencing for the study of development, physiology and disease. *Nat Rev Nephrol* **14**, 479–492 (2018).

338. Williams, C. G. *et al.* An introduction to spatial transcriptomics for biomedical research. *Genome Med* **14**, 1–18 (2022).

339. Ogata, H. *et al.* KEGG: Kyoto Encyclopedia of Genes and Genomes. *Nucleic Acids Res* **27**, 29–34 (1999).

340. Gillespie, M. *et al.* The reactome pathway knowledgebase 2022. *Nucleic Acids Res* **50**, D687–D692 (2022).

341. Consortium, T. G. O. *et al.* The Gene Ontology knowledgebase in 2023. *Genetics* **224**, (2023).

342. Ashburner, M. *et al.* Gene Ontology: tool for the unification of biology. *Nature Genetics 2000 25:1* **25**, 25–29 (2000).

343. Shannon, P. *et al.* Cytoscape: a software environment for integrated models of biomolecular interaction networks. *Genome Res* **13**, 2498–2504 (2003).

344. Pirttiniemi, A. *et al.* Long-chain polyphosphates inhibit type I interferon signaling and augment LPS-induced cytokine secretion in human leukocytes. *J Leukoc Biol* (2023) doi:10.1093/JLEUKO/QIAD058.

345. Lin, W. *et al.* IGFBP5 is an ROR1 ligand promoting glioblastoma invasion via ROR1/HER2-CREB signaling axis. *Nat Commun* **14**, 1–16 (2023).

346. Zhou, Z. *et al.* Comparative transcriptome analysis provides insight into the molecular targets and signaling pathways of deer TGF-1 regulating chondrocytes proliferation and differentiation. *Mol Biol Rep* (2023) doi:10.1007/s11033-023-08265-z.

347. Kizawa, H. *et al.* An aspartic acid repeat polymorphism in asporin inhibits chondrogenesis and increases susceptibility to osteoarthritis. *Nat Genet* **37**, (2005).

348. Davidson, E. N. B. *et al.* Increase in ALK1/ALK5 Ratio as a Cause for Elevated MMP-13 Expression in Osteoarthritis in Humans and Mice 1. *The Journal of Immunology* **182**, 7937–7945 (2009).

349. Valdes, A. M. *et al.* Genetic variation in the SMAD3 gene is associated with hip and knee osteoarthritis. *Arthritis Rheum* **62**, 2347–2352 (2010).

350. Lyon, M. *et al.* The Interaction of the Transforming Growth Factor-βs with Heparin/Heparan Sulfate Is Isoform-specific. *J. Biol. Chem* **272**, 18000–18006 (1997).

351. Ruppert, R. *et al.* Human bone morphogenetic protein 2 contains a heparin-binding site which modifies its biological activity. *Eur J Biochem* **237**, 295–302 (1996).

352. Di Guglielmo, G. M. *et al.* Distinct endocytic pathways regulate TGF-β receptor signalling and turnover. *Nature Cell Biology 2003 5:5* **5**, 410–421 (2003).

353. van Caam, A. *et al.* TGFβ1-induced SMAD2/3 and SMAD1/5 phosphorylation are both ALK5-kinase-dependent in primary chondrocytes and mediated by TAK1 kinase activity. *Arthritis Res Ther* **19**, 1–13 (2017).

354. Holtzhausen, A. *et al.* Novel bone morphogenetic protein signaling through Smad2 and Smad3 to regulate cancer progression and development. *FASEB J.* **28**, 1248 (2014).

355. Líbalová, H. *et al.* Global gene expression changes in human embryonic lung fibroblasts induced by organic extracts from respirable air particles. *Part Fibre Toxicol* **9**, 1 (2012).

356. Sebollela, A. *et al.* Amyloid-β oligomers induce differential gene expression in adult human brain slices. *J. Biol. Chem* **287**, 7436–7445 (2012).

357. Yoshihara, K. *et al.* High-Risk Ovarian Cancer Based on 126-Gene Expression Signature Is Uniquely Characterized by Downregulation of Antigen Presentation Pathway. *Diagnosis, Prognosis Clin Cancer Res* **18**, (2012).

358. Desagher, S. *et al.* Genes Regulated in Neurons Undergoing Transcription-dependent Apoptosis Belong to Signaling Pathways Rather than the Apoptotic Machinery. *J. Biol. Chem* **280**, 5693–5702 (2004).

359. Shigemizu, D. *et al.* Using Functional Signatures to Identify Repositioned Drugs for Breast, Myelogenous Leukemia and Prostate Cancer. *PLoS Comput Biol* **8**, (2012).

360. Synnergren, J. *et al.* Molecular Signature of Cardiomyocyte Clusters Derived from Human Embryonic Stem Cells. *Stem Cells* **26**, 1831–1840 (2008).

361. Hong, G. *et al.* Separate enrichment analysis of pathways for up- and downregulated genes. *J R Soc Interface* **11**, (2014).

362. Wang, J. F. *et al.* ITGA5 Promotes Tumor Progression through the Activation of the FAK/AKT Signaling Pathway in Human Gastric Cancer. *Oxid Med Cell Longev* **2022**, (2022).

363. Masuzaki, R. *et al.* Integrin β1 Establishes Liver Microstructure and Modulates Transforming Growth Factor β during Liver Development and Regeneration. *Am J Pathol* **191**, 309–319 (2021).

364. Arias-Salgado, E. G. *et al.* Src kinase activation by direct interaction with the integrin beta cytoplasmic domain. *PNAS* **100**, 13298–13302 (2003).

365. Lundin, L. *et al.* Differential tyrosine phosphorylation of fibroblast growth factor (FGF) receptor-1 and receptor proximal signal transduction in response to FGF-2 and heparin. *Exp Cell Res* **287**, 190–198 (2003).

366. Dai, X. X. *et al.* The expression of ERK and JNK in patients with an endemic osteochondropathy, Kashin-Beck disease. *Exp Cell Res* **359**, 337–341 (2017).

367. Effects of Pleiotrophin (PTN), a heparin-binding growth factor, on chondrocytes | Enhanced Reader.

368. Pufe, T. *et al.* Vascular endothelial growth factor (VEGF) induces matrix metalloproteinase expression in immortalized chondrocytes. *Journal of Pathology* **202**, 367–374 (2004).

369. Ashikari-Hada, S. *et al.* Specific inhibition of FGF-2 signaling with 2-O-sulfated octasaccharides of heparan sulfate. *Glycobiology* **19**, 644–654 (2009).

370. Denker, A. E. *et al.* Formation of cartilage-like spheroids by micromass cultures of murine C3H10T1/2 cells upon treatment with transforming growth factor-beta 1. *Differentiation* **59**, 25–34 (1995).

371. Tracy Ballock, R. *et al.* TGF-beta 1 prevents hypertrophy of epiphyseal chondrocytes: regulation of gene expression for cartilage matrix proteins and metalloproteases. *Dev Biol* **158**, 414–429 (1993).

372. Hollnagel, A. *et al.* Id Genes Are Direct Targets of Bone Morphogenetic Protein Induction in Embryonic Stem Cells*. *J. Biol. Chem* **274**, 19838–13845 (1999).

373. Pagano, M. *et al.* Cyclin A is required at two points in the human cell cycle. *EMBO J* **11**, 961–971 (1992).

374. Matsuoka, S. *et al.* Linkage of ATM to cell cycle regulation by the Chk2 protein kinase. *Science* **282**, 1893–1897 (1998).

375. Cheeseman, L. P. *et al.* Specific removal of TACC3-ch-TOG-clathrin at metaphase deregulates kinetochore fiber tension. *J Cell Sci* **126**, 2102–2113 (2013).

376. Zeitlin, S. G. *et al.* CENP-A is phosphorylated by Aurora B kinase and plays an unexpected role in completion of cytokinesis. *J Cell Biol* **155**, 1147–1157 (2001).

377. Moldovan, G. L. *et al.* PCNA, the Maestro of the Replication Fork. *Cell* **129**, 665–679 (2007).

378. Yao, R. *et al.* TACC3 is required for the proper mitosis of sclerotome mesenchymal cells during formation of the axial skeleton. *Cancer Sci* **98**, 555–562 (2007).

379. Kok, Y. P. *et al.* Overexpression of Cyclin E1 or Cdc25A leads to replication stress, mitotic aberrancies, and increased sensitivity to replication checkpoint inhibitors. *Oncogenesis* **9**, 1–15 (2020).

380. Carloni, V. *et al.* CHK2 overexpression and mislocalisation within mitotic structures enhances chromosomal instability and hepatocellular carcinoma progression. *Gut* **67**, 348–361 (2018).

381. Sebastian, A. *et al.* Single-cell RNA-seq reveals transcriptomic heterogeneity and post-traumatic osteoarthritis-associated early molecular changes in mouse articular chondrocytes. *Cells* **10**, 1462 (2021).

382. Shrestha, R. L. *et al.* Mislocalization of centromeric histone H3 variant CENP-A contributes to chromosomal instability (CIN) in human cells. *Oncotarget* **8**, 46781–46800 (2017).

383. Maehara, K. *et al.* CENP-A Reduction Induces a p53-Dependent Cellular Senescence Response To Protect Cells from Executing Defective Mitoses. *Mol Cell Biol* **30**, 2090–2104 (2010).

384. Rose, J. *et al.* DNA damage, discoordinated gene expression and cellular senescence in osteoarthritic chondrocytes. *Osteoarthritis Cartilage* **20**, 1020–1028 (2012).

385. Zhang, F. *et al.* Cell cycle-related lncRNAs and mRNAs in osteoarthritis chondrocytes in a Northwest Chinese Han Population. *Medicine* **99**, E19905 (2020).

386. Sun, J. *et al.* Identification of genes associated with osteoarthritis by microarray analysis. *Mol Med Rep* **12**, 5211–5216 (2015).

387. Chou, C. H. *et al.* Genome-wide expression profiles of subchondral bone in osteoarthritis. *Arthritis Res Ther* **15**, 1–12 (2013).

388. Tuckwell, D. S. *et al.* Conformation dependence of integrin-type II collagen binding. Inability of collagen peptides to support alpha 2 beta 1 binding, and mediation of adhesion to denatured collagen by a novel alpha 5 beta 1-fibronectin bridge. *J Cell Sci* **107 (Pt 4)**, 993–1005 (1994).

389. Haglund, L. *et al.* Identification and Characterization of the Integrin α2β1 Binding Motif in Chondroadherin Mediating Cell Attachment. *J. Biol. Chem* **286**, 3925 (2011).

390. Danen, E. H. J. *et al.* The fibronectin-binding integrins α5β1 and αvβ3 differentially modulate RhoA–GTP loading, organization of cell matrix adhesions, and fibronectin fibrillogenesis. *Journal of Cell Biology* **159**, 1071–1086 (2002).

391. Humphries, J. D. *et al.* Integrin ligands at a glance. *J Cell Sci* **119**, 3901–3903 (2006).

392. Wang, Q. *et al.* Dysregulated integrin αVβ3 and CD47 signaling promotes joint inflammation, cartilage breakdown, and progression of osteoarthritis. *JCI Insight* **4**, (2019).

393. Wright, M. O. *et al.* Hyperpolarisation of cultured human chondrocytes following cyclical pressure-induced strain: evidence of a role for alpha 5 beta 1 integrin as a chondrocyte mechanoreceptor. *J Orthop Res* **15**, 742–747 (1997).

394. Vielreicher, M. *et al.* Dynamic Interaction between Src and C-terminal Src Kinase in Integrin αIIbβ3-mediated Signaling to the Cytoskeleton. *J. Biol. Chem* **282**, 33623–33631 (2007).

395. Chiu, S.-J. *et al.* Hepatocyte Growth Factor Upregulates Integrin in Madin-Darby Canine Kidney Cells: Implications in Tubulogenesis. *J Biomed Sci* **9**, 261–272 (2002).

396. Klein, S. *et al.* Integrin Regulation by Endogenous Expression of 18-kDa Fibroblast Growth Factor-2. *J. Biol. Chem* **271**, 22583–22590 (1996).

397. Basson, C. T. *et al.* Differential modulation of vascular cell integrin and extracellular matrix expression in vitro by TGF-beta 1 correlates with reciprocal effects on cell migration. *J Cell Physiol* **153**, 118–128 (1992).

398. Kobayashi-Miura, M. *et al.* Decrease in Glycosaminoglycan with Aging in Normal Rat Articular Cartilage Is Greater in Females than in Males. *Cartilage* **13**, (2022).

399. Shen, H. *et al.* Enhancing the Potential of Aged Human Articular Chondrocytes for High-quality Cartilage Regeneration. *FASEB J* **35**, e21410 (2021).

400. Williams, A. *et al.* Differential recovery of glycosaminoglycan after IL-1-induced degradation of bovine articular cartilage depends on degree of degradation. *Arthritis Res Ther* **5**, R97 (2003).

401. Shamdani, S. *et al.* Heparan sulfate functions are altered in the osteoarthritic cartilage. *Arthritis Res Ther* **22**, 1–14 (2020).

402. Izvolsky, K. I. *et al.* Systemic Inactivation of Hs6st1 in Mice Is Associated With Late Postnatal Mortality Without Major Defects in Organogenesis. *Genesis* **46**, 8–18 (2008).

403. Do, A. T. *et al.* Overexpression of heparan sulfate 6-O-sulfotransferases in human embryonic kidney 293 cells results in increased N-acetylglucosaminyl 6-O-sulfation. *J. Biol. Chem* **281**, 5348–5356 (2006).

404. Johnson, C. E. *et al.* Essential Alterations of Heparan Sulfate During the Differentiation of Embryonic Stem Cells to Sox1-Enhanced Green Fluorescent Protein-Expressing Neural Progenitor Cells. *Stem Cells* **25**, 1913–1923 (2007).

405. Al Mahbuba, D. *et al.* Dynamic Changes in Heparan Sulfate Nanostructure in Human Pluripotent Stem Cell Differentiation. *ACS Nano* **17**, 7207–7218 (2023).

406. Lamanna, W. C. *et al.* Heparan sulfate 6-O-endosulfatases: discrete in vivo activities and functional co-operativity. *Biochem J* **400**, 63–73 (2006).

407. Wang, M. *et al.* Decorin knockdown affects the gene expression profile of adhesion, growth and extracellular matrix metabolism in C-28/I2 chondrocytes. *PLoS One* **15**, e0232321 (2020).

408. Glasson, S. *et al.* Deletion of active ADAMTS5 prevents cartilage degradation in a murine model of osteoarthritis. *Nature* **434**, 644–648 (2005).

409. Garg, A. *et al.* Biological Activity Assessment of a Novel Contraceptive Antimicrobial Agent. *J Androl* **26**, 414–421 (2005).

410. Longobardi, L. *et al.* Effect of IGF-I in the chondrogenesis of bone marrow mesenchymal stem cells in the presence or absence of TGF-beta signaling. *Journal of Bone and Mineral Research* **21**, 626–636 (2006).

411. Ekenstedt, K. J. *et al.* Effects of chronic growth hormone and insulin-like growth factor 1 deficiency on osteoarthritis severity in rat knee joints. *Arthritis Rheum* **54**, 3850–3858 (2006).

412. Maile, L. A. *et al.* The association between integrin-associated protein and SHPS-1 regulates insulin-like growth factor-I receptor signaling in vascular smooth muscle cells. *Mol Biol Cell* **14**, 3519–3528 (2003).

413. Maile, L. A. *et al.* Integrin-associated protein binding domain of thrombospondin-1 enhances insulin-like growth factor-I receptor signaling in vascular smooth muscle cells. *Circ Res* **93**, 925–931 (2003).

414. Nam, T. J. *et al.* Thrombospondin and Osteopontin Bind to Insulin-Like Growth Factor (IGF)-Binding Protein-5 Leading to an Alteration in IGF-I-Stimulated Cell Growth. *Endocrinology* **141**, 1100–1106 (2000).

415. Yuan, X. *et al.* Recent Advances of SHP2 Inhibitors in Cancer Therapy: Current Development and Clinical Application. *J Med Chem* **63**, 11368–11396 (2020).

416. Song, Z. *et al.* Tyrosine phosphatase SHP2 inhibitors in tumor-targeted therapies. *Acta Pharm Sin B* **11**, 13–29 (2021).

417. Nyberg, P. *et al.* Endostatin Inhibits Human Tongue Carcinoma Cell Invasion and Intravasation and Blocks the Activation of Matrix Metalloprotease-2, -9, and -13. *J. Biol. Chem* **278**, 22404–22411 (2003).

418. Sipola, A. *et al.* Endostatin inhibits endochondral ossification. *J Gene Med* **9**, 1057–1064 (2007).

419. Sipola, A. *et al.* Endostatin affects osteoblast behavior in vitro, but collagen XVIII/endostatin is not essential for skeletal development in vivo. *Calcif Tissue Int* **85**, 412–420 (2009).

420. Hamano, Y. *et al.* Lack of Collagen XVIII/Endostatin Exacerbates Immune-Mediated Glomerulonephritis. *J Am Soc Nephrol* **21**, 1445 (2010).

421. Bausch-Fluck, D. *et al.* A Mass Spectrometric-Derived Cell Surface Protein Atlas. *PLoS One* **10**, 121314 (2015).

422. Schiess, R. *et al.* Analysis of Cell Surface Proteome Changes via Label-free, Quantitative Mass Spectrometry. *Molecular & Cellular Proteomics* **8**, 624 (2009).

423. Saegusa, J. *et al.* The Direct Binding of Insulin-like Growth Factor-1 (IGF-1) to Integrin αvβ3 Is Involved in IGF-1 Signaling. *J. Biol. Chem* **284**, 24106–24114 (2009).

424. Elbediwy, A. *et al.* Integrin signalling regulates YAP and TAZ to control skin homeostasis. *Development* **143**, 1674–1687 (2016).

425. Deng, Y. *et al.* Reciprocal inhibition of YAP/TAZ and NF-κB regulates osteoarthritic cartilage degradation. *Nature Communications 2018 9:1* **9**, 1–14 (2018).

426. Wilusz, R. E. *et al.* Micromechanical mapping of early osteoarthritic changes in the pericellular matrix of human articular cartilage. *Osteoarthritis Cartilage* **21**, 1895–1903 (2013).

427. Dupont, S. *et al.* Role of YAP/TAZ in mechanotransduction. *Nature* **474**, 179–183 (2011).

428. Paszek, M. J. *et al.* Tensional homeostasis and the malignant phenotype. *Cancer Cell Int* **8**, 241–254 (2005).

429. Levental, K. R. *et al.* Matrix Crosslinking Forces Tumor Progression by Enhancing Integrin signaling. *Cell* **139**, 891 (2009).

430. Bursell, L. *et al.* Src kinase inhibition promotes the chondrocyte phenotype. *Arthritis Res Ther* **9**, 1–12 (2007).

431. Khurana, S. *et al.* A novel role of BMP4 in adult hematopoietic stem and progenitor cell homing via Smad independent regulation of integrin-α4 expression. *Blood* **121**, 781–790 (2013).

432. Van Caam, A. *et al.* TGFβ-mediated expression of TGFβ-activating integrins in SSc monocytes: Disturbed activation of latent TGFβ? *Arthritis Res Ther* **22**, 1–9 (2020).

433. Delcommenne, M. *et al.* Control of integrin expression by extracellular matrix. *J. Biol. Chem* **270**, 26794–26801 (1995).

434. Basson, C. T. *et al.* Differential modulation of vascular cell integrin and extracellular matrix expression in vitro by TGF-β1 correlates with reciprocal effects on cell migration+. *J Cell Physiol* **153**, 118–128 (1992).

435. Mcclurg, O. *et al.* Targeting Cartilage Degradation in Osteoarthritis. *Pharmaceuticals* **14**, (2021).

436. Briggs, M. D. *et al.* New developments in chondrocyte ER stress and related diseases. *F1000Res* **9**, (2020).

437. Fujita, Y. *et al.* Fragmentation of Golgi apparatus of nigral neurons with alpha-synuclein-positive inclusions in patients with Parkinson's disease. *Acta Neuropathol* **112**, 261–265 (2006).

438. Hu, Z. *et al.* The study of Golgi apparatus in Alzheimer's disease. *Neurochem Res* **32**, 1265–1277 (2007).

439. Sasaki, K. *et al.* PGSE Is a Novel Enhancer Regulating the Proteoglycan Pathway of the Mammalian Golgi Stress Response. *Cell Struct Funct* **44**, 1–19 (2019).

440. Singer, M. S. *et al.* SULF2, a heparan sulfate endosulfatase, is present in the blood of healthy individuals and increases in cirrhosis. *Clin Chim Acta* **440**, 72–78 (2015).

441. Jiang, T. *et al.* SULF2 promotes tumorigenesis and inhibits apoptosis of cervical cancer cells through the ERK/AKT signaling pathway. *Brazilian Journal of Medical and Biological Research* **53**, 1–11 (2020).